**TECHNISCHE
UNIVERSITÄT
WIEN**

**VIENNA
UNIVERSITY OF
TECHNOLOGY**

D I S S E R T A T I O N

Assessing river bed changes by morphological and numerical analysis

ausgeführt zum Zwecke der Erlangung des akademischen Grades eines Doktors der technischen Wissenschaften unter der Leitung von

O. Univ. Prof. Dipl.-Ing. Dr. techn. Dr. h.c. Dieter Gutknecht

E 222

Institut für Wasserbau und Ingenieurhydrologie

eingereicht an der Technischen Universität Wien

Fakultät für Bauingenieurwesen

von

Dipl.-Ing. Tim Fischer-Antze

0026881

Große Mohrengasse 24-26/3/2, 1020 Wien

Wien, im Dezember 2005

Acknowledgements

Kurzfassung

Die vorliegende Arbeit befasst sich mit der Beurteilung von Flussbettveränderungen durch Anwendung unterschiedlicher Analysemethoden. Hierfür werden regelmäßig durchgeführte Sohlgrundaufnahmen der Donau östlich von Wien bis zur österreichisch-slowakischen Staatsgrenze über einen Zeitraum von 10 Jahren ausgewertet. Zur Beschreibung und Quantifizierung relevanter morphologischer Strukturen und Prozesse werden Erosions-Anlandungs-Muster erstellt und analysiert, bestehende morphologische Parameter angewendet und neue Parameter vorgestellt. Numerische Methoden werden durchgeführt, um das Verständnis der den gemessenen Flussbettveränderungen zugrunde liegenden Prozesse zu erweitern. Für diesen Zweck wird das dreidimensionale numerische Modell *SSIIM* zur Berechnung von ungleichförmigen Sedimenttransportprozessen modifiziert. Die Sediment-transportformeln von *Wu et al. (2000b)*, die einen Ansatz zur Beschreibung von Verbergens- und Expositionsvorgängen enthalten, werden in das bestehende Modell implementiert. Das modifizierte Modell wird an Laborexperimenten in einer Gerinnekrümmung mit einer Sedimentmischung unter instationären Verhältnissen validiert. Sowohl Sohlverformungen als auch Sortierungsprozesse werden berechnet. Der Nutzen des implementierten Ansatzes wird anhand eines Vergleichs von berechneten Ergebnissen des modifizierten und des ursprünglichen Modells mit gemessenen Daten ermittelt. Anschließend wird das validierte Modell an einem 6 km langen Donauabschnitt angewendet. Hierbei werden instationäre Berechnungen von Strömung und Sedimenttransport eines 100-jährlichen Hochwasserereignisses durchgeführt. Die berechneten Ergebnisse werden mit gemessenen Sohlhöhenveränderungen verglichen.

Abstract

This study deals with the assessment of river bed changes using different analysing methods. Regular bed level surveys of the Danube river between Vienna and the Austrian-Slovakian border are processed over a period of ten years. Erosion-deposition patterns are analysed, commonly applied morphological parameters are used, and new parameters are introduced to describe and quantify relevant morphological structures and processes. Numerical studies are performed to enhance the understanding of the processes leading to measured river bed changes. Therefore, the three-dimensional numerical model *SSIIM* is modified to compute nonuniform sediment transport processes. The sediment transport formulas of *Wu et al. (2000b)* considering hiding-exposure algorithms are incorporated into the existing model. The modified numerical model is validated on laboratory experiments in a channel bend under unsteady flow conditions using graded bed material. Both bed deformation and sorting processes are computed. The benefit of the newly incorporated approach is assessed by comparing the computed results of the modified model and the default model to measured data. Afterwards, the validated model is applied to compute unsteady flow and sediment transport processes of a 6 km long reach of the Danube river induced by a 100 year flood event. The computed results are compared to measured river bed changes.

Table of Contents

List of Tables

List of Figures

1   Outline

The aim of the present study is to analyse the morphological structures and morphological changes of the free flowing Danube river reach between Vienna and the Austrian-Slovakian border by processing bed level surveys and by applying the three-dimensional numerical model *SSIIM* which was originally developed by *Olsen (1991)* to calculate sediment movements in water intakes. The model is modified to calculate morphological changes at graded gravel-bed rivers. It is validated on laboratory experiments in a channel bend comprising relevant processes of morphological changes occurring in nature.

In nature most rivers comprise morphological structures or bed forms such as bars, scours, islands, crossings, ripples, and dunes. Different morphological structures develop depending on the grain size distribution of the bed material, the flow conditions, and the geometrical features of the rivers. Induced by the interaction of flow and sediment transport processes, the structures can change their dimensions and positions over time. Often river beds are in a stage of a general long-term development with either dominating deposition or erosion processes. In many cases, past or present river training measures, such as river straightening, installations of hydropower stations, bank revetments, dredging measures, and groyne installations influenced the long-term development.

The current study is motivated by the need to understand morphological processes at the Danube river. The reach is characterised by a general trend of erosion introducing various problems for navigational purposes and the ecology of the river. The reach comprises developed morphological structures including alternate bars, point bars, and crossings. The general erosion trend is documented in various studies (*Kresser (1988)*, *Bors (1992)*, *Stiefelmeyer (2001)*), but little information is available of the local bed change processes at individual morphological structures and their influence on the flow such as variations of water levels. An assessment of the current morphological status of the river reach can serve as a basis for planning concepts in terms of stabilising the river bed.

Currently, in practical applications mostly one-dimensional approaches are used for the computation of sediment transport processes. With rapidly growing computer resources, multi-dimensional models gain in importance for solving practical open-channel problems with respect to the computations of flow and sediment transport. In many cases, engineering specifications are complex and cannot be solved suitably using one-dimensional approaches. Thus, often laboratory experiments are employed to solve complex tasks including flow and transport processes. Multi-dimensional approaches can serve as an alternative to expensive laboratory investigations, provided that the numerical model captures the relevant morphological processes. This study contributes to the possibilities of multidimensional modelling for complex flow and transport situations. Possibilities and limitations are discussed based on model verification studies using laboratory experiment data and real river bed survey data. Three-dimensional modelling including approaches for fractional sediment transport can be used to complement laboratory investigations.

Bed level surveys of the Danube river reach are analysed over a period of ten years (Chapter 2) to gain insight into the relevant morphological processes reflected by the observed bed levels. The morphological structures are visualised by creating bathymetric maps of different surveys. Therefore,

the measured bed levels are interpolated onto equidistant grids. Difference maps showing erosion and deposition patterns are obtained by subtracting the interpolated grids from different surveys. These methods are performed to draw a concise picture of the relevant processes at different morphological structures. Both short-term and long-term changes are investigated. Moreover, commonly applied parameters are used to quantify and describe the morphological features and changes of the river reach. The observed morphological changes are discussed with reference to maintenance measures performed in the study period and to the hydrological conditions. The impact of the morphological changes on the hydraulics such as water level reductions is investigated. New morphological parameters are derived to gain deeper insight into the processes under the specific conditions of the Danube river.

The numerical model *SSIIM* is modified by incorporating a formulation for nonuniform sediment transport (*Wu et al. (2000b)*) accounting for hiding and exposure effects for the sediment transport of graded bed load. The modified model is validated on laboratory experiments in a channel bend (*Yen & Lee (1995)*) comprising three-dimensional bar forming processes and grain sorting processes under unsteady flow conditions (Chapter 3). Furthermore, the morphological changes are computed using the originally incorporated approach (*v.Rijn (1984a)*)). These results are compared to the results of the modified model to discuss the improvements and effectiveness of the incorporated nonuniform sediment transport formula. Additionally, sensitivity studies of several sediment parameters are performed to investigate their influence on the results in terms of bed deformation and sorting processes.

Based on the processed bed level surveys, a reach of the Danube river is chosen to test the modified model (Chapter 4) on actual river bed changes. The flood event in 2002 is simulated. The computed results are validated based on the pre and post flood surveys. A method to assess the quality of the computed bed changes is introduced by creating difference maps of measured and computed bed changes and comparing the deviations. A mean measure of error is introduced to compare computational results of several sensitivity studies. Moreover, the computed sorting processes and the temporal evolution of bed levels at characteristic locations (e.g. bars, crossings) are processed and discussed.

2 Morphology and morphodynamics of the Austrian Danube river east of Vienna

2.1 Introduction

Rivers are exposed to morphological changes. If erosion and sedimentation processes are balanced over longer time periods, the river is in a stage of dynamic equilibrium. Induced by human interferences including retained sediments in the reservoirs of hydropower stations, dredging measures, and structural regulation measures such as groynes or spur dykes, the dynamic equilibrium can be considerably disturbed. Then rivers are in a long-term stage of erosion or deposition.

The 40 km long reach of the Danube river from Vienna to the Austrian-Slovakian border is investigated in this Chapter. As one of two remaining free flowing reaches of the Danube in Austria, this part of the river is of special importance. The study reach is in a general process of erosion, having impacts on the economical functions such as navigability and the ecology of the river. In this Chapter the morphological processes of the reach are assessed over a period of ten years. The morphological structures are visualised in terms of bathymetric maps and morphological changes are visualised using difference maps allowing to detect erosion and deposition patterns. Appropriate existing parameters such as mean bed levels, thalweg development, cumulative bed volume changes, and width-to-depth ratios are applied to quantify the morphology and morphodynamics of the reach. Furthermore, new parameters such as profile symmetry, lateral slopes, and spatial and temporal profile shape variations, are developed to gain deeper insight into the morphological processes happening at the study reach. The analysis serves as basis for validating a numerical morphodynamic model on a sub-reach of the Danube river (see Chapter 4).

2.1.1 Morphological features in rivers

The term morphology is generally described as the study of structure or form. It is used in a number of different disciplines, such as in biology, where it is applied for describing the form and structure of animals and plants or in language sciences where morphology is a study and description of word formation or finally in geological sciences where the external structure of rocks in relation to the development of erosion forms or topographic features is described.

Morphology in the context of river or fluvial hydraulics deals with the description of the structure and the form of the river bed. Since these structures are usually variable with time, a second term, morphodynamics, is introduced, dealing with the changes of forms and structures over time. Both morphological features and morphological changes of the Austrian Danube river east of Vienna are addressed in this study.

The morphological classification of rivers is often based on their planimetric structure. *Leopold & Wolman (1957)* distinguish three general channel types, straight, meandering, and braided channels. A schematic is given in Figure 2.1. Straight river reaches are very rare in nature, they can be found mostly as a result of river training activities. According to *Mangelsdorf & Scheurmann (1980)*, straight rivers, in a strict geometrical meaning, do not exist in nature. Rivers are denoted as straight when they

are characterised by very small river bed development in the plan view. Even "straight" rivers usually show minor curvature after a maximum length of ten times the river width. Meandering channels are characterised by alternating curvature in the plan view. *Mangelsdorf & Scheurmann (1980)* subdivide two types of meanders depending on their evolution. Free or river meanders develop in their own alluvion and incised or valley meanders have an impressed stream course that is based on the relief of the terrain. Besides these two general types, a variety of transitional meander forms are found in nature. The straight and the meandering channels are typically characterised by a relatively narrow river bed. The water is solely flowing within the limited width of the main channel for discharges smaller than the bankfull discharge. Braided rivers, on the other side are characterised by wide river widths and intensive bed load transport. Here, the flow is subdivided into a number of branches that usually change their geometrical features for each flood event. The areas between the branches can be considered as bars of different configuration that are usually free of vegetation. Besides these three main types of channel configurations, a variety of transitional types can be distinguished. A relevant transitional type is the configuration of alternate bars.
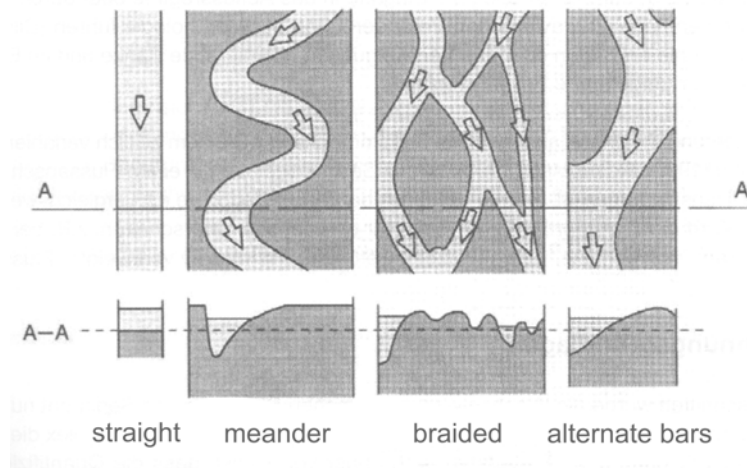
Figure 2.1: Plan view and cross-sections of alluvial rivers (from: *Zarn (1997)*)

Bars are found with different configurations in a lot of river courses. Due to their asymmetric shape and their variability over time, bars are considered as valuable structures from an ecological perspective. Structural diversity and small lateral gradients towards the banks of the river represent favourable habitat conditions. On the other side, bars on waterways are relevant for navigation, such as the reach of the Austrian Danube river east of Vienna. Here, the presence of bars leads to an alternating thalweg configuration. Therefore, the navigation channel is aligned accordingly which can cause gorge portions and critical shallow reaches at the transition from one bar to another (crossings). Intensive river training works in the 19th century at a number of European rivers comprised straightening measures in many cases. In these straightened reaches, the geometrical features of the rivers such as river width, depth, and slope were changed significantly. Therefore, often the morphology changed from an originally braiding to an alternate bar configuration. For this reason the description of river reaches with alternate bar configurations by means of defining appropriate parameters is a practical and scientific issue that is addressed in this study.

Seminara & Tubino (1989) distinguish between two types of bars, alternate (free) and stationary (forced or point) bars. The term free emphasizes the spontaneous character of an instability process as opposed to the development of point bars in curved channels that are controlled by the forcing effects of curvature. The process leading to point bars at the inner bends of rivers is based on the unbalance between transverse pressure gradient, practically uniform along the vertical, and centrifugal forces which decrease from the free surface to the bottom. This leads to secondary circulations, directed outwards at the surface and inwards close to the bottom, characterised by transverse shear stresses able to compensate for the above dynamic unbalance (*Rozovskij (1957)*). If the channel bed is cohesionless, the action of bottom shear stresses associated with the secondary flow makes sediment particles deviate towards the inner bank, thus establishing a transverse slope of the bottom which reaches an equilibrium condition when the transverse bottom stress acting on the particle is balanced by the downslope component of gravity. Figure 2.2 shows the result of this mechanism, the bottom deepens along the concave bank and the water depth becomes shallower along the inner bank (*v.Bendegom (1963)*, *Engelund (1974)*, *Kikkawa et al. (1976)*, *Naudascher (1987)*).
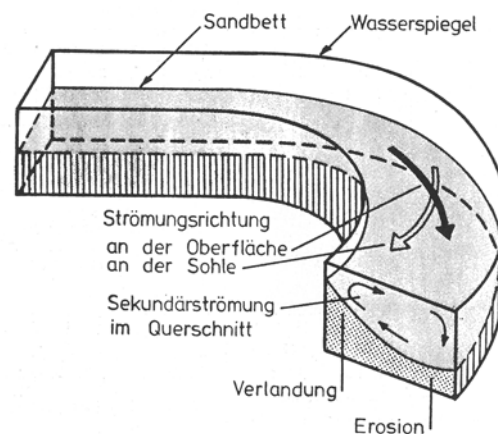
Figure 2.2: Secondary current and morphology in a channel bend (from: *Naudascher (1987)*)

Seminara & Tubino (1989) set up a theoretical framework that draws a picture of the various phenomena involved in the initial process of meander formation in alluvial channels. "Let us consider an originally straight channel with uniform grain sizes. Unless the channel is too narrow or too wide, it undergoes an instability process, which, on a relative fast time scale, leads to the formation of migrating perturbations, alternate bars. As channel widening proceeds, provided the width ratio exceeds a second threshold value above which spatial disturbances may grow, the channel undergoes a second instability process, a planimetric one. The latter process, the details of which still require to be elucidated, is not primarily determined but is definitely affected by the presence of free bars. As the amplitude of meanders increases, so does sinuosity, so that free bars tend to decrease their amplitude till they disappear, leaving only forced bars to induce bank erosion."

Having various morphological structures in rivers that are based on different processes, the *ASCE (1966)* introduced a classification scheme for various bed forms. According to the definition of the *ASCE*, bars fall within the group of bed forms. Typically, bed forms are ripples, dunes, anti dunes, and bars. The *ASCE* subdivides 'bars' in transverse bars, point (or forced) bars, alternate (or free)

bars and tributary bars. Bars are also parts of braided rivers. A schematic of the characteristic bar types is given in Figure 2.3. *Jäggi (1983)* characterises transverse bars as bed forms, where the bar front is positioned in a lateral direction to the flow direction. Their widths coincide with the channel width and they are similar to large dunes. Point bars (forced bars) remain immobile for a longer period, and they comprise bar heights larger than the water levels at medium discharge resulting in an emerging arrangement. They are mostly found at the inner banks of river bends. Alternate bars are situated in straight or mildly curved channels. They are attached to the left and the right banks in an alternating alignment. In the vicinity of tributary flows, particular bars are built in the main channel initiated by the deflection of the main flow.
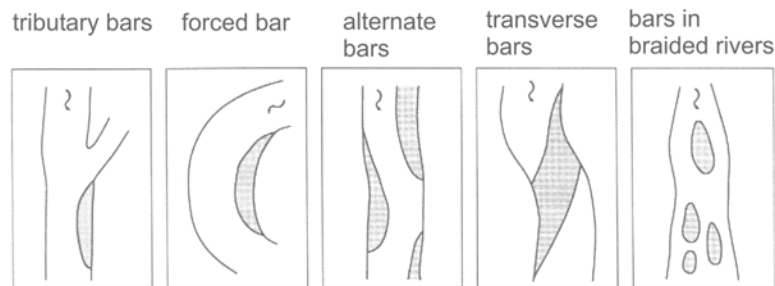
Figure 2.3: Typical bar configurations (from: *Zarn (1997)*)

Often, bars evolve as a pre-stage of islands. After *Scherle (1999)* islands and bars can be distinguished by the presence of vegetation. Islands are covered permanently by vegetation, while bars show no or only temporary vegetation coverage that is removed by the passage of flood events exceeding a critical discharge. *Maryono (1999)* introduces an alternative classification by using the height of the element to distinguish between bar and island. Islands show heights approaching the water depths at medium discharge, while bars comprise significantly lower heights. Due to sedimentation processes, preferably after flood events, bars may become islands. *Yalin & da Silva (2001)* distinguish dunes or bars, that are initiated by turbulent eddy structures and riffles that develop in the viscous sub layer in a fluvial channel. Therefore, the size of ripples is invariant of the size of the channel geometry. The authors differentiate between dunes and bars by the characteristic length of the bed form. The characteristic lengths of the dunes and bars are proportional to the flow depth and the channel width, respectively. The authors mainly investigated different configurations of bars. Depending on the river width, alternate (one row) or multiple bars are found in natural rivers.

Yalin & da Silva (2001) explain the evolution of bars by the presence of horizontal macroturbulent eddies. Horizontal, burst-forming eddies originate predominately near the water surface at the bank where a perturbation is initiated. The size of the eddy grows as it moves away from the banks and is conveyed downstream by the flow. Eventually, when the eddy reaches the bank on the opposite side, the size acquires its maximum value at the river width. At this size, the eddy breaks up. From measurements of the turbulence structure, the length of the eddy structure from its initiation till break up was determined to be six times the width of the channel. For a sufficiently large width-to-depth ratio, the eddy rubs and imprints its structure on the river bed (see Figure 2.4). According to *Yalin & da Silva (2001)*, this process is responsible for the evolution of bars in straight

rivers. For small width-to-depth ratios, the eddy achieves the opposite bank without rubbing the bed. In this case, the eddy cannot produce any bed forms.
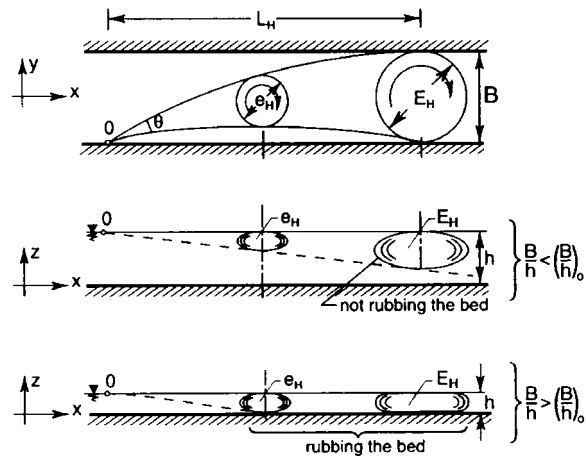
Figure 2.4: Horizontal burst-forming eddies(from: *Yalin & da Silva (2001)*)

Based on the master thesis of *da Silva (1991)*, the authors *Yalin & da Silva (2001)* considertwo significant ratios for determining the morphological classification of a river, the width-to-depth ratio *(B/h)* and the ratio of water depth and mean grain diameter *(h/d)*. Depending on these two parameters, different morphological structures evolve in a river. The authors derived empirically existence regions in the *(B/h) – (h/d)* plane of different morphological characteristics including multiple bars, braiding rivers, alternate bars, meanders, and regime channels (see Figure 2.5). Although the scatter was large, the authors were able to detect the zones (existence regions) for the different morphological classes. It was possible to define an upper boundary for alternate bar, meandering, and regime rivers. Above this line, multiple bars and braiding rivers are preferentially situated. Although the upper boundary of the alternate bars and the regime rivers is the same, their lower boundaries are different. The lower solid line in Figure 2.5 represents the lower boundary of the alternate bars and the dashed line characterises the lower boundary of meandering and regime rivers. *Zarn (1997)* used these relationships to discuss two general types of channel geometries under varying discharge conditions. A narrow river is characterised by a flat river bed for low flow. According to Figure 2.5 and to observations in nature, this river bed configuration remains generally unchanged for a flood event. Different behaviour is observed in the case of wide rivers. Often, wide rivers show braided river bed configurations for low water levels. With increasing discharges (flood), the width-to-depth ratio (*B/h*) decreases and (*h/d*) increases so that the river bed configuration can change to alternate bars, and, even to the configuration of a flat river bed. With the falling limb of the flood, again a braided river bed configuration develops that usually shows different features than the pre flood river bed configuration.
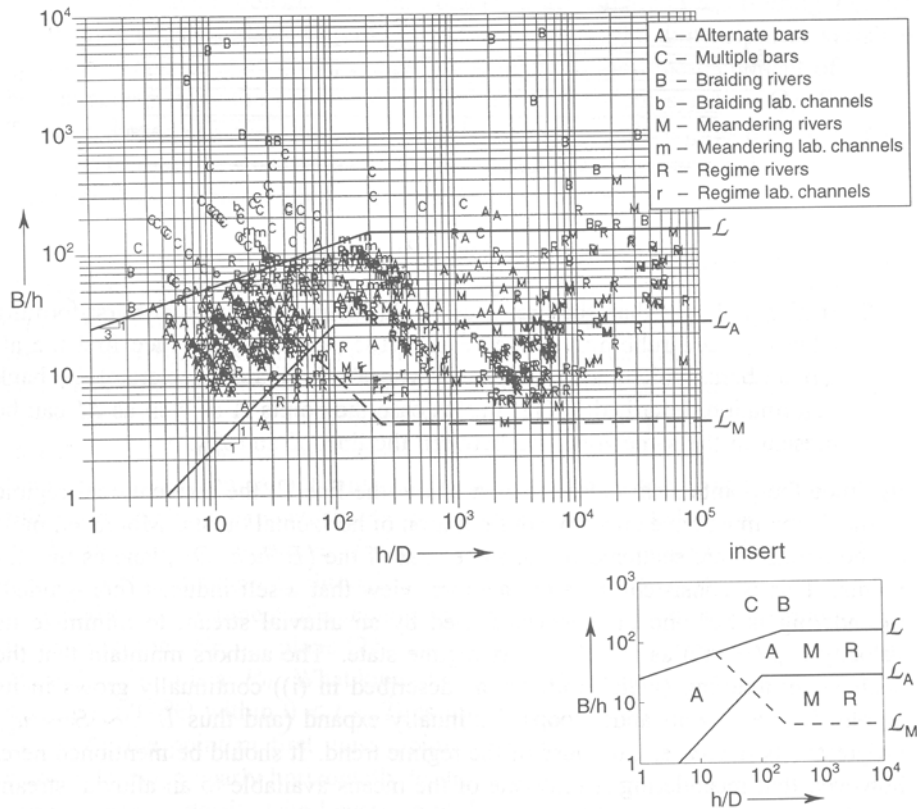
Figure 2.5: Existence region of morphological structures (from: *Yalin & da Silva (2001)*)

Jäggi (1983) introduces alternative criteria for the evolution of alternating bars. By arranging empirical data in groups with constant width and grain diameter, the author develops the minimum bed slope for the existence of alternate bars as a function of the ratio of channel width and grain size diameter. The existence region in the *(B/d, J)* plane is given in Figure 2.6.
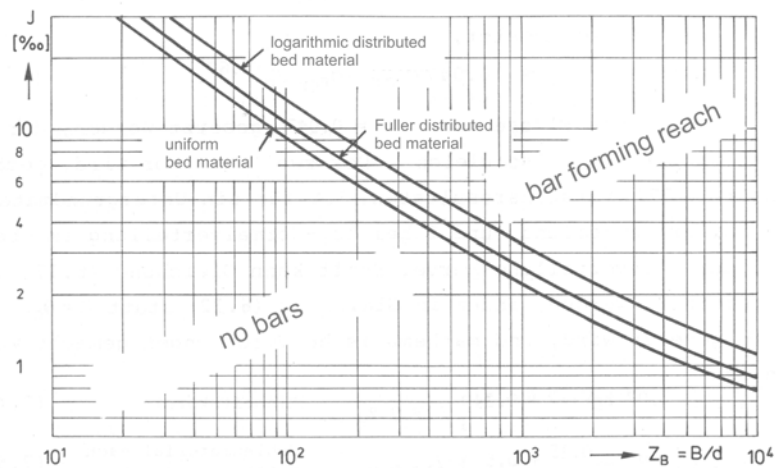
Figure 2.6: Existence region of bars (from: *Jäggi (1983)*)

The question of the existence of morphological structures leads to the question of the geometrical dimensions. A focus is drawn on the dimensions of alternate bar structures. According to *Seminara & Tubino (1989)*, the main features of alternate bars are fairly steep consecutive diagonal

bar fronts, deep pools at the downstream face of each front along the channel banks followed by relatively gentler riffles along the upstream faces of the fronts, bar heights in the order of the average flow depth, bar lengths in the order of a few channel widths, and migration velocities much smaller than the average flow velocity (see Figure 2.7). In gravel bed rivers, free bars form at flood stage and are subject to minor variations at lower stage. In sand bed streams, bars coexist with dunes and significant variations of the bar structure may occur as the flow stage varies. After *Knaapen (2001)*, alternate bars are wave patterns, where the crest and trough alternate between the banks of the channel. The bars move downstream at a speed of several meters per day. Their existence reduces the navigability and influences the water capacity of the channel.
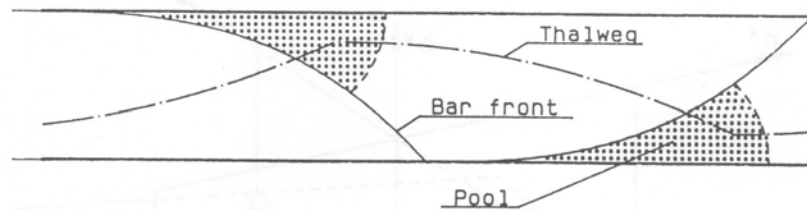
Figure 2.7: Sketch of a sequence of developed free bars (from: *Seminara & Tubino (1989)*)

A number of research groups considered the geometrical dimensions of alternate bars. Mostly, indicators for the lengths and the heights of the bars are found. *Yalin & da Silva (2001)* determine the lengths of the bars by the geometrical nature of the horizontal macroturbulent eddies. Following this reasoning, the mean bar length is defined by six times the river width. *Jäggi (1983)* processed laboratory data on bar formation and approximated the bar length with ten times the river width. Also, for the definition of the bar height, an exclusive formula cannot be given. According to *Bechteler et al. (1998)*, the bar height h_B can be determined by the double distance from the mean bed level. The asymmetric nature of the bar height was accounted for by *Jäggi (1983)*. The scour depth has to be considered when estimating the total height of the bar element. According to *Jäggi (1983)*, the total height is defined as the sum of the maximum heights of the bed form above mean bed level and the scour depth, which is measured from the mean bed level. *Jäggi (1983)* found empirically, that the total bar height Δ_B, the bar height h_B, and the scour depth S can be written as:

$$\Delta_B = 0.22 \ B \ / \ (B/d_m)^{0.15}, \quad h_B = 0.24 \ \Delta_B \quad \text{and} \quad S = 0.76 \ \Delta_B \ (= 0.17 \ B \ / \ (B/d_m)^{0.15})$$

Comparing of the above equation for the scour depth S with field data showed that good agreement was obtained, when the channel width B was replaced by a reduced significant width of $B_r = B - 2 \ast n \ast S$, where the bank slope is given by 1/n. This modification accounts for the generally trapezoidal shape of natural cross-sections.

Yalin (1992) criticises that a conversion of the bar height equation as given by *Jäggi (1983)* reveals a monotonous functionality of the *B/h* and *h/d$_m$* ratios. Therefore, an alternative approach was introduced, indicating the alternate bar height scales with *h/d$_m$* and the channel width B:

$$\Delta_B \approx 0.18 \ast B \ast (h/d_m)^{-0.45}$$

2.1.2   Processing morphological structures in rivers

In *Nestmann & Büchele (2002)*, an extensive joint research project was performed on the morphodynamics of the Elbe river, focussing predominantly on the 568 km long German reach of the channel. The major goal was to describe the main abiotic parameters and processes in the river and the floodplains. Assessment and analysis of the current river conditions in the field of morphology, hydrology, hydraulics, and groundwater dynamics, gives deeper insight into the understanding and evaluation of the ecological and economical functions of rivers. To support decisions on a sustainable regional development, the study provides instruments for quantifying long-term effects and scenarios. Among numerous studies, the morphological situation of the Elbe river was assessed, both historically and at the present time. The Elbe river was characterised by severe human disturbances in terms of river training activities in the 18th and 19th century effecting the morphology from then on till present. Activities including river straightening, bank protection, structural regulation measures such as building groynes and spur dykes, and the removal of islands influenced the spatial and temporal morphological development considerably. Typical morphological changes including incision processes were some of the consequences that were observed at the river. The reaches of intensive straightening coincide well with the reaches of major erosion processes. For these reasons, *Nestmann & Büchele (2002)* attribute the observed incision processes to river training measures in the past, especially river straightening and bank protection. Historical data of the river bed was assessed in terms of a possible eco-morphological concept. The data allowed to define typical natural profile shapes. Various parameters describing the current morphological status were developed and provided for pre-defined, morphologically consistent sub-units. Morphological parameters were processed including geographical data (such as chainage and bank lines), grain size distributions of the bed material in longitudinal profiles, mean and maximum bed levels in the centre of the river course, thalweg development, width of the bank regions, width-to-depth ratios, degree of human impact in the bank regions, and flood areas. Special focus was drawn on the with-to depth ratio, as it proved to serve as an efficient measure to quantify the human impact on the river bed morphology when comparing historical and present width-to-depth ratios. While typically the present cross-sectional profiles are characterised by narrow river widths and large depths induced by incision processes, the historical status was characterised by wide profile shapes combined with shallow water depths. Mean width-to-depth ratios of 90 (for mean discharges) to 245 (high discharges) were achieved at present stage, while historically significantly higher ratios of 245 (mean discharges) to 665 (high discharges) were determined. The historically higher width-to-depth ratios are correlated with higher variabilities of width and depth. Within the framework of the joint research project, the historical status was defined as the specific mission approach for future near-natural river planning activities. Moreover, a hydrological sediment-transport balance model was developed including discharge-transport relationships and longitudinal transport rate distributions. Both bed load and morphological relevant suspended load were considered.

Within the scope of a joint research project, the Salzach river was subject of intensive morphological investigations (*WRS (2000)*). In 1816, the Salzach river became a borderline between Germany and Austria. After a number of river training measures, the Salzach river was finally regulated resulting in a mean river width of 114 m and a predominantly straightened course of the

river. The regulation measures started in 1873 and were continued until the beginning of the 20th century. Due to a reduced channel width, erosion processes started to become a severe problem for the river. A heterogeneous, natural morphology of the river is not given, the river is characterised by uniform cross-sectional profile geometries and continuous bank protection measures. Straightening measures and a reduced supply of bed load lead to river bed lowering involving a lowering of the near-river groundwater levels. The riparian wetlands were successively cut off from the river eco-system. The study reach, defined by the borderline between Austria and Germany is one of very few free flowing reaches within the Alpine region. The main objectives of the joint research project were oriented on an overall environmental concept based on the historical morphological status in the year 1817. Achieving a dynamical stability of the river bed and improving the flood protection were the major issues for the planned measures at the Salzach river. Within the scope of a catalogue of measures the morphological current status of the river was analysed. A morphological classification on the basis of the morphological regions as defined by *da Silva (1991)* was applied for the river using present and historical data and a variety of relevant discharges. Based on the reference year in 1817, a clear shift from the region of braided rivers to alternate bars or meandering rivers was one result of the analysis. The shift is explained by the severe river training measures in this period that lead to significantly different morphological structures of the Salzach. Formerly braided rivers or, in some parts, alternate bar configurations disappeared as a consequence of human activities. Observations of the river partially reflect the result of the analysis after the *da Silva (1991)* classification. Generally different morphological processes were observed at two sub-reaches. At the upper sub-reach (Freilassinger Becken), a sediment deficit at the entrance caused significant erosion processes and fining of the sediment size distribution over the last decades. As a consequence, the originally developed alternate bar features reduced considerably. Cross-sectional profile shapes developed towards more uniform and symmetrical features. Further analysis were performed concentrating on the mean scour depths and the mean bed levels in the sub-reach. The results indicated that the mean bed levels reduced only to a minor degree from the reference level in 1817 to the year 1920. However, from 1920 to 1995, stronger reductions of the mean bed levels occurred. Also, due to the intensive reductions of the channel widths, the scour depths reduced considerably. The eroded material caused less sediment deficit in the downstream sub-reach (Tittmoninger Becken). Thus, erosion processes occurred only to a reduced extend and alternate bars in this region persisted and were not characterised by decaying processes. In addition, the dynamics and the dimensions of the alternate gravel bars were investigated by analysing the thalweg development at different surveys. The wavelengths of the bars were determined by a complete oscillation of the thalweg. In the case of the Tittmoninger Becken bar wavelengths of 1200 to 1400 m were found that fit well the findings of *Leopold & Wolman (1957)* giving 10 to 14 times the river width, resulting in 1000 to 1400 m. The thalweg dynamics in vertical directions proved to be considerably different at the sub-reaches Tittmoninger and Freilassinger Becken. While the first sub-reach was characterised by minor thalweg changes, the latter showed continuously reduced amplitudes of the thalweg from 1953 to 1995. The migration speed was determined for the periods 1953-1959 and 1973-1977. For the two periods, the migration speed was determined as 120 m/a and 85 m/a, respectively in the Freilassinger Becken, while the reach at Tittmoninger Becken showed velocities of 110 m/a and 180 m/a, respectively.

Volume changes and mean bed levels of the Salzach river were computed. In most cases, a reference level and two verticals were given for each cross-section to compute the differences of the cross-sectional area. Volume changes were given by multiplying the area changes by the longitudinal spacing of the cross-sections. From 1920 to 1998, most of the river reaches eroded. Different types of erosion processes in several sub-reaches were observed. While the reach from km 60 to 40 was mostly characterised by rotational erosion processes with mean erosion depths of 4 m on the upstream and 1 m on the downstream end, the succeeding sub-reach from km 40 to km 20 showed relatively continuous lowering of 1 m. Also a narrow valley type sub-reach, from km 20 to km 0 showed considerable local erosion processes.

Savova (2002) investigated some morphological parameters of the Danube river east of Vienna based on cross-sectional bed level surveys performed in 1996. Among others, an asymmetry parameter was determined describing the spatial development with respect to successive bar and crossing regions. Bar regions proved to exhibit significant asymmetrical cross-sectional shapes while crossings were significantly more symmetrical. This analysis was used in the present study to further analyse the temporal development of the river reach with respect to its symmetric features.

A whole network of alluvial rivers in Tuscany, Italy was investigated by *Rinaldi (2003)*. Morphological changes were observed in both vertical and horizontal direction. The analyses in terms of vertical bed changes were based on two data sets. Both topographic longitudinal profiles of different years and field observations were processed. Horizontal bed changes, such as channel width adjustments were investigated by comparing available aerial photographs taken in the 1950's and in the 1990's. Human disturbances, including sediment mining activities, construction of weirs and dams, proved to be the dominant factor for river bed changes. Significant incision processes were observed at virtually all the fluvial systems. Sediment mining activities from 1945 to 1980 caused considerable acceleration of channel incision. The highest rates of bed level lowering were observed along the Arno river, whereas rivers located on the Southern parts experienced significantly smaller amounts of incision. *Rinaldi (2003)* also tried to correlate vertical bed changes with hydrological data. Little evidence of significant changes in magnitude or frequency of floods were found to explain the acceleration of channel incision observed in the second half of the 20th century at the Arno river. Channel narrowing represented a second major morphological change, and occurred simultaneously or following bed-level lowering along most of the analysed reaches. *Rinaldi (2003)* described different types of channel adjustments, depending on the initial channel morphology. "Rivers that were originally sinuous with alternate bars to braided generally adjusted by a moderate incision and a moderate to intensive narrowing, whereas sinuous – meandering channels mainly adjusted vertically, with a minor amount of narrowing." (*Rinaldi (2003)*).

Similar investigation methods were applied by *Ham & Church (2000)*. Also in this study, aerial photographs were processed to analyse morphological changes, the investigated site was the Chilliwack River in British Columbia. Using an analytical stereoplotter, channel features were extracted from five surveys in the second half of the 20th century. The specific sedimentologic situation at this study reach, the river drains a large lake allowing to assume that bed-material output from the lake is zero, allowed to derive a sediment budget approach. Two main patterns of instability were

experienced along the river. Upper channel reaches remained relatively stable due to large particle sizes and the moderating effect of the lake on the flow intensity. The lower reaches, on the other side, were considerably wider which was associated with an increase in sediment supply, a decline in bed-material size and an increase in flood flow intensity and variability. Here, floods caused extensive bank erosion including deposition upstream a crossing in the short–term. In the mid-term, the deposited material was removed by small floods occurring several times per year, so that no persistent long-term aggradation was observed upstream the crossing during the study period. According to *Ham & Church (2000)*, the main limitation of mapping channel changes from aerial photographs of different surveys is, that water levels may not be similar for all individual surveys. This suggests to introduce a correction factor to account for these differences

Various technologies exist for the assessment of morphological structures and their changes over time. Common measures are processing of aerial photographs or conducting field measurements. *Fuller et al. (2003)* compare two types of field measurements and the corresponding processing approaches within a 1 km long reach of the gravel bed river Coquet in Northern England. "The techniques utilise: (i) channel planform and cross-section surveys based on a theodolite/electronic distance measurement (EDM) survey of 21 monumented channel cross-section and channel and gravel bar margins, and (ii) theodolite-EDM survey generating a series of x, y, z coordinates, from which digital elevation models (DEMs) of the reach were constructed. Calculating the difference between DEM surfaces provided a volumetric change between surveys carried out during the spring of 1999 and 2000." (*Fuller et al. (2003)*). The cross-sectional approach was performed in a way that the spacing of the profiles was regular and small enough to cross each bar in the reach by at least one cross-section. In this way, the cross-sectional approach represented the geometry of a bar and its changes in most cases by only one measured cross-section. A budgeting approach was performed on a morphological unit base based on the cross-sectional measurements. Vertical changes in areas along each cross-section were calculated and multiplied by the corresponding planform area to give a net gain/loss volume for each morphological unit. For the second approach, a DEM was created on the basis of approx. 3000 measured irregularly distributed points for each survey. The DEMs were interpolated using kriging. This methodology provided a distinct characterisation of spatial patterns of erosion and deposition, which cross-section based approaches at this site failed to identify. Comparison of the two approaches showed apparent and consistent underestimation of the magnitude of sediment losses using the cross-section approach. The authors explain these discrepancies by significant morphological changes taking place between the cross-sections.

Recent advances in analytical photogrammetry allowed to gain insight of the spatial distribution of the river bed topography often used to analyse morphological changes in rivers. *Brasington et al. (2000)*, however, point out the limitations of photogrammetric methodologies in the context of morphodynamics, since they are usually restricted to emerging river bed structures. An alternative approach was presented providing topographic survey of both exposed and submerged areas of the reach using the Global Positioning System (GPS). Two field programmes were performed in 1998 and 1999 to assess the morphological changes of the Fershie River in Scotland. A GPS base station was placed over a master bench mark and survey points were collected using a roving receiver. The river

reach showed relatively little changes. Anyway, the methodology allowed to detect local changes including the propagation of submerged bar fronts and scours along major channel thalwegs.

Brockmann et al. (2001) present an advanced methodology for creating a DEM for rivers that satisfies the special requirements for hydrological problems. A methodology was developed to filter out irregular measuring errors applying the software package *Scop*. A least square interpolation, denoted as *Krige* estimation was applied. The filtered interpolation results proved to achieve higher accuracies than results that were obtained without the introduced filter technology. Moreover, break lines were considered for creating the DEM allowing to combine data from different sources such as echosounder and laser scanner data. The methodology was introduced in the context of the hydrological geo-information system of the German river Saar.

Habersack & Schneider (2000) analysed historical maps of the Mur River in Austria to derive morphological parameters as an alternative to prevailing descriptive analyses used for defining overall environmental concepts. Typical processed parameters included river width, slope, radius of curvature, and sinuosity. Processing of all parameters revealed that the prevailing problem of successive bed erosion at the Mur river is best solved when changing the crucial parameter "river width" in order to achieve the goal of increased morphodynamics.

2.1.3   The Danube river in Austria

The Danube river is the second longest river in Europe after the Wolga river (3534 km). The source of the Danube river is located in Donaueschingen, Germany, given by the confluence of the two headwaters (Brigach and Breg). The Danube river flows through Germany, Austria, Slovakia, Hungary, Croatia, Serbia, Romania, Bulgaria, and the Ukraine. With a large estuary it flows into the Black Sea. Its total length is 2880 km and the total catchment area comprises 817,000 km². With a navigation length of 2,400 km it is one of the most important waterways in Europe connecting the West and the East of Europe. This function gives rise to an intensive demand of maintenance considering hydraulical, navigational, and ecological aspects (*Savova (2002)*).

The longitudinal river bed development of the Danube river (Figure 2.8) shows two major discontinuities with respect to the slope allowing to subdivide the river into three characteristic reaches. The upper reach is limited by the source of the river and approx. stream km 1800. Here a mean bed slope of 0.4 m/km is present. The river reach represents a mountainous character. It flows through Austria over a length of 350 km. At the German-Austrian border, near Passau downstream the confluence of the Inn river, the river drains a catchment area of 75,000 km², at the Austrian-Slovakian border the catchment area increases to 131,000 km². The 40 km long river reach investigated in this study ranges from stream-km 1920 in Vienna to stream-km 1880 at the Austrian-Slovakian border. It is thus located within the upper river reach. The medium reach is limited by the discontinuity at stream-km 1800 and the Iron Gate at stream-km 950. Here, the mean bed slope decreases significantly, the lower Danube reach with a further decrease of the bed slope ranges from the Iron Gate to the mouth of the river at the Black Sea.
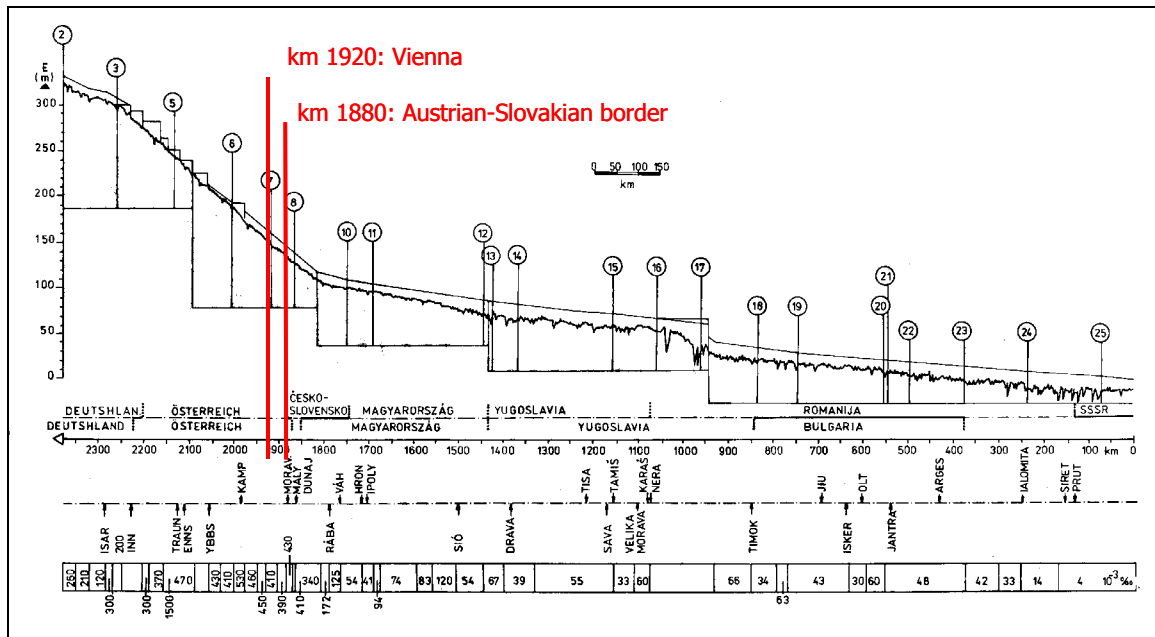
Figure 2.8: Longitudinal profile of the Danube river

The Austrian Danube river was subject to several phases of human interferences over the last two centuries. According to *Kresser (1988)*, the development off the Austrian Danube river can be divided into three phases. The first phase is the time prior to significant river training measures. These measures were performed from 1869 till 1875 (*Mohilla & Michlmayr (1996)*). The measures included improvements of flood protection by building dams along the banks of the river, performing cut-offs to concentrate the flow on a main channel, deactivating side branches, and drainage of wetlands. The measures sustainably modified the river regime and are considered as the beginning of progressive erosion processes at the Danube (*Stiefelmeyer (2001)*). From this time, the Austrian Danube was considered a heavily modified river body and it lost its natural morphological dynamics to a great extent. Originally, the Danube was a braided river within the basin regions consisting of several branches. Islands that were partially vegetated divided the flow. Some of the branches were subject of changes in the planform. High floods were able to change the course of the river considerably. However, within the narrow valley reaches the Danube river was characterised as a one-branch river with compact cross-sectional shapes. Here, the course of the river remained unchanged until present. The second phase ranges from the post river regulation time till the installations of hydropower stations that started in the 1950s. In total, 9 hydropower stations have been installed on the Danube river in Austria. The installation of the embankment dam of the last station, Freudenau, situated at the downstream end of the Austrian cascade of hydropower stations, was finished in 1996. The operational reservoir level was partially set in March 1996 and the maximum operational reservoir level was set in November 1997. Most of the originally free flowing reaches of the Austrian Danube river were successively influenced by the backwater of the dams. Only two river reaches remained free of the backwater influence of the hydropower stations. The first free flowing reach (Wachau) is located downstream the station Melk ranging from km 2037 to 2002, and the second free flowing reach is located downstream the hydropower station Freudenau ranging from km 1920 to 1880. This

reach is analysed in this study. Figure 2.9 shows a longitudinal profile of the Austrian reach of the Danube river including the hydropower station cascade.
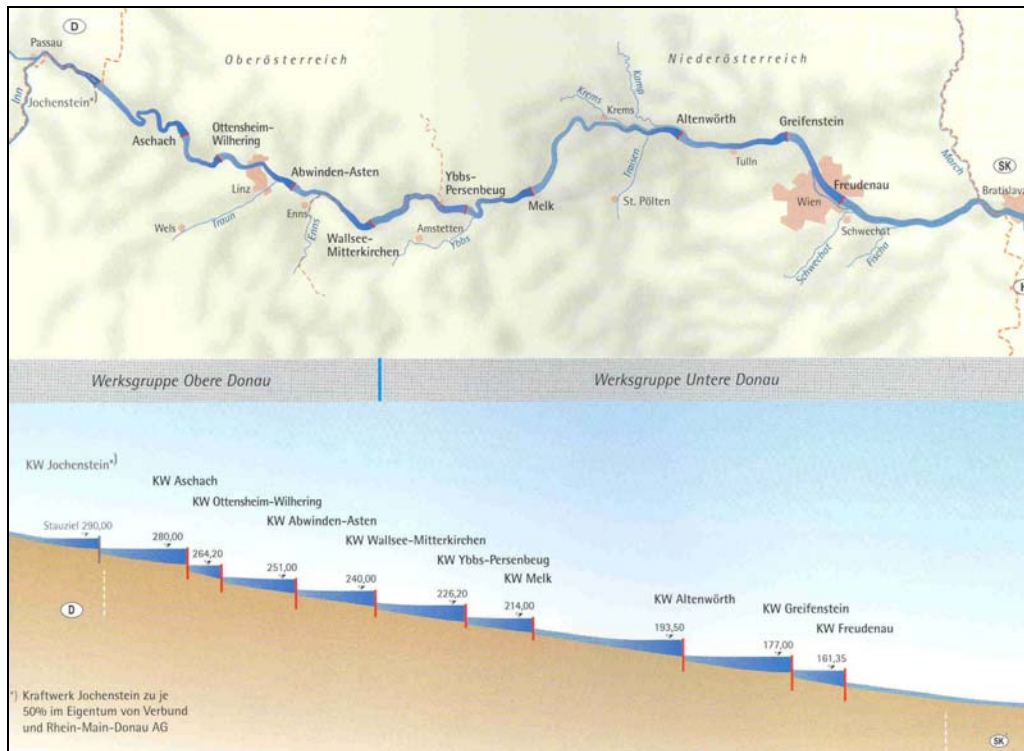
Figure 2.9: Longitudinal profile of the Austrian reach of the Danube river (from: *Verbund (2005)*)

The last phase is the time of further river training measures to enable heavy navigation at the Austrian Danube. River training measures included low water level regulations such as installation of 169 groynes from 1905 till 1911 between Fischamend and Bad Deutsch Altenburg (*Schmautz et al. (2002)*).

The river reach investigated in detail in this study is indicated by a red rectangle in Figure 2.10. A detailed map in Figure 2.11 shows a river length of 40 km of the river reach that is limited by the hydropower station Freudenau in Vienna at the upstream entrance and by the Austrian-Slovakian border at the confluence of the March river at the downstream end. It is assumed that the water levels are not or only to a minor degree affected by the next hydropower station downstream (Gabcikovo at stream-km 1819). Thus, the study reach is characterised as a free flowing reach.

Figure 2.10: Map of Austria, red rectangle indicated the study reach of the Danube river
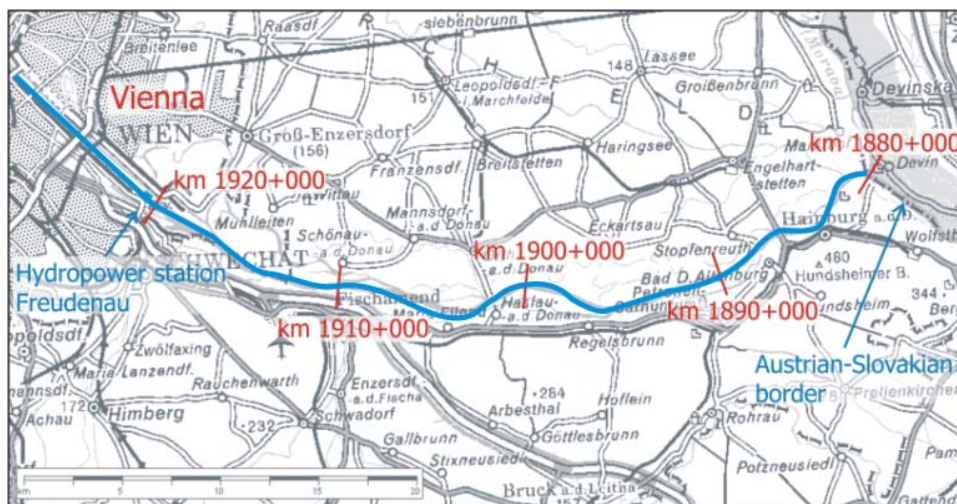
Figure 2.11: Map of the 40 km long study reach of the Danube river

The Austrian Danube river east of Vienna (km 1920 to km 1880) is subject to successive erosion processes that are presumably related to the river training measures performed in the 19th century. The river bed development over the last 50 years before installation of the power station Freudenau can be determined implicitly by analysing the low water level development from 1949 to 1996 at chosen gauging stations. The mean annual erosion rates derived from the low water level development is shown in Table 2.1. The erosion trend was observed at all gauging stations. The annual lowering until 1970 is mostly below 1 cm per year, the erosion rates intensified in the later period from 1970 to 1996 showing erosion rates of 2 cm or more per year. The increasing erosion rates are caused by the successive installation of hydropower plants at the Danube river and its tributaries. *Kresser (1988)* investigated low water levels of the Austrian Danube east of Vienna. The analysis was based on the reference low water levels from 1959 to 1986. Also this analysis revealed a

progressive erosion trend at the Danube reach. All cross-sections experienced significant erosion tendencies with a magnitude of 1 to 2 cm per year with an increasing erosion trend based on the later reference water levels. Analysis of the rating curves at the gauging stations showed that the stations near the downstream end, such as Bad Deutsch-Altenburg (km 1886) or Hainburg (km 1883.92), experienced significantly higher erosion processes compared to the stations upstream. These observations are possibly induced by a reverse erosion process initiated in Bratislava, which is situated 30 km downstream the Austrian-Slovakian border at stream km 1852.

Table 2.1: Mean annual erosion rates from 1949 to 1996 (from: *Klasz (2002)*)

Gauging Station	Stream-km	Mean erosion rates 1949 to 1970 [cm/a]	Mean erosion rates 1970 to 1996 [cm/a]
Donaukanalmündung	1919.43	-0.7	-2.0
Wildungsmauer	1894.72	-1.1	-2.0
Hainburg	1883.92	-0.3	-2.7

Bors (1992) investigated quantitatively the morphological changes of the Danube river in Austria over the last decades. Generally morphological changes at two types of reaches are distinguished, the reaches that are influenced by the backwater curves in the reservoirs of the dams, and the free flowing river reaches. The reservoirs are characterised by significant deposition processes. The river beds of the reservoir reaches upstream the hydropower stations are characterised by deposited fine sediments. The free flowing reaches are generally characterised by severe erosion activities. Bed level erosion processes have significant impact on the slope, the water levels, and the ground water levels. From 1960 to 1990, a maximum deposition volume of 22 million m³ was measured in the reservoir of the hydropower station Aschach. The two remaining free flowing reaches in Austria, Wachau and east of power station Greifenstein (at the time of the study, the hydropower station Freudenau was not installed) were analysed. They exhibit different morphological dynamics. While the reach Wachau remains virtually stable over many years, the long-term development of the latter reach achieves mean erosion rates of 1 to 3 cm per year. Similar to other studies, *Bors (1992)* attributes the progressive erosion trend to intensive river training measures and a bed load deficit due to the construction of dams at the Danube river and its tributaries.

With a catchment area of approx. 100,000 m³, the Danube river in Vienna has a mean discharge of *MQ* = 1,915 m³/s. Further characteristic discharges are derived by the waterway directorate (*WSD (1996)*) using duration curves over a period of 30 years (1961 to 1990) and statistical flood analysis (Table 2.2). Tributaries of the study reach are the rivers Schwechat at km 1913.7 and Fischa at km 1904.7. Both tributaries have a mean discharge of approximately 8 m³/s. Thus, they have a negligible influence on the hydraulics and morphodynamics of the Danube river.

Table 2.2: Characteristic discharges at the Danube river (source: *WSD (1996)*)

	Name	Discharge at study reach	Definition
RNQ	Reference low discharge	910 m³/s	Discharge with a duration of exceedance of 94 % (approx. 343 days per year).
MQ	Mean discharge	1,915 m³/s	Determined on the basis of the arithmetic mean of the mean annual discharges over the given 30 year period.
HSQ	Highest discharge for navigation	5,010 m³/s	Discharge with a duration of exceedance of 1 % (approx. 3.6 days per year).
HQ$_{100}$	Discharge for the 100 year flood	10,400 m³/s	Discharge with a return period of 100 years.

Zottl & Erber (1987) investigated the bed material sediment size distribution of the Danube river in the context of the planned hydropower station Freudenau. 30 sediment samples were taken from km 1940 to km 1880. Within the reach east of Vienna, 20 processed sediment samples are available. On average, a mass of 550 kg was grabbed per sample. The grabber closed completely so that fine material was preserved for sieve analysis. The quality of the samples is assumed to be high, since it was possible to sample large amounts preserving all fractions for further sieve analysis. An extract of the processed sieve analysis is shown in Figure 2.12. The red curve indicates the mean sediment curve that was averaged over the 20 sediment samples east of Vienna. In Table 2.3, characteristic diameter sizes are shown that are derived from the mean sediment curve (mA). With a d_{16} = 5.7 mm and a d_{90} = 57.6 mm the Danube river falls within the range of a gravel bed river, which is limited by 2 and 60 mm for fine and coarse gravel, respectively.
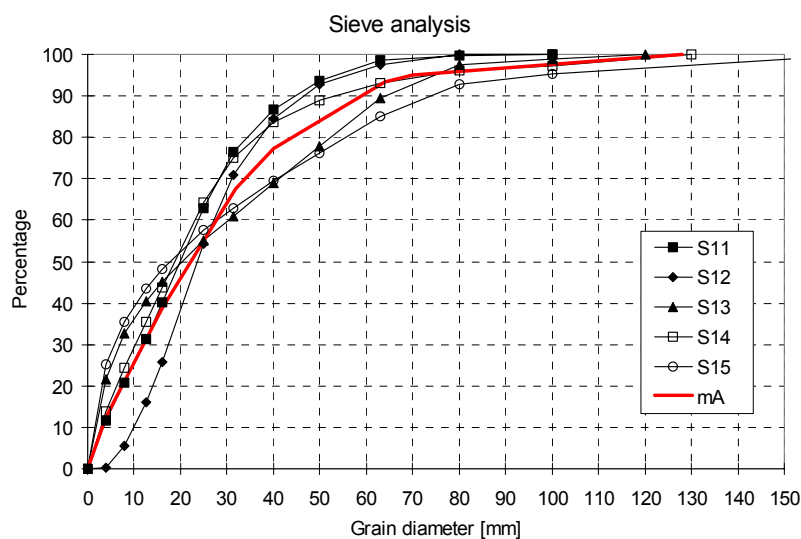
Figure 2.12: Sieve curves of bed samples at the Danube river (from: *Zottl & Erber (1987)*)

Table 2.3: Characteristic grain diameters at the Danube study reach (from: *Zottl & Erber (1987)*)

d_{90}	d_{84}	d_{50}	d_{16}	d_m
57.6 mm	48.1 mm	21.6 mm	5.7 mm	26.3 mm

Analysing the processed mean grain diameters along the course of the river gives insight into the longitudinal development of the bed material. The processed results are shown in Figure 2.13. A general trend of decreasing mean grain diameters is given representing abrasion processes in the river reach. The mean grain diameters d_m and a relationship describing the abrasion of the grains introduced by Sternberg are shown as a function of the upstream longitudinal distance. At km 1920 and at km 1887, mean grain diameters of 27.6 mm and 23.8 mm were determined, respectively.

Sternberg introduced in 1875 a relationship for abrasion as a function of the longitudinal distance *x* based on the reference mean grain diameter $d_{m,0}$. The coefficient *c* [km^{-1}] is determined empirically according to the specific morphological situation at the river :

$$d_m(x) = d_{m,0} \cdot e^{-c \cdot x / 3}$$

Zottl & Erber (1987) performed a regressional analysis by adjusting the empirical parameter *c*. A least square errors fit was performed to achieve the parameter *c* = 0.0137. The empirically determined parameter fits well to the values given in literature for the Danube river.

In the *WRS (2000)* study, abrasion of the Salzach river was determined by the German Federal Institute of Hydrology (BfG). Also here, the approach of Sternberg was used to determine abrasion processes. The abrasion coefficient here was determined to c = 0.005 km^{-1} and was therefore considerably smaller compared to the Danube river. However, sensitivity studies using numerical models on the Salzach river showed, that the variation of the abrasion coefficient had minor effect on the morphodynamics of the river.

At the Danube river, samples from scours exhibited generally coarser grain diameters than at the bars (*Zottl & Erber (1987)*). However, the variations within one cross-section were relatively small. Although, the samples were taken almost 20 years ago, the data is used for various analyses in the current study such as for the morphological classification and for the numerical computations, assuming that the mean sediment size distribution (mA) still represents the current sedimentologic conditions at the Danube river reach.
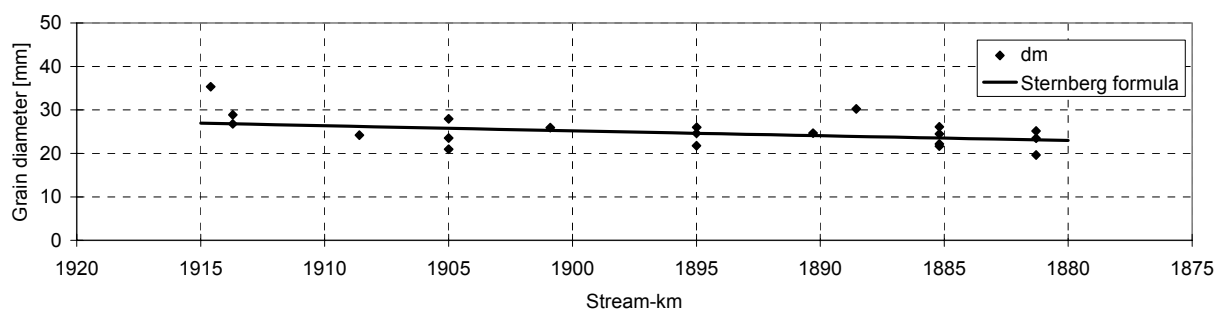
Figure 2.13: Mean grain diameters from km 1915 to 1880 (derived from: *Zottl & Erber (1987)*)

In a study by *Donauconsult (1997)*, the mean sediment size distribution from Table 2.3 was used to calculate the sediment transport capacity of the Danube reach east of Vienna for characteristic discharges. The sediment transport formula of *Meyer-Peter & Müller (1949)* and a characteristic cross-sectional profile that was produced by an averaging procedure of the hypsographic curves of the considered cross-sectional profiles were used for the computations of the sediment transport capacities. Table 2.4 shows, that according to the formulas of *Meyer-Peter & Müller (1949)*, sediment transport is initiated when a critical shear stress is exceeded. At the Danube river this is achieved for a discharge of *MQ* = 1,915 m³/s where a negligible amount of sediments is set into motion. A sediment transport capacity of more than 600 kg/s is achieved for a 100 year flood. Using a discharge duration curve over a period of 20 years (1971 to 1990) gives the average annual sediment transport capacity that achieves a value of almost 300,000 m³/a.

Table 2.4: Sediment transport capacity at the study reach (from: *Donauconsult (1997)*)

	Sediment transport capacity
RNQ	0.0 kg/s
MQ	1.9 kg/s
Q = 3500 m³/s	40.0 kg/s
HSQ	220.1 kg/s
Q = 8000 m³/s	441.5 kg/s
HQ_{100}	635.8 kg/s
Annual transport capacity	297,700 m³/a

River training measures were successively performed including the installation of groynes and spur dykes along the study reach. These river training measures improving the navigability at the Danube river were partially realised up to an extensive degree. Improved navigability is achieved by the effect of groynes to raise low water levels and to concentrate the flow on the navigation channel. Various formulas exist in literature parameterising the raising effect. *Krouzecky (2004)* introduced an empirical relationship to calculate water levels at the presence of groynes considering the hydraulic conditions (discharge, slope, roughness), the geometry, and the longitudinal spacing of the groynes. Within the reaches of extensive groyne configurations, a longitudinal spacing of approximately 100 to 200 m is given at the Danube reach. Figure 2.14 shows an example of the alignment of the groynes in a 2 km long reach from km 1896 to 1894. The yellow points on the banks of the river represent the breakpoints given for all cross-sectional profiles at a distance of 100 m. Here, intensive groyne installations are shown on the inner bend on the left side. The lengths of the groynes may reach up to 170 m, covering approx. 45 % of the channel width. Smaller groynes are found on the outer bend on the right side achieving lengths of up to 50 m. The morphological changes of the groyne fields are not monitored consistently, since these shallow reaches cannot or only be reached partially by the measuring device (boat). The sediment size distribution in the groyne fields consists mostly of fine

material that deposited from suspended sediment transport within the shallow regions of the groyne with small flow velocities. Typically, the morphological structures at a groyne field consists of a scour in flow direction downstream the groyne heads, which is followed by a deposition region on the side and the downstream face of the scour (*Spannring (1999)*). Groynes fulfil several functions in a river. They serve to protect the banks of a river by reducing the widths of the cross-sectional profiles and concentrating the flow in the main channel. The flow concentration leads to deposition processes in the groyne fields and thus erosion processes in the main channel due to increased shear stresses. The flow concentration can have positive effects on navigation. From an ecological perspective, groyne fields can serve as valuable secondary habitats *Krouzecky (2004)*.

Figure 2.15 shows the presence of groynes and spur dykes at the Danube reach. The results show that 44 % of the cross-sections on the left, and 39 % on the right side are influenced by groynes or spur dykes. The construction intensity significantly increases in the lower half of the river reach. In the upper half, where alternate bar configurations are present, the extent of river training measures in terms of low water regulations is comparably smaller.
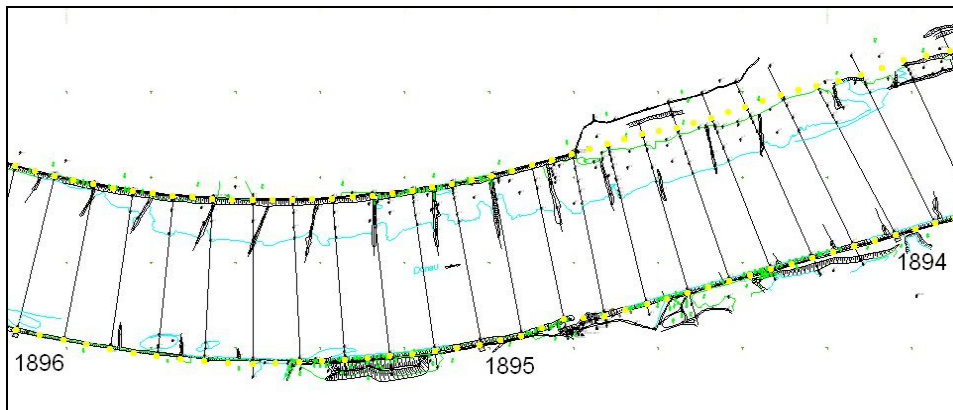
Figure 2.14: Navigation map of Danube river from km 1896 to 1894
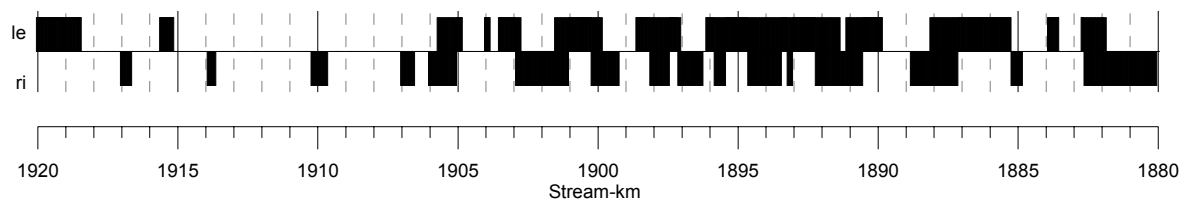
Figure 2.15: Presence of groynes and spur dykes

The Danube river is characterised by regular dredging measures for maintaining the navigation channel. A considerable amount of the dredged material is returned to the main channel of the Danube river (grain feeding). Material is also used for structural river training measures near the banks of the river. In this case, the material is elevated onto its new position (*Bors (1992)*). Presumably, the elevated material lies outside the measured bed level surveys in most cases while the surveys completely cover the reach of the grain feeding. In Figure 2.16, the positions and years of the dredging and grain feeding measures are shown. In total, amounts of 1.1 million m³ and 0.4 million m³ were

dredged and fed over the ten year period, respectively. The largest dredging activities were performed at the crossings (see Table 2.5). Here, the crossing Hainburg was characterised by the largest dredgings by far. The confluence reach of the *Neue Donau* at stream-km 1917 also demands regular significant dredging measures. These hot spots have to be considered when interpreting the measured morphological changes at the Danube river.

Table 2.5: Overview of dredgings at crossings from 1993 to 2003

Name of crossing	Stream-km	No. of dredgings	From	To	Total cubature [m³]
Schwechatmündung	1913.7	4	1995	1997	148,000
Buchenau	1912	1	2002	2002	16,000
Kuhstand	1910	1	1998	1998	14,000
Fischamend	1908	1	2001	2001	11,000
Orth	1902	4	1997	2002	69,000
Regelsbrunn	1898	3	1998	2002	74,000
Rote Werd	1896	2	2001	2002	38,000
Treuschütt	1888	2	2000	2000	43,000
Hainburg	1884	8	1994	2003	467,000
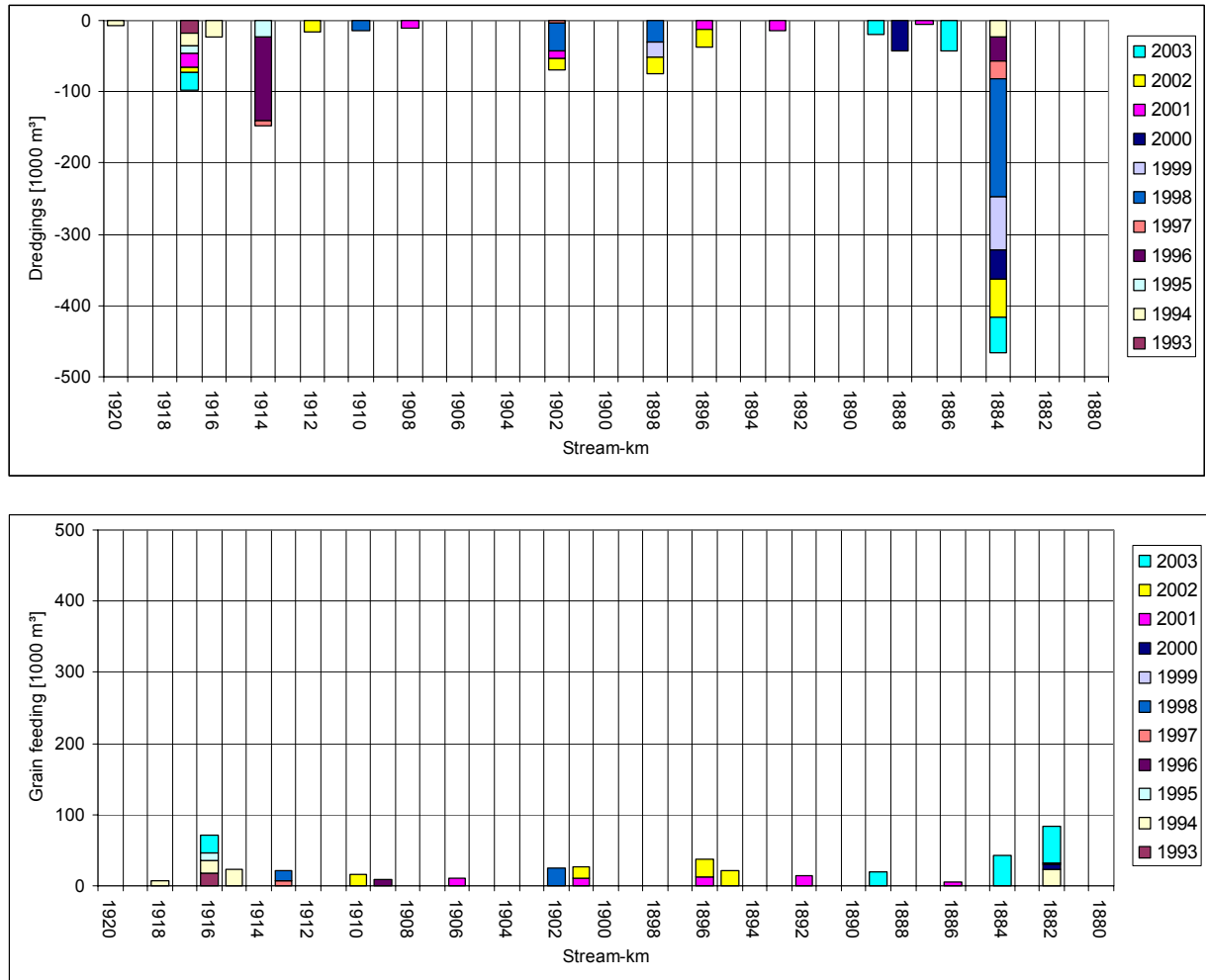
Figure 2.16: Dredging and grain feeding measures from 1993 to 2003

The operator of the hydropower station Freudenau is committed to regularly release sediment material (grain feeding) to compensate for the retaining effect of the dam on the free passage of the sediments. The general erosion trend that was presumably initiated at this reach of the Danube river after termination of the river training measures in the 19th century is not compensated by the operator. The grain feeding started in 1996 (after installation of the hydropower station). Analysis of the transported material before 1996 yielded an average amount of 160,000 m³ per year that was transported into the study reach (*Donaukraft (1995)*). On average, this amount was determined to be artificially released into the study reach by grain feeding measures. This average value has to be modified with respect to the hydrologic situation of each year. For years exceeding the average water volumes, larger amounts of sediment have to be fed into the river. The mean amount of 160,000 m³ is smaller than the potential sediment transport capacity of the river reach (300,000 m³, see Table 2.4). Therefore, the successive erosion trend at the Danube river reach cannot be solely compensated by the operator's grain feeding measures. The first 10 km downstream the hydropower station from km 1920 to 1910 (denoted as maintenance reach) are used for the grain feeding measures. Table 2.6 shows the grain feeding measures that were performed from 1996 to 2003, the sum of the grain feedings for the periods between the bed level surveys is shown in Table 2.7. Additionally, the operator performed local scour fillings in the years 1994 to 1995 (see Table 2.8) to protect these

sensitive regions from further erosion processes (*Lanschützer (2005)*). These filling and feeding measures have to be considered for the analysis of measured bed levels at different surveys.

Table 2.6: Grain feeding measures performed by the operator of the hydropower station Freudenau

Year	Feeding [m³]	Stream-km	Time	Survey period
1996	10,000	1918.0	?	95-96(?)
	47,000	1912.7	?	95-96(?)
	27,300	1917.2-1917.7	10.03.-07.04.	95-96
	11,400	1915.5-1915.8	08.04.-15.04.	95-96
	10,000	1914.4-1915.0	16.04.-22.04.	95-96
	14,400	1912.2-1912.7	23.04.-06.05.	95-96
	14,200	1919.1-1919.5	06.05.-28.05.	95-96
	22,800	1917.7-1918.8	02.06.-25.06.	95-96
	157,000			
1997	8,000	1917.7-1918.8	26.06.-02.07.	97-98
	68,200	1920.0-1918.6	02.07-22.10.	97-98
	35,800	1918.2-1917.6	01.07.-19.11.	97-98
	23,900	1916.5-1915.4	19.11.-17.12.	97-98
	17,100	1916.5-1915.4	12.01.-20.01.	97-98
	3,300	1920.0-1919.3	21.01.-26.01.	97-98
	156,300			
1998	36,800	1920.0-1919.3	26.01.- 29.04.	97-98
	78,600	1918.8-1917.9	21.01.- 23.04.	97-98
	44,700	1916.9-1915.5	24.04.- 19.11.	97-98
	3300	1915.4-1915.5	19.11.-24.11.	97-98
	9100	1914.8-1915.2	24.11.-09.12.	97-98 (?)
	24,100	1920.0-1919.7	10.12.-13.01.	98-99
	196,400			
1999	42,100	1920.3-1919.4	09.03.-14.12.	98-99(?)
	83,200	1918.8-1917.3	26.04.-08.09.	98-99(?)
	40,700	1916.9-1915.4	14.09-18.11.	99-00
	165,900			
2000	81,600	1920.3-1919.4	17.04.-07.11.	00-01(?)
	45,000	1920.0-1919.4	18.09.-11.10.	00-01
	42,800	1913.1-1912.4	12.07.-29.11.	00-01
	11,500	1915.0-1914.5	23.10.-29.11.	00-01
	199,100			
2001	46,900	1917.3-1916.5	26.11.-06.03	00-01
	40,100	1918.8-1918.0	28.05.-12.02	01-02(1)
	87,000			
2002	44,700	1912.8-1912.3	11.09.-04.12.	02(1)-02(2) (?)
	109,500	1918.1-1917.3	04.06-10.09.	02(1)-02(2)
	93,500	1920.2-1919.3	06.03.-03.06.	02(1)-02(2)
	247,600			
2003	62,000	1912.8-1912.3	01.02.-31.08.	02(2)-03(1)
	17,000	1912.8-1912.3	01.02.-31.08.	03(1)-03(2)
	36,000	1915.8-1914.3	01.03.-31.08.	02(2)-03(1)
	30,000	1915.8-1914.3	01.03.-31.08.	03(1)-03(2)
	62,000	1918.1-1917.3	01.03.-31.08.	02(2)-03(1)
	15,000	1918.1-1917.3	01.03.-31.08.	03(1)-03(2)
	222,000			

Table 2.7:Grain feeding measures at the survey periods

Period	Feeding [m³]
95-96	157,100
96-97	0
97-98	328,800
98-99	149,400
99-00	40,700
00-01	146,200
01-02(1)	40,100
02(1)-02(2)	247,700
02(2)-03(1)	160,000
03(1)-03(2)	62,000

Table 2.8: Scour fillings

Scour	Stream-km	Year
1	1915.6 - 1916.3	1995
2	1913.4 - 1915.2	1994
3	1912.0 - 1913.1	1995
4	1910.0 - 1912.0	1995

2.2 Methods

2.2.1 Measuring technique

The river bed of the Danube river east of Vienna is regularly surveyed. The surveys are performed to gain insight into the river bed morphology and morphodynamics. Additionally, the amounts of regular grain feeding, the river training measures such as dredgings, and the navigability within the navigation channel are monitored. The river bed surveys consist of measurements of bed heights in pre-defined cross-sectional lines. The longitudinal spacing of the cross-sections is 100 m, thus, the whole 40 km long reach is represented by 400 cross-sectional profiles. In plan view, the cross-sectional lines are defined by two breakpoints on the banks of both sides of the river. The breakpoint positions are given in a cartesian local co-ordinate system denoted as *Gauss-Krüger Österreich*.

The bed levels are surveyed by a measuring boat navigating along the pre-defined cross-sectional lines. The position of the boat is determined by a D-GPS (differential global positioning system) technology. This technology uses at least two GPS receivers to improve the accuracy of the measurements. One receiver, the base station, is mounted over a breakpoint with known position, another receiver, the rover, is mounted on the boat. The base station transmits the deviation between known and measured position to the rover which allows to increase the measured accuracy. Then, deviations such as artificially produced errors by a GPS-jammer applied for military reasons are eliminated. With this technology an accuracy of the position of less than 1 m is achieved. The captain of the boat is provided with online information of the current boat position. Considering the cross-

sectional line, the captain gets information on the current offset, allowing to adjust the boat position continuously, and therefore to minimise operational position errors.

The height of the boat is determined by water levelling performed at each cross-section. The water depth is determined by a single beam echo-sounder system. The technology is based on a swinger that gives an impulse towards the bed of the river with a frequency of approximately 100 kHz. The sound waves are reflected by the river bed and received by a mounted sound transformer. The water depth can be derived from the temporal delay and the velocity of propagation of the sound waves. The velocity of propagation strongly depends on temperature and salinity of the water. Therefore, the measuring devices have to be calibrated before each use. The absolute bed levels are computed by the height of the boat and the measured water depths. Accuracies of less than 10 cm in height are achieved by this technique.

Approximately 400 to 500 measured points per profile are collected, allowing to analyse precisely the river bed morphology in lateral direction at the cross-sectional lines. The positions of the cross-sectional lines remain unchanged for all surveys. The data of the measuring points are given in a cartesian local co-ordinate system. To enable direct cross-sectional comparison of different measurement campaigns, the measured data have to be pre-processed in two steps. First, the offsets are eliminated by transforming the points orthogonally onto the cross-sectional lines, assuming that the measured height is characteristic for the cross-sectional position. Then, the data is converted from the cartesian co-ordinate system into a cross-sectional system, the point of origin is set equal to the left breakpoint in flow direction for each cross-section. River bed data is available from 1993 till 2001 in yearly intervals, in the years 2002 to 2003 the frequency was increased to bi-annual intervals.

Table 2.9 shows the durations of the surveys and the periods between the surveys computed by the differences of the mean survey dates. In most cases the duration of the survey campaigns is 1 to 2.5 months. However, in three cases, the surveys require a measurement duration of more than 100 days. For long-term measurement campaigns, the possibility is given that the survey does not capture the momentary river bed morphology. Then morphological changes within the campaigns have to be expected. The periods between the surveys are ranging from 0.5 to 2.1 years. Smaller survey intervals (bi-annual) are realised from the year 2002 on.

Table 2.9: Dates and periods of the bed level surveys

Survey	Start	End	Duration of survey [d]	Mean	Days between surveys	Years between surveys
1993	26.04.1993	27.05.1993	31	11.05.1993	-	-
1995	20.03.1995	10.08.1995	143	30.05.1995	749	2.1
1996	29.04.1996	26.08.1996	119	27.06.1996	394	1.1
1997	10.04.1997	11.06.1997	62	11.05.1997	318	0.9
1998	16.09.1998	30.11.1998	75	23.10.1998	531	1.5
1999	06.04.1999	16.06.1999	71	11.05.1999	200	0.5
2000	20.03.2000	10.05.2000	51	14.04.2000	339	0.9
2001	05.03.2001	18.04.2001	44	27.03.2001	347	0.9
2002(1)	25.02.2002	15.04.2002	49	21.03.2002	360	1.0
2002(2)	09.10.2002	07.11.2002	29	23.10.2002	216	0.6
2003(1)	30.04.2003	25.06.2003	56	28.05.2003	217	0.6
2003(2)	04.09.2003	31.12.2003	118	02.11.2003	158	0.4

Besides the echo-sounder measurements that mainly cover the deeper regions of the river bed, a photogrammetric flight was performed in 2003 at low flow providing bed levels at dry river regions. The data of the photogrammetric flight is also given in the local cartesian co-ordinate system. It is processed to complement the cross-sectional information. The combination of both data sets, photogrammetric flights and echo-sounder measurements, gives improved river bed information. Still, data gaps remain at shallow water areas. The combination of echosounder and photogrammetric data is used to generate a numerical grid for a test reach of the Danube river as described in Chapter 4.2. The photogrammetric data is not appropriate for analysing measured morphological changes.

The river bed surveys provide data to analyse the morphology and the morphological changes of the river reach. Nevertheless, some limitations have to be considered when interpreting the processed data. The accuracies of the height and position of the measurement points are limited. Assuming randomly distributed errors, a large number of measurements can compensate for measured inaccuracies with respect to processed averaged information, such as the mean bed level in a cross-section. Besides randomly distributed errors, the system can also introduce bias errors. For example the conversion of the measured water depths by the echo-sounder into bed levels on the basis of the water levelling for each cross-section neglects any influences from laterally inclined water levels. In river bends, this leads to a bias that is partially compensated when only the differences from one survey to another are considered. Although, aerial measurements can complement echo-sounder data, gaps still remain in shallow water areas. This technology gives a large data measurement density within the cross-sectional lines, but there is no information given between the cross-sections in longitudinal direction. Morphological structures, such as ripples or dunes that have much smaller dimensions than the longitudinal spacing of the cross-sections cannot be measured by this technology. Offsets from cross-sectional lines induced by inaccurate navigation of the measuring boat can only be corrected in position but not in height. The duration of the measurement campaigns is one to two months on average. Morphological changes that happened during one campaign influence the accuracy of the results. The interval of six months to one year is not sufficient to resolve all relevant

morphological processes such as immediate morphological response to a flood event. The lengths of the measured profile lines depend on the present water levels. Therefore, these lengths may vary from one campaign to another. For some of the morphological characteristics such as bed volume changes or mean bed levels, data processing has to be performed within reduced widths covering all surveys.

2.2.2 Processing technique

The measured heights of the river bed provide a large data set of topographic information. On average, 200,000 points are measured at each survey for the 40 km long Danube river reach. A total of 12 surveys is analysed. Processing of the data is performed in terms of parameters describing the morphology and morphodynamics of the river reach. Computer routines are written in *Matlab 7* to handle the large data sets. Techniques requiring a number of processing steps are presented here.

To enable a visual analysis of the morphology and morphodynamics of the study reach, the measured bed levels at the cross-sections are used to establish contour maps showing water depths below a pre-defined fixed low water level (bathymetric maps). Furthermore, maps of morphological changes are created by subtracting the bed levels from different surveys. This allows to analyse morphological features from the bathymetric maps and to oppose them directly to the morphological changes that occurred between two surveys. The water depths are achieved by subtracting the measured bed levels from the reference low water levels. This conversion allows to disregard the influence of the streamwise slope of the river. In this way, it is possible to apply a smaller colour range since the streamwise lowering of the river bed does not have to be considered. Large-scale morphological features including bars, pools, and crossings are represented by a sufficient number of cross-sectional measurements, so that contour maps can display these characteristics adequately. Small-scale features such as ripples or dunes cannot be visualised by this measuring and processing technique. *Fuller et al. (2003)* introduced a budgeting approach comparing DEM's (digital elevation model) that were created on the basis of different surveys providing a characterisation of spatial patterns of erosion and deposition. This methodology is denoted as DEM differencing. In this study, a cross-section-based approach failed to identify morphological differences. Therefore, it is crucial to consider the scale of the morphological structures of interest. When the data is based on cross-sectional measurements, differencing of contour maps is only meaningful for a sufficient number of profiles given for each morphological structure. *Brasington et al. (2000)* introduced DEM differencing on the basis of detailed topographic survey of the exposed and submerged areas of a river reach.

The Danube river reach is processed similarly. Since the cross-sectional frequency proves to be sufficiently large to represent relevant morphological structures such as bars, pools and crossings, DEM's are created for the bed level surveys of the years 1993, 1996, 2002(1), 2002(2), and 2003(2). The numbers in brackets indicate that more than one survey was performed in the given year. In 2002 and 2003, two surveys were performed per year, the numbers 1 and 2 indicate spring and autumn surveys, respectively. The computed water depths for each survey are interpolated onto a rectangular 10 m x 10 m grid using a kriging methodology. The water depths of all processed surveys are interpolated onto identically positioned grids. In this way, direct comparison of water depths of different surveys is possible at any grid point. The boundaries of the surveys are extracted from the first and last measured points in each cross-section. Closed polygon lines are generated serving as a boundary

for each survey. The software package *Surfer* is applied to generate the grids and to visualise the results. Contour maps using a colour band ranging from blue to brown colours are created, blue colours indicating large water depths corresponding to deep bed levels (e.g. scours on the opposite sides of the bars), while brown regions represent shallow water depths corresponding to higher bed levels (e.g. bar and crossing regions). Also negative values are present indicating regions where the bed levels lie above the reference low water level, that was fixed in 1996.

Maps of the bed changes are obtained by subtracting the grids of the individual surveys from each other. The water depths of the later survey are subtracted from the water depths of the earlier survey. Positive and negative numbers of the difference grids indicate deposition and erosion processes, respectively. This DEM differencing method allows to assess the bed changes in a period between two chosen periods in terms of erosion and deposition patterns. Maps that are appropriate for interpreting morphological changes can be drawn from the difference grids, giving insight into spatially and temporally varying morphological processes. The chosen colour band ranges from blue to red representing erosion and deposition processes, respectively. The difference maps are plotted inside the overlapping reach of both surveys that are compared to each other.

While the bathymetric and difference maps give a rather qualitative impression of the bed changes at the river reach, the morphology and morphodynamics are described quantitatively by computing appropriate parameters for different surveys. An important parameter to assess the averaged configuration and dynamics of a river is the mean bed level (or the mean water depth). Analysing mean bed levels of different surveys give insight into the bulk development of the Danube morphology, both in space and in time. Comparing the mean bed levels to the reference low water levels allows to analyse different morphological structures such as bar and crossing structures. Additionally, when comparing mean bed levels of different surveys, the width averaged dynamics of the Danube river bed are assessed. Apparently, the parameter is easily determined, but in fact, depending on the data situation, it is rather involved to define a significant and unambiguous definition of the mean bed level. The definition of mean bed levels differs in literature (*WRS (2000)*). Generally the mean water depth (water level minus bed level) can be computed by the ratio of the area that is bounded by the cross-sectional geometry and a reference line, such as the low water level (LWL) and the river width. Often, it is meaningful to limit the averaging procedure by fixed verticals defined on both sides of the river.

In this study, the low water level is not used as a basis for the computation of the mean bed levels. Individual surveys produce individual low water level widths depending on the intersection points of the cross-sectional profiles with the water level. As it is an objective of this study to compare mean bed levels of different surveys, it is important to define a reference width that is invariant to the individual surveys! Therefore, a characteristic width is determined that fulfils two criteria. (1) The width is independent of the survey and (2) the width covers most of the measured geometry. These considerations are also important for further processing of the data, such as the computation of bed volume changes. A characteristic width limiting averaging procedure is chosen based on the fixed width of the navigation channel (B_{nc}). The navigation channel is characterised by a virtually constant width of 120 m and it is situated at regions with large water depths within the main channel. Thus, the

measuring device always covered this reach regardless of the geometrical configuration of the cross-section or the given water levels. Additionally, an extended width is defined having a length of B_{ext} = 1.5 * B_{nc}. Based on the position of the navigation channel, the extended fixed width is positioned as to best fit into the measured profile. A schematic of a cross-section is shown in Figure 2.17 visualising the positions of the navigation channel and the extended width. Note, that the extended width completely covers the measured profile. This applies for all profiles in all surveys. The extended width B_{ext} covers approximately 75 % of the width of the low water levels and represents therefore a limited section of the morphological processes within the cross-sections. The mean bed level z_m is determined within the extended width (B_{ext}) by a coextensive approach, where A is the area below the cross-section that is limited by the verticals of the extended width and the datum line (0 m a.s.l.):

$$z_m = \frac{A}{1.5 \cdot B_{nc}}$$

(2.1)
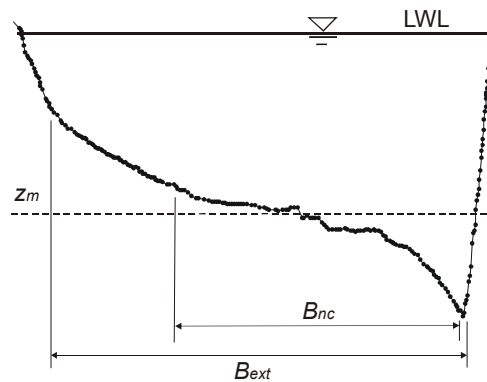
Figure 2.17: Schematic of cross-section for determining mean bed levels

On the basis of the mean bed levels, further parameters are determined. A characteristic parameter describing the compactness of the geometry of a cross-sectional profile is the width-to-depth ratio. The widths and the width-to-depth ratios are analysed for all cross-sectional profiles. The compactness of a profile allows to clearly distinguish between different morphological structures, since wide river reaches often coincide with small water depths and vice versa. The interplay of typical changes at crossings, bars and pools is analysed by the width-to-depth ratios of the cross-sections over time. The schematic of a cross-section shown in Figure 2.18 illustrates how the widths are determined. The width of a profile is defined as the distance of the intersection points of the water level and the river bed geometry representing the lateral extent of the water level. The parameters width and width-to depth ratio are computed for three discharges corresponding to the low, the mean, and the bankfull water level. In the case of emerging structures such as islands, the inner intersection points are used to determine the width. In this way only the width of the relevant main channel contributing to the discharge is considered. The water depths are computed from the differences of water levels and mean bed levels.
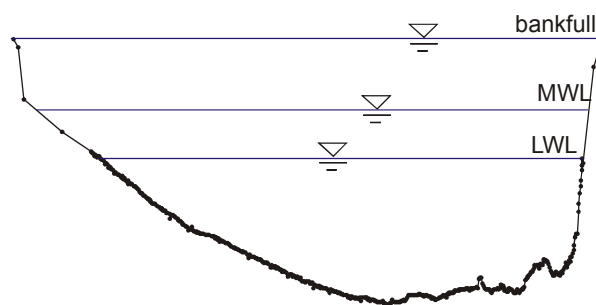
Figure 2.18: Schematic of cross-section for determining the water widths

Generally, cross-sectional geometries differ considerably depending on the morphological structure of a river. Profiles within bar regions are characterised by undercut banks and slip-off-slope banks in the vicinity of the scours and bars, respectively. Thus, typical cross-sectional profiles at the bars are characterised by pronounced asymmetrical shapes. On the other side, the cross-sectional profiles of the crossings are comparably more symmetrical (see Figure 2.40). Based on the study of *Savova (2002)*, a parameter is derived to quantify these features of the cross-sections. The symmetry of a profile is determined based on the thalweg position. Within a cross-section, the total cross-sectional area A_{tot} limited by the reference low water level is computed. A vertical line crossing the thalweg position is used to divide the total area into two sub-areas on the left and the right side of the thalweg position, denoted as A_{left} and A_{right} (see Figure 2.19). Adding the two sub-areas yields the total cross-sectional area: $A_{left} + A_{right} = A_{tot}$. The ratio A_{left}/A_{tot} is chosen for characterising the symmetry in a profile. To be in line with other parameter studies only the main channel is considered for these computations. A perfectly symmetrical profile would exhibit identical sizes of the two sub-areas and thus the symmetry parameter would give 0.5. On the range of values [0, 1], values greater 0.5 give asymmetrical profiles skewed to the right side, while values smaller 0.5 indicate profiles skewed to the left side.

Additionally to the symmetry computations as a function of the stream-km, a frequency analysis is performed using the first and last survey available, performed in the years 1993 and 2003(2), respectively. For this analysis, a different symmetry parameter is used computed by the ratio of the smaller sub-area and the total area, A_{small}/A_{tot}. Thus, this parameter has a range of values of [0, 0.5]. Perfect symmetry is achieved for a value of 0.5. A_{small}/A_{tot} does not provide directional information (left or right), so that it can be further processed with respect to its difference from the 0.5 line. Maximal asymmetry is given for the asymptote $A_{small}/A_{tot} \rightarrow 0$. The cumulative frequencies are then used as an integrative measure for the entire study reach to characterise the symmetrical configuration and the changes of the symmetry. Comparing the cumulative frequencies of different surveys allows to assess and quantify the morphodynamic variability in terms of the symmetry changes of the river reach.
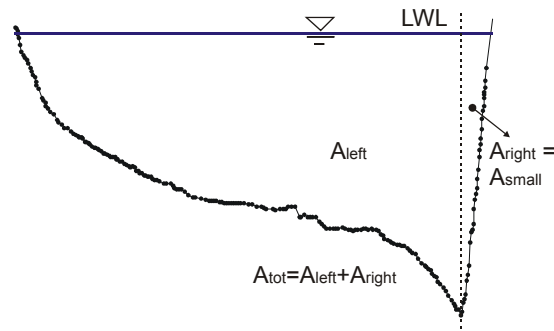
Figure 2.19: Schematic of cross-section for determining symmetry parameter

The symmetry parameters describing the cross-sectional shapes are supplemented by a parameter describing the lateral slopes of the cross-sections. The main objective of this analysis is to further quantify the characteristics of the bars in the Danube river. Information is also gathered on the lateral slopes of the banks. Thalweg positions within the cross-sections are used to distinguish between the left and the right side of the profiles. The cross-sectional profiles are processed within the range defined by the reference low water level (LWL). Two methods are developed to calculate the lateral slope values on the sides of the river, that are given as the mean and the median slope. The intersection points of the low water level and the cross-sectional profile are determined. The mean slope is then computed by the ratio of the height difference and the lateral distance of the intersection points and the thalweg points on both sides (see Figure 2.20). The median lateral slopes are also processed representing better the characteristic/dominant slope of a bar by "filtering out" the extreme slope gradients. In an intermediate processing step all cross-sections are interpolated onto an equidistant lateral raster. Based on the interpolated points, the lateral distribution of the cross-sectional slopes is computed and sorted allowing to determine the median slope from the distribution. Depending on the dominance of the lateral profile shape, the median slope can become both smaller and larger than the mean slope.
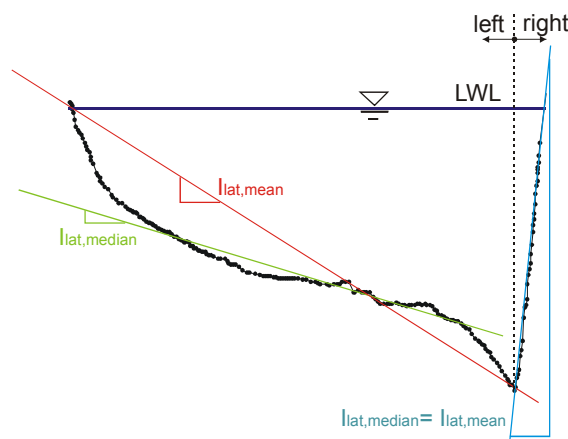
Figure 2.20: Schematic of cross-section for determining lateral slopes

Another parameter based on the mean bed levels is found when computing the bed volume changes. This parameter is used to estimate the sediment balance for a given river reach over a specific time period. Accumulation of the cross-sectional bed volume changes allows to quantify the total sediment deficit or sediment aggregation at a chosen river reach. The bed volume changes are

obtained by comparing cross-sectional profiles at identical positions measured at two different surveys. From the measurements of the bed levels, cross-sectional areas limited by characteristic widths are computed for the two surveys. Subtracting the cross-sectional areas gives the area change for each cross-section. The results can be both positive or negative area changes indicating averaged erosion or deposition processes over the widths of each cross-section. Assuming that the computed area changes at one cross-section are characteristic for the unobserved section between two cross-sections, the bed volume changes are obtained by multiplying the difference areas with the longitudinal cross-sectional distance given with 100 m. Cumulative bed volume changes are achieved when summing up the computed bed volume changes obtained for each cross-section.

The processing techniques allow to analyse temporal cross-sectional changes, giving information where and to which extent the river bed changes over time. These temporal changes are presumably related to the spatial variability of the river bed. An approach is introduced to investigate the temporal variations of the cross-sectional profile shapes with respect to spatial morphological changes. Spatial and temporal changes and the relationship of both changes are considered. The method of the analysis is to investigate the similarity of successive cross-sectional profile shapes (spatial similarity) and the similarity of a cross-sectional profile measured at different surveys (temporal similarity) and compare the computed similarities with each other. A similarity measure is derived by computing the root mean square error (*RMSE*) for two respective cross-sectional measurements. In a pre-processing step the two cross-sections are interpolated onto an equidistant raster in order to compare the measured profiles at identical lateral positions. Then, the error e_i at each individual position *i* within the cross-sectional profile is computed. The root mean square error *RMSE* is then defined as given in Table 2.10.

Table 2.10: Error and root mean square error used as measure for similarity

$e_i = \Delta h_{XS1,i} - \Delta h_{XS2,i}$	Error
$RMSE = \sqrt{\dfrac{1}{n}\sum e_i^2}$	Root mean square error

Analysing two different cross-sectional profiles, different either in time or in space, provides a similarity measure given as the *RMSE* value for each comparison. The more similar the two cross-sections, the smaller are differences in height and thus the errors e_i. As a consequence the mean error *RMSE* also becomes small. The cross-sectional data is processed below the reference low water level. The breakpoints of the profiles do not consistently follow the streamline of the river. Discontinuities of the longitudinal breakpoint lines with respect to the streamlines of the river require appropriate data pre-processing preceding the spatial similarity computations. A module is implemented performing lateral, horizontal transformations of the cross-sectional profiles. The optimum transformation is found when the minimum *RMSE* value is achieved assuming that this represents best the spatial similarity of the two cross-sections. The transformation procedure is demonstrated at five cross-sections in Figure 2.46. Preceding transformation computations are not necessary for the temporal *RMSE* computations, as identical break points are used here.

Different approaches in terms of the characteristic widths are chosen to compute the bed volume changes. In Figure 2.21, the different characteristic widths used for bed volume computations are shown. In approach 1, the characteristic width is defined as the commonly measured length within a cross-section that is measured by both surveys. This approach allows to use a maximum of the available bed level information to derive the averaged bed volume changes. Depending on a variety of factors, such as the cross-sectional geometry, the water levels on the days of the measurement campaigns, or the chosen boat, the common widths may vary significantly, both spatially and temporally. Therefore processing based on the common widths may introduce bias errors. In approach 2, the navigation channel is used as the reference width. As shown in Figure 2.21, the width of the navigation channel B_{nc} covers only parts of the cross-sectional geometry. Using the navigation channel as characteristic width implies a cut-off of relevant cross-sectional information in the shallow river reaches. Morphological changes occurring in these regions are then ignored. Approach 3 represents a combination of the two approaches discussed above. The bed volume changes are computed within a fixed reference width defined as B_{ext} = 1.5 B_{nc} ($\approx$ 180 m). Its position is determined by the position of the navigation channel with respect to the cross-sectional profile delimited by the left and right breakpoints. Thus, the position of the extended width is chosen as to best fit into the measured cross-sectional profiles. The extended width B_{ext} is the maximum width that is covered by all surveys.
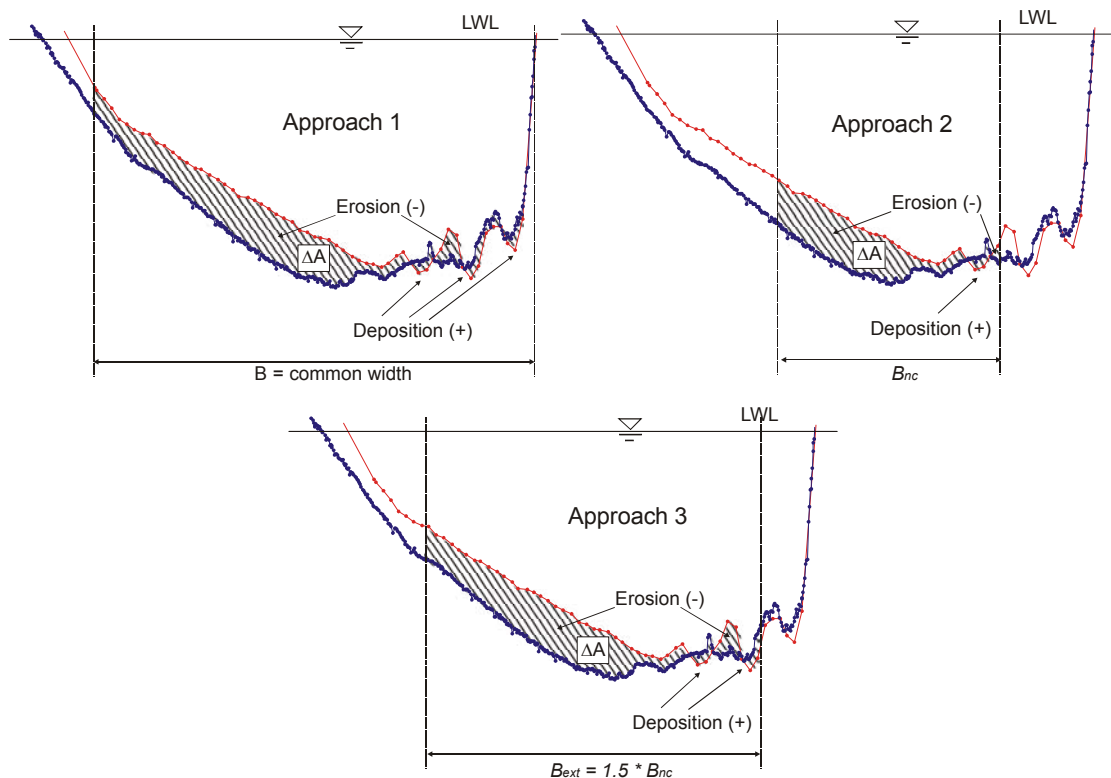
Figure 2.21: Different characteristic widths used for the computation of bed volume changes

A tentative analysis is performed to investigate the relationship of morphological changes and the hydrologic variations of the Danube river. This analysis gives information on the influence of hydrological events on the changes of the morphology. The bed level surveys are performed in half

year to one year intervals, so that bed changes are related to the water volumes over these time periods.

The net bed changes are achieved by subtracting the regular grain feeding measures performed by the operator of the hydropower station from the computed total volume changes based on the extended navigation channel (B_{ext}). The water volumes are computed from the flow hydrographs that are integrated over the survey periods (Table 2.9). Two approaches are applied. In the first approach, the total water volume passing the Danube reach between two surveys is computed, for the second approach, only the water volume exceeding a threshold value of Q_{cr} = 2000 m³/s is determined. The latter approach is based on the assumption that sediment transport is initiated when a critical shear stress is exceeded. From literature, it is given that initial sediment transport at the Danube river is initiated for an excess of approximately 2000 m³/s (Table 2.4). A relationship can be given when considering the fact, that the hydropower station Freudenau at the upstream end of the study reach serves as a virtually complete barrier to the passage of sediments. Therefore budgeting is justified, giving the relationship that high discharges produce high erosion rates.

2.3   Results

In this Chapter the results of the processed cross-sectional bed level surveys are presented. Parameters are defined in Chapter 2.2.2 to describe and quantify the morphological development of the 40 km long Danube river reach east of Vienna to the Austrian-Slovakian border. Both the spatial and the temporal development of the fluvial morphology are determined. Starting from bulk and averaged parameters such as the mean bed levels, water depths, and thalweg configuration, the coarse development of morphological structures is discussed. Based on these results, more specific and detailed parameters are given with respect to the particular morphological situation at this river reach that is characterised over a significant length by pronounced alternate bar structures. Typical bar geometries, the cross-sectional symmetry of morphological structures, the lateral slopes of the bars and the banks are analysed both with respect to their spatial and temporal development. Spatial development is related to temporal development by comparing cross-sectional shapes by means of a similarity measure. Assessing the net sediment balance over a period of ten years using all available bed level surveys gives information on the volumetric bed changes. The relationship of the bed changes and the water volumes for the periods between the bed level surveys is finally evaluated.

2.3.1   Morphological classification

In order to achieve an overview where the morphology of the Danube river reach is positioned with respect to other rivers, the classification scheme of *Yalin & da Silva (2001)* is applied here. All available data based on the 2002(2) survey are used to derive averaged values for B/h_m and h_m/d_m. The results are plotted for three discharges in Figure 2.22. The results show that all analysed water levels (low discharge (*LWL*), mean discharge (*MWL*), and bankfull discharge (*bankfull*)) of the Danube river lie within the common reach of alternate bars, meanders, and regime channels. This empirical classification by *Yalin & da Silva (2001)* fits well the observed configuration of the Danube river as shown in Figure 2.23 to Figure 2.26.

The Danube river's B/h_m ratio decreases with rising water stages. This phenomenon is characteristic for wide rivers with large width-to-depth ratios. Then, a large width is already achieved for small discharges. Within the bankfull flow, higher discharges produce minor increase of the width. This results in comparably stronger depth than width enhancement for rising discharges. Due to limited data availability, overflowing discharges are not analysed. Presumably the trend would reverse for overflowing discharges. From bankfull to over-bankfull flow, the width increases rapidly with only slight changes of the water depth.
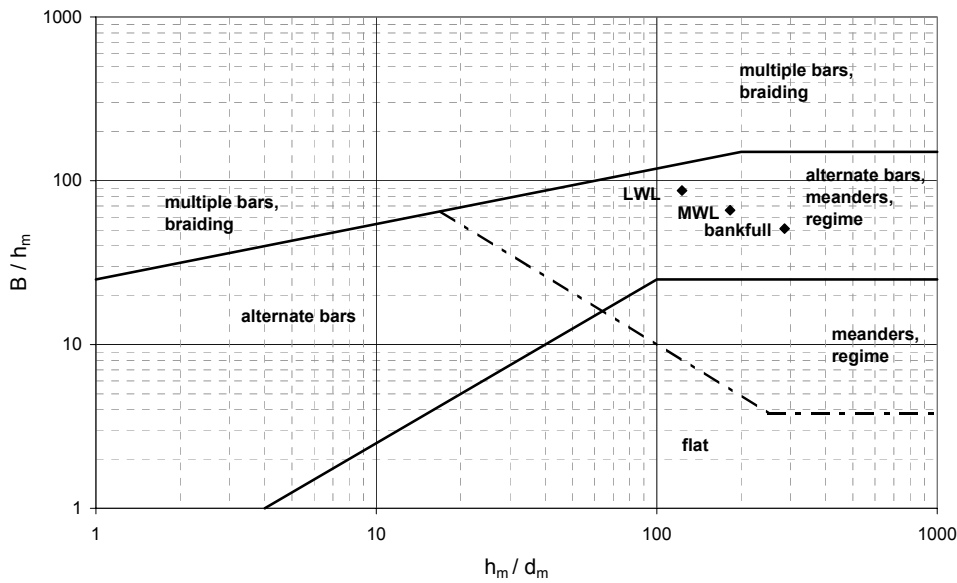
Figure 2.22: Morphological classification after *Yalin & da Silva (2001)*

2.3.2   Erosion-deposition patterns

Cross-sectional bed level surveys are used to generate contour maps of water depths (bathymetric maps) and bed changes. Figure 2.23 to Figure 2.26 show water depths and bed changes. Here, a focus is drawn on the long-term development of the river reach. For presentation purposes, the reach is subdivided into four units each having a length of 10 km. The water flows from the left to the right. According to the convention applied at the Danube river, the given stream-km's are assigned against flow direction originating at the river mouth of the Danube river at the Black Sea. The maps indicated by letter (a) show the water depths below the reference low water level based on the 2002(2) survey visualising different morphological structures at the Danube river reach.

Within the upper 20 km, from km 1920 to 1900, a distinct alternate bar configuration is seen. The bars alternate from one side of the channel to the other side over a generally stretched course of the river. From km 1905 to 1903, the course of the river shows different planform characteristics. In this region, a slight river bend can be observed. As observed in most alluvial channels, a developed bar is present at the inner bend and a scour at the outer bend. Different from alternate bars, bars in river bends show stationary character and are denoted as point bars. The transitional reaches from one bar to another are characterised by comparably shallow water depths. These reaches are denoted as crossings. For navigational purposes, the crossing regions often exhibit hot spots in terms of critical water depths. To enable undisturbed navigation most of the crossings are characterised by regular

dredging measures. An overview of dredging measures performed over the study period from 1993 to 2003 is given in Table 2.5 and Figure 2.16. On the opposite side of the bars, scours are given with large water depths. They often reach their maximum water depths on the opposite sides of the second half of the bars. At the lower half of the river reach alternate bar configurations are not developed. Here, some of the morphological parameters, such as the maximum river width or the mean bed slope in flow direction, are similar to the 20 km reach upstream but the intensity of river training measures, such as the installation of groynes and spur dykes (see Figure 2.15) increases considerably in this region so that the natural development of the river is considerably disturbed here. From km 1900 to km 1890, the bed level variability is significantly reduced. The river bed is comparably more uniform represented by steep banks and minor variations of the main channel. Further downstream, from km 1890 to km 1880, the curvature of the river course increases. As a consequence, mostly point bar structures develop, characterised by stationary bar configurations at the inner bends of the river. Scours are located on the opposite sides of the point bars and crossings are located in between the bars.

When subtracting the grids of two surveys from each other, a difference grid (DEM differencing) is obtained which is used to display erosion and deposition patterns. The maps labelled (d) show the long-term development of the Danube river bed for a period of ten years from 1993 to 2003(2). Generally the erosion regions (blue colours) dominate the deposition regions (red colours) clearly. Thus, the designated general erosion trend (e.g. *Kresser (1988)*, *Bors (1992)*, *Stiefelmeyer (2001)*) is reflected in the difference maps. However, the maps show that the trend is not homogeneously distributed over the entire study reach. Both significant erosion processes and significant deposition processes are present over the ten year study period. The characteristics of the bed changes vary significantly over the 40 km reach and are discussed separately for this reason. Within the upper 10 km, from km 1920 to 1910, both strong erosion and deposition patterns are available. A considerable fraction of the bed changes exhibit large absolute values ranging from 0.8 to 5 m. When comparing the bed changes to the morphological structures as shown in maps (a), a distinct process within the bar region becomes evident. Within the period of ten years, significant deposition processes occur in the scour regions while the bar regions exhibit considerable erosion processes. Obviously, the cross-sectional shape of the bars is substantially transformed from an originally strongly asymmetrical shape towards a more uniform shape. This is discussed in detail in Chapter 2.3.7. Moreover, regular dredging measures occurred at the river reach for maintaining the navigation channel (see Figure 2.16). Also, the crossings are characterised by distinct bed changes. Here, erosion processes with less intensity than at the bars are found. Within the upper 10 km reach two relevant locations are subject to regular dredgings, found at km 1917 and km 1914. The material is partially re-fed into the main channel approximately 1 km downstream. The accuracy of the exact dredging positions is limited. In the long-term development (10 years), the effect of the dredging and re-feeding measures are superimposed by the before mentioned bed change processes. The tendency towards unified cross-sectional profiles within the bar regions are a combination of human interferences and natural processes. These observations are in line with decay processes of the alternate bar dimensions at the Salzach river at a 10 km long reach (*WRS (2000)*). Here, distinct alternate bars were observed in the

1950's, that substantially decayed in the 1970's, and that were finally almost non-detectable in the 1990's.

At the Danube river, the succeeding 20 km downstream, from km 1910 to 1890, are characterised by a significant reduced spatial variability of bed changes. Here, the erosion processes clearly dominate over the deposition processes. Although partly still in the region of alternate bars, the processes of the decay of distinct bar geometries cannot be observed here. In parts of the alternate bars the trend is opposed compared to the upper 10 km reach. Almost the whole 20 km reach is characterised by erosion processes that differ in their intensity. The last 10 km, from km 1890 to 1880, are characterised by an increased spatial variability of erosion and deposition patterns similar to the upper 20 km reach. The Danube river here also shows erosion processes in most parts. In this reach, the strongest erosion is found at approximately km 1884. These changes are attributed to the most intensive dredging measures here (see Figure 2.16). Parts of the dredged material is re-fed into the main channel at km 1882. The deposition processes observed from km 1882 to km 1881 can be partly attributed to these measures.

Maps (b) and (c) represent the morphological changes from 1993 to 1996 and 1996 to 2003(2), respectively. The temporal split is motivated by the installation of the hydropower station Freudenau in 1996 (partial operational reservoir level in March 1996, maximum operational reservoir level in November 1997) that is situated at the upstream end of the study reach and has a substantial impact on the morphological development of the river reach. Before 1996, local filling measures were performed at four scours from km 1916.3 to 1910.0 (see Table 2.8). In the years 1994 and 1995, these measures were implemented to protect the river bed at these hot spots from further erosion. From 1996 on, regular grain feeding measures started (see Table 2.6 and Table 2.7)) to compensate for the sediment deficit induced by the retaining effect of the dam. The feeding measures were performed at the upper 10 km reach with special intensity in the regions from km 1919 to 1918.5, km 1918 to 1917, around km 1916, and km 1913 to 1912. Exact positions of the feedings are not available. Presumably, deep reaches were preferentially supplied.

From km 1920 to km 1910, the maps (b) and (c) show that both periods contribute to the above mentioned "decaying" processes of the alternate bars at different positions. While the decaying of the alternate bars for the later period is observed mainly from km 1920 to 1915, the earlier period shows damping at alternate bar configurations from km 1915 to 1910. The regions of feedings are reflected in map (c) by distinct deposition reaches that are not available or only to a smaller degree at map (b). The processes of the earlier period are partly ascribed to the artificial filling measures. The early bed level surveys (map (b)) clearly reflect the scour filling measures.

The overall magnitudes of erosion and deposition heights within the upper 10 km are similar. At the succeeding sub-reach, from km 1910 to km 1890, erosion processes are dominating for both periods. Areas of strong erosion are present at different positions for both periods that contribute to the total morphological changes in the long-term. Strong erosion processes from km 1910 to km 1909 are mainly caused by the second period. At some locations, a trend of erosion or deposition is reversed to the opposite trend, such as the erosion processes at around km 1904 and at around km 1899 that are reversed into a deposition process at the latter period. At km 1890 to 1880 erosion processes can be

observed at the gorge portion downstream km 1884 for both periods. These effects accumulate to a distinct erosion area here (that is also influenced by dredging measures as discussed above). Strong erosion processes correspond to the increased flow velocities inducing an increased shear stress. The deposition of the scour at the outer bend from km 1882 to 1881 continuously develops in both periods.
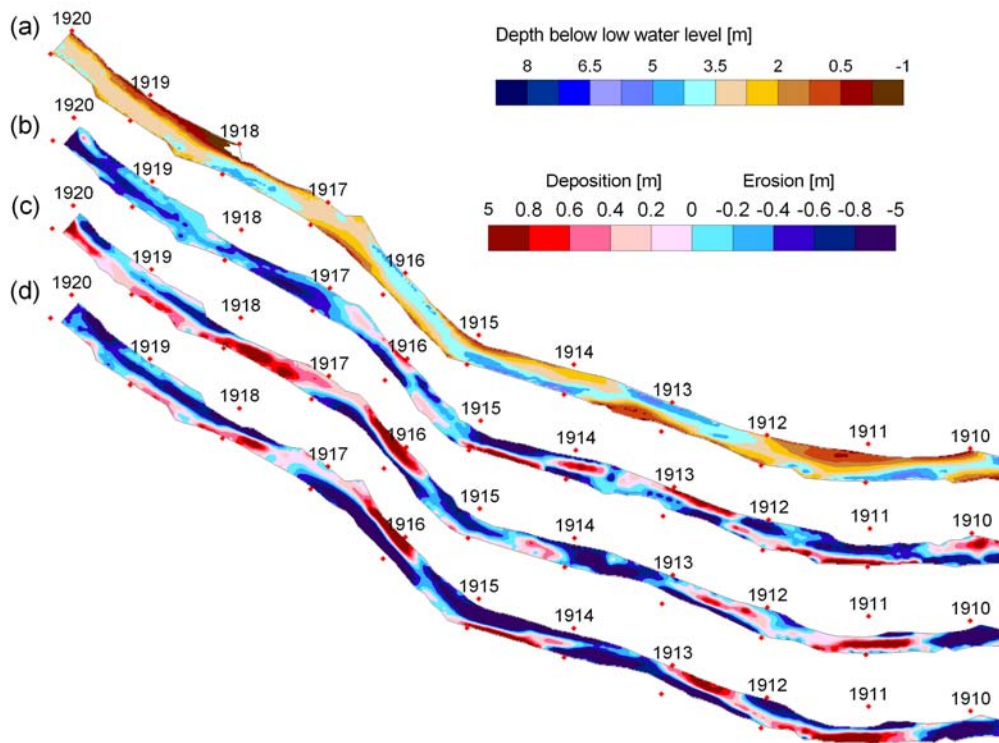
Figure 2.23: Water depths and bed changes from km 1920 to 1910: (a) water depths 2002(2), (b) bed changes 1993-1996, (c) bed changes 1996-2003(2), (d) bed changes 1993-2003(2)
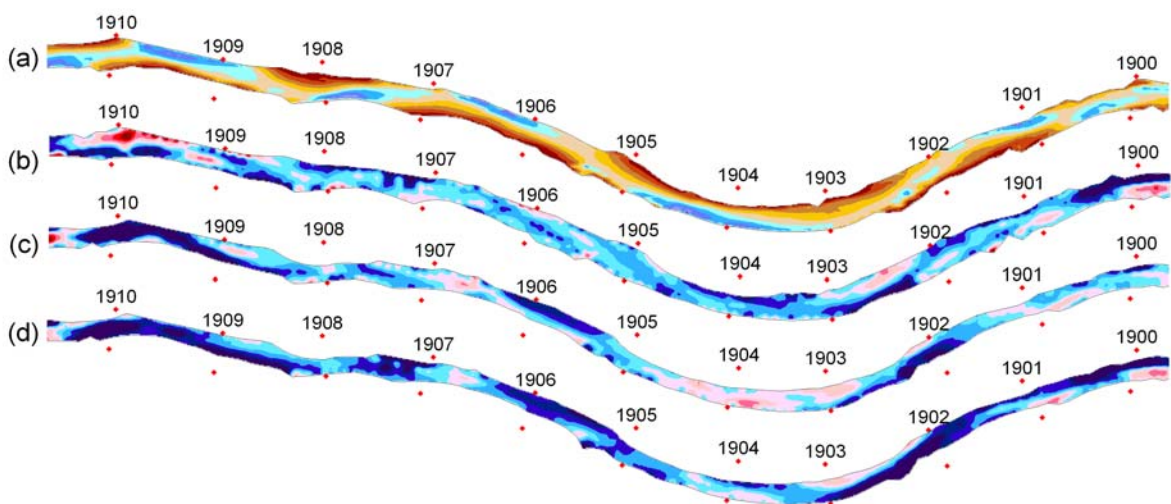
Figure 2.24: Water depths and bed changes from km 1910 to 1900: (a) water depths 2002(2), (b) bed changes 1993-1996, (c) bed changes 1996-2003(2), (d) bed changes 1993-2003(2)
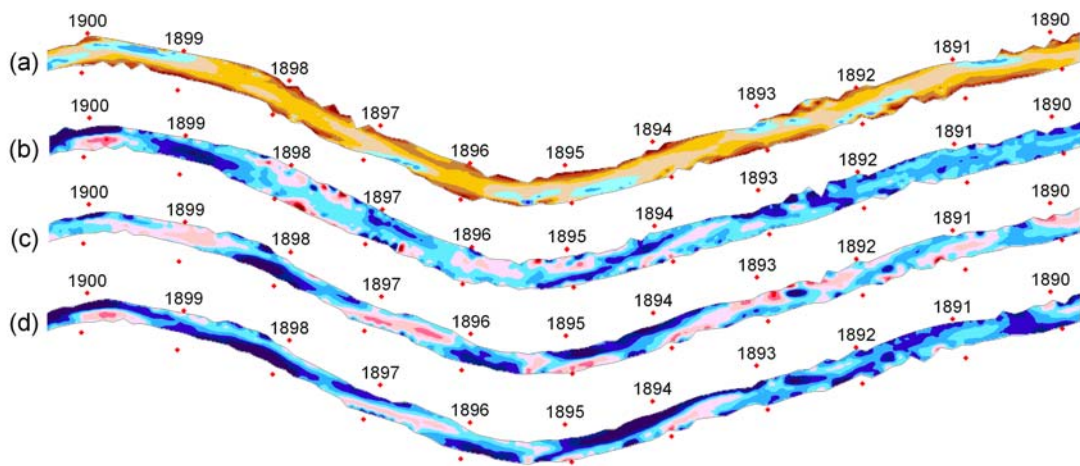
Figure 2.25: Water depths and bed changes from km 1900 to 1890: (a) water depths 2002(2), (b) bed changes 1993-1996, (c) bed changes 1996-2003(2), (d) bed changes 1993-2003(2)
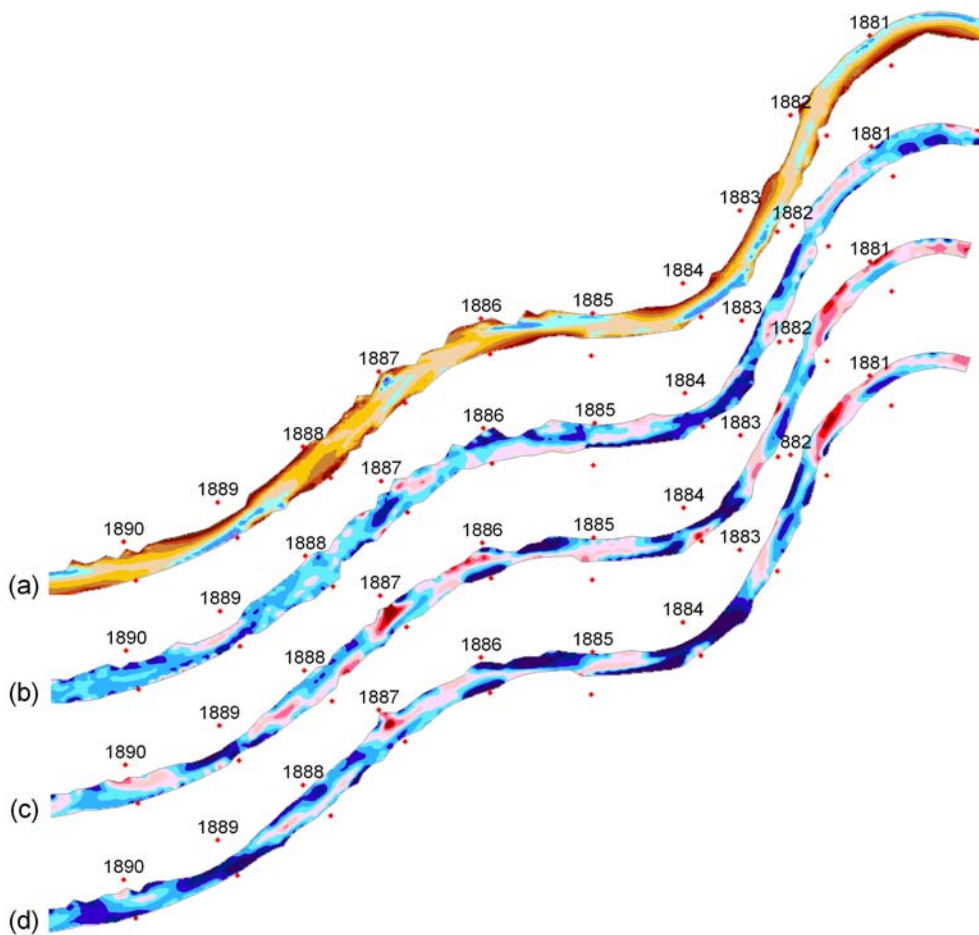
Figure 2.26: Water depths and bed changes from km 1890 to 1880: (a) water depths 2002(2), (b) bed changes 1993-1996, (c) bed changes 1996-2003(2), (d) bed changes 1993-2003(2)

Additionally to the long-term development, bed level surveys are processed for a short-term period in 2002, when a 100 year flood passed the Danube river. Pre and post flood surveys, 2002(1) and 2002(2), are analysed to investigate the influence of the 100 year flood on the bed level changes. The results are shown in Figure 2.27 to Figure 2.30. Map (a) shows the water depths before, and map (b) after the flood event. The morphological changes are visualised by the difference map (c). The positions and shapes of the morphological structures (bars, crossings, scours) are subject to minor changes induced by the passage of the flood event. The results also indicate, that stronger bed change heights occur at the alternate bar reach within the upper 20 km than at the downstream 20 km reach. These general short-term results are in line with the long-term development. Strong local changes in the range ± 1 m occur preferentially at the upper half of the river reach. Local discontinuities, such as holes at km 1902.3 or 1887.0 are partially filled up during the flood event. The overall deposition processes seem to dominate the erosion processes. This is partly explained by intensive grain feeding measures at around km 1919.5, 1917.5, and 1912.5. The deposition phenomenon is further discussed in Chapter 2.3.10. Three bars are subject to slight dynamical development, that is best observed when analysing the difference maps. The bars from km 1914 to 1912.5, from 1912 to 1910, and from 1907.5 to 1905.5 are characterised by erosion in the upper half of the bars and deposition in the second half. These sediment re-distributions might indicate small bar propagations induced by the 100 year flood. However, the overall morphological configuration remains unchanged.
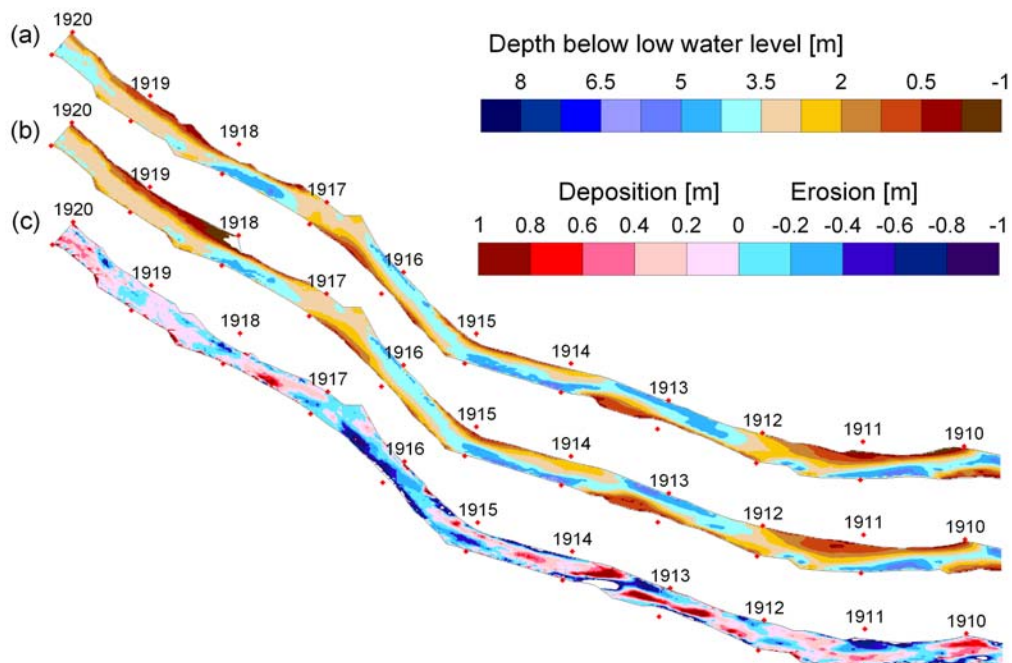
Figure 2.27: Water depths and bed changes from km 1920 to 1910: (a) water depths 2002(1), (b) water depths 2002(2), (c) bed changes 2002(1)-2002(2)
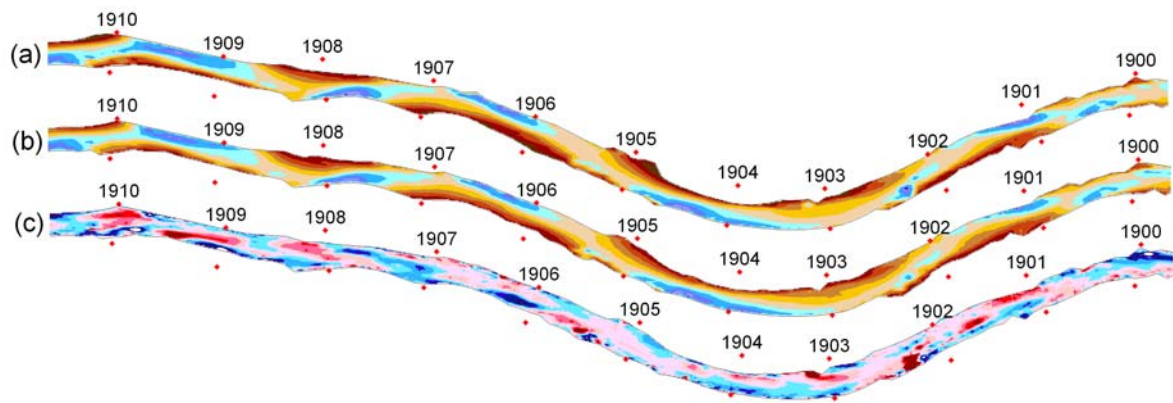
Figure 2.28: Water depths and bed changes from km 1910 to 1900: (a) water depths 2002(1), (b) water depths 2002(2), (c) bed changes 2002(1)-2002(2)
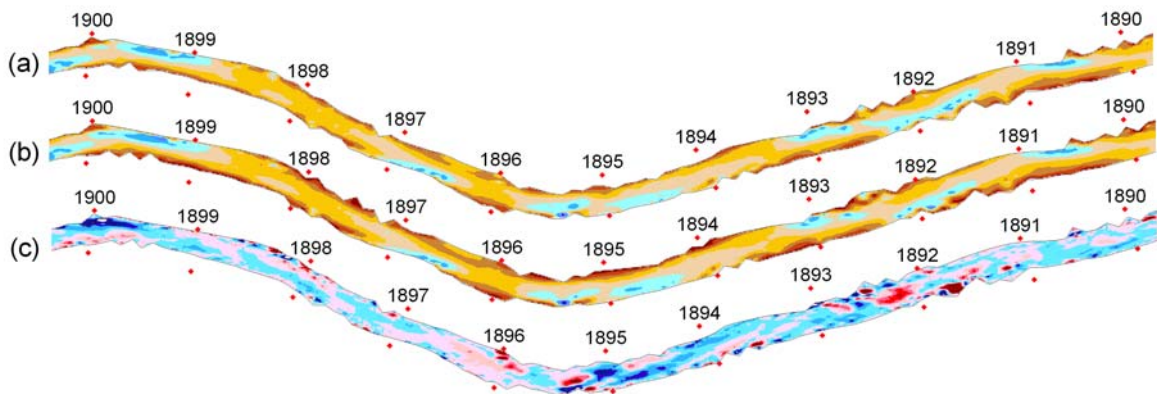
Figure 2.29: Water depths and bed changes from km 1900 to 1890: (a) water depths 2002(1), (b) water depths 2002(2), (c) bed changes 2002(1)-2002(2)
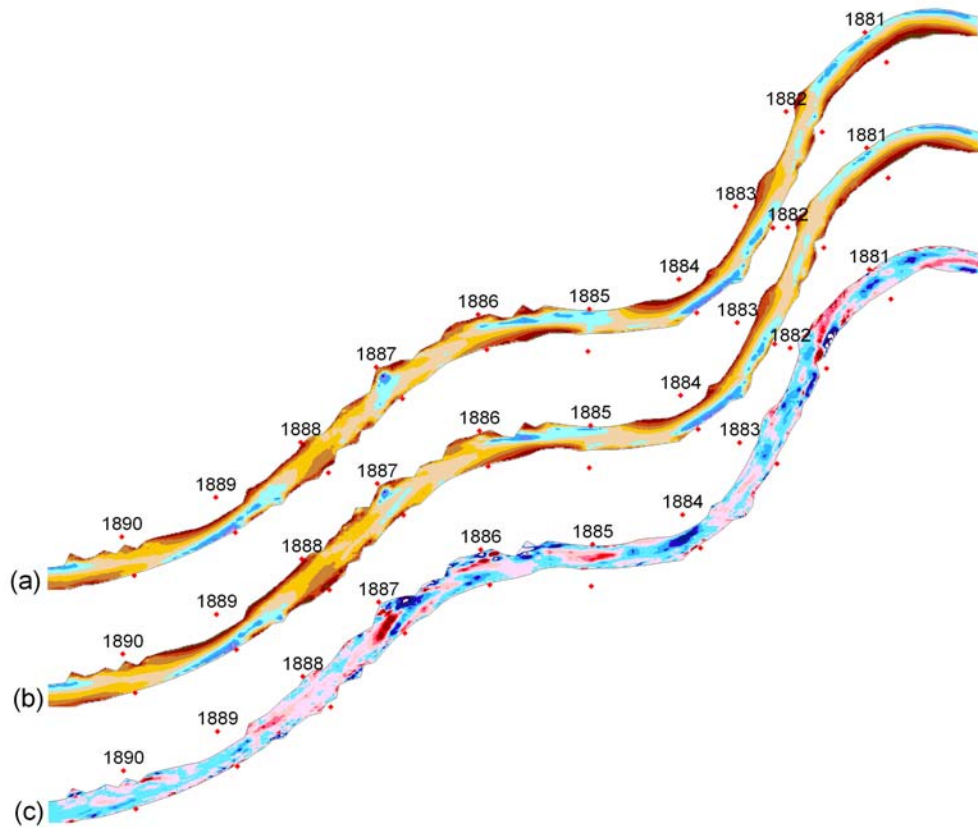
Figure 2.30: Water depths and bed changes from km 1890 to 1880: (a) water depths 2002(1), (b) water depths 2002(2), (c) bed changes 2002(1)-2002(2)

2.3.3 Mean bed levels and water depths

Based on the extended width of the navigation channel B_{ext} =1.5 B_{nc} (see Chapter 2.2.2), mean bed levels are computed for the river reach for the surveys 1993, 1996, 2002(1), 2002(2), and 2003(2). Figure 2.31 and Figure 2.32 show the long-term development of the mean bed levels and mean water depths, respectively. Over the study period of ten years, distinct bed level reductions appear induced by erosion processes. Generally the reductions in shallow river reaches are stronger than in the deep areas.

Averaged over the whole study reach, the mean bed levels decrease 19.5, 6.0, and 25.5 cm in the periods 1993-1996, 1996-2003(2), and 1993-2003(2), respectively. From Table 2.9, the times of the periods 1993-1996, 1996-2003(2), and 1993-2003(2) are calculated as 3.1, 7.3, and 10.5 years, respectively. From these periods, average annual erosion rates are computed as 6.3, 0.8, and 2.4 cm/year. A substantial decline of the erosion rates after 1996 is in line with regular grain feeding measures that commenced in this year.

Comparing the longitudinal development of the mean bed levels in 1993, 1996, and 2003(2) shows that a majority of the crossings is characterised by severe erosion processes over the ten year period (Figure 2.31). In particular, the crossings Schwechatmündung (km 1913.7), Kuhstand (km 1910), Orth (km 1902), Regelsbrunn (km 1898), Rote Werd (km 1896), Treuschütt (km 1888), and Hainburg (km 1884) (see Table 2.5) are facing significant erosion processes over the study period.

Only the crossings Buchenau (km 1912) and Fischamend (km 1908) remain nearly unchanged. In these two crossings only minor dredging activities are necessary. Thus, the crossings with intensive erosion tendencies are characterised by considerable dredging activities, so that the observed bed level reductions of the crossings represent a combination of natural processes and local river training measures. The water depths below the reference water level are shown in Figure 2.32. Two of the crossings, Kuhstand (km 1910) and Hainburg (km 1884) exhibit water depths smaller than 2 m based on the early surveys in 1993 and 1996. Survey 2003(2) shows, that none of the crossings fall below water depths of 2 m. In Chapter 2.3.2, it is shown that the bed development in the bar regions is characterised by an distinct process in the long-term development: Deposition processes in the scours coincide with erosion processes of the bars. When computing an averaged value over the cross-section such as the mean bed level, these processes cannot be quantified. Therefore the parameter "mean bed level" is not adequate to describe these processes. Thus, different parameters considering specific processes within the bar regions are developed.

In Figure 2.33, the seven year development of the low water levels is shown. In *Gutknecht & Fischer-Antze (2005)*, an approach is introduced to compare low water levels originating from different surveys. Since two water level surveys are generally not measured for identical hydrological conditions, i.e. identical discharges, the comparability needs to be developed using appropriate methods. The method is based on generating virtual rating curves for each cross-section by applying a one dimensional numerical model. Then, the discharge variations during the low water level surveys are considered and it is possible to derive water levels for identical constant discharges for both surveys.

The results show that the differences of the low water level fixations in 1996 and 2003 are mostly negative. The changes are obviously induced by erosion processes of the river bed over the seven year period. However, water level changes show different characteristics than the bed level changes. The water level changes are divided into three characteristic regions. While only minor water level reductions occur at the upstream end of the study reach (km 1920), the region from km 1920 to 1910 is characterised by severe water level reductions with a maximum of more than 40 cm. The succeeding reach, from km 1910 to 1892, is characterised by constant reductions of approximately 20 cm followed by smaller water level reductions over the last 12 km of the Danube reach. On average, the water levels lower 19.5 cm over the seven year period. Compared to the mean erosion of the river bed from 1996 to 2003(2), where 7.3 cm are measured, the water levels decrease significantly more than the bed levels on average. An explanation for this discrepancy can be given when considering the effect of the strong (partly man-made) erosion processes at the crossings on the water levels. As the crossings are regions of high bed levels by definition, a decrease of these crossings has a severe impact on the water levels from a hydraulical point of view. The crossings have a backwater effect on the water levels. Thus, they influence the water levels up to a considerable distance upstream the crossing. Strong gradients of the water level differences coincide well with the lowering of some crossings. The lowering of the crossing at Hainburg (km 1884) for example cause the water levels to sink more than 10 cm. Lowering crossings (i.e. reducing the backwater effect) lead to significant water level reductions in upstream direction. Further upstream, the erosion of the crossings at Buchenau (km 1910) and Schwechatmündung (km 1913.7) lead to further decrease of

the water levels. Upstream km 1915, the crossings are characterised by only minor erosion processes leading to a maintaining backwater effect. Thus, the water level differences increase. The results show that crossings are sensitive morphological structures. Any changes (natural or manmade) have severe consequences on the fluvial system.
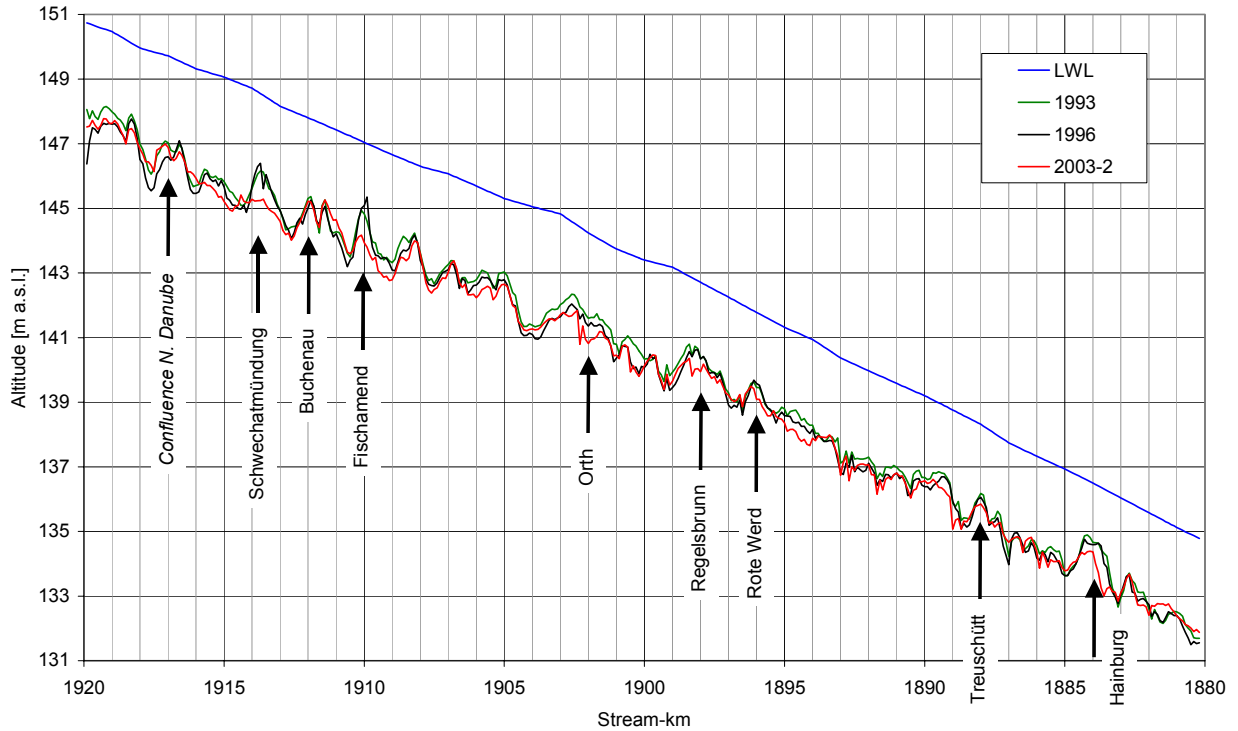
Figure 2.31: Mean bed levels 1993, 1996, 2003(2)
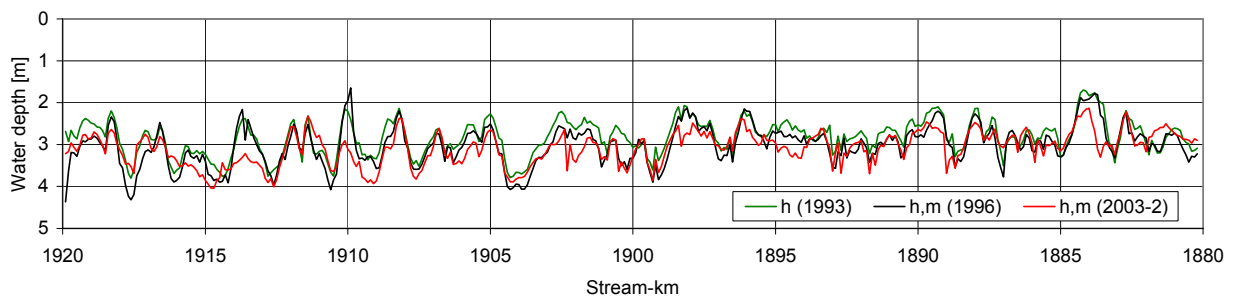
Figure 2.32: Mean water depths 1993, 1996, 2003(2)
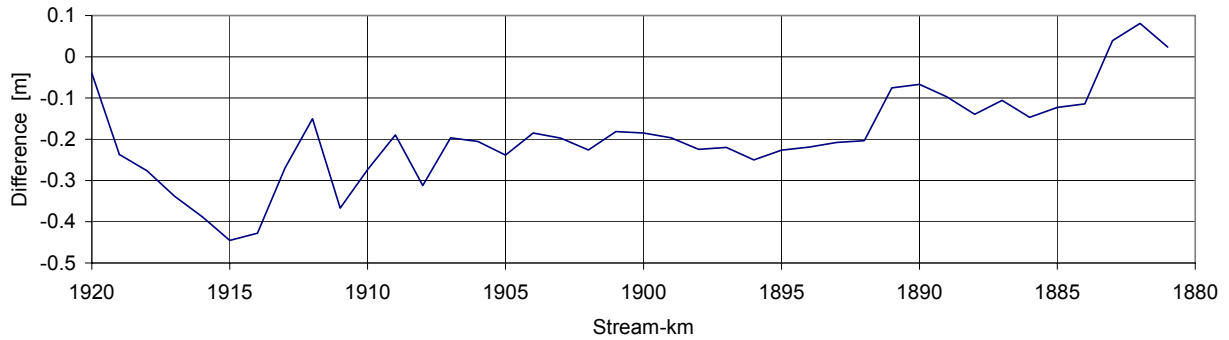
Figure 2.33: Low water levels 1996 and 2003(2)

Further analyses are performed for the short-term development within the scope of the flood events in 2002. The river bed surveys 2002(1) and 2002(2) are processed analogously to the long-term analysis. The results are shown in Figure 2.34 and Figure 2.35. Generally small changes of the mean river bed features occur between the two surveys. Locally, some systematic changes can be observed. Water depths achieving values close to 4 m in the survey 2002(1), generally reduce as a consequence of the flood event. These pool regions are generally characterised by large water depths. Significant depth reductions are observed at km 1917.5, 1912.6, 1909.4, 1902.3, 1901.0, 1887.1, and 1885.0. Apparently, the flood event locally causes a smoothing of the steep pools by filling up the discontinuities (holes). An analysis of the bed changes within the cross-sections show, that the deposition processes occur predominantly around the lower regions of the profile close to the thalweg.

The crossing Hainburg at km 1884 experiences water depths smaller than 2 m. From Table 2.5 and Figure 2.16 it can be inferred that this crossing is characterised by the most intensive river training measures. Dredging activities have to be performed here almost once a year. All other crossings show water depths of more than 2 m and remain virtually unchanged in terms of their mean bed levels.
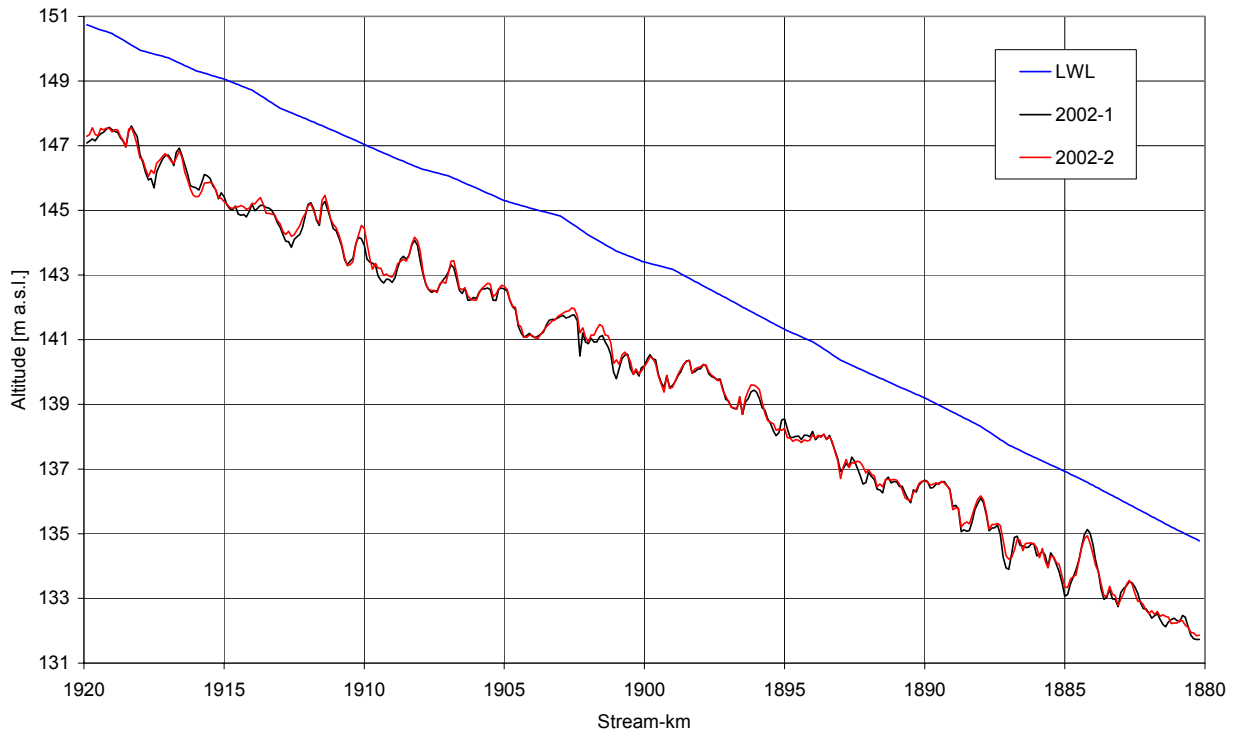
Figure 2.34: Mean bed levels 2002(1) and 2002(2)
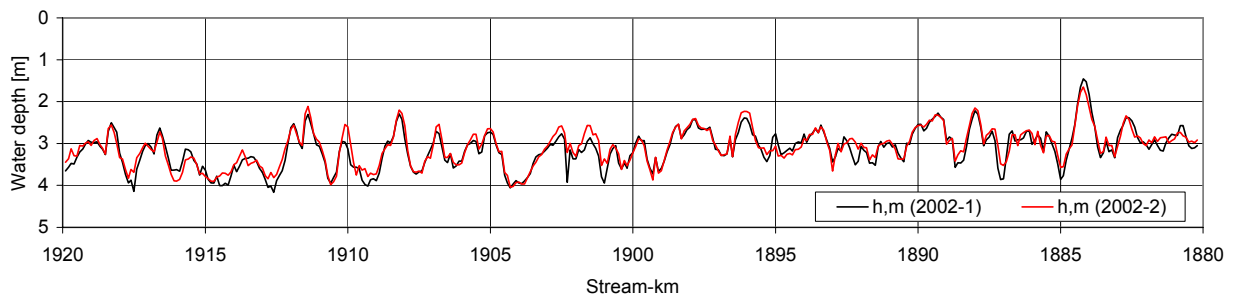
Figure 2.35: Mean water depths 2002(1) and 2002(2)

2.3.4 Thalweg

The cross-sectional bed-level surveys are processed with respect to the lowest position in each cross-section, denoted as thalweg. The positions of the thalweg as a function of the longitudinal distance give insight into the alignment and the dynamics of the morphological structures. For the same surveys as shown in Chapter 2.3.3, 1993, 1996, 2002(1), 2002(2), and 2003(2), the thalweg development is plotted. Figure 2.36 and Figure 2.37 show the long- and short-term development of the thalweg positions, respectively.

Within the upper 20 km of the Danube reach the spatial thalweg development shows a regular periodicity. The deepest point is not positioned in the centre of the cross-section represented by regular symmetrical profiles, but on its sides giving rise to a distinct asymmetrical cross-sectional configuration within this reach. The asymmetry of the cross-sectional profiles is further parameterised

in Chapter 2.3.7. The periodic changes of the thalweg from one bank to another are the consequences of developed alternate bar structures. The position plot of the thalweg is further used to derive characteristic parameters of the bars, such as the wave length. Further downstream, from km 1900 to 1887, the thalweg shows stronger fluctuations, the periodicity is damped. As shown in Figure 2.23 to Figure 2.26, this reach is not characterised by alternate bars. Here, intensive installations of groynes, inhibit the natural development of alternate bar structures. The lowest reach, from km 1887 to km 1880 is characterised by point bar structures. Thus, here the thalweg development shows longer periods induced by the given curvature of the river.

The thalweg dynamics can be determined when analysing the thalweg positions from different surveys. The results show that the upper 20 km with alternate bar structures are characterised by minor thalweg dynamics. From this analysis, it can be concluded that the alternate bars practically do not migrate over the study period of ten years. Unlike in literature, where alternate bars move several metres per day (*Knaapen (2001)*), which would suggest a bar migration in the order of a kilometre per year, the bars at this Danube reach appear to be virtually immobile. The results of the Danube reach are in line with *Zarn (2005)* where analysis of the dynamics of alternate bars in mountainous rivers showed that the bars remained practically immobile. The retaining effects of vegetational elements, fixations by river training measures, and slight curvature effects, that may represent a transitional status for the Danube bars between alternate and point bars, are inhibiting factors for the mobility of the bars. The succeeding reach, from km 1900 to approx. km 1886 shows more thalweg dynamics. Here, the cross-sectional geometry is more uniform in some regions with steep banks on both sides and a flat river bed at the main channel. Therefore, the thalweg position can have an arbitrary character, and thus change significantly from one survey to another. The considerations concerning spatial thalweg development and thalweg dynamics are valid for both the long-term and short-term analysis. Also in the short-term (Figure 2.37), the dynamics within the alternate bar and the point bar reach are negligible, while the dynamics increase for the river reach, where uniform cross-sections are present. The positions of the bars remain virtually constant even for the 100 year flood passing the Danube river in 2002. A substantially stable river bed configuration with respect to the positions of the morphological structures can be inferred from the thalweg analyses.
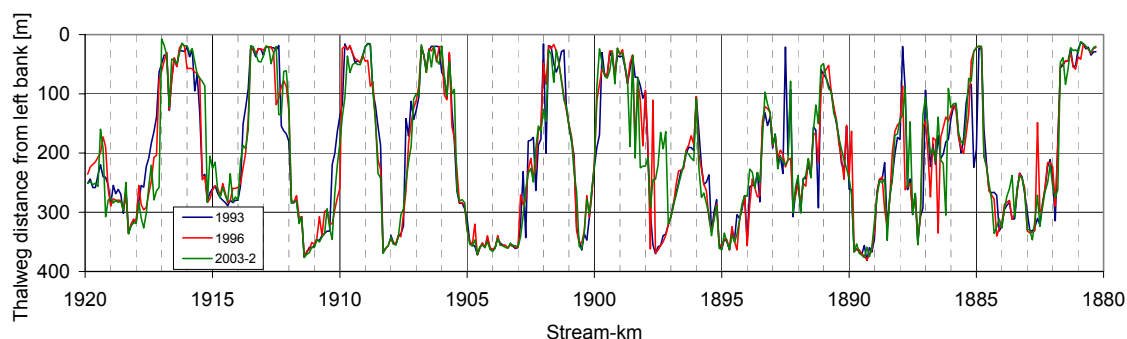
Figure 2.36: Thalweg positions 1993, 1996, 2003(2)
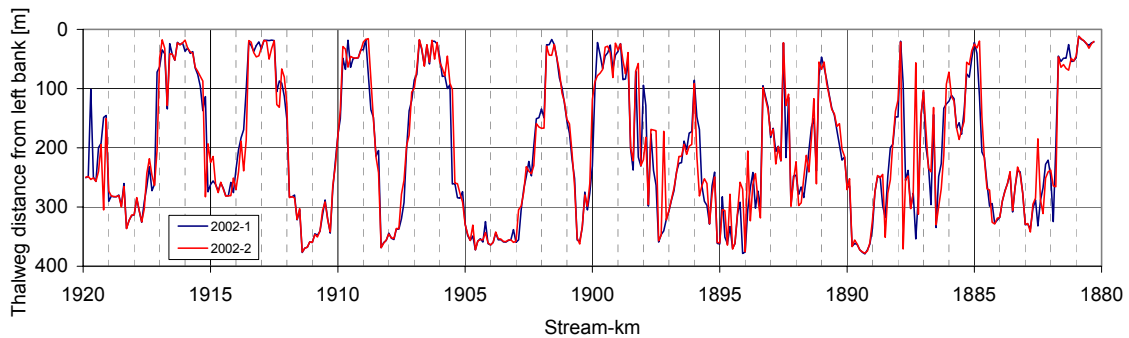
Figure 2.37: Thalweg positions 2002(1) and 2002(2)

2.3.5   Widths and Width-to-depth ratios

Based on the cross-sectional bed level surveys, parameters are derived describing the lateral variability and the compactness of the geometry of a river bed profile. The survey in 2002(1) is used as a reference for analysing these morphological features of the Danube river. The results of the widths and the width-to-depth ratios of this survey are shown in Figure 2.38. For low water levels (*LWL*) the mean width is 256 m with a standard deviation of 37 m. The mean width of the mean water levels (*MWL*) is 297 m with a standard deviation of 34 m and the bankfull discharge given at the breakpoints of the profiles (*bankfull*) shows a mean width of 366 m with a standard deviation of 37 m. For small and mean discharges, the variations of the river widths along the course of the river are strong at the upper 20 km followed by smaller variations of the reach from km 1900 to 1890. The 10 km reach from km 1890 to 1880 again exhibits increased river width variations. These variations correspond to the morphological diversity over the length of the river reach. Relating the computed widths to the morphology of the Danube reach as given in Figure 2.23 to Figure 2.26 shows that the regions of the crossings are characterised by *LWL* widths of approx. 300 m, while the bar regions exhibit significantly smaller *LWL* widths of 200 to 250 m.

An analysis of the width-to-depth ratio, a parameter often used for characterising the compactness of the cross-sectional shape shows that the values for the small discharges (*LWL*) are higher than for the higher discharges. This trend could possibly change for flood events, where inundations produce large widths.

Comparing the width-to-depth ratios to the morphological structures as given in Figure 2.27 to Figure 2.30 shows that the crossing regions generally exhibit larger width-to-depth ratios than the bar regions for the low water levels. These observations reflect the fact that crossings are usually shallow areas that have wide widths in order to convey the water flow, while the bar regions are characterised by asymmetric shapes (see Chapter 2.3.7) that have comparably larger water depths and reduced widths. The effect of significantly different width-to-depth ratios for the bar and crossing regions is best observed for the low water levels. The effect decreases for the higher discharges including mean (*MWL*) and bankfull water levels. While for *MWL* the differences are significantly reduced but still detectable, the width-to-depth ratios for the water depths near the bankfull discharge are more uniform and virtually not influenced by the morphological features of the river.

A hot spot is given at the crossing Hainburg (km 1884). Here, large widths and small water depths lead to maximum width-to-depth ratios. Comparing this local and regional maximum to the dredging activities as given in Table 2.5, reveals that a sudden spatial increase (peak) of the width-to-depth ratio can cause severe navigational problems. These hot spots are potential areas of deposition that need to be maintained in the scope of regular navigation activities.

In Appendix A further widths and width-to-depth ratios for the years 1993, 1996, 2002(2), and 2003(2) are shown. Comparing the width-to-depth ratios of the individual years show that the variations of the ratios reduce over the ten year period. Focussing on the width-to-depth ratios for *LWL* reveals that in the first year, in 1993, the values are ranging from 50 to more than 150, while in 2003(2) the ratios are found mostly in the range 50 to 100. The mean values for the width-to-depth ratios in 1993 and 2003(2) reduce slightly from 94 m to 83 m, respectively, while the standard deviations reduce substantially from 26 m in 1993 to 15 m in 2003(2).
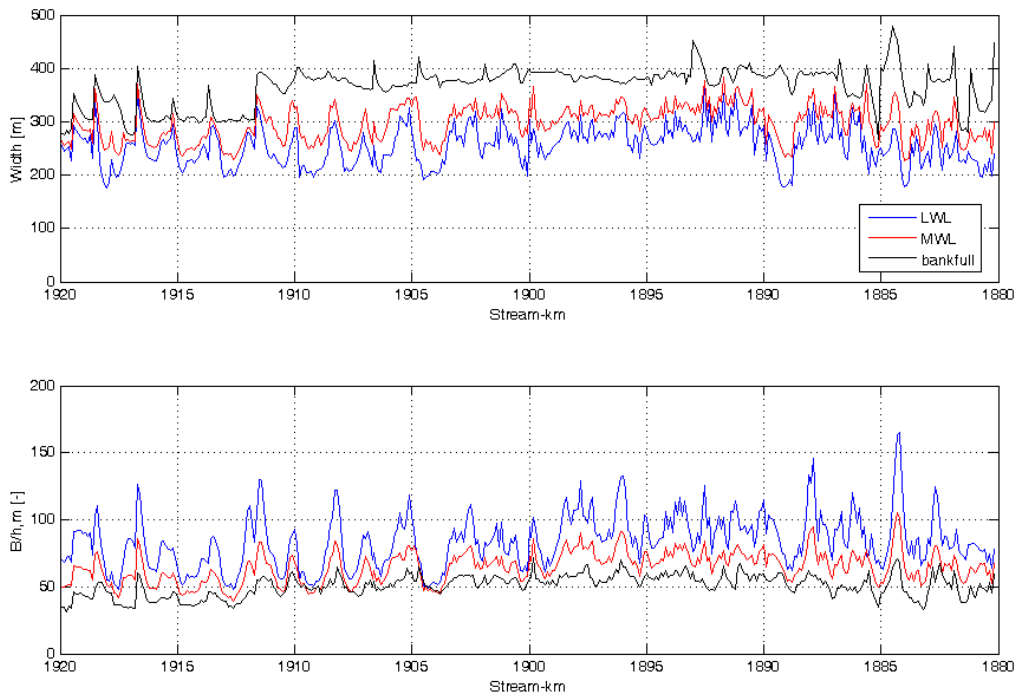
Figure 2.38: Widths and Width-to-depth ratios 2002(1)

A comparison of the development of the width-to-depth ratios for *LWL* within the bar region from km 1920 to 1900 is given in Figure 2.39. The first and last survey after the power station is installed, 1996 and 2003(2), are chosen for comparison. The figure shows that pronounced overall changes of the width-to-depth ratios and thus changes of the shapes of the cross-sections occur during the seven year period. Within the bar regions a slight increase of the ratio is present corresponding to the erosion of bars and deposition of the scours (see Figure 2.40a). In the regions of the crossings the width-to-depth ratios change significantly stronger compared to the changes in the bar regions in the same period. This especially applies to the crossings having large ratios in 1993. The two crossings, Schwechatmündung (km 1913.7) and Kuhstand (km 1910) are characterised by the strongest

changes. Both slight reductions of the widths and intensive water depth increases lead to reduced with-to-depth ratios and the cross-sectional development as shown in Figure 2.40b. These temporal bed developments are apparently a combination of natural processes and human interferences. The grain feeding measures that are performed from the year 1996 contribute to the described cross-sectional bed changes in the bar regions. As a response to the grain feeding measures in the scours, parts of the bars erode in order to convey the water discharges. This leads to a trend of more uniform/compact cross-sectional profile shapes. Also the erosion processes at the crossings are influenced by human interferences (dredgings), that lead to significant reductions of the width-to-depth ratios at the cross-sectional profiles of the crossings.
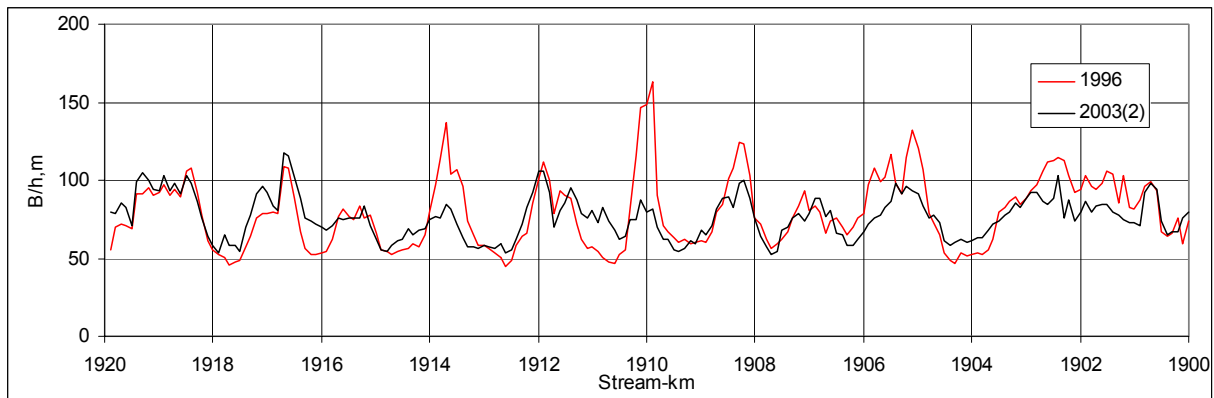
Figure 2.39: Width-to-depth ratios 1996 and 2003(2) in the bar region
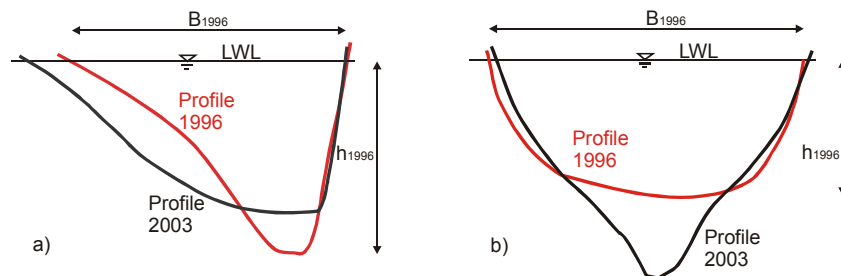
Figure 2.40: Schematic of cross-sectional profiles in a bar region (a) and in a crossing region (b).

2.3.6 Bar wave lengths

The averaged parameters introduced in Chapters 2.3.3 to 2.3.5 are used to distinguish different morphological structures over the course of the river reach. Measures are found to differentiate typical bar and crossing regions, strongly developed at the upper half of the study reach. A typical feature of a bar is its wavelength. *Jäggi (1983)* defines the bar wave length as the distance between two successive bars on the same side of the river. The wavelengths of the bars are analysed within the upper 20 km of the Danube river reach. Generally the bar wavelengths can be derived from the processed parameters based on the widths, the depths, or the configuration. The bars are best distinguished by the thalweg positions in map view (Figure 2.36 and Figure 2.37). Therefore, the wavelengths are determined based on the thalweg development using the local extreme values of the thalweg fluctuations. The longitudinal differences of the extreme values represent the wave lengths of the bars.

The results are shown in Figure 2.41. Five bars on the left and five bars on the right side are detected within the upper half of the study reach. Most of the bar wave lengths lie within 3000 and 4000 m. The results show that the bar wave lengths are limited by a rather small range along the course of the river. With the presence of curvature, the wave lengths of the bars deviate from the preceding bar wave lengths. The lengths show the same tendencies on both sides of the river. At the beginning, small curvature determines the configurations of the first bars, having both lengths smaller 3500 m. The adjacent bars within a straight river reach (bars 2 and 3) have lengths of 3000 to 3500 m followed by a significant increase of the lengths for bars 4. Here, the course of the river is characterised by slight curvature determining the lengths. The bars 4 on both sides and bar 5 on the right side are aligned at the inner bends of curves. While the bars 4 on both sides represent the maximum lengths, the adjacent bar lengths downstream decrease on both sides. The mean bar wave length is computed with 3400 m for the upper half of the study reach. The magnitude of the bar wave lengths corresponds well with theoretical considerations of *Jäggi (1983)*, where the length of the bar is defined as Λ_a = 10 *B* = 10 * 366 = 3660 m when considering the width based on bankfull discharge. The theoretical formula of Yalin Λ_a = 6 *B* underestimates the mean length of the bars. Similar results have been obtained for the morphological analysis of the Salzach river (*WRS (2000)*).
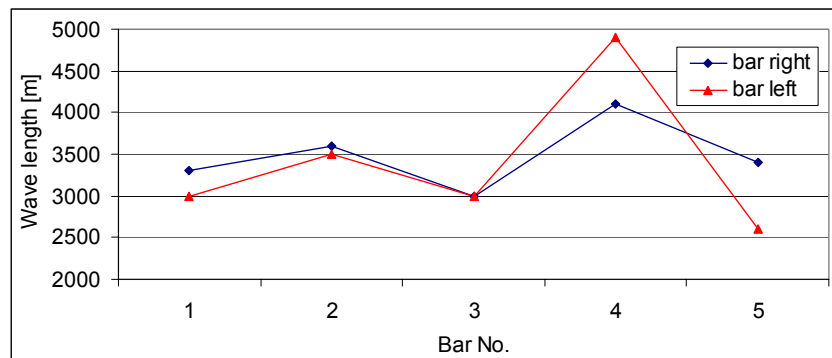
Figure 2.41: Bar wave lengths

2.3.7 Profile symmetry

As indicated earlier, cross-sectional geometries differ considerably depending on the morphological structure of the river. Typical profiles in the bar regions are characterised by an asymmetric shape, while comparably symmetrical features are inherent to the profiles of the crossings (see Figure 2.40). A parameter describing the symmetry of a profile is introduced. Figure 2.42 shows the results of the analysis. The total areas of the cross-sections are shown on the top plot based on the 2002(1) survey. On average, an area of 695 m² is achieved with a standard deviation of 95 m². The symmetry parameter of the profiles is achieved by computing the area A_{left} limited by a vertical passing the thalweg position and the reference low water level and dividing it by the total area A_{tot} limited by the reference low water level. Thus, the symmetry parameter is defined as A_{left}/A_{tot}. Perfect symmetry is given when the parameter achieves a value of 0.5. The longitudinal distribution of the symmetry parameter is shown in the lower plot (Figure 2.42). The dashed line represents the original values, and the solid line represents an averaged, smoothed development. It is computed by a 5 point moving averaging procedure.

The plot shows, that intensive asymmetric features are present at the Danube river, especially in the region of alternate bars, within the upper 20 km of the reach. Here, strong deviations from the "symmetry" line 0.5 are computed representing pronounced asymmetric cross-sectional profile geometries. Virtually all bar profiles are characterised by symmetry parameters exceeding 0.8 (skewed right) or falling below 0.2 (skewed left). The crossing reaches characterised by symmetrical profiles in the vicinity of A_{left}/A_{tot} = 0.5 are comparably small so that the transition from one bar to another is realised within short distances. The general trend of asymmetric profiles continues in the lower half of the study reach from km 1900 to 1880. Here, alternate bar configurations are inhibited by the presence of intensive installations of groynes (see Figure 2.15). Nonetheless, an asymmetric configuration is still present showing an increased variability of the symmetry parameter. Near the downstream end, from km 1887 to 1880, the cross-sectional asymmetry is given by the curvature of the river implying fixed bar structures at the inner bends of the river. Here, asymmetry parameters slightly smaller than in the alternate bar reach occur. Asymmetry parameters of different surveys are shown in Appendix A. Comparing the symmetry parameters of the different surveys shows that the temporal changes are small over the ten year period of investigation.
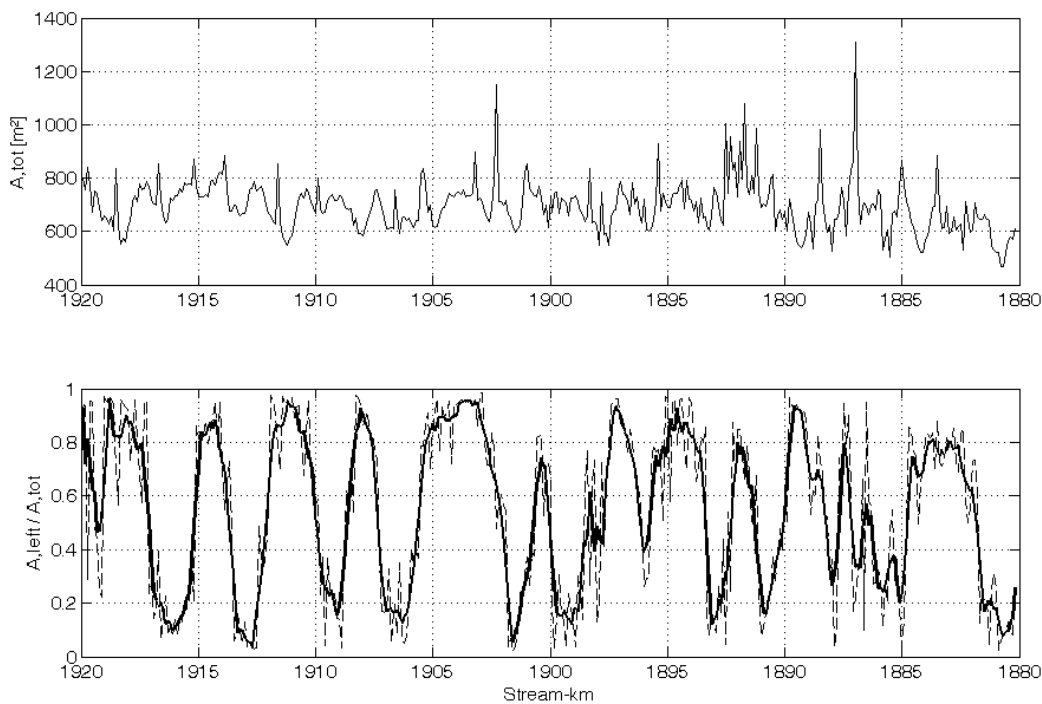
Figure 2.42: Symmetry in 2002(1) survey

In order to quantify the visual impression of minor temporal variability of the symmetry parameter over the study period, a frequency analysis of the parameter values is performed. Therefore, the symmetry parameter is slightly modified (see Chapter 2.2.2) by representing only the symmetry of a profile and neglecting the directional information (left or right). The modified parameter is defined by the ratio of the smaller sub-area and the total area, A_{small}/A_{tot}. This parameter has a range of values of [0, 0.5]. The first and the last surveys, 1993 and 2003(2) are chosen for the frequency

analysis. In Figure 2.43, the cumulative relative frequencies are plotted over the range of the parameter A_{small}/A_{tot}. The results show that the two lines are almost identical and thus the frequency distribution of the symmetry parameter is virtually invariable over the ten year time period. Both lines represent an overall asymmetry of a high extent. 30 % of the 400 cross-sections show symmetry parameters smaller than 0.1 giving an extensive asymmetry. 50 % of the cross-sections show smaller symmetry parameters than 0.18, that is considered a large asymmetry. Only 15 % of the profiles exhibit symmetrical shapes characterised by symmetry parameters larger than 0.4. They are preferentially located in the crossing regions between the alternate bars (see Figure 2.42). From this analysis a stable geometrical configuration of the river reach with respect to its cross-sectional symmetrical features can be inferred. Asymmetrical cross-sectional shapes are dominant at the river reach that remain virtually unchanged over a time period that is influenced by severe river training measures, including the installation of a hydropower station and regular grain feeding measures.
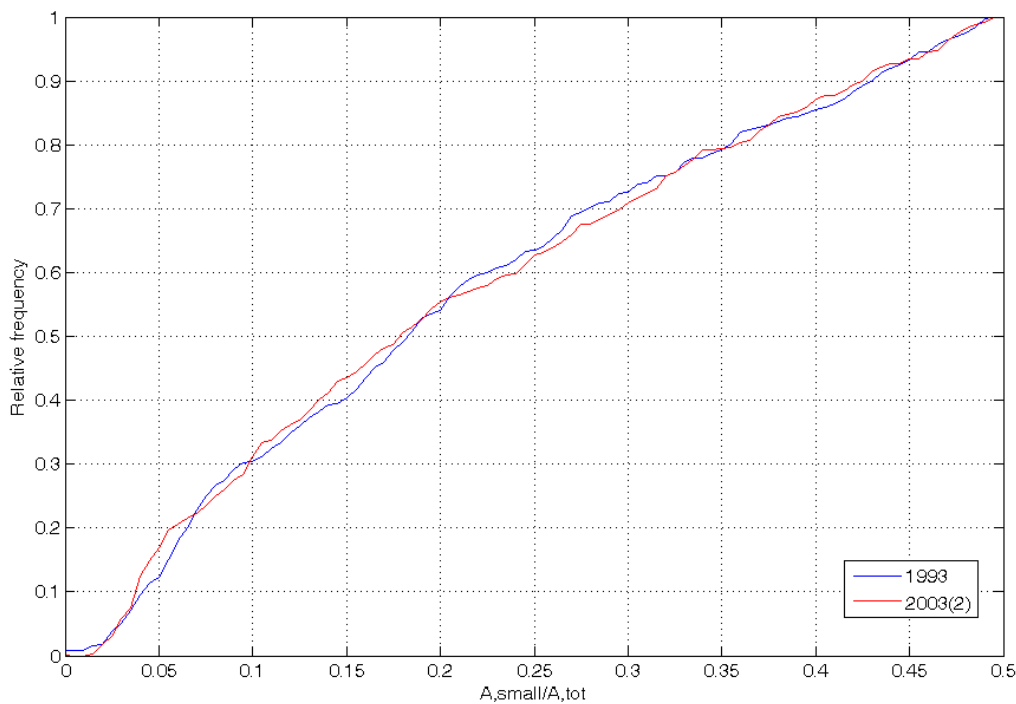
Figure 2.43: Symmetry in 1993 and 2003(2) surveys

2.3.8   Lateral slopes

For further quantifying the characteristics of the bars in the Danube river, the lateral slopes of the cross-sectional profiles are analysed. Two parameters, the mean and the median lateral slope are determined (see Chapter 2.2.2). The median slope represents better the characteristic slopes of the bars by filtering out the extreme gradients. The analysis focuses on the 2002(1) survey. The results are shown in Figure 2.44 and Figure 2.45. Further analysis of the other surveys are depicted in the Appendix A. To distinguish the two sides, the slopes on the right sides are multiplied with (-1). Comparing the results of Figure 2.44 to the bathymetric maps (Figure 2.27 to Figure 2.30) shows that the high-gradient slopes such as undercut banks are represented by absolute values greater than 0.1

and the slopes of the bars are typically smaller than this value. The undercut slopes can achieve values of up to 60 %. Bank slopes of this extend are secured by bank revetments. In most cases, the median and mean values of the high-gradient slopes do not differ considerably. In the reach from km 1905 to km 1903 on the right side, the mean slope values achieve higher values than the median values. This is an indication that the dominant slope is smaller than the linear approach that characterises the mean slope (see Chapter 2.2.2).
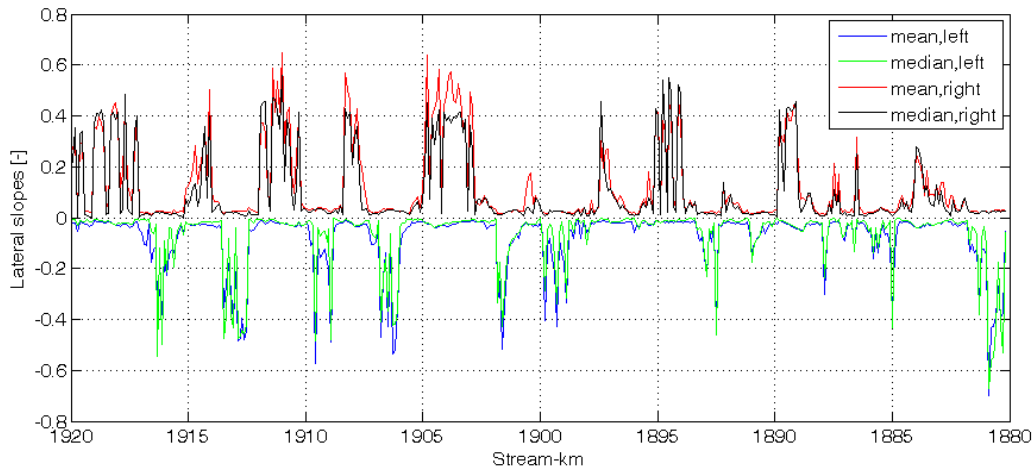
Figure 2.44: Lateral slopes in the survey 2002(1)

Focussing on the lateral slopes of the bar regions is achieved by filtering out all gradients exceeding the range of –0.1 to 0.1 (Figure 2.45). The reach of the alternate bars from km 1920 to km 1900 is analysed. The centre positions of the bars are derived from Figure 2.36. They are found at: km 1918.5, 1916.0, 1914.5, 1913.0, 1911.0, 1909.5, 1908.0, 1906.5, 1904.0, 1901.5, and 1900.5. At these positions the majority of the lateral bar slopes lie at around 0.025 = 2.5 %. Considering a mean longitudinal slope of 0.04 % at this reach of the Danube river, the lateral slope is more than 60 times larger than the longitudinal slope on average. These morphological features have implications on the selective sediment transport producing these structures. Sorting processes induced by fractional sediment transport highly interact with the lateral bed development (see Chapter 3). Generally the median slopes are smaller than the mean slopes. Due to the filtering effect, the median slopes represent the characteristic slope at the bars more accurately in the case of highly varying lateral slope gradients within a bar profile. In regions with similar values for the mean and median slopes, the bars are fairly uniform and linear. In Appendix A, lateral slopes of further surveys are shown. Comparison of the results show, that the lateral slopes of the early surveys are slightly larger compared to the later surveys. This reflects the effects of bar erosion and scour deposition increasing the compactness of the cross-sectional profiles.
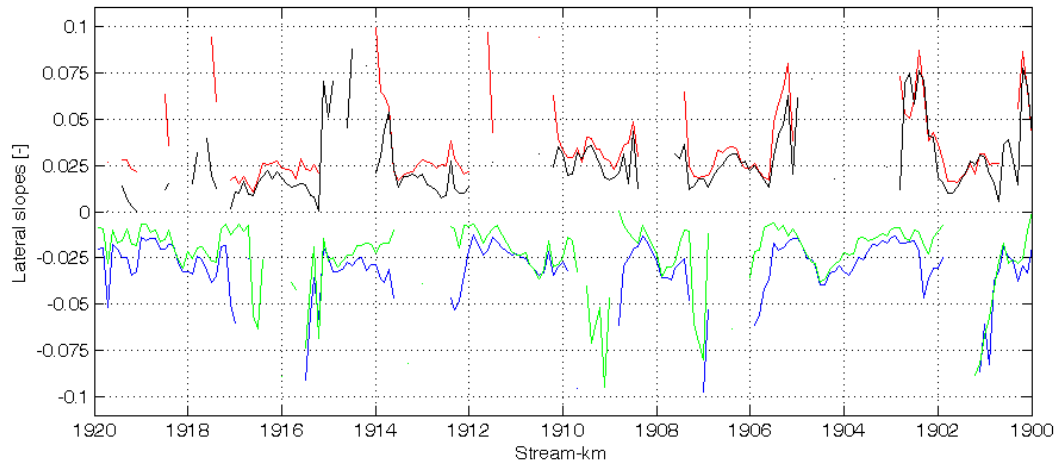
Figure 2.45: Lateral slopes on the bars in the survey 2002(1)

2.3.9   Profile shape variations

The study reach of the Danube river is partly characterised by intensive local bed changes analysed by comparing measured bed levels in cross-sectional profiles at different surveys. Temporal bed changes may vary significantly over the course of the river reach as reflected by considering the non-linearity of the cumulative bed volume changes. The processes producing the temporal variability of the bed changes are addressed in this Chapter assuming that the temporal changes are related to the spatial variability of the profiles. To get deeper insight into these processes, spatial and temporal similarities of the cross-sectional surveys are computed and compared. For accurately representing the spatial similarities, the cross-sections are horizontally shifted until an optimum similarity is achieved (see Chapter 2.2.2).

Figure 2.46 gives an example of similarity analysis at some cross-sections. The cross-sections are compared to their neighbouring cross-sections upstream (spatial analysis). For the temporal analysis, all cross-sections measured by a first survey are compared to cross-sections at identical positions measured at another survey. The figure shows cross-sections at five positions (including their neighbouring positions for the spatial analysis). The red cross-sections from survey 2002(1) are used to find similarities (*RMSE* parameters) in comparison with their spatial neighbour cross-sections in upstream direction (blue cross-sections) and with another survey at the same position (black cross-section, survey 2002(2)). On the left side of Figure 2.46, the original positions of succeeding cross-sections are plotted (dotted lines). The upstream blue cross-sections are shifted horizontally until the spatial *RMSE* values achieve their minimum. The shifted cross-sections are plotted with blue thin lines. The numeric results for these profiles are given in Table 2.11 showing that the necessary transformation lengths range from less than 10 m to almost 100 m. As shown in Figure 2.46 (right side) and Table 2.11, the temporal *RMSE* values are mostly smaller than the spatial *RMSE* values, i.e. compared to the spatial variability the temporal changes are small. Here, shifting procedures are not necessary to compute the temporal *RMSE* values. The influence of spatial similarity on the temporal changes is best explained at cross-section km 1902.3. Here, the neighbouring profile is significantly different which produces considerable deposition of the profile at km 1902.3 as observed in the later

survey (2002(2)). These temporal changes are unambiguously motivated by the upstream morphological structures.

Spatial similarity	Temporal similarity
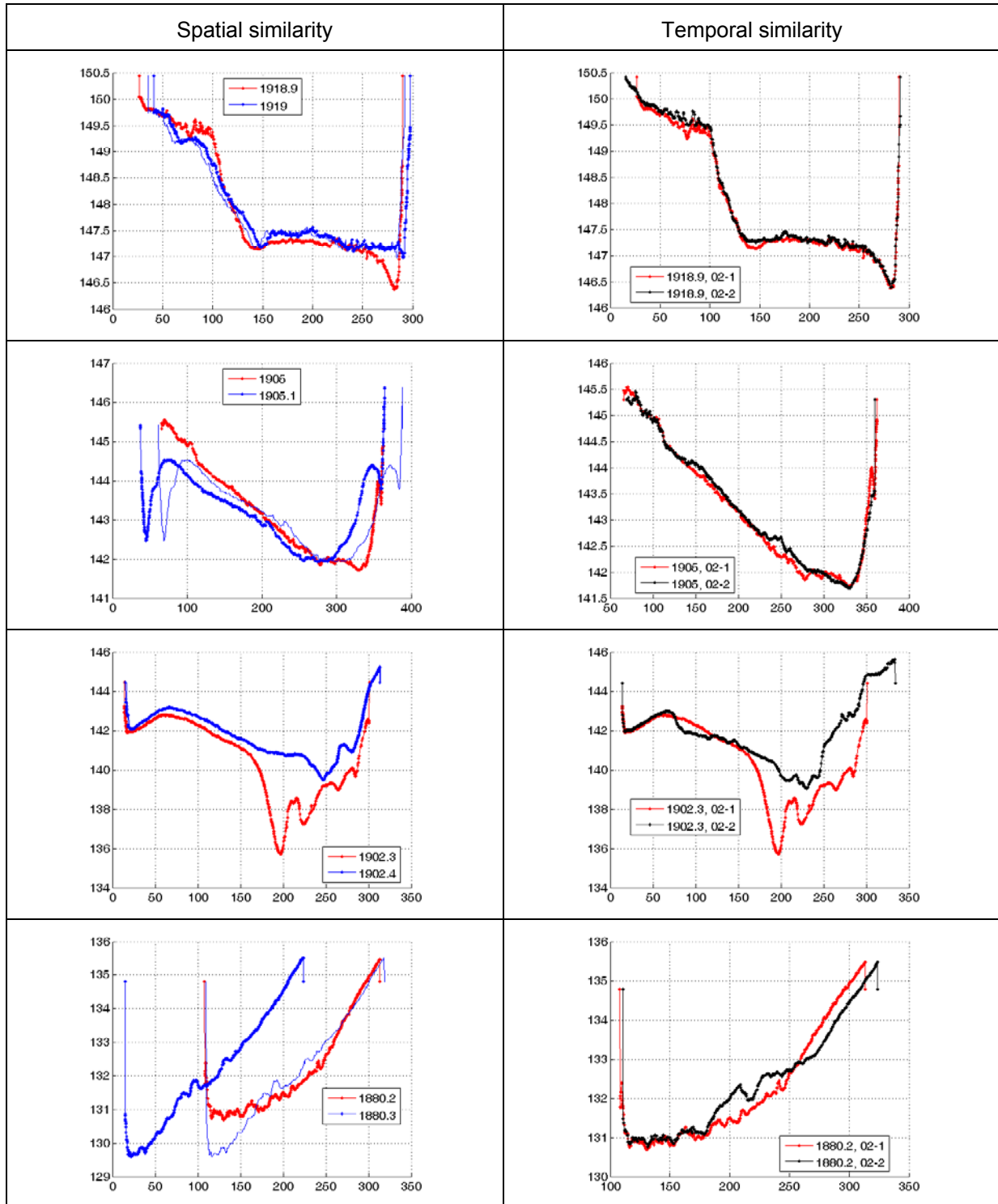
Figure 2.46: Selected cross-sections for 2002(1) and 2002(2) survey

Table 2.11: *RMSE* values and transformation lengths for selected cross-sections for 2002(1) and 2002(2) survey

Profile	RMSE	RMSE, trans	L, trans	RMSE, time
1918.9	0.52	0.32	-6	0.10
1905.0	0.88	0.67	24	0.15
1900.3	0.95	0.64	-6	0.52
1880.2	2.92	0.54	95	0.47

The *RMSE* values representing the similarities between two cross-sections and the transformation lengths are plotted over the entire study reach. Both spatial and temporal *RMSE* values are computed and compared. The results of the similarities of the surveys 2002(1) and 2002(2), using the 2002(1) survey for spatial analysis, are shown in Figure 2.47 and Figure 2.48. All cross-sections over the course of the river reach are used for the analysis. The first plot in Figure 2.47 shows spatial *RMSE* values for the Danube reach from km 1920 to 1880. The second plot shows the computed transformation lengths to obtain the optimal spatial *RMSE* values. In the upstream half of the river reach significantly lower transformation lengths are necessary to achieve the optimum spatial similarities. Obviously, the deviations of streamlines and breakpoint lines are smaller here. The temporal *RMSE* values are shown in the third plot. The similarity parameters (*RMSE* values) focus on cross-sectional changes of the shapes of the profiles. Therefore, the temporal *RMSE* values can show different trends than averaged parameters such as changes of the mean bed levels. Direct comparison of the *RMSE* values (Figure 2.48, top plot) shows some minor similarities. A smoothing filter using a moving average window with a span of 5 points is applied to reduce fluctuations (bottom plot). Focusing on the peaks shows agreement at some locations indicating that instantaneous spatial changes induce strong temporal changes. The overall relationship of spatial and temporal similarity is rather weak for the short-term analysis. The results further show, that generally the spatial cross-sectional changes exceed the temporal changes indicating that even for a 100 year flood, the impressed spatial variability influences the temporal changes only to a minor degree.
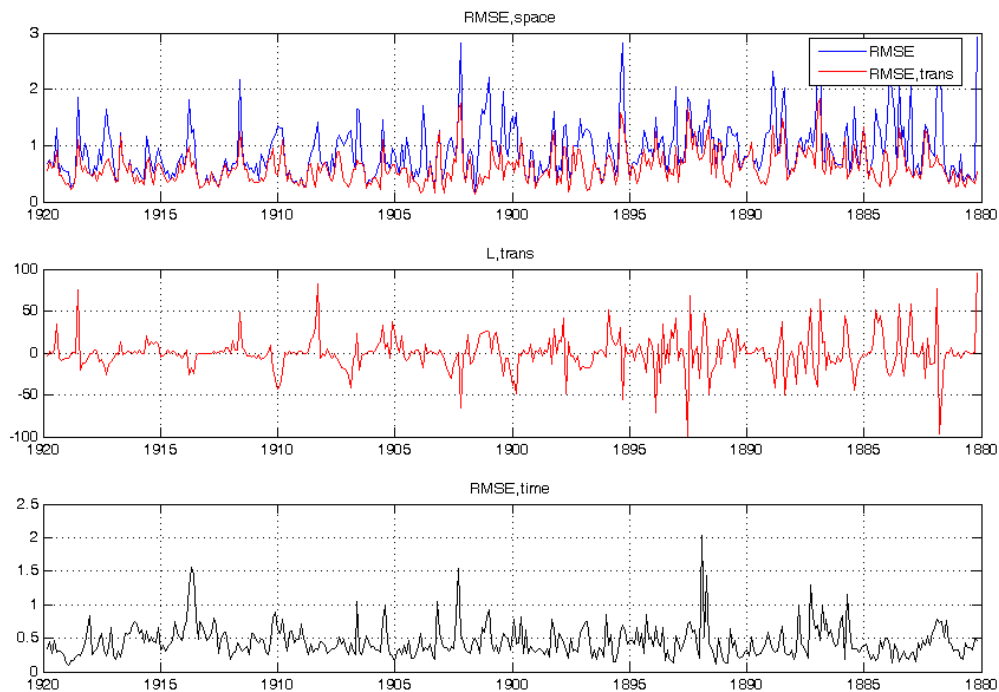
Figure 2.47: Spatial and temporal RMSE values and transformation lengths for 2002(1) and 2002(2) survey
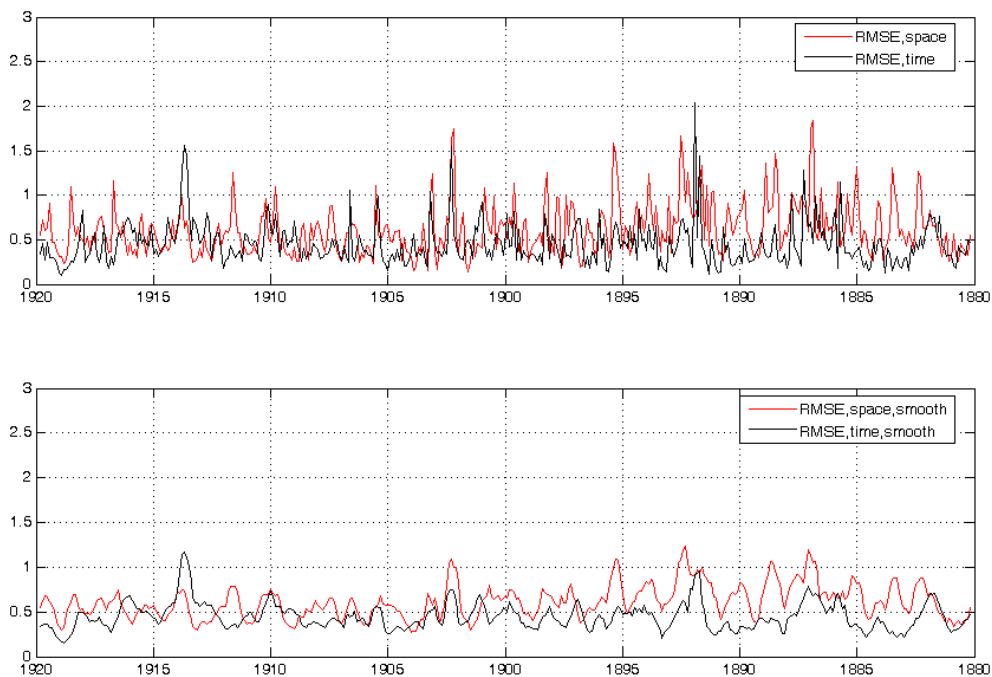
Figure 2.48: Comparison of spatial and temporal *RMSE* values for 2002(1) and 2002(2) survey

The long-term development of the Danube river, from 1996 to 2002(2) is processed in an analogous way. The time between these surveys represents the long-term period after installation of the hydropower station Freudenau. The results are shown in Figure 2.49 and Figure 2.50. In 1996, the differences of succeeding profiles are generally higher than in the 2002(1) survey. This applies especially to the second half of the Danube river reach. Here, *RMSE* values of 1 are regularly exceeded while this occurs only at some limited locations at the 2002(1) survey. This implies, that during the seven year period, the Danube river harmonises to a certain degree. Comparing the smoothed spatial and temporal *RMSE* values (Figure 2.50, bottom plot) of the long- and short-term development reveals that the relationship of spatial and temporal development is stronger for the long-term development. An agreement of small *RMSE* values indicates, that small spatial diversity induces small temporal changes. This indicates stable, minor mobile river reaches. On the other side, an agreement of large *RMSE* values indicates, that strong spatial diversity induces similar strong temporal changes. This is an indication for mobile river reaches where the cross-sectional profile shapes over time adjust to the upstream profile shapes. Another process can be inferred from the general trend of higher temporal *RMSE* values at the upper 10 km reach that is induced by strong temporal changes that are virtually not correlated to the smaller spatial variability. This is characteristic for the alternate bar region that is characterised by intensive vertical changes in a region of a stable planimetric configuration.
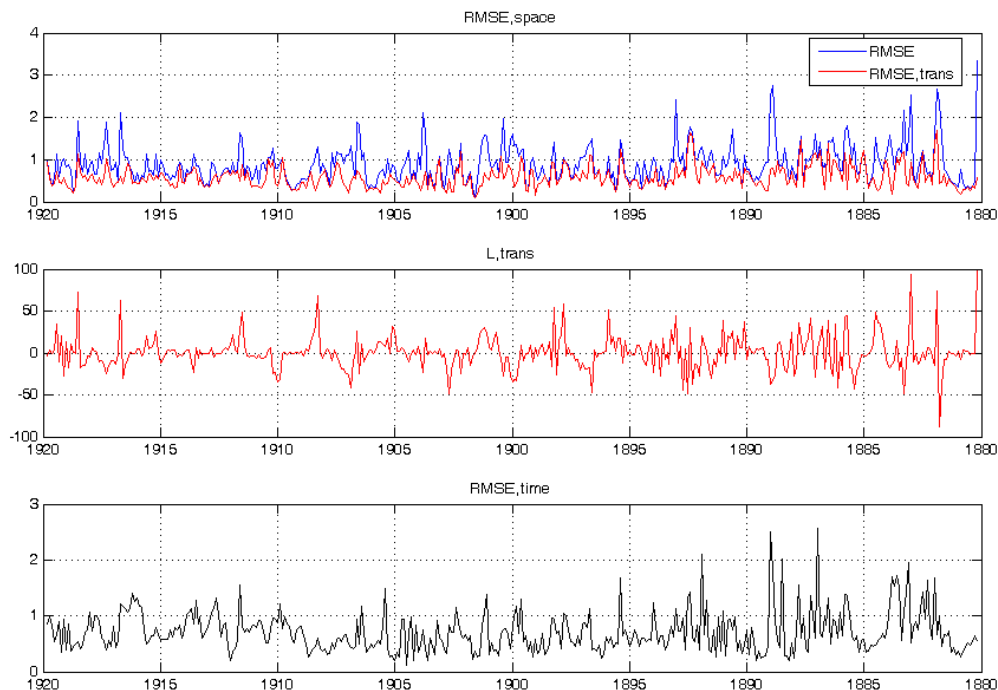
Figure 2.49: Spatial and temporal *RMSE* values and transformation lengths for 1996 and 2002(2) survey
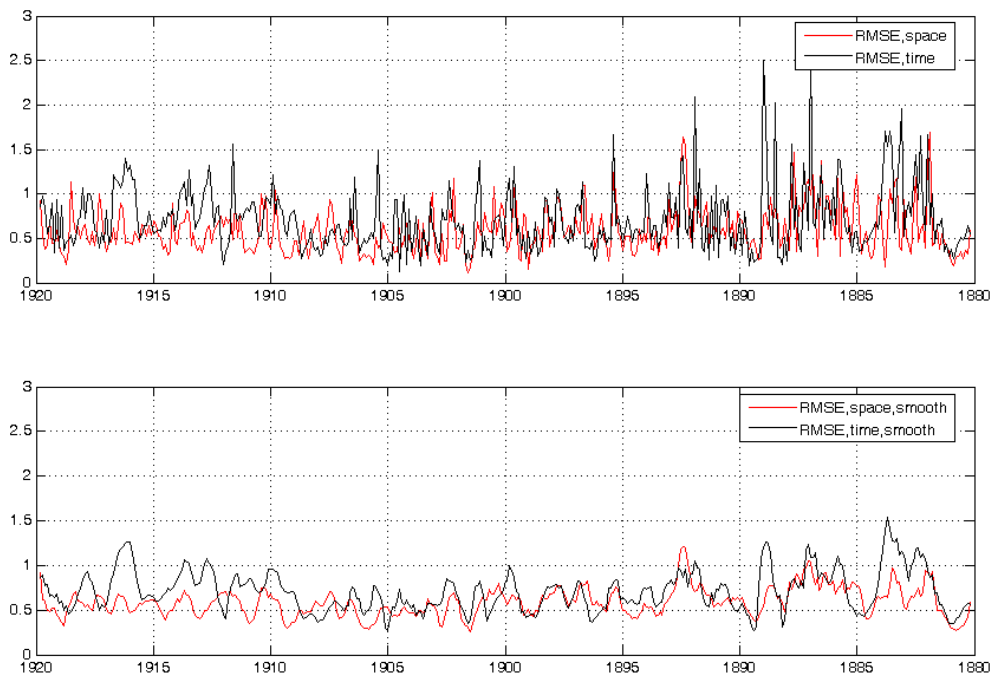
Figure 2.50: Comparison of spatial and temporal *RMSE* values for 1996 and 2002(2) survey

2.3.10 Bed volume changes

Bed volume changes of the Danube river are calculated based on 12 bed level surveys performed over a ten year period (see Table 2.9). The results of the cumulative bed volume changes for 11 periods (12 surveys) are shown in Figure 2.51 to Figure 2.53. Positive and negative gradients of the line plots indicate deposition and erosion processes, respectively. Three approaches (common width, width of navigation channel, extended width, see Chapter 2.2.2) are chosen to compute the bed volume changes. All approaches show wide scatters of cumulative bed volume changes for the individual periods. The widest scatter of deviations occur for approach 1 (common width). The scatter becomes smaller when using approach 3 (extended width) and further decreases for approach 2 (navigation channel). Approach 3 (extended width), that is most suitable for bed volume computations, is discussed in detail. Over the course of the river, erosion and deposition processes alternate, as indicated by the changing gradients of the cumulative bed volume change curves. To assess the large-scale heterogeneity of the bed change processes, the river reach is divided into four units each having a length of 10 km. The overall bed change processes are analysed for each unit. This large scale analysis reveals that six periods out of eleven (93-95, 95-96, 97-98, 98-99, 01-02(1), 02(1)-02(2)) show monotonous trends of bed changes, i.e. in these periods a total deposition (erosion) is composed of deposition (erosion) processes in all four units. Two periods (99-00, 03(1)-03(2)) generally also show monotonous trends with minor trends in the opposite direction while three periods (96-97, 00-01, 02(2)-03(1)) exhibit contrary trends within the units. Thus, generally a majority of eight periods exhibits monotonous trends of erosion or deposition. Also local river training measures influence the cumulative bed volume changes such as intensive dredging measures performed at the crossing Hainburg (km 1884) for the period 97-98. In this period the dredging measures are reflected

by a sudden drop of the cumulative curve. In the first instance the monotonous trend of deposition for the pre and post flood surveys in 2002 (02(1) and 02(2)) is unexpected. Considering the inhibited passage of bed load material over the dam of the upstream hydropower station, the monotonous deposition processes during the flood period can be attributed to laterally mobilised sediment from unobserved shallow water regions. The two periods before the installation of the hydropower station (93-95 and 95-96) are characterised by severe erosion processes. Grain feeding measures started in 1996, for this reason the erosion volumes reduce after this time.
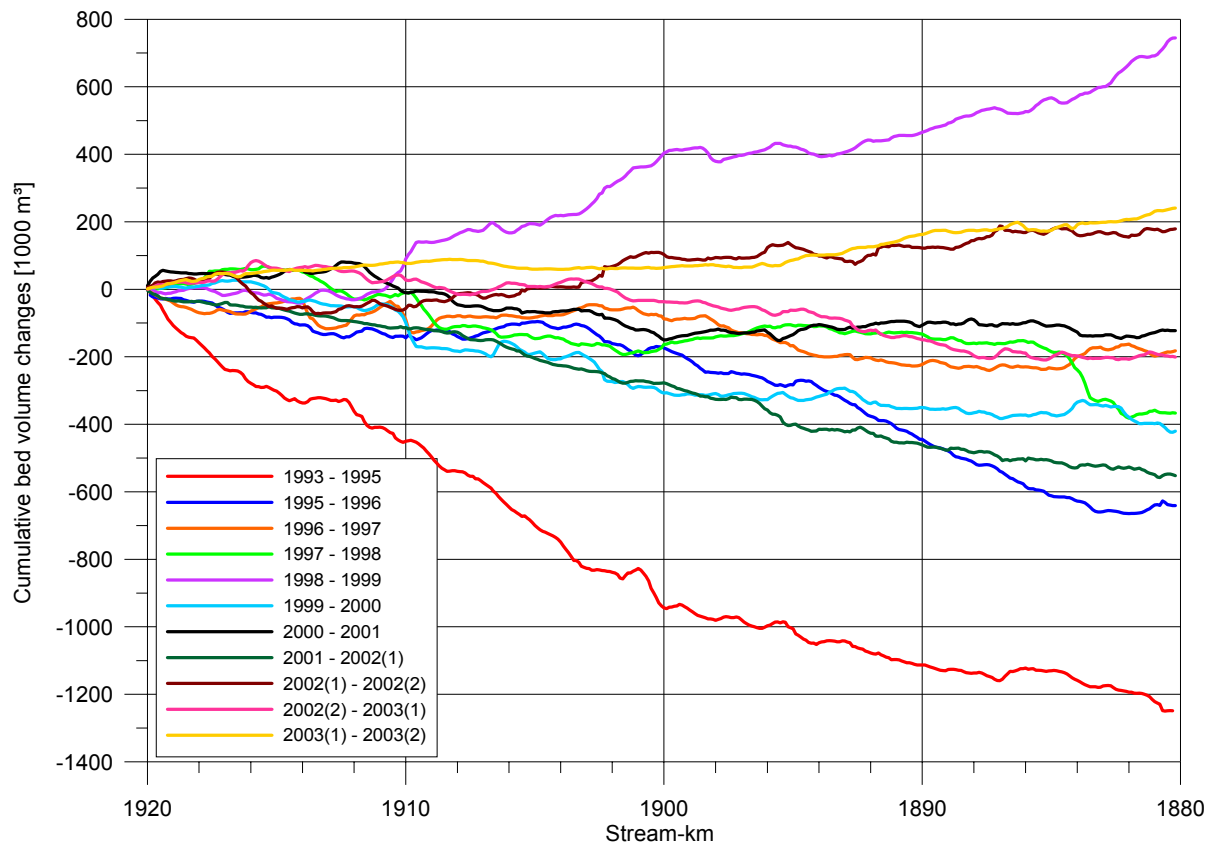
Figure 2.51: Cumulative bed volume changes based on "common width"
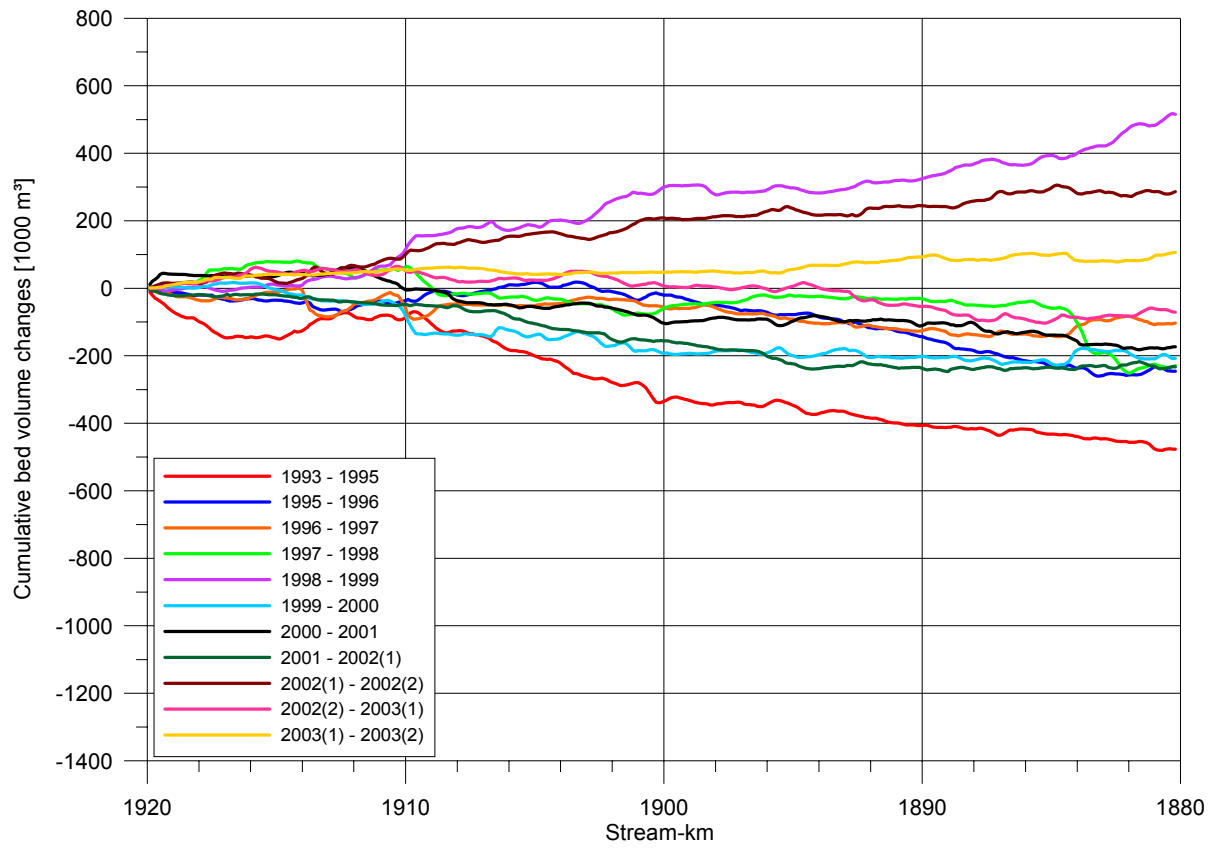
Figure 2.52: Cumulative bed volume changes based on width of navigation channel
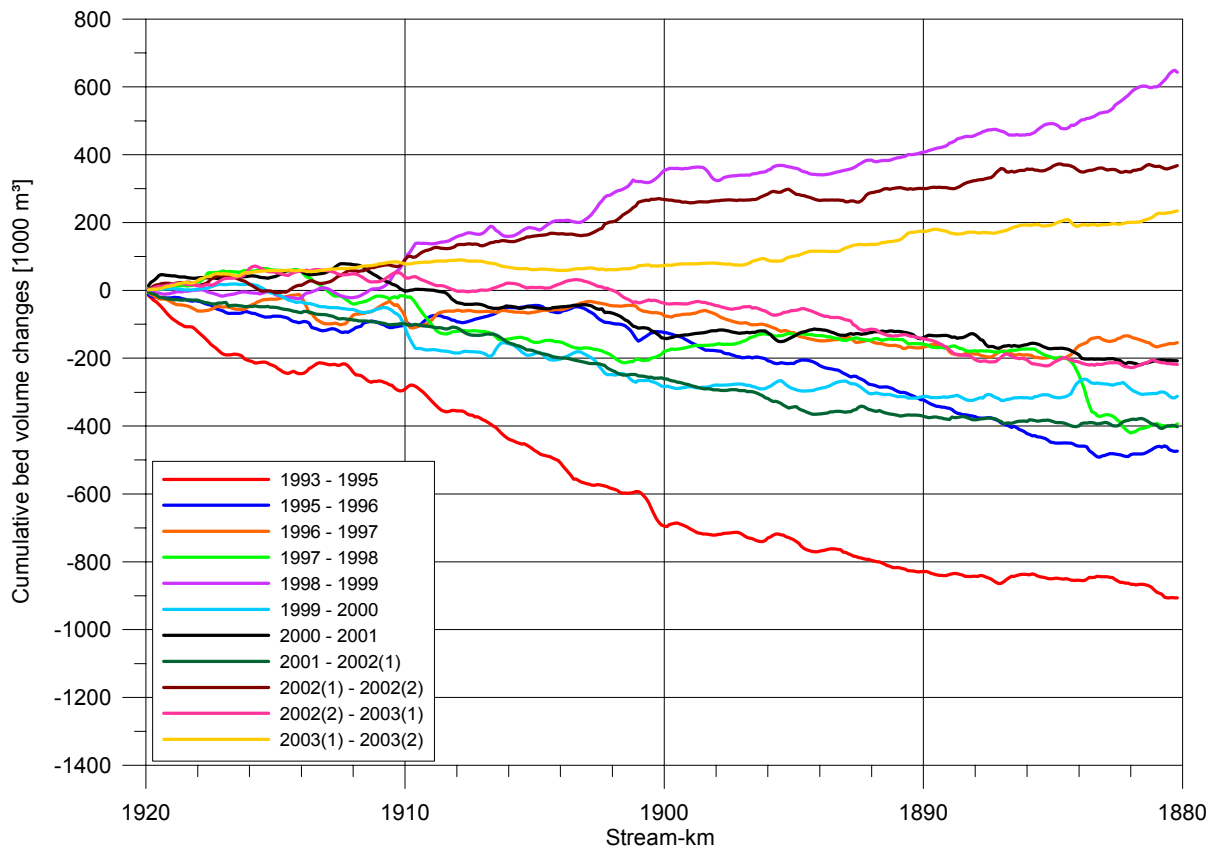
Figure 2.53: Cumulative bed volume changes based on extended width

The survey periods are further analysed in terms of their total bed volume changes (Figure 2.54). Additionally the annual bed volume changes are computed (light colours). The non-monotonous character of the bed level changes is seen in this overview plot. Eight periods erode and three periods show depositions in total. Generally the total bed volume changes increase with increasing reference widths. However, this trend does not apply to the periods 00-01 and 02(1)-02(2). The fact that the total deposition volume for the common width of the 02(1)-02(2) survey is smaller than for the limited width approaches is an indication that sediment is transported from the shallow regions into the main channel. The relationship of the total bed volume changes and the hydrological conditions is discussed in Chapter 2.3.11.

Considering a width of B_{ext} = 180 m and a length of 40 km, the total cumulative bed volume changes are converted into mean bed level changes by dividing the total bed volume change with the planimetric area given as the length times the width:

$$dh = dV / (40000 * 180) \tag{2.2}$$

	93-95	95-96	96-97	97-98	98-99	99-00	00-01	01-021	021-022	022-031	031-032
Common width	-1249	-641	-182	-367	745	-420	-122	-552	179	-201	241
Common width/a	-609	-594	-209	-253	1360	-452	-129	-560	302	-339	557
Nav. channel	-477	-246	-103	-230	515	-207	-173	-233	286	-71	106
Nav. channel /a	-232	-228	-118	-158	940	-223	-182	-237	484	-120	246
1.5x nav. channel	-907	-474	-154	-393	643	-311	-206	-402	367	-218	234
1.5x nav. channel/a	-442	-439	-177	-270	1173	-335	-217	-408	620	-368	541

Figure 2.54: Volume balances for the Danube reach between km 1920 and 1880

The long-term development of the Danube river reach, represented by the periods 93-03(2), 93-96 and 96-03(2) is shown in Figure 2.55. Applying the above equation, a mean erosion rate in the ten year period from 1993 to 2003(2) of $\varDelta h$ = 1.8*10⁶ / 40000 / 180 = 25 cm is calculated that corresponds to an annual mean erosion rate of 2.4 cm/a. Comparing the periods before and after the installation of the hydropower station reveals that the major erosion (78 %) of the ten year development occur in the three years before installation of the power station, while the following seven years only contribute with 22 %. While the period 93-96 is characterised by virtually monotonously decreasing cumulative bed

volume changes, i.e. almost over the whole river reach erosion processes dominate, the later period, 96-03(2), shows considerably different morphodynamics. In this period, deposition regions alternate with erosion regions resulting in significantly reduced total erosion rate. The upper 10 km, from km 1920 to 1910 denoted as maintenance reach, are used for regular grain feeding measures. This reach shows a volume balance of almost zero in the period 96-03(2). Here, obviously the grain feeding measures achieved a stabilising effect of this reach.
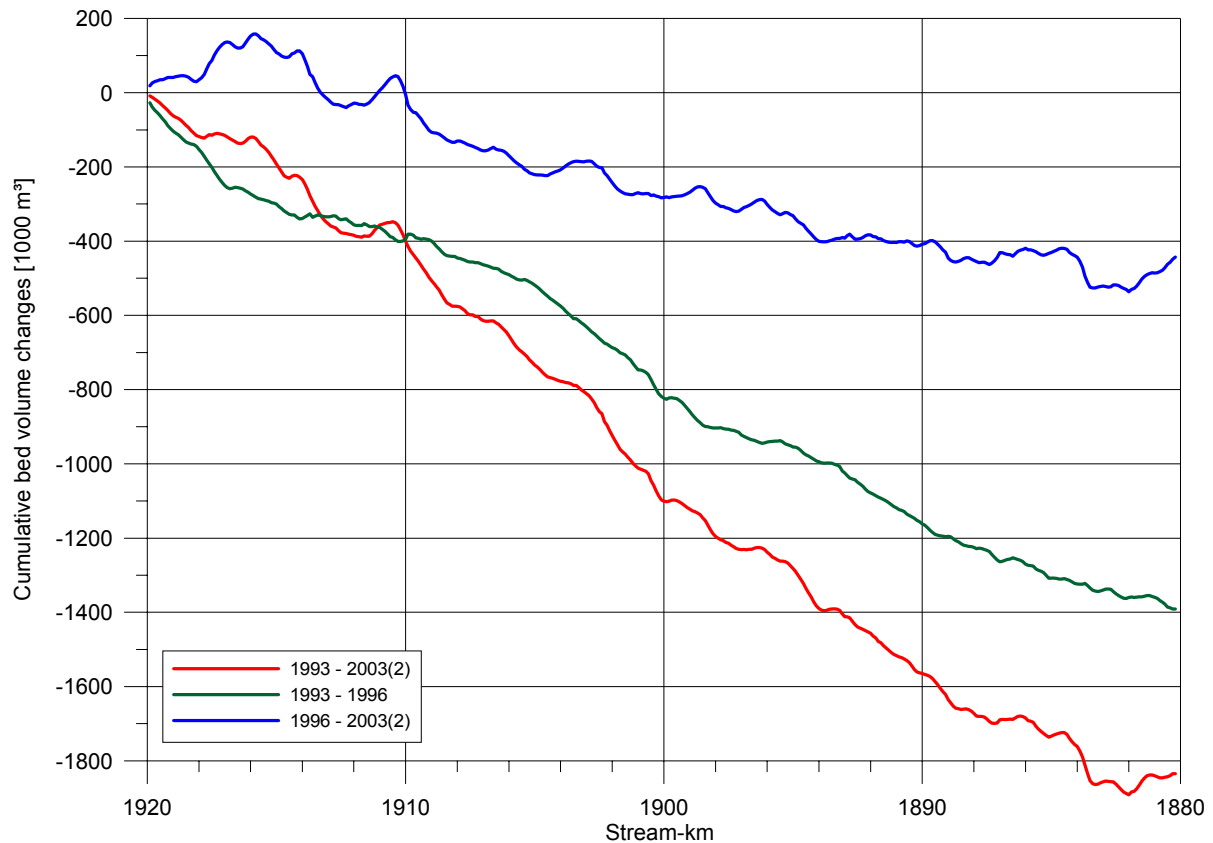
Figure 2.55: Long-tern development (93-03(2), 93-96, and 96-03(2)) based on the extended width

2.3.11 Relationship hydrology – morphodynamics

The relationship of cumulative bed volume changes and the hydrology of a river is influenced by a variety of external conditions. From literature (e.g. *Zanke (1982)*) relationships are given to estimate sediment transport rates for given hydrologic conditions either by applying appropriate sediment transport formulas or by performing transport measurements allowing to derive cumulative discharge and sediment transport curves. However, calculated sediment transport capacities do not necessarily coincide with prevailing sediment transport rates. Sediment deficits induced for example by river training measures can significantly disturb the predicted sediment transport capacities. Also in this study, uncertainty including limited knowledge of the initial movement of sediments, rough information on the amounts of grain feeding, limited knowledge on volumetric changes in the shallow regions of the river, is given. Therefore, comparing morphological changes with hydrological conditions represents a qualitative analysis.

Figure 2.56 and Figure 2.57 show the results of the computed water volumes versus the computed cumulative bed volume changes. The bed level surveys from 1996 to 2003(2) are

considered for the analysis. The water volumes and the water volumes exceeding a threshold of 2000 m³/s are computed for the periods between the bed level surveys. A tendency is given showing that generally highly negative bed volumetric changes (erosion) correspond with the presence of large water volumes. Also, small to medium negative bed volumetric changes correspond well with medium water volumes. Positive bed volumetric changes (deposition) correspond with small water volumes.

The cumulative bed volume changes are reduced by the regular grain feeding measures as given in Table 2.7. The results show that three periods 1998-1999, 2002(1)-2002(2), and 2003(1)-2003(2) show positive bed changes, i.e. deposition processes. When assuming that the passage of bed load is inhibited by the power station and that the measurement accuracy is sufficiently high to compute a plausible sediment balance, it can be inferred that sediment is transported from the unobserved shallow side areas outside the extended navigation channel towards the main channel. The assumption of complete retained bed load material upstream the hydropower station cannot consequently be met for flood events. According to *Donaukraft (1995)*, bed load transport is completely inhibited for discharges of up to 3000 m³/s. However, for higher discharges where the weirs are opened, certain amounts of bed material can be transported from the reservoir into the study reach. Quantitative information is not given. Thus, deposition processes are probably based on both cross-sectional re-arrangements and entrained material from the upstream reservoir.

When introducing a threshold value of 2000 m³/s the distribution remains essentially unchanged except for period 97-98 that significantly changes its position. The relationships slightly deteriorates compared to using the total water volumes. This can be due to the effect, that already smaller discharges, such as Q>1000 m³/s contribute to relevant bed volume changes. The deviation might also indicate erroneous surveys either in 1997 or in 1998.
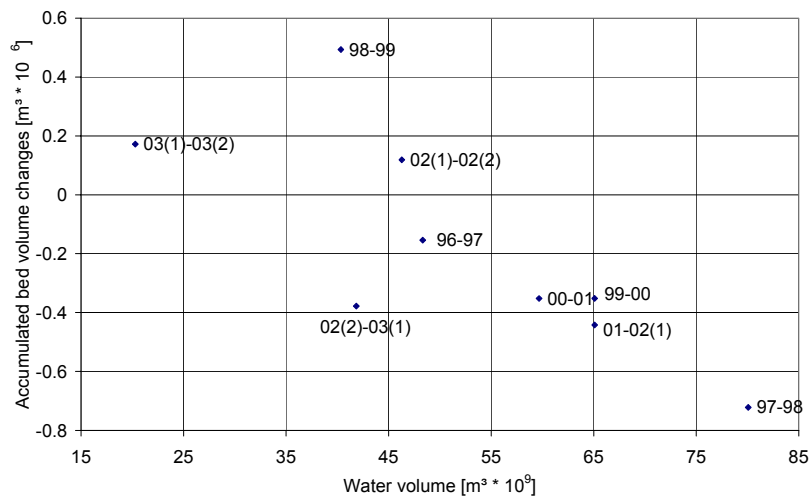
Figure 2.56: Relationship of water volumes and bed volume changes
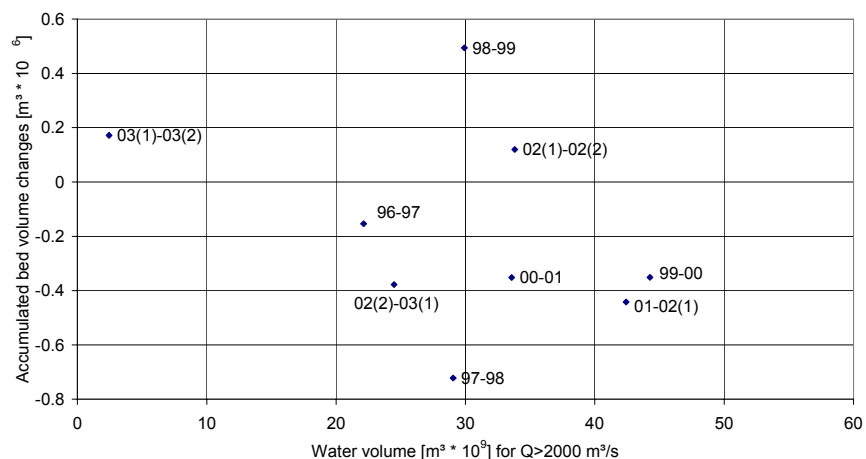
Figure 2.57: Relationship of water volumes and bed volume changes for Q>2000 m³/s

2.4   Summary and conclusions

The Danube river in Austria fulfils several important functions. As the second longest river in Europe, it serves as an important waterway connecting the West with the East of Europe. Furthermore, the river and its adjacent wetlands serve as an important habitat that needs to be protected and preserved. In the 19th century, major parts of the river were characterised by intensive river restoration works. The flow of the originally braiding river was concentrated on the main channel. Several issues were addressed by these measures. The navigability was enhanced, wetlands were drained for agricultural purposes, and the conditions for flood protection were improved. At a length of 350 km the Austrian Danube reach comprises nine hydropower stations. Thus, most of the river is influenced by the backwater effect of the dams, only two free flowing reaches remain. One of these reaches is investigated in this study.

With a length of 40 km, the study reach is situated between Vienna downstream the hydropower station Freudenau and the Austrian-Slovakian border. The sediments that are retained by the upstream dam have to be artificially fed into the reach by the hydropower station operator. In 2002, a 100 year flood passed the Danube reach.

The study reach is characterised by substantial progressive erosion processes induced by river training measures and a significant sediment deficit caused by the installation of the hydropower stations at the Austrian Danube river and its major tributaries (Inn, Traun, Enns, Ybbs). The motivation of this study is to analyse the morphological structures and the morphological changes of the 40 km long study reach under the given conditions by applying existing and deriving new methods to describe and quantify the relevant features. The analysis is based on regular annual or bi-annual bed level surveys over a period of ten years. The morphological situation is interpreted and compared to other rivers exhibiting similar morphological features. The observed river bed levels are processed and described in a way, that they can be used as for testing a numerical morphodynamic model at an appropriate sub-reach (see Chapter 4).

The river bed configuration is visualised by interpolating the measured bed levels onto an equidistant grid which is used as a base for producing bathymetric maps of the reach. Moreover,

morphological changes are visualised in terms of producing difference maps based on the bathymetric maps from different surveys. This method allows to visualise erosion and deposition patterns giving a concise impression of the morphological changes between two surveys. Existing parameters, such as mean bed levels, thalweg development, cumulative bed volume changes, and width-to-depth ratios, describing the morphological situations at rivers, are applied and interpreted. In some cases, the sensitivity of the parameters using different characteristic lengths is investigated (such as computing cumulative bed volume changes based on different characteristic profile widths). The study is complemented by introducing new parameters that are derived based on the specific morphological situation at the Danube river reach, describing and quantifying morphological processes more detailed than what is commonly done in comparable studies. The developed new parameters, such as profile symmetry, lateral slopes, and spatial and temporal profile shape similarities, allow to gain deeper insight into the morphological processes happening at the study reach.

A morphological classification scheme (*Yalin & da Silva (2001)*) based on the ratios of width to depth and depth to grain size shows that the Danube river reach is characterised by an alternate bar configuration. Alternate bar structures are also observed at similar rivers, such as the Elbe, Rhine, and Salzach. The analysis based on the bathymetric maps confirms the classification. Distinct alternate bars are found at the upper half of the study reach. Here, developed bars are found with a mean wave length of 3,400 m. This characteristic length fits into the study of *Jäggi (1983)* who provides an empirical relationship giving similar results. Parts of the lower half are characterised by significant river training measures such as intensive installations of groynes and spur dykes. The development of alternate bar structures is based on natural river forming processes that are inhibited at this part of the river reach. While the majority of the study reach is characterised by a stretched river course, the lowest few kilometres exhibit stronger curvature. This leads to point bar characteristics at this part of the river with typical bar formations at the inner sides of the bends and scours at the outer sides.

The repeatedly discussed erosion processes at this river reach in literature (*Kresser (1988)*, *Bors (1992)*, *Stiefelmeyer (2001)*) using different methods to determine the erosion rates, such as analyses of low water level fixations or changes of rating curves at gauging stations, can be confirmed by the current study when analysing the river bed surveys. Over the study period of ten years, a mean annual erosion rate of 2.4 cm per year is computed. This result fits well into the findings of other studies. Intensive river restoration works in the 19th century (flow concentration on the main channel, bank revetments, cut-off of side arms), installations of hydropower plants at the Danube river and its tributaries, and improvements of navigability (groynes) are responsible manmade reasons for the erosion of bed levels. These measures caused a significant increase of bed shear stress combined with a sediment deficit at the free flowing reaches.

Processing successive bed level surveys with respect to the sediment balance show both overall erosion and overall deposition processes. Although the river reach is in a stage of erosion, this general trend is not reflected by all surveys. Comparing the hydrological conditions with the morphological changes reduced by the regular grain feeding measures shows that generally high water volumes produce large overall erosion rates and reduced water volumes cause smaller bed level reductions, or in some cases depositions. When computing sediment balances one has to be

aware of possible uncertainties introduced by (a) inaccurate bed level surveys, (b) unknown amounts of bed load material transported over the dam of the upstream power station, and (c) sediment exchanges from unobserved shallow water reaches and the measured main channel. Uncertainties with respect to the short-term sediment balance can be eliminated by averaging over long time-periods to achieve a reliable mean trend of annual river bed changes.

Mean bed level changes exhibit distinct local longitudinal variations (fluctuations of erosion and deposition processes) in the short-term. In the case of the pre and post flood surveys these local variations are caused by the process of smoothing out discontinuities by the 100 year flood event. On a large scale (averaging over 10 km units), the bed changes exhibit continuous tendencies in most cases. A long-term analysis of the cumulative bed volume changes reveals stability at the upper 10 km of the study reach. Here, regular grain feeding measures prevent the river bed from erosion processes in the long-term (maintenance reach).

Several processing methods prove that over the ten year period, the positions of the morphological structures remain unchanged. Thus, from a planimetric perspective, the Danube river reach comprises a stable configuration. Even the 100 year flood causes solely minor re-distributions of the bar elements. Obviously, minor curvature, installation of groynes, and vegetation, protect the bars from propagation processes.

While the positions of the bars remain stable, distinct morphological changes are observed with respect to height changes at various morphological structures. At the alternate bar reach (upper half of the study reach), distinct deposition processes of the scours occur. As a consequence, the bars located at the opposite sides, are characterised by intensive erosion processes. These long-term river bed changes are partly attributed to scour filling measures that happened in the first half of the 1990's and grain feeding measures increasing the bed levels predominantly in the scour regions. As a consequence, these morphological changes lead to a decay of the geometrical features of the bars. Over a long-term period, these decay processes were also observed at the Salzach river. Further characteristic morphological processes at the study reach are observed at the crossings located between the alternate bar elements. These structures are characterised by considerable long-term bed level reductions. Intensive river dredging measures were performed at the crossings so that these changes are most likely not based on natural processes. Local erosion at the crossings have significant impact on the water levels induced by the reduced backwater effect of these structures. Analysis of the low water level fixations over a long-term period shows that on average the water level reductions are significantly larger than the bed level reductions. Compared to the bar reach (upper half), the groyne reach (lower half) is characterised by remarkably reduced spatial variability leading to monotonous erosion processes in the long-term.

Analysis of the profile shapes reveals that 80 % of the profiles at the Danube reach shows distinct asymmetrical profile shapes. The asymmetric profiles are typically found at the bar regions. Here the thalweg position is considerably skewed to one side of the river, while the other side comprises smooth slip-off slope banks. The asymmetric features of the reach remain virtually unchanged over the study period. The slip-off slope banks representing the bars comprise lateral

slopes of 2.5 % on average. The lateral slopes are 60 times larger than the longitudinal (0.04 %) indicating potential sorting processes at the bars (see Chapter 3).

In order to get a deeper insight into the morphodynamic processes, the spatial profile shape variations of successive profiles are compared to temporal profile shape variations. In the short-term, when processing the pre and post flood surveys, an overall weak relationship of spatial and temporal changes is given. Thus, the impressed spatial variability influences the temporal changes only to a minor degree. However, instantaneous spatial changes (peaks) induce increased temporal changes, indicating temporal adjustments to strong spatial changes. For the long-term development, spatial and temporal profile shape changes are considerably better related. Three types are distinguished: (a) stable, minor mobile reaches (small spatial diversity induces small temporal changes), (b) mobile reaches characterised by strong temporal changes induced by strong spatial diversity (cross-sectional profile shapes over time adjust to the upstream profile shapes), and (c) strong temporal changes (mostly at the upper 10 km) that are virtually not related to the smaller spatial variability. This is characteristic of the alternate bar region that is characterised by intensive vertical changes in a region of a stable planimetric configuration.

3 Numerical computation of bed deformation and sorting processes in a laboratory bend

3.1 Introduction

In Chapter 3 the morphological processes in river bends are investigated. A focus is drawn on numerical methods for calculating bed deformation and sorting processes. Morphological processes in river bends are discussed, and the possibilities of numerical models to describe these complex processes are shown. Bed deformation and sorting processes in a laboratory bend are computed by a modified three-dimensional numerical model. The laboratory experiments comprise unsteady flow and nonuniform sediment transport processes. The results are discussed with respect to the accuracy of the computations, and the sensitivity of relevant sediment parameters. On the basis of the gained experiences for the computation of morphological processes in a laboratory bend, the numerical model is tested on morphological processes of the Danube river (Chapter 4).

3.1.1 Processes in river bends

The morphology of natural rivers can be subject to considerable temporal and spatial changes. Variations of water discharge and water levels cause fluctuations of sediment transport leading to changes of the morphology of a river. Even for steady flow, sediment transport is organised in batch-wise movements, bed forms are built that propagate with different velocities. As a consequence of morphological changes, a river can significantly change its curvature over time. Anthropogenic measures such as the installation of hydropower plants, can intensify the variations and consequently cause a sustainable change in river bed morphology. Typical river bed configurations, found in nature are: (1) alternate bars in straight river reaches, (2) meandering of rivers, and (3) point bars in river bends. The grain size distributions of the river bed develop as a consequence of bed elevation changes. Longitudinal, lateral and vertical sorting processes in river beds can be observed. Usually the upper layers of natural river beds are composed of coarser sediments protecting the finer sediment layers below, a process denoted as armouring. Morphological changes in rivers have a great ecological impact and need to be carefully investigated.

There are many complex physical processes that are responsible for river bed deformations. To a certain degree, natural rivers always exhibit curvature. Therefore a special focus is drawn on processes in river bends in this Chapter. The processes of sediment transport in river bends are generally more complex compared to sediment transport in straight channels. The bed material in channel bends is subject not only to longitudinal transport but also to transverse transport induced by a spiral motion of the flow. Thus, bars develop at the inner bank and scours occur at the outer bank of the river bend. Additionally, the river bed in bends is subject to sorting processes. The secondary currents generally cause fine material to deposit at the inside of the curves, while erosion takes place at the outer bank, so that coarser material remains in this region. In combination with bed forms, this effect can cause spatial variation in the roughness of the bed in a bend influencing the flow field. Thus, there is a direct interaction of flow, sediment transport, and erosion and deposition processes in a

bend. The bed changes induced by erosion and deposition affect the flow which in turn influences the distribution of the bed shear stress and thus the bed load component and finally the bed topography.

When dealing with engineering problems concerning river bends, the practising engineers often face highly complex flow and sediment situations with highly nonuniform sediment size distributions and transport under unsteady flow conditions. Therefore it is of great importance to support engineers with powerful tools that are able to predict river bed changes accurately.

3.1.2 Literature review on bed changes and sorting processes

Complex phenomena of flow and morphodynamics in river bends have been broadly investigated in literature. Methods to describe or quantify the dynamics are quite diverse. Experimental, numerical, and analytical approaches are documented.

A study for sediment transport on side slopes was introduced by *Engelund (1974)*. The formula was based on static considerations of forces acting on a grain on side slopes. The approach was further developed by *Engelund (1981)*, by introducing an empirically derived modified Shields parameter considering the skin friction of the sediments resulting in a deviation angle between the sediment transport direction and the near flow direction. The input parameters are the transversal slope of the channel bed $\partial h/\partial n = \tan(\alpha)$, the Shields parameter related to the skin friction, and the specific weights of water and sediment.

Parker & Andrews (1985b) described sorting processes of bed load sediment in meander bends analytically. Their model is based on a relation between transverse and downstream bed load transport, considering the inward transverse pull on bed load grains due to secondary currents, and the lateral downslope pull on bed load grains due to gravity. A transverse force balance holds at first order for some grain sizes near the overall mean size of the surface bed material. This balance determines bed topography. The lateral downward pull, however, increases with grain size. According to *Parker & Andrews (1985b)*, as a consequence, for coarser grains the outward layer gravitational pull exceeds the inward pull of the secondary currents, and a net outward flux of coarse material is realized. In a similar way, finer material moves towards the inside of the bend. This sorting process is initiated at the upstream inflection point of a bend and is terminated at the downstream inflection point. The locus of coarse material moves constantly outwards as the bend is traversed in the downstream direction. For periodic bends, the locus of coarse material crosses from the inside to the outside at a point where the downstream centreline direction is parallel to the valley direction. This point is typically at or near the bend apex, i.e. the point of maximum centreline curvature.

Julien & Anthony (2002) investigated sorting mechanisms in a field study in the sharp meander bends of Fall River, Colorado. The authors derived a model from a three-dimensional moment analysis to account for the effect of particles resting on an embankment inclined at a side slope. The model predicts the downstream and transverse shear stress components and the particle orientation angle that allows an assessment whether a particle moves towards the point bar or the thalweg. The input parameters are particle size d, water depth h, downstream channel slope angle Θ_0, side slope angle Θ_1, and bed shear stress τ_b. The field measurements in two meander bends corroborate the theoretical model: particles finer than d_{50} (1 mm) preferentially move up the point bar and particles

coarser than d_{50} move towards the thalweg. The measured deviation angle between the mean trajectory of 0.125 mm and 32 mm particle reaches 20° near the bend apex.

Lanzoni (2000b) investigated the development of alternate bars in a straight laboratory flume using a nearly uniform sand under controlled steady flow conditions. Experimental values of bar wavelength and bar celerity were compared to the theoretical estimates obtained from a model developed within the classical framework of linear stability analysis, that gave quantitatively satisfactory predictions of bar wavelength. In a companion study by *Lanzoni (2000a)*, the role of the nonuniform character of sediment often exhibited by river beds was discussed. Laboratory experiments were performed in the same flume, but for this study using a bimodal sediment mixture in a range of flow conditions was used, such that the initially flat bed became unstable enhancing the development of alternate bars. The mean geometric grain diameter was chosen to be the same as in the experiments with uniform sediments. The comparison suggested that sediment heterogeneity may appreciably affect bed form characteristics. The development of small scale and mesoscale sediment waves tended to be inhibited thus allowing a decrease in flow resistance. *Lanzoni (2000a)* observed, that selective transport of individual grain size fractions, coupled with the characteristic bar topography pattern led to an intensive longitudinal sorting which accreted the coarser particles on bar crests. Furthermore, bar migration caused, through scour and fill, a significant vertical sorting. As a consequence of these sorting processes and in accordance with previous experimental observations, bar height turned out to be damped with respect to the uniform sediment experiments.

Odgaard & Bergs (1988) studied the dynamic features of the flow and sediment transport in a 180° constant-radius, recirculating laboratory channel with a trapezoidal shape of the cross-sections. The channel bottom was filled at the beginning of the experiment with a 23 cm thick flat horizontal layer of sand with d_{50} = 0.35 mm and d_{90} = 0.53 mm. During the run, the discharge was kept constant at a rate of 0.153 m³/s, the sediment moved mainly as bed load at an inflow rate of 3.7 g/(cm*min). The experiment was run until an equilibrium steady state for the bed bathymetry and the flow was reached. The bed and water surface elevations and the depth averaged velocities at several sections were measured for equilibrium conditions. At equilibrium conditions, characteristic erosion and deposition patterns were measured. According to *Odgaard & Bergs (1988)*, one of the most important observations in this study was the effect, that changes in curvature had on the bend flow processes. The flow and bed topography responded to a curvature change like a damped oscillating system. The experiments of *Odgaard & Bergs (1988)* were used by numerous numerical investigations for validation purposes (*Wu et al. (2000a)*, *Minh Duc et al. (2004)*, *Zeng et al. (2005)*).

3.1.3 Relevance of numerical models

In addition to the use of laboratory experiments or field studies, more and more numerical models are used to gain insight into the phenomena and processes of complex hydraulics and morphology. Over the last two decades, the computational power has increased tremendously, and numerical models have become progressively more a competitive tool to laboratory experiments. While there is a well-defined state-of-the-art for computing the hydraulics of flows in channels and natural rivers, complex computations of sediment transport and associated morphodynamics are still in a state of research. Due to the need of excessive computational resources, especially for

multidimensional modelling, the application and development of numerical-morphodynamic models is mainly limited to research institutions. There exists a number of 1D, 2D, and 3D approaches for the computation of the dynamics of flow and morphology. 1D approaches are well documented but they are inherently limited to 1D flow and sediment transport problems, such as section integrated erosion or deposition processes in a straight river reach. Local bed changes cannot be computed using 1D methods. A widely used alternative to 1D approaches are 2D models, that can predict morphological changes satisfactory when the 3D nature of the processes is of minor importance, such as in many open channel flows, when the width-to-depth ratio is large, so that the vertical velocity component is much smaller than the horizontal components and the pressure distribution is virtually hydrostatic.

The difficulty with respect to 2D models is that they neglect the influence of secondary flows. Empirical parameters are often introduced trying to compensate significant 3D effects in 2D models, such as the lateral migration of channel banks or the effects of secondary flows on sediment transport and morphological changes.

According to *Olsen (2003)*, the main simplifications of 2D models with respect to flow and sediment computations are:

> ➢ removing all terms that include the vertical velocity
> ➢ assuming a hydrostatic pressure distribution in the vertical direction
> ➢ assuming a vertical streamwise velocity profile that follows a power law formula
> ➢ assuming an empirical vertical distribution of the transverse velocity
> ➢ assuming isotropic distribution of the eddy viscosity
> ➢ assuming the bed shear stress direction is the same as the depth-averaged water velocity
> ➢ assuming all derivatives to be zero
> ➢ assuming the water velocity and water depth to be constant along the centreline of the flow.

After *Zeng et al. (2005)* a 2D model and even a 3D hydrostatic model would not be able to accurately predict flow and transport phenomena in regions where the flow is strongly 3D and large adverse pressure gradients and/or massive separations are present (e.g. river reaches containing hydraulic structures). Realistic computations of flow and morphodynamics, where 3D effects are not parameterised but computed directly can only be performed using a fully 3D non-hydrostatic model. The advantage of 3D approaches is that many of the processes in a meandering or curved channel are modelled directly instead of using simplifications. For curved channels, the helical (secondary) flow exists due to the difference between the centrifugal forces acting on the upper and lower layers of flow. The helical flow plays an important role in the evolution of channel topography. The application of a fully 3D model should give superior results compared to a parameterised 2D model when calculating flow and sediment transport in channel bends.

3.1.4   Literature review on numerical models

In recent years, several 2D and 3D numerical morphodynamic models have been developed, for predicting bed deformation and in some cases sorting processes for graded sediment size distributions.

Minh Duc et al. (2004) propose a 2D depth-averaged model using a finite volume method with boundary-fitted grids. The sediment transport module is comprised of semi-empirical models for suspended and non-equilibrium bed load transport. The secondary flow transport effects are taken into account by calibrating the dimensionless diffusivity coefficient in the depth-averaged k-ε turbulence model. A quasi 3D flow approach is used to simulate the effect of secondary flows characterised by channel curvature on bed load transport. For the calculation of the bed shear driven resultant bed load, the empirical formulas by *v.Rijn (1984a)* are used. Among others, the model is validated on laboratory experiments in river bends of *Odgaard & Bergs (1988)* and *Yen & Lee (1995)*. The model set up for validating the experiments by *Yen & Lee (1995)* are simplified by assuming the uniform instead of a graded sediment size distribution. Thus, relevant observed sorting processes are neglected by the 2D model.

Wu & Wang (2004) propose a 2D depth-averaged model for computing flow and sediment transport in curved channels. Owing to the fact that helical flow significantly affects the flow, sediment transport, and morphological evolution in curved channels, a semi-empirical formula is presented to determine the cross-stream distribution of the helical flow intensity in the developed regions of a channel bend. It is used to evaluate the dispersion terms in the depth-averaged 2D momentum equations and suspended load transport equation as well as the bed load transport angle. The sediment transport formulas introduced by *Wu et al. (2000b)* are implemented. By calibrating two parameters of the introduced helical flow intensity model, the experiments by *Yen & Lee (1995)* are used for validation. Here, eight sediment size fractions are chosen to represent the nonuniform sediment mixture, so that the sediment sorting processes are computed by the model.

A 3D model for the calculation of flow and sediment transport is proposed by *Wu et al. (2000a)*. The flow is calculated by solving the Reynolds-averaged Navier-Stokes equations with the k-ε turbulence model. Suspended load transport is simulated by the general convection-diffusion equation with an empirical settling velocity term. Bed load transport is simulated using a non-equilibrium method and the bed deformation is obtained from an overall mass-balance equation. The empirical formulas of *v.Rijn (1984a)* and *v.Rijn (1984b)* are implemented for the computation of bed and suspended load. The model is not able to account for the effect of transverse bed slope on the bed load transport. The model is tested by calculating the flow and sediment transport of the experiments by *Odgaard & Bergs (1988)*. Due to the fact, that uncertainties remain with respect to the description of parameters of the non equilibrium term, the model is only tested for near-equilibrium steady state situations.

Olsen (2003) introduces calculations of a self-forming meandering channel. The model results are compared to results from laboratory studies by *Zimpfer (1975)*. The fully 3D numerical model is based on the finite volume method using an unstructured grid with dominantly hexahedral cells. The k-ε model is used to for turbulence modelling and the SIMPLE method is chosen to compute the non-hydrostatic pressure. The sediment transport is computed as bed load in addition to solving the convection-diffusion equation for suspended sediment transport. The empirical formulas by *v.Rijn (1984a)* and *v.Rijn (1984b)* are used for the computation of bed and suspended load. The formulas are based on predicting transport of fine sand and silt in a marine environment for grain diameters up to 2 mm.

Fischer-Antze et al. (2004) simulate morphological bed changes in a reach of the Danube river as a consequence of a flood event. The numerical model is modified by incorporating sediment transport formulas by *Wu et al. (2000b)* to account for hiding and exposure effects. Significant bed changes in the river reach are successfully modelled by the modified approach. The same numerical model is applied by *Ruether & Olsen (2005)* to simulate the velocity distribution and bed level changes over time in a 90° channel bend by a fully 3D numerical model. The authors introduce relationships to determine the particle flow direction on a lateral slope. The results give an increased accuracy when introducing a particle deviation approach.

Zeng et al. (2005) present a fully 3D model to solve the flow, bed load transport and bed morphology changes in open channel flows. The non-hydrostatic model solves the 3D Reynolds averaged Navier-Stokes equations with integrations up to the wall such that the use of wall functions is avoided. The k-Ω model is implemented, a non-equilibrium bed load sediment transport model is used with additional introduction of down-slope gravitational force effects. The empirical formulas proposed by *v.Rijn (1984a)* for the equilibrium bed load transport rate are used in the study. Among others, the experiments by *Odgaard & Bergs (1988)* are employed to validate the model.

In this study, the fully 3D non-hydrostatic model *SSIIM*, developed by *Olsen (2004)*, serves as the basis for the computation of unsteady flow, sediment transport, and morphological changes. The sediment transport module of the model is modified by incorporating the nonuniform sediment transport formulas by *Wu et al. (2000b)* considering hiding-exposure effects.

The concept of the study is to expand the possibilities of the numerical model, that was originally designed to compute sedimentation processes in water reservoirs of hydropower plants. The original model computes sediment transport processes using the formulas of *van Rijn* (*v.Rijn (1984a)* and *v.Rijn (1984b)*). The formulas are based on predicting transport of fine sand and silt in a marine environment and are therefore mostly tested for sedimentation processes. For situations with prevailing bed load transport of gravel material, the originally incorporated formulas are not appropriate.

In a study performed by *Scheer et al. (2002)*, the behaviour and verification of sediment transport formulas for graded sediments are investigated. 17 transport formulas of ten authors/research groups (*Ackers&White, Parker, Engelund&Hansen, Meyer-Peter&Müller, Van Rijn, Hunziker, Gladkow&Söhngen, Wu et al., Wilcock&Crowe and Ribberink*) are tested. Bed load transport formulas for uniform and nonuniform sediments are considered. Three different parameters are chosen to investigate the validity range of the formulas: the median grain size of the bed material (d_{50}), the geometric standard deviation (σ_g) of the bed material, and the Shields parameter (θ). The formula of *Wu et al. (2000b)* proved to have the largest validity range of all analysed formulas. This formula is based on a large set of experimental and field measurements.

The transport formulas are verified by comparing transport predictions with measurements originating from ten sets of laboratory experiments. The results show that the fractional formula of *Wu et al. (2000b)* gives the best transport rate predictions. Moreover, the formula of *Wu et al. (2000b)* gives the best transport composition predictions. Generally the fractional formulas show superior

results compared to their uniform counterparts. All formulas show deviations when predicting the transport composition at low Shields parameters. Many formulas show good transport rate predictions for experiments with a median grain size smaller than their validity range. "Based on the study, it can be concluded that the formulas of *Wu et al. (2000b)* is the best formula for sediment transport." (*Scheer et al. (2002)*).

Based on the study of *Scheer et al. (2002)*, *Kroekenstoel & van Welzen (2003)* performs morphological computations in a comparative study on two laboratory case studies (*Günter (1971)* and *Ribberink (1987)*). *Günter (1971)* examined erosion processes and the evolution of armouring layers, and *Ribberink (1987)* investigated sedimentation processes. Two 1D morphodynamic models are applied to test three transport formulas:

The Swiss model MORMO is applied to test the formula of *Hunziker (1995)* and the Dutch model SOBEK-Graded is applied to test the formulas of *Meyer-Peter & Müller (1949)* and *Wu et al. (2000b)*. For both case studies, the Hunziker formula performs best and the *Wu* formula achieves a good second place. The tests on two case studies are not necessarily representative for the quality of the three formulas and/or the chosen mathematical models, but the results generally suit the findings by *Scheer et al. (2002)*.

Due to the good performance of the *Wu et al. (2000b)* formula presented in the two studies, this approach is incorporated into the existing numerical three-dimensional model *SSIIM*. The motivation is to modify the numerical model to account for the effects of sorting, hiding-exposure and to predict sediment transport and bed-changes for an enhanced range of applicability more accurately than the original model. The modified model is validated on laboratory experiments in a 180° channel bend performed by *Yen & Lee (1995)*. These experiments are challenging for a numerical model as they combine four important processes that are often found in natural river flows:

- ➢ flow in a bend with predominating secondary currents,
- ➢ unsteady flow using a triangle hydrograph,
- ➢ bar development in a mobile bed channel bend , and
- ➢ graded bed material used.

3.2 Laboratory experiments

The laboratory data used for validating the numerical model introduced in this study are performed by *Yen & Lee (1995)*. The experiments are conducted in a laboratory channel bend having a central angle of 180°, a radius of curvature along the central line in the bend of r_c = 4 m, and a width of B = 1 m. The bend is connected with a stilling basin, an upstream straight reach of 11.5 m, a downstream reach of the same length, and a sediment settling tank. The laboratory geometry is shown in Figure 3.8. The water depth is controlled by a weir at the downstream end, which is positioned as to produce a uniform flow along the bend with the base flow discharge. Each cross-section of the bend is identified by its respective angular position. In the upstream straight reach, it is identified by the distance from the beginning of the bend (negative), and in the downstream straight reach by the distance from the end of the bend (positive). The base flow is set at Q_0 = 0.02 m³/s, corresponding to a base flow depth of h_0 = 5.44 cm and a shear velocity of the base flow of u_{*0} = 0.031 m/s. The

sediments are specified by the initial median diameter of d_{50} = 1.0 mm and the standard deviation of sediment-size gradation of σ_0 = 2.5 (see Figure 3.2).
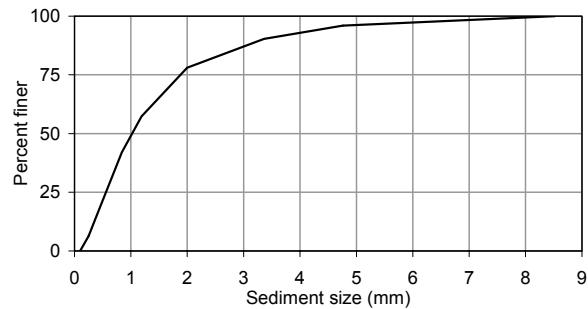
Figure 3.1: Initial sediment size gradation curve

All experiments have an initial bed slope of I_0 = 0.002. Bed topography and transverse sediment sorting are investigated. Five experiments are performed, each having the same initial sediment-size gradation but different inflow hydrographs. At various sections of the bend, bed elevations are measured and bed surface sediments are sampled at the peak and the end of the hydrograph in each experiment. The sediment settling tank is lifted for sampling and the sediment accumulated during the period is weighed. At the end of the runs, sampling of the surface bed layer is conducted at six locations with a melted wax procedure.

The results indicate that for all experiments bars evolve at the inner bank while scours evolve at the outer bank of the channel. As a consequence, lateral sorting processes occurre with the largest intensity in the area around 90°, indicated by diameters larger d_{50} at the outer bank and smaller d_{50} at the inner bank. The maximum deposition height is situated between section 75° and 90°, and the maximum scour depth occurs between 165° and 180°. The measurements indicate that the characteristics of the hydrograph has prominent influences on bed topography and transverse sediment sorting. According to *Yen & Lee (1995)*, the cases with a higher ramping rate of the hydrograph have greater deposition heights near the inner bank and larger scour depths near the outer bank. Furthermore, the sediment is finer near the inner bank and coarser near the outer bank in cases with a higher ramping rate.

In this study, run #4 is applied to validate the numerical model. As shown in Figure 3.2, the duration of this run is 300 min, using a triangle-shaped hydrograph with a linearly rising and falling limb. The peak discharge of Q_P = 0.053 m³/s is reached at t_P = 100 min.
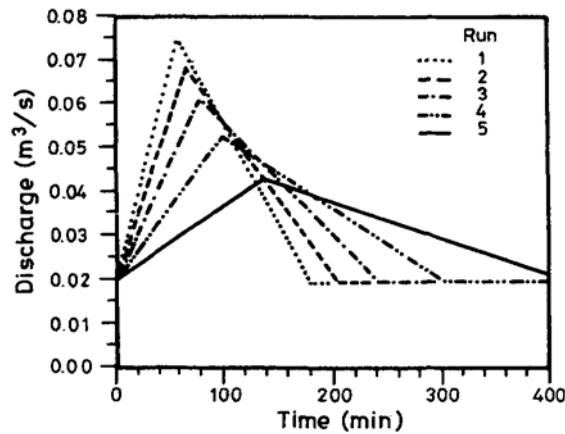
Figure 3.2: Hydrographs for laboratory experiments by *Yen & Lee (1995)*

3.3 Methods

The three-dimensional numerical model *SSIIM* used in this study was originally developed by *Olsen (1991)* for the simulation of sediment movements in water intakes with multiblock option. Originally, the model run under the operating system OS/2 and was applied for the computations of suspended sediment transport of fine sediments by solving the convection-diffusion equations. Enhancements of the model included unsteady calculations of the water flow, free surface calculations instead of fixed backwater calculations, and improved post processing options. In 2001, the model was restructured, it was ported to Microsoft Windows and compiled using DLL's (dynamic link libraries) (*Olsen (2004)*). This model structure allows cooperating researchers to modify outsourced parts of the code without changing the main hydrodynamic module. In this study the bed module (beddll) was modified. Nonuniform sediment transport routines including a hiding-exposure approach (*Wu et al. (2000b)*) were incorporated allowing to consider the interaction of different sediment size fractions.

3.3.1 Computing the flow

Numerous new developments of three-dimensional hydrodynamic models have been introduced over the last two decades by a variety of researchers (e.g. *Tritthart (2005)*, *Hervouet et al. (1994)*, *Fluent (2003)*, *Luijendijk (2001)*). Details on the derivation of the governing equations and numerical implementations can be found there and in *Olsen (2004)*. An overview of the relevant theoretical background is given here.

The numerical model *SSIIM* (*Olsen (2004)*) computes the hydrodynamics for a general three-dimensional geometry by solving the Reynolds averaged Navier-Stokes equations using the continuity equation:

$$\frac{\partial U_i}{\partial x_i} = 0 \tag{3.1}$$

$$\frac{\partial U_i}{\partial t} + U_j \frac{\partial U_i}{\partial x_j} = \frac{1}{\rho} \frac{\partial}{\partial x_j} \left(-P \delta_{ij} - \rho \overline{u_i u_j} \right) \tag{3.2}$$

U is the velocity averaged over the time t, x is the spatial geometrical scale, ρ is the water density, P is the pressure, δ_{ij} is the Kronecker delta, and u_i is the velocity fluctuation in time. The left

term on the left side of equation (3.2) is the transient term. The next term is the convective term. The first term on the right side is the pressure term. The second term on the right side of the equation is the Reynolds stress term which is modelled by a turbulence model.

The correlations of the fluctuations $\overline{u_i u_j}$ characterise the turbulent motion in a flow. This value is a measure for the momentum exchange caused by the fluctuations. It can be considered as an internal shear stress. When multiplied with the density of water ρ, the Reynolds stress term is obtained representing the transport of momentum or mass due to the fluctuating turbulent motion. $-\rho \cdot \overline{u_i u_j}$ is the transport of x_i-momentum in the direction x_j or vice versa. The Reynolds stress term is not found in the original Navier-Stokes equations but is a product of the averaging procedure, that is added to the flow velocities in the three directions and the pressure. For the closure of the system of equations, additional equations are needed. Empirical or semi-empirical turbulence models are used to estimate the value and the distribution of the turbulent shear stresses (Reynolds stresses). The turbulence model cannot serve to compute all details of the turbulent motion, but it represents their effect on the averaged flow *Rodi (1984)*.

The k-ε turbulence model is chosen in this study. Based on an eddy viscosity concept, the turbulent shear stresses are related to the gradients of the velocities.

$$-\overline{u_i u_j} = v_t \left(\frac{\partial U_i}{\partial x_j} + \frac{\partial U_j}{\partial x_i} \right) - \frac{2}{3} k\, \delta_{ij} \quad \text{with} \quad v_t = \frac{c_\mu \cdot k^2}{\varepsilon}, \tag{3.3}$$

The turbulence features can be described by two parameters, k, the turbulent kinetic energy, and ε, the dissipation rate of the turbulent kinetic energy. These parameters determine the eddy viscosity v_t and they are obtained from the following semi-empirical equations:

$$\frac{\partial k}{\partial t} + U_j \frac{\partial k}{\partial x_j} = \frac{\partial}{\partial x_j} \left(\frac{v_t}{\sigma_k} \frac{\partial k}{\partial x_j} \right) + P_k - \varepsilon \tag{3.4}$$

$$\frac{\partial \varepsilon}{\partial t} + U_j \frac{\partial \varepsilon}{\partial x_j} = \frac{\partial}{\partial x_j} \left(\frac{v_t}{\sigma_\varepsilon} \frac{\partial \varepsilon}{\partial x_j} \right) + C_{\varepsilon 1} \frac{\varepsilon}{k} P_k - C_{\varepsilon 2} \frac{\varepsilon^2}{k} \tag{3.5}$$

The production of turbulent kinetic energy P_k is defined as:

$$P_k = v_t \frac{\partial U_i}{\partial x_j} \left(\frac{\partial U_j}{\partial x_i} + \frac{\partial U_i}{\partial x_j} \right) \tag{3.6}$$

The empirical constants are determined from measurements by *Launder & Spalding (1974)*:

Table 3.1: Values of the constants in the k-ε model

C_μ	$C_{\varepsilon 1}$	$C_{\varepsilon 2}$	σ_k	σ_ε
0.09	1.44	1.92	1.0	1.3

The computation of the bed shear stress τ_b plays an important role for the computation of sediment transport. Since most empirical sediment transport formulas are based on an excess shear

stress concept, the bed shear stress acts as the interface of flow and sediment transport computations. Following the boundary conditions for rough walls, the log law, the bed shear stress τ_b is written as:

$$U_0^+ = \frac{\kappa \cdot U_0}{\ln(\frac{30y}{k_s})}$$

(3.7)

$$\tau_b = \rho \left(U_0^{'+}\right)^2$$

(3.8)

When assuming that the production of turbulence is equal to the dissipation near the boundary *Rodi (1984)*, one obtains:

$$\tau_b = \sqrt{c_\mu}\,\rho k$$

(3.9)

The control volume method is used for discretisation. Therefore the geometry is divided into elements or finite volumes. The convective terms and the orthogonal diffusive fluxes in the Navier-Stokes equations are solved by the second order upwind (SOU) scheme using equation (3.10) for the velocity in cell *P*, where the neighbouring cells of cell *P* in all directions (*E* = east, *W* = west, *N* = north, *S* = south, *T* = top, *B* = bottom) and the neighbours of the neighbours (*EE* = east of east cell, *WW* = west of west cell, *NN* = north of north cell, *SS* = south of south cell, *TT* = top of top cell, *BB* = bottom of bottom cell) are considered. The non-orthogonal fluxes are neglected:

$$a_p U_p = \sum_{nb=1}^{12} a_{nb} U_{nb} , \qquad nb = EE, E, WW, W, NN, N, SS, S, TT, T, BB, B$$

(3.10)

where the a_{nb} coefficients are weighting factors for the 12 cells surrounding cell *P*. A detailed discussion of the SOU scheme is given in *Olsen (1999)* and *Olsen (2004)*. An implicit method is used for time integration and the pressure field is computed with the SIMPLE method (*Patankar (1980)*). The acronym stands for semi-implicit method for pressure-linked equations. The algorithm is based on a guess-and-correct procedure for the calculation of the pressure. The Rhie and Chow interpolation (*Rhie & Chow (1983)*) is applied to compute the velocities and the fluxes at the cell surfaces.

3.3.2   Computing sediment transport

In river hydraulics, sediment is defined as solid material that is transported by the water flow. Usually, the sediments consist of mineral materials, that form the mobile bed of a channel. Whether the particles get mobilised or remain on the river bed is related to the flow intensity and the properties of the material (*Schröder & Zanke (2003)*).

The motion of particles in rivers can be classified by the mode they are conveyed by the flow. Three modes of sediment transport can be distinguished, suspended, wash, and bed load transport. Suspended load transport takes place over the whole water body. Sediment particles may reach the ground but generally they are conveyed in suspension. This transport mechanism may change as the topography of the channel changes. For instance, a widening of a river causes the flow velocity to decrease and particles in suspension may settle. Very small particles are transported as wash load being in suspension so they never get into permanent contact with the channel bed. They do not

contribute to morphological bed changes. Coarser particles are mainly conveyed near the ground as bed load transport. Two modes of transport are distinguished, rolling and saltating movements. In the rolling mode, the sediment is constantly in contact with the river bed. Mainly, the sediment particles with large diameters are transported in this way. In the saltating mode, the sediment particle is not constantly in contact with the river bed. With the flow, the particle leaves the river bed and falls back onto it, the saltation movement is characterised by a saltation height. According to *v.Rijn (1984a)* the saltation of small particles is dominated by drag forces resulting in long but flat particle trajectories, while the saltation of large particles is dominated by lift forces resulting in short but high trajectories. The parameter u* or the excess from the critical parameter (u*-u*$_{cr}$) can be used to differentiate between these two modes. From these findings, by using the saltation height and the particle velocity, *v.Rijn (1984a)* derived a bed load transport formula for small size particles ranging from 0.2 to 2 mm. In the present study morphological phenomena are investigated that are mainly induced by bed load transport processes. Therefore approaches describing these processes are presented herein.

In a morphodynamic model, the boundary conditions at the bed are given by sediment transport relations. In the default configuration of the morphodynamic model, fractional bed load transport is computed by the formulas of *v.Rijn (1984a)* applied individually for each fraction. Interaction between each individual grain size is not considered:

$$\frac{q_{b,i}}{d_i^{1.5} \cdot \sqrt{\frac{(\rho_s - \rho) \cdot g}{\rho_s}}} = 0.053 \cdot \frac{\left(\frac{\tau - \tau_{c,i}}{\tau_{c,i}}\right)^{1.5}}{d_i^2 \left(\frac{\rho_s / (\rho - 1) \cdot g}{\nu^2}\right)^{0.1}} \qquad (3.11)$$

For fractional transport with nonuniform sediments, *Wu et al. (2000b)* introduces an approach considering the interaction between different size fractions. A correction factor accounts for hiding and exposure mechanisms and is assumed to be a function of the hiding and exposing probabilities, stochastically related to the size and gradation of the bed material. A definition sketch of the exposure height is shown in Figure 3.3.
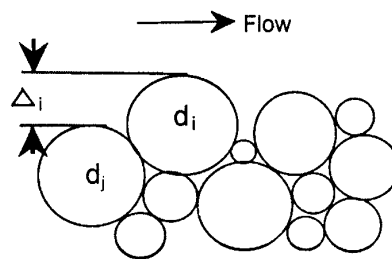
Figure 3.3: Definition of exposure height of bed material (from: *Wu et al. (2000b)*)

The probability of particles d_j staying in front of particles d_i is assumed to be the percentage of particles d_j in the bed material, p_{bj}. Therefore, the probabilities of particles d_i hidden and exposed by particles d_j is obtained as:

$$p_{hi} = \sum_{j=1}^{N} p_{bj} \frac{d_j}{d_i + d_j} \qquad (3.12)$$

$$p_{ei} = \sum_{j=1}^{N} p_{bj} \frac{d_i}{d_i + d_j} \qquad (3.13)$$

$$\eta_i = \left(\frac{p_{ei}}{p_{hi}}\right)^m \qquad (3.14)$$

where N is the total number of particle size fractions of nonuniform sediment mixtures, p_{bi} and d_i are the percentage and the diameter of the ith fraction, respectively, η_i is the correction factor and m is a constant determined to be –0.6 by default. The exponent in the hiding function is often used as a calibration parameter in morphodynamic models.

The hiding and exposure factor is used to modify the criterion for incipient sediment motion for each fraction,

$$\frac{\tau_{ci}}{(\gamma_s - \gamma)d_i} = \theta_c \cdot \eta_i \qquad (3.15)$$

where τ_{ci} is the critical shear stress for particle d_i in nonuniform sediment mixtures, γ_s and γ are the specific weights of sediment and water, respectively and θ_c is a constant set to 0.03. The non-dimensional fractional bed-load transport rate ϕ_{bi} is defined as

$$\phi_{bi} = \frac{q_{bi}}{p_{bi}\sqrt{(\gamma_s - \gamma)gd_i^3}} \qquad (3.16)$$

where q_{bi} is the transport rate of the ith fraction of bed-load per unit width. By a regression analysis using least square curve fitting, the following relationship is obtained,

$$\phi_{bi} = 0.0053 \left[\left(\frac{n'}{n}\right)^{1.5} \frac{\tau_b}{\tau_{ci}} - 1\right]^{2.2} \qquad (3.17)$$

where n' is Manning's coefficient corresponding to grain roughness, here calculated with $n' = d_{50}^{1/6}/20$, n is the Manning's coefficient for the channel bed and τ_b is the bed shear stress.

Various approaches are documented in literature describing the movement of particles situated on side slopes, that are usually found in river bends with developed bar structures (e.g. *Kikkawa et al. (1976)*, *Ikeda (1982)*, *Parker & Andrews (1985a)*,). In these situations, the direction of particle movement deviates from the streamline direction. The morphodynamic model *SSIIM* accounts for side slope effects applying two approaches, (1) reducing the critical shear stress for incipient sediment motion, and (2) computing the deviation angel between flow direction and sediment transport on laterally inclined slopes. The first approach was introduced by *Brookes (1963)*. In this study, a factor K is given, that is used to reduce the critical shear stress for sediments on slopes. K is a function of the sediment's friction angle of repose, the transversal slope, and the direction of the near bed velocity:

$$K = -\frac{\sin\alpha \cdot \sin\delta}{\tan\Phi} + \sqrt{\left(\frac{\sin\alpha \cdot \sin\delta}{\tan\Phi}\right) - \cos^2\Phi\left[1 - \left(\frac{\tan\alpha}{\tan\Phi}\right)\right]}$$ (3.18)

where δ =angle between the stream line and the direction of the near bed flow velocity, α = transversal slope of the channel bed, Φ = slope parameter similar to the sediment's friction angle of repose. The second approach accounts for the deviation angle on side slopes, it was introduced by *Engelund (1974)*. The formula is based on static considerations of forces acting on a grain on side slopes. The approach was further developed by *Engelund (1981)*, by introducing an empirically derived modified Shields parameter considering the skin friction of the sediments:

$$\tan\Psi = \frac{0.6}{\sqrt{\theta'}} \cdot \frac{\partial h}{\partial n}$$ (3.19)

$$\theta' = 0.4 * \theta^2 + 0.06$$ (3.20)

$$\theta = \frac{\tau_b}{(\gamma_s - \gamma)d}$$ (3.21)

where Ψ = angle between the sediment transport direction and the near flow direction, $\partial h/\partial n$ = $\tan(\alpha)$ = transversal slope of the channel bed, θ' = Shields parameter related to the skin friction, θ = Shields parameter. In a river bend with an initially flat bed, the bed load particle moves in the direction of the near bed flow which is skewed inwards as a consequence of secondary currents. However, as the deformation of the bed develops, the direction of the particle starts deviating from the flow direction. The more the side slope is developed, the more the particle is oriented towards the outer bend as an effect of gravity (*Ruether & Olsen (2004)*). This mechanism is shown in Figure 3.4.
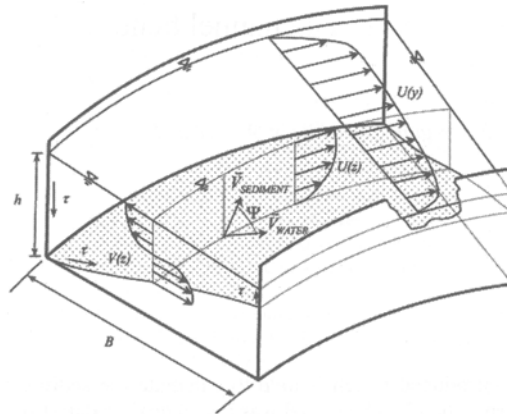
Figure 3.4: Velocities and sediment directions on a sloping bed in a channel bed (from: *Ruether & Olsen (2004)*)

The computation of sediment transport and morphological processes requires a good choice of appropriate sediment transport formulas. The transport formulas are based on empirical relationships that have been tested for different ranges of applicability. In the last three decades approximately thirty sediment formulas have been published, usually derived from different laboratory flume tests under various flow and sediment conditions and tested on laboratory and field data. The deviation of

computed and measured quantities can achieve up to three orders of magnitude, especially for low Shields parameters ($\theta < 0.1$) (*Kroekenstoel & van Welzen (2003)*).

For the case of fractional sediment transport formulations *Kroekenstoel & van Welzen (2003)* give three sediment parameters that are crucial for the interaction of flow, sediment composition, and sediment transport. These parameters are often used for adjustments. The data for deriving sediment transport formulas often cover large ranges of flow situations, geometrical configurations, and grain sizes. Thus, the derived formulas represent an averaged approach that might deviate considerably from individual test data relations. On this account, morphodynamic computations generally need adjustments of relevant sediment parameters to reproduce the morphological processes correctly. Relevant sediment parameters are:

> ➢ critical bed shear stress for incipient sediment motion
> ➢ ripple factor
> ➢ hiding and exposure coefficient

In the present study, parameter variations were performed and the sensitivity on the computed bed changes was investigated.

3.3.3 Boundary and initial conditions

For the numerical solution of the flow and transport equations, boundary conditions are needed for the whole simulation period on all boundaries being the inflow, the outflow, and the walls (bed and side wall). Two types of boundary conditions can be distinguished,

> ➢ Dirichlet boundary conditions specify values of the variables
> ➢ Neumann boundary conditions specify their gradients, often set to zero.

Initial conditions have to be specified at the beginning of the computations. A one-dimensional back water calculation is performed to obtain the initial water level. Initial conditions need to be specified for all variables. The pressure is set to zero, using a logarithmic vertical velocity profile, the velocities in flow direction are specified from the backwater calculation. The flow velocities in cross-streamwise and vertical direction are initially set to zero. The mean sieve curve of the bed material needs to be specified. The sieve curve is uniformly distributed over the whole river reach. The initial roughness can either be set constant or computed by the model as a function of the sediment size distribution. Both approaches are tested in this study.

Zero gradient boundary conditions are used for all variables at the outflow boundary. The temporal variations of the water levels are given over the whole simulation period as a stage hydrograph at the outflow boundary for sub-critical flow conditions. No boundary conditions need to be specified for the pressure at the outflow.

Velocities are specified at the inflow boundary (Dirichlet boundary condition). The temporal variation of the inflowing discharge is specified as flow hydrograph. The sediment inflow is specified for each time step on the inflowing cross-section.

The flux through the bed or wall is zero, so theoretically, boundary conditions set to zero can be given. However, the flow gradient towards the wall is steep, requiring a large number of grid cells to

resolve the gradient sufficiently. To avoid an extensive vertical grid resolution usually wall laws for rough boundaries that consider the roughness k_s are defined for the first cell at the bed or side wall. Wall laws introduced by *Schlichting (1979)* are used at the side walls and the bed:

$$\frac{U}{u_*} = \frac{1}{\kappa} \ln \frac{30y}{k_s}$$

(3.22)

where k_s is the wall roughness, u_* is the shear velocity, y is the distance from the wall and κ is the Karman constant, set to 0.4. Wall laws are used for both the velocities and the turbulence parameters. At high Reynolds numbers, k and ε near the wall are defined as:

$$k = \frac{u_\tau^2}{\sqrt{c_\mu}}$$

(3.23)

$$\varepsilon = \frac{u_\tau^3}{\kappa y_p}$$

(3.24)

Further details can be found in (*Rodi (1984)*, *Ferziger & Peric (2002)*). The sediment concentrations at the bed are defined by equilibrium concentrations in the cell close to the bed determined by the sediment transport formulas.

The water surface was modelled as a symmetry plane, thus the streamwise and cross-streamwise velocities are set equal to the values in the layer below. The vertical velocity is set to zero. *Ferziger & Peric (2002)* suggests zero values for the turbulence parameters.

3.3.4 Computing morphological changes

The vertical bed changes are based on sediment continuity for the bed cell, they are computed from the difference of inflowing and outflowing sediment fluxes. The defect is converted into a vertical bed elevation by dividing it by the submerged density of the sediments (1320 kg/m³) to find the volume of the deposition or erosion for each time step. This is then transformed into bed level changes for the grid. Both the sedimentation and the erosion processes are modelled using the same approach:

$$\Delta z_0 = \frac{\Delta t \, r \, (Flux_{in} - Flux_{out})}{A}$$

(3.25)

$$Flux_{In} = \sum_{nb} a_{nb} \, c_{nb}$$

(3.26)

$$Flux_{Out} = c_{bed} \sum a_{nb}$$

(3.27)

where r is the ratio of the compact sediment density (2650 kg/m³) and the submerged sediment density of the bed (approx. 1320 kg/m³). $Flux_{in}$ and $Flux_{Out}$ are the inflowing and outflowing sediment fluxes in a cell.

When fractional transport is computed, sorting mechanisms are considered by the definition of an exchange layer (denoted as active layer) and an inactive layer where the sediment continuity equation is solved separately for each fraction. The river is subdivided into three layers, (1) a water layer near the river bed, with a mixture of water and sediments, (2) an upper sediment layer (active) where sediments do not move with the water; depending on the relevant process, material is entrained

or deposited (exchange process with water layer), and (3) a lower sediment layer, denoted as inactive layer. The vertical size of the active layer is usually kept constant, the size of the inactive layer is set to a large value. The grain size distributions in the two bed layers are obtained by considering sediment continuity for each fraction. If deposition occurs, each fraction f_a in the active layer is computed as:

$$f_a = \frac{f_{a,0}\, z_a + f_d\, z_d}{z_a + z_d} \qquad\qquad (\,3.28\,)$$

where z_a is the height of the active layer, z_d is the height of the deposition, f_a and f_d denote the fractions in the active layer and of the deposited material, respectively. Because the vertical size of the active layer remains constant, material has to be transferred into or from the inactive layer.

$$f_i = \frac{f_{i,0}\, z_i + f_a\, z_a}{z_i + z_a} \qquad\qquad (\,3.29\,)$$

where the index *i* denotes the inactive layer. Erosion processes are computed analogously.

3.3.5   Linking hydrodynamic and morphodynamic module

In order to understand the interaction of water flow and sediment transport, the underlying physical processes and the forces on a grain are considered. The flow features determine, if a particle is stable on the ground or if it is transported with the flow. The classical approach to determine the initiation of sediment transport is an equilibrium of forces on a particle on the river bed in the flow. As shown in Figure 3.5 the dominant forces acting on a particle are (1) the shear force induced by the flow and (2) the resistance force of the grain (*Dittrich (1998)*). At critical stage, or at the initiation of motion, these two forces are in equilibrium.
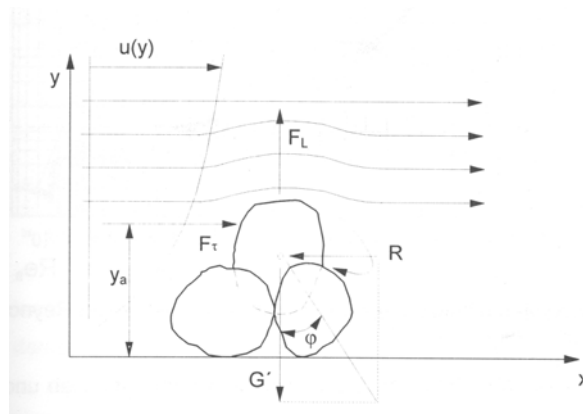
Figure 3.5: Forces on a grain at the river bed (from: *Dittrich (1998)*)

The processes in a river with respect to hydraulics, sediment transport, and morphological changes can numerically not be treated separately. The computed bed changes induced by deposition or erosion affect the flow which in turn influence the distribution of the bed shear stress and thus the bed load component and ultimately the bed topography. In the morphodynamic model, these interactions are considered by changing the bed after each time step. As a consequence, the hydraulics have to be recalculated for each time step. In Figure 3.6, the interaction of the modules in the numerical model *SSIIM* are shown.
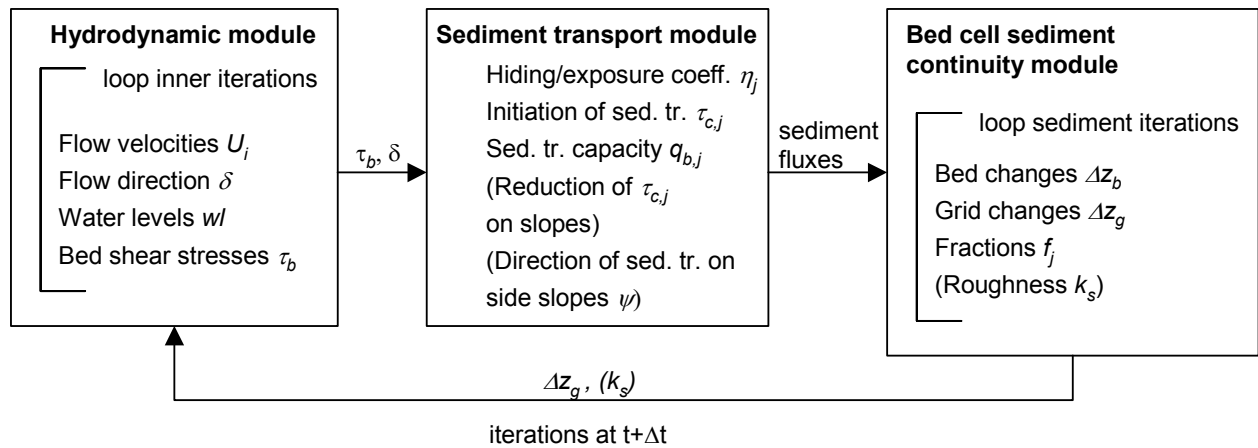
Figure 3.6: Interaction of the modules used in *SSIIM*

3.3.6   Validation

For validating the introduced numerical model, the geometry of the laboratory experiments of *Yen & Lee (1995)* has to be discretized. A three-dimensional, structured, non-orthogonal, vertically adaptive, and curvilinear grid is set-up. 254 hexahedral cells in the streamwise, 20 cells in the lateral, and 5 cells in the vertical direction are used. Figure 3.8 shows plan views of the numerical grid. Both the full extent and the region of the bend are shown. The numerical grid of the model represents the laboratory flume completely, including the full lengths of the upstream and downstream straight reaches, as to maintain an undisturbed developed flow field in the bend region of interest.

The grid is adaptive in the vertical direction, but not in the horizontal directions. A time step of 20 s is chosen. After each time step, both the water surface and the bed surface are updated. For discretization of the sediments, the continuous initial bed sediment sieve curve is decomposed into seven size fractions ranging from 0.3 to 6.6 mm. Figure 3.9 shows the initial sediment size distribution. The original blue curve shows the sieve curve used by *Yen & Lee (1995)*. The pink curve shows the seven fractions used for the simulations with the numerical model. The numerical values of the seven fractions used in *SSIIM* are given in Table 3.2. In order to accurately reproduce the original sediment curve, the breakdown of the fractions are chosen to be 20, 20, 20, 20, 10, 5, 5 percent. The uneven distribution of the fractions is justified by the decreasing gradient of the curve leading to finer discretisation of the larger sediment diameters. The characteristic diameters representing a fraction are positioned in the centre of a fraction.

Table 3.2: Fractions used for the computations in the laboratory bend

#	fractions [%]	sum [%]	position	diameter size [m]
1	**5**	100	97.5	**0.0066**
2	**5**	95	92.5	**0.0041**
3	**10**	90	85	**0.0028**
4	**20**	80	70	**0.0017**
5	**20**	60	50	**0.0010**
6	**20**	40	30	**0.0006**
7	**20**	20	10	**0.0003**

The flow field is computed by a pre-run for steady initial base flow conditions to provide a developed flow field for the main run including sediment transport processes and unsteady computations. The computed flow properties of the pre run – the velocity components *u, v, w*, turbulent kinetic energy *k* and dissipation of turbulent kinetic energy ε - are assigned to the main run. This procedure allows to initiate the morphodynamic-hydraulic computations based on a developed and numerically converged flow field.
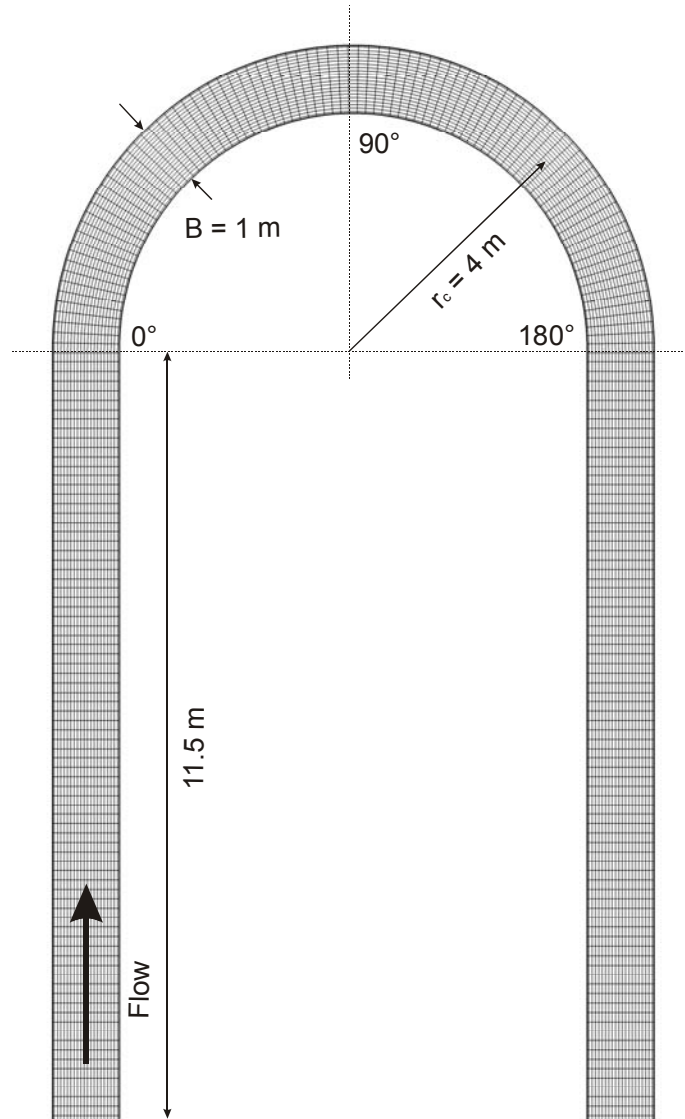
Figure 3.7: Map view of numerical grid, full extent
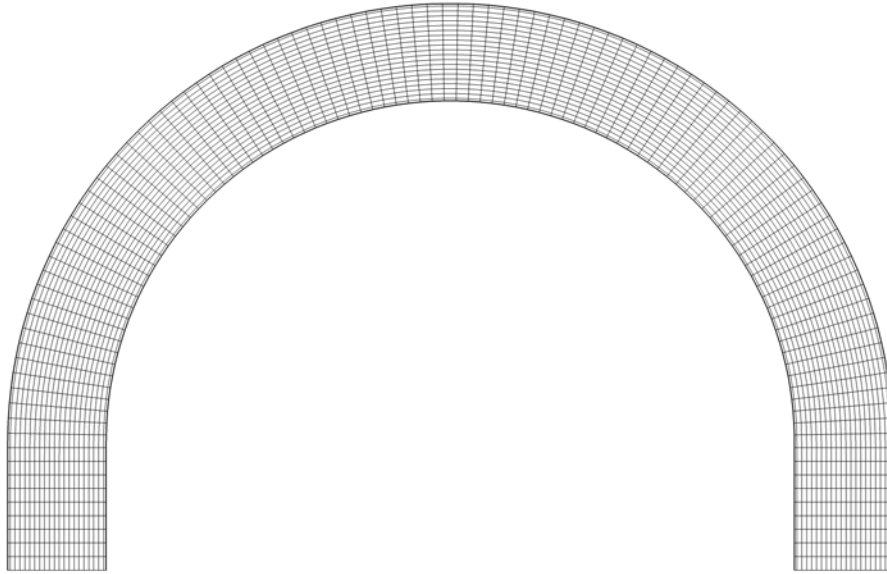
Figure 3.8: Map view of numerical grid, detail
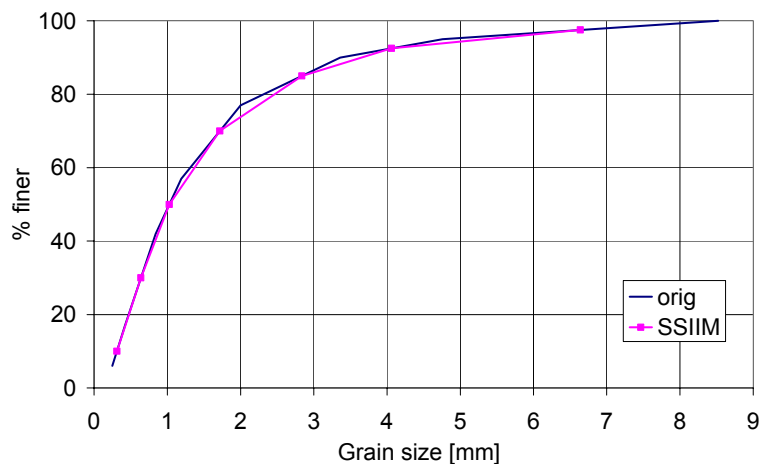
Figure 3.9: Initial sediment size distribution

3.4   Results and discussion

3.4.1   Flow

The pre-run is performed under steady flow conditions applying the initial base flow Q_0 = 0.02 m³/s, corresponding to the initial water depth of h_0 = 5.44 cm. The water surface develops according to the computed pressure field, i.e. the model is able to represent laterally inclined water levels in curved channels.

In Figure 3.10 on the left side a plan view of velocity vectors in two layers is given. The small vectors represent the velocities in the bottom cell closest to the bed and the large vectors are the velocities in the top cell closest to the water surface. The different sizes represent the vertical velocity distribution in open channel flows characterised by small velocities near the ground and high velocities at the water surface. In the upstream straight reach the velocity distribution is rather uniform in lateral direction. This is an indication for the small roughness at the side walls, that evidently has a minor

influence on the water flow. In the region of the bend the velocity vectors at the bed and at the water surface deviate significantly. The near bed vectors are pointing towards the inner bank and the surface vectors towards the outer bank. This corresponds with typical flow patterns in river bends, the velocities in bends are driven by a helical flow, also denoted as secondary current. These secondary flow processes in river bends produce characteristic morphological structures. The inwards directed velocity vectors cause mobile river beds to transport material from the outer to the inner bank that deposits there (point bars). The lack of sediment material leads to erosion processes (scours) at the outer bank. The computations show that the influence of the inclined lateral velocity distribution with small velocities at the inner and higher velocities at the outer bank induced by the channel bend propagates into the downstream straight reach and vanishes not before half of the straight length.

Figure 3.11 shows cross-streamwise velocity vectors in seven cross-sections, two located in the upstream and downstream centres of the straight reaches, respectively, and five evenly distributed along the flume bend at 0°, 45°, 90°, 135°, and 180°. The secondary flow pattern is shown in the cross-sections of the bend. The secondary flow effect becomes strongest at section 90° at the bend apex. In the straight reaches, the velocity vectors are directed in flow direction, so that virtually no lateral or vertical velocity components appear indicating that the straight reaches at these positions are free of secondary flow patterns. A rather symmetrical pattern over the water depth is computed, that represents the helical flow motion. As a consequence of the secondary flow, a laterally inclined water surface is computed. The model's ability to calculate lateral gradients of the water surface is based on the computed non-hydrostatic pressure field. Figure 3.10 on the right side gives the water surface elevations, with an initial downstream water depth of h_0 = 5.44 cm. The water surface is inclined within the region of the bend which propagates downstream into the straight reach. The longitudinal gradient of the water surface corresponds to the initial longitudinal bed slope, indicating uniform flow conditions at the initial stage.
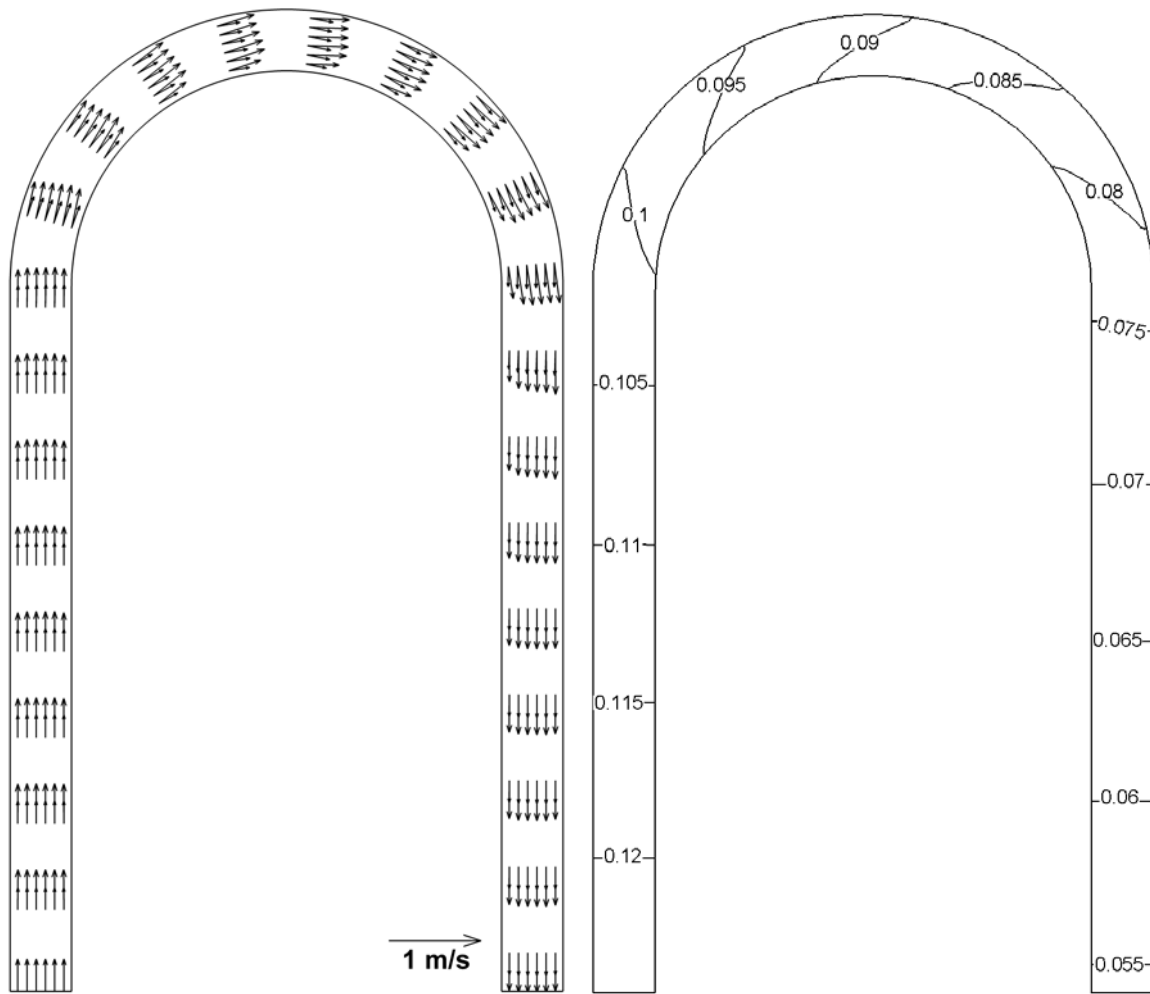
Figure 3.10: Velocity vectors at the water surface and near the bed (left), and contours of water surface elevation in meters (right)
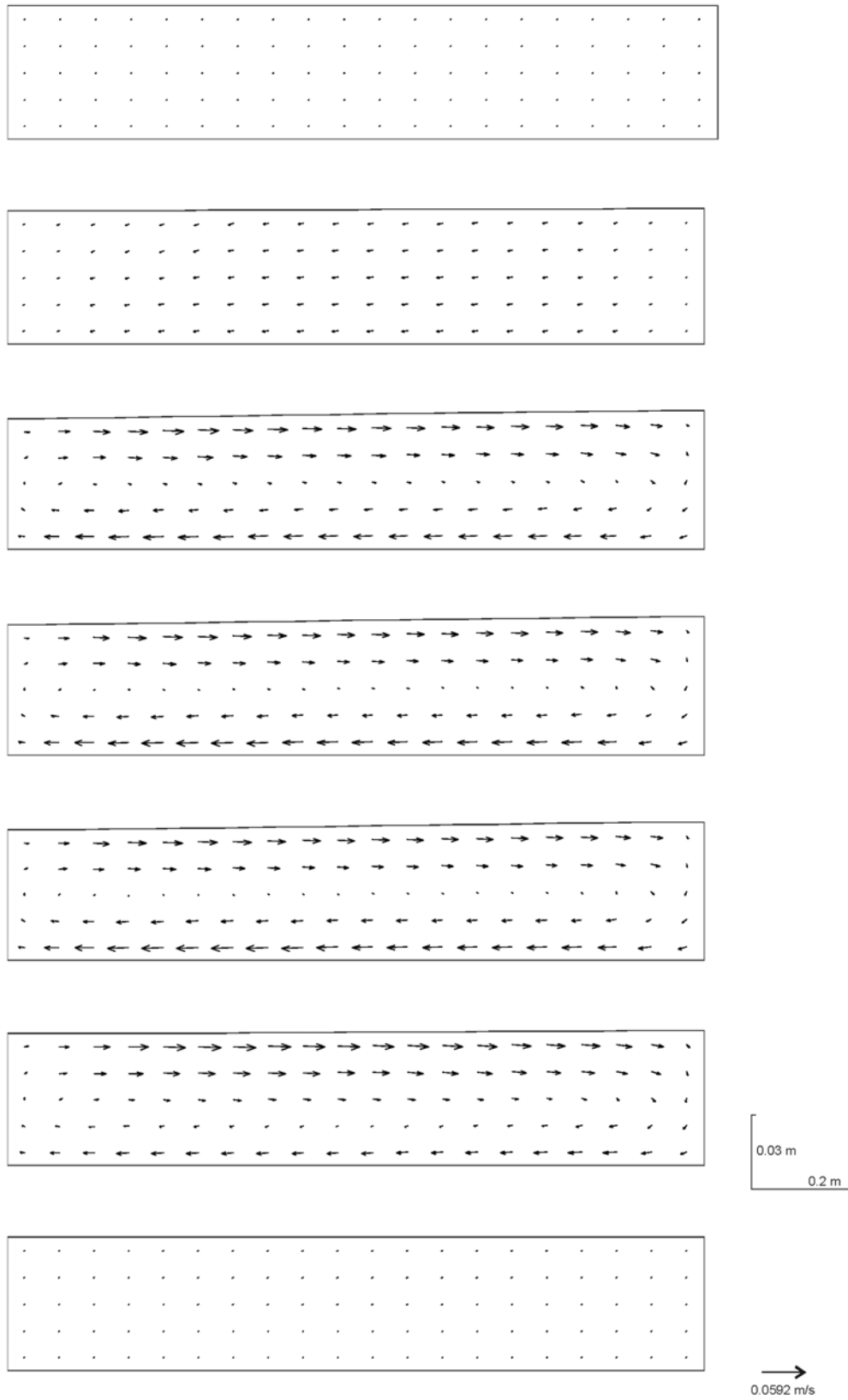
Figure 3.11: Cross-streamwise velocity vectors at cross-sections -5.75 m, 0°, 45°, 90°, 135°, 180°, +5.75 m (plotted against flow direction)

Following the theory of frictionless slip streams, the 1D relationship of the lateral water surface gradient can be derived (*Jirka & Lang (2005)*):

$$\frac{dh}{dr} = \frac{V^2}{gr}$$

(3.30)

An approximation of the formula gives the lateral difference of the water surface elevation Δh:

$$\Delta h \approx \frac{V^2}{gR_0} B$$

(3.31)

Applying the 1D formula for estimating the influence of curvature to the lateral slope of the water surface at the U-bend, one obtains very good agreement of the values derived by the empirical formula and the computed numerical model. Analytical and numerical differences of the water surface at the bend apex are given in Table 3.3. These results indicate that the flow features in the river bend are computed plausibly.

Table 3.3: Analytical and numerical differences of the water surface at the bend apex

Discharge	$\Delta h_{analytical}$	$\Delta h_{numerical\ model}$
0.02 m³/s (Q_0)	3.4 mm	3.3 mm

Figure 3.12 shows the unsteady development of the water surface induced by the triangle flow hydrograph computed at the main run. The results of the pre-run are used as input to provide a developed flow field. The unsteady computations result in a time varying water surface inclination. The triangle shaped hydrograph is characterised by a linearly rising period of the water surface from initiation to minute 100 with a peak discharge of Q_P = 0.053 m³/s and a corresponding water depth of h_P = 0.103 m. Subsequently, a linearly falling period from minute 100 to minute 300 is employed approaching the base flow at Q_0 = 0.02 m³/s and h_0 = 0.0544 m (see Figure 3.2). The computed results show that the general arrangement of the inclined water surface contours (WL) remains the same for the whole transient run. For higher discharges the lateral slope of the water surface increases representing the proportionality of the lateral difference of the water surface elevation and the squared velocities (see Equation (3.31)).
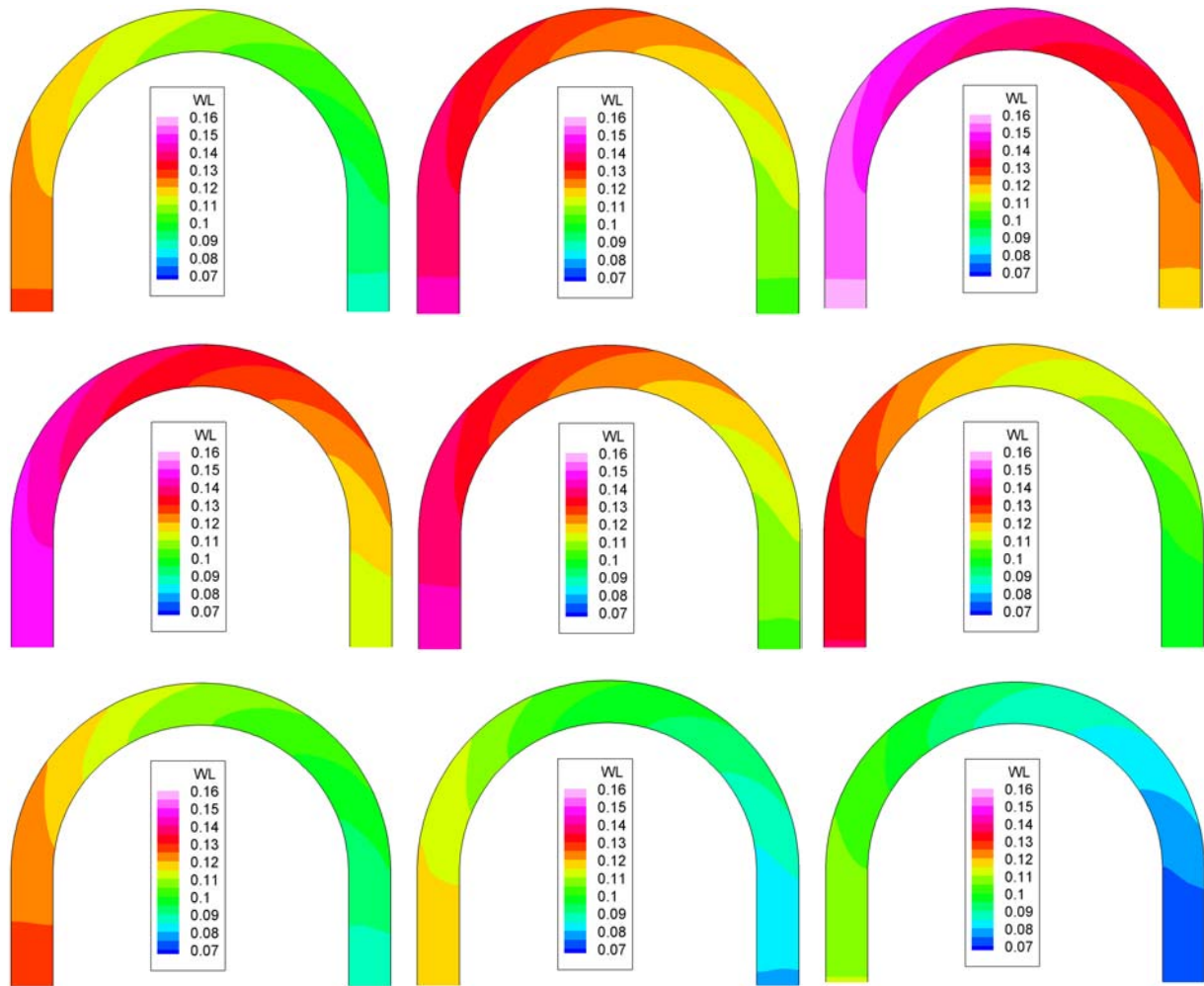
Figure 3.12: Evolution of the water surface at t = 33, 67, 100, 133, 167, 200, 233, 267, 300 min

The distribution of bed shear stress at the beginning and the end of the main run is given in Figure 3.13. At the beginning of the main run, an increased bed shear stress is computed at the downstream end of the outer bend at profile 180°. A slight lateral bed shear stress gradient is computed from the inner to the outer bend inducing reduced and increased sediment transport at the inner and outer bends, respectively. In combination with secondary flow patterns, bar and scour developments are induced at the inner and outer banks, respectively. At the end of the run a distinct lateral gradient of the bed shear stress is computed. The bed shear distribution interacts with the computed morphological changes leading to a consolidated lateral gradient.

Figure 3.13: Distribution of bed shear stress at the beginning and the end of the run

3.4.2   Morphological changes

Figure 3.14 shows contour plots in plan view of the bed deformations and median sediment sizes. Both the measured results by *Yen & Lee (1995)* and the computed results of this study are shown. The contours are displayed in a dimensionless form, the bed deformations are normalized by the initial water depth (h_0 = 5.44 cm), and the median sediment diameter (d_0 = 1 mm). The bed changes and sorting processes are shown at the end of the unsteady computation after 300 minutes. The computed results are obtained by applying the introduced sediment transport formula by *Wu et al. (2000b)*. Generally three parameters in the formula are used for adjustments, (1) factor α, that modifies the sediment transport rate, (2) the exponent m in the hiding-exposure function, and (3) the critical shear stress θ_c. The factor α is introduced in Equation (3.32), which is based on Equation (3.17). The factor α is unity by default.

$$\phi_{bi} = \alpha \cdot 0.0053 \left[\left(\frac{n'}{n} \right)^{1.5} \frac{\tau_b}{\tau_{ci}} - 1 \right]^{2.2} \qquad (3.32)$$

As can be seen from Table 3.4, the parameters α and θ_c remain unchanged for the numerical computations, while parameter m is modified. The effect of all parameters on the modelled results is shown and discussed later in this study.

Table 3.4: Chosen and default parameter sets of the sediment formulas

	chosen	default
α	1	1
m	-0.3	-0.6
θ_c	0.03	0.03

Figure 3.14 shows that the deposition processes leading to bar development at the inner bank and the erosion processes leading to scour development at the outer bank are well represented by the model. Moreover, both measured and calculated results lie within the range of $\Delta z/h_0$ = [0.75,-0.75].

Typical deposition processes at the inner bank and scour processes at the outer bank are correctly modelled. A deviation from the measured contours can be observed for the position of the maximum depositions at the inner bank. While the maximum deposition ($\Delta z/h_0$ = 0.75) is measured only slightly upstream the bend apex (cross-section 90°), the computed maximum deposition is situated at the first half of the bend. Both measured and calculated maximum depositions occur in a comparably small region. Between section 180° and section +2 m, the maximum scour ($\Delta z/h_0$ = -0.75) is measured at the outer bank due to the increased bed shear stress in this region (see Figure 3.13, right side), that declines after a short distance in downstream direction in the straight channel reach. This process is well reproduced by the numerical model. Special focus is drawn on the contour line -0.25. This contour line is computed and measured at approximately the same position, commencing at section 15° at the entrance of the bend, proceeding to the centre of the bend and finally leaving the depicted reach at the left side of the channel width in flow direction. Generally a satisfying agreement of measured and calculated bed deformation is achieved.

The contours of the measured median sediment sizes indicate a generally constant gradient over the length of the bend. The measured median sediment sizes are derived from undisturbed bed samples. With a melted wax technique, the sediment samples are extracted as wax sheets from the channel bed. The numerical results represent the sediment size distribution in the active layer of the model. The comparative results show that the model is able to reproduce the processes of the sorting processes with a satisfying agreement. The total fining (0.5 at inner bend) is well reproduced by the model while the measured coarsening (3.0 at outer bend) is slightly overestimated by the model. The sorting mechanism starts at the entrance of the bend, where it develops until the apex of the bend is reached. From the apex on downstream, the sorting configuration remains roughly preserved. The contours do not vary significantly over the width downstream the apex. The pattern of the contours, the development upstream of the apex and the uniformity downstream of the apex are well reproduced by the model.
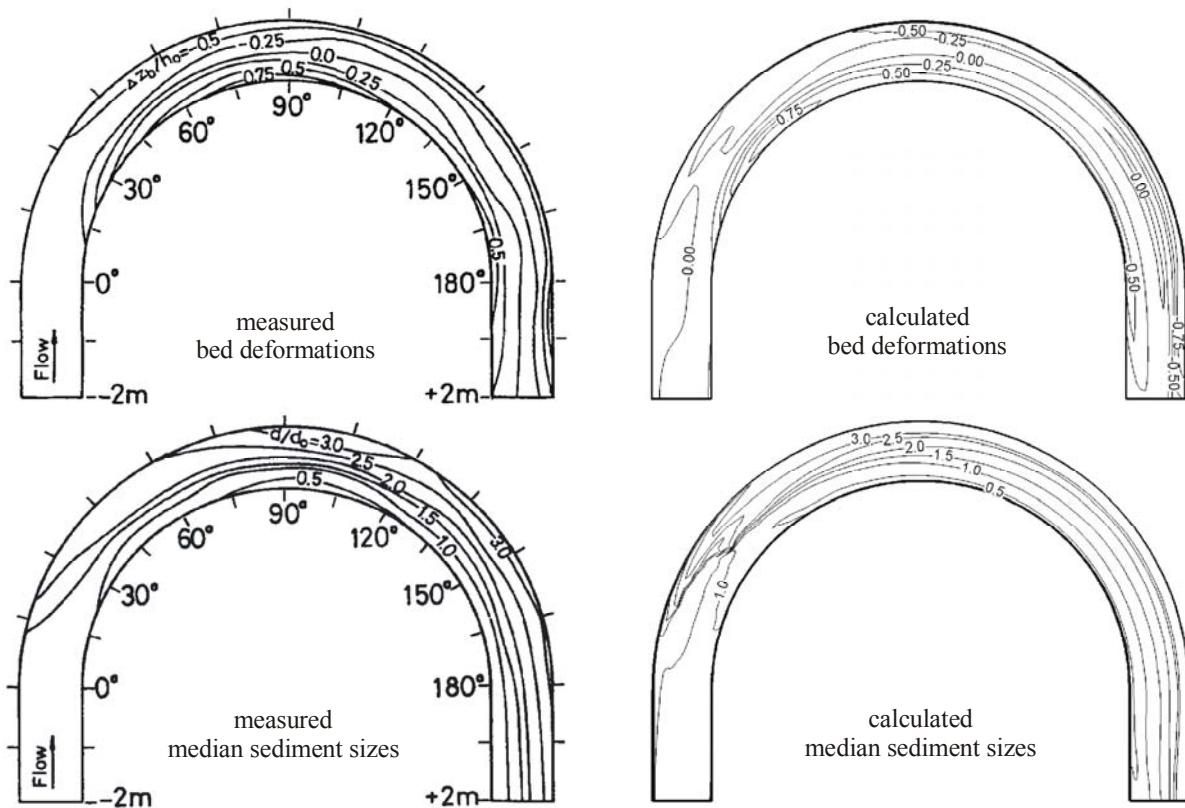
Figure 3.14:   Plan view of measured (left) and calculated (right) bed deformations and median sediment sizes

Figure 3.15 illustrates the temporal evolution of the channel bed using the same time intervals as in Figure 3.12. The initiation of a bar at the inner bend can be observed at minute 67. At the peak of the hydrograph (100 min), the bar establishes at approximately 30°, simultaneously the initiation of a scour evolves at the end of the outer bend at section 180° due to an increased shear stress in this region. While the sediment transport decreases after minute 100, the bed further develops during the falling limb of the hydrograph. While the peak of the bar slightly propagates downstream, a bar formation occurs throughout the whole length of the inner bank. As observed in the laboratory experiment, the bar develops stronger at section 180° (end of the bend). The scour develops against flow direction initiated by the scour hole at section 180°. A plateau-like area near the centreline of the bend remains throughout the whole duration of the run, while erosion and deposition processes with stronger gradients occur near the outer and inner banks, respectively.
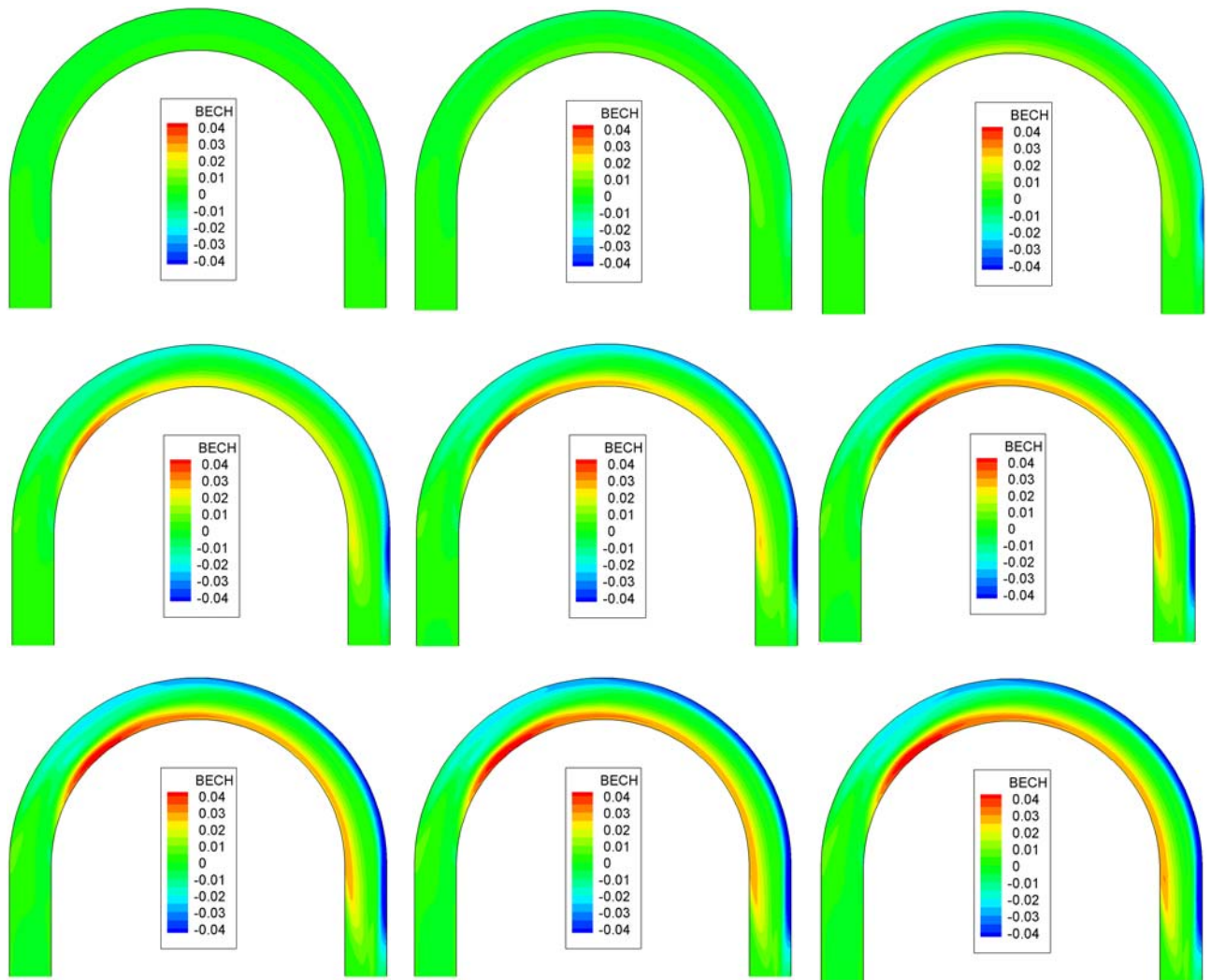
Figure 3.15: Evolution of bed at t = 33, 67, 100, 133, 167, 200, 233, 267, 300 min

Figure 3.16 shows computed versus measured bed changes at four cross-sections at the first half of the bend (45°), the bend apex (90°), the second half of the bend (135°), and the end of the bend (180°). Figure 3.14 on the left side illustrates the positions of the cross-sections in plan view. The dashed lines in Figure 3.16 represent the results of the original configuration of the numerical model, computed with the default formulas of *v.Rijn (1984a)*. The general features of the bed changes are satisfyingly represented by the numerical model. The total erosion and deposition heights are approximately within the correct range. The width of the scour is determined by a sudden inception of a strong downwards gradient at a distance of about 0.2 m from the outer bank. The scour width and scour depth are well represented by the default *van Rijn* formulas. However, the bar evolution, located at the inner bank, is significantly over predicted. The over prediction is present in all cross-sections.

Additionally to the results of the default approach, the solid lines in Figure 3.16 represent the results of the *Wu* approaches, respectively. The hiding-exposure coefficient m = -0.3 is applied, while for the parameters α and θ_c default values are used. The results indicate that a significant improvement of the computed bed levels is achieved compared to the results of the original *van Rijn*

formula. While the scour depths are modelled with a similar accuracy compared to the default *van Rijn* model, the deposition heights at the inner bank are significantly damped and thus they fit better to the measured bed changes. Also, the distinctive region of the scour near the outer bank is well represented by the nonuniform approaches. Furthermore, the plateau-like central region and the shape of the bar evolution is modelled with good agreement. The results indicate that the consideration of hiding and exposure mechanisms significantly improves the modelled bed deformation results.

In Figure 3.17, the variations of the median sediment diameters are shown for the default configuration and for the *Wu* approach. The default approach (dashed lines) generally predicts the variations of the median sediment size with the correct tendency, such that fining is modelled at the inner bank and coarsening at the outer bank. However, the fining processes at the inner bank and the coarsening processes at the outer bank are over estimated. The results of the nonuniform approach (solid lines) represent the measured data considerably better than the default model. The measured gradient of the sorting process is well represented and the values are computed within the correct range. The effect of the hiding and exposure approach, characterized by small particles that hide behind coarser particles and are therefore better protected from being transported, is well represented in the results. When comparing the results with and without consideration of hiding-exposure corrections, the underlying physical processes become evident. One can see that less coarsening occurred for the hiding-exposure approach near the outer bank, because the fine particles are protected and are therefore transported to a smaller extent. On the other hand, the inhibited transport of fine material that preferentially deposits at the inner bank leads to a better agreement of the median sediment size at the inner bank region. The reduced deposition heights at the inner bank of the hiding-exposure approaches in comparison with the default approach, as depicted in Figure 3.16, can be interpreted by the reduced amount of fine material available from sediment transport and therefore not being available for deposition at the inner bank. As a result, the fining at the inner bank is less pronounced.

The results of this study show, that both bed changes and sorting processes are modelled with superior agreement when a hiding-exposure approach is applied. The superior agreement with respect to the default approach shows that these mechanisms play an important role in nature and that they should be considered when modelling morphological changes with nonuniform sediments.
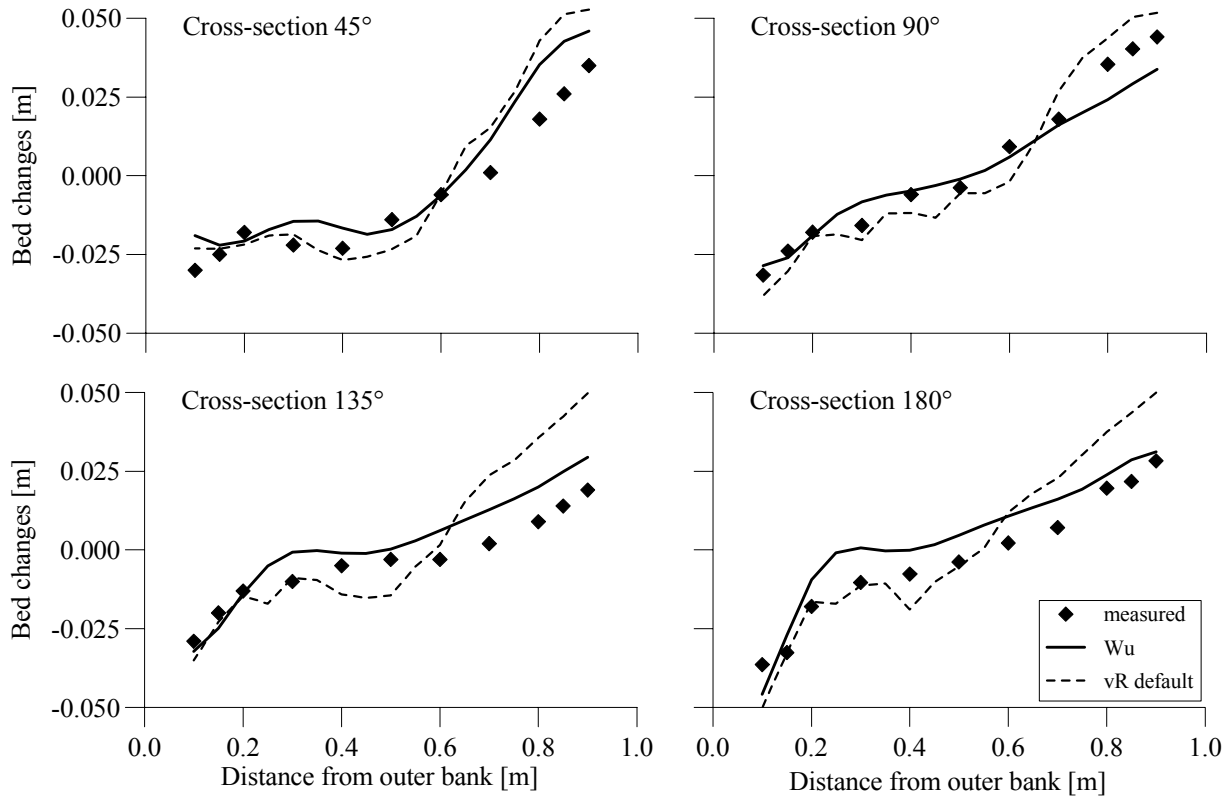
Figure 3.16: Bed changes at four cross-sections using the default *van Rijn* and *Wu* formulas
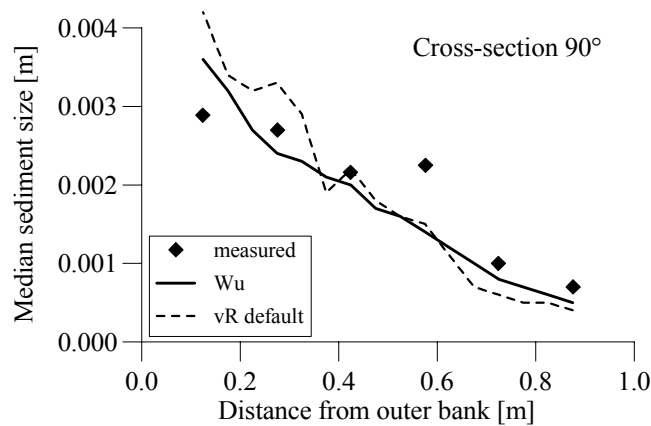
Figure 3.17: Median sediment sizes at the bend apex using the default *van Rijn* and *Wu* formulas

Additionally to the detailed comparisons of measured and computed morphological features, an integrative comparison of the default and the hiding-exposure approach is shown in Figure 3.18. This figure depicts the accumulated sediment outflow at the outlet of the laboratory flume over time. Measurements of the outflowing sediments are performed at two points in time, at the peak discharge at t_p = 100 min and at the end of the experiment at t_{max} = 300 min the outflowing sediments are collected and weighed. Both the computed sediment outflow using the *Wu* and the default *van Rijn* approach are shown. As can be seen from the sediment hydrographs, the tendency of the measured outflow is represented in a plausible way by both approaches, characterized by an increase of outflow from t_0 to t_p followed by a decreased outflow from t_p to t_{max}. While the *Wu* approach only slightly underestimates the measured sediment outflow, the default *van Rijn* approach considerably

overestimates the outflow. For two reasons the *van Rijn* approach over predicts the measured outflow, (1) the tested sediment size range for the default *van Rijn* approach is limited to a maximum of 2 mm, while the *Yen & Lee (1995)* experiments range to a maximum of 8.5 mm, and (2) the lack of considering hiding-exposure mechanisms leads to an increased total transport, since small particles are not protected.
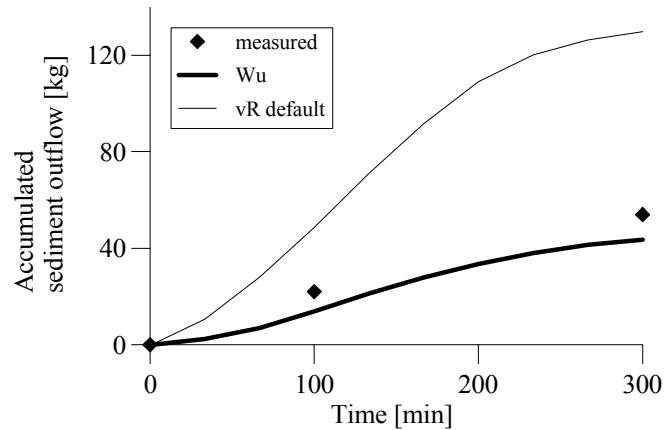
Figure 3.18: Accumulated sediment outflow using the *Wu* and default *van Rijn* formulas

The present configuration of the hiding-exposure approach using the sediment transport formulas by *Wu et al. (2000b)* and applying the sediment parameters given in Table 3.4, is chosen to compute another run of the laboratory experiments by *Yen & Lee (1995)*, denoted as run #1. It differs from the current run (run #4) by using a steeper triangle hydrograph, as indicated in Figure 3.2. For this run, detailed measured size gradation of the bed sediments at the outer bank is provided. The initial and measured sieve curves for three sections at the outer bend are documented in Figure 3.19. The general coarsening process is well represented by the model. The results in Figure 3.14 reveal, that the distribution of the median sediment diameter is well reproduced, while here it is shown that the computed sediment sieve curves at the end of the run generally represent the measured curves well. Both the values and the shapes of the curves are well reproduced. However, a minor measured tendency towards a decrease in the coarsening in flow direction from section 90° to 180° cannot be reproduced by the model. The computed results show that the coarsening remains nearly unchanged along the flow direction. As indicated in Figure 3.19, and also seen in Figure 3.16, the model tends to slightly overestimate the coarsening process.
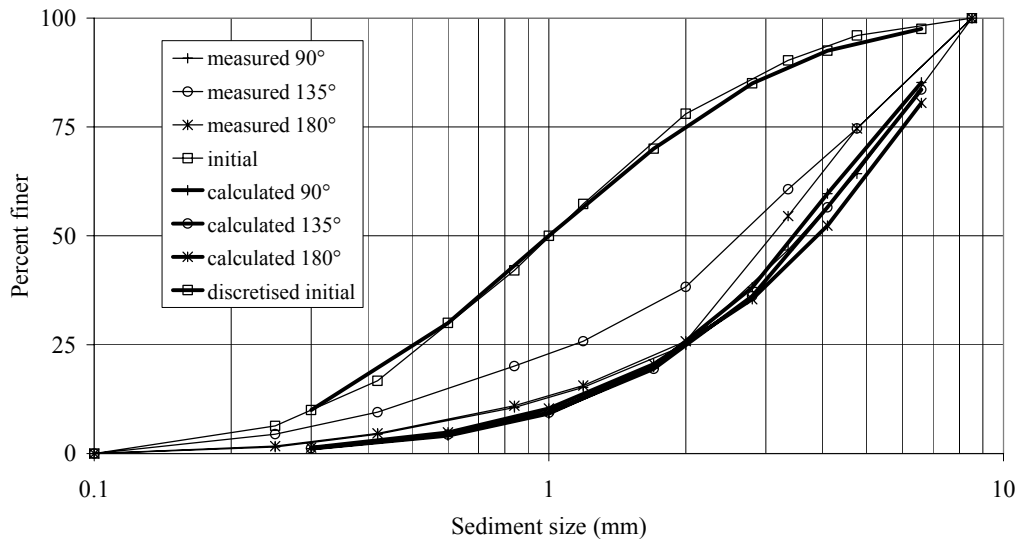
Figure 3.19: Sediment size gradation curves at end of run 1 (measured and calculated)

3.4.3   Sensitivity analysis

The sensitivity of the three sediment parameters (m, α, θ_c) presented in the formula of *Wu et al. (2000b)* is investigated in this section. These parameters are generally appropriate for adjusting morphodynamic models. In Figure 3.20, measured and computed bed changes are shown using the default value of the exponent for the hiding-exposure function, m = -0.6, and the chosen exponent, m = -0.3. The results show, that in all cross-sections, the bed changes computed by the default exponent (dashed lines) tend to underestimate the deposition heights slightly. The gradients are smaller than the measured gradients near the inner banks. As a consequence, the computed bed changes in the central region of the cross-sections are slightly overestimated using the default exponent. The scour depths are modelled with comparable accuracy. Compared to the sensitivity of the other parameters, the sensitivity of the parameter m is of minor relevance. The differences between the default and the chosen exponent become more evident when analysing the distribution of the median sediment sizes as given in Figure 3.21. Here, the results of the default exponent significantly underestimate the measured sorting processes, while the results of the chosen exponent give good agreement. In Equations (3.12) to (3.14), it can be seen that the effect of the hiding-exposure mechanism decreases when the absolute value of m decreases (from –0.6 to –0.3). The inhibited sorting for the default exponent shown in Figure 3.21 conforms well the theoretical considerations. Apparently, the absolute value of the proposed default exponent by *Wu et al. (2000b)*, m = -0.6, should be reduced in this case, as shown for both the bed changes and the sorting processes. Comparing the computed bed changes of the *van Rijn* approach with the results using the default sediment parameters of the *Wu* approach (dashed lines in Figure 3.16 to Figure 3.20) shows that slightly better agreement for the *Wu* approach is obtained. Here, the bed deformation heights are generally predicted correctly, while the *van Rijn* approach overestimates the deposition heights considerably. This indicates, that hiding-exposure approaches should be considered when modelling nonuniform sediment transport processes. However, better agreement can be obtained when adjusting relevant sediment parameters.

Figure 3.20: Bed changes at four cross-sections, variations of *m*
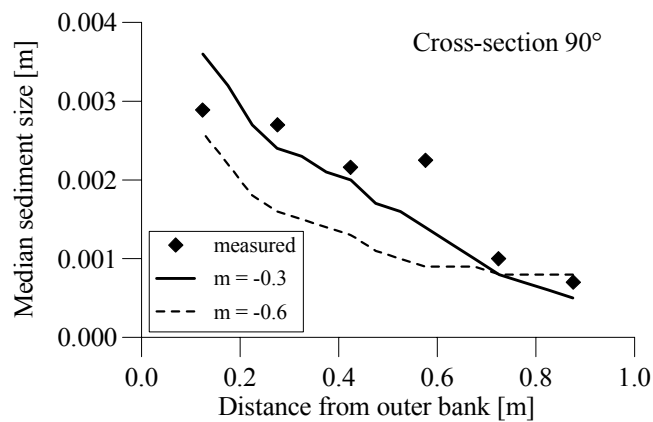
Figure 3.21: Median sediment sizes at the bend apex, variations of *m*

The second sediment parameter tested for sensitivity is the factor α, that is multiplied with the fractional sediment transport rate (see Equation (3.32)). By default, α is unity. Two variations are analysed, computing half (α = 0.5) and double (α = 2) of the fractional sediment transport rate. The results of the bed changes are given in Figure 3.22. Generally the effect of a reduced or increased sediment transport rate is a reduced or increased lateral gradient of the bed levels, respectively. A doubled rate significantly increases the scour depth compared to the default approach starting from section 90° with increasing tendency in downstream direction. Figure 3.23 shows the effect of the modified transport rate on the median sediment diameter distribution. The same results as found for the bed changes also apply to the sorting. With an increase of the transport rate, the sorting processes intensify. For both, the bed changes and the median sediment distribution, the default value of α gives

best results indicating that the original fractional sediment transport rate, as given by *Wu et al. (2000b)*, is appropriate to use in the three-dimensional model in this case.

Figure 3.22: Bed changes at four cross-sections, variations of α
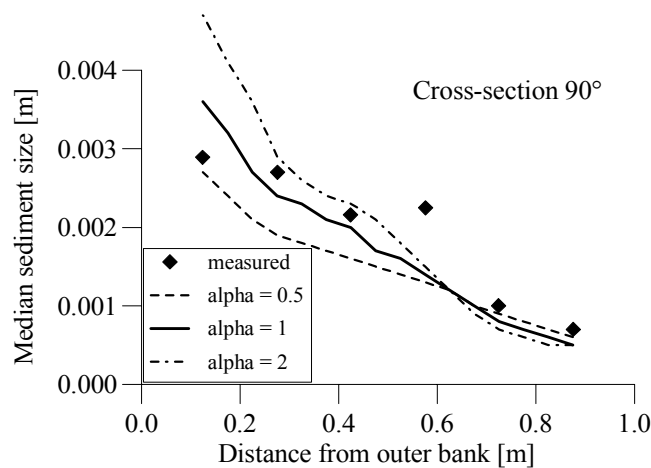
Figure 3.23: Median sediment sizes at the bend apex, variations of α

The third sensitivity analysis is performed with the sediment parameter θ_c. This parameter can be interpreted as the non-dimensional critical shear stress for the corresponding uniform sediment or the mean size of bed materials. As shown in Equations (3.14) and (3.15), in combination with the hiding-exposure function, θ_c determines the incipient motion of nonuniform sediments and therefore serves as a threshold value. The default value of $\theta_c = 0.03$ is reduced and increased by a value of 0.01 to test its sensitivity on the results. The results of the bed changes in Figure 3.24 show that a

modification of the non-dimensional critical shear stress reacts very sensitive on the computed bed changes. While the increased value of θ_c = 0.04 leads to a reduced transport that results in reduced bed changes, the reduced value of θ_c = 0.02 has great effects on the computed bed changes. The lateral gradient increases considerably, and the computed scour depth achieves large values in combination with a sharp point of inflection. In Figure 3.25, the same tendency can be observed for the sorting, the increased critical shear stress inhibits sorting processes and the reduced critical shear stress leads to a strong sorting. Also for this parameter, the default value proposed by *Wu et al. (2000b)* gives best results and does therefore not need to be modified. The non-dimensional critical shear stress proves to be a very sensitive parameter.
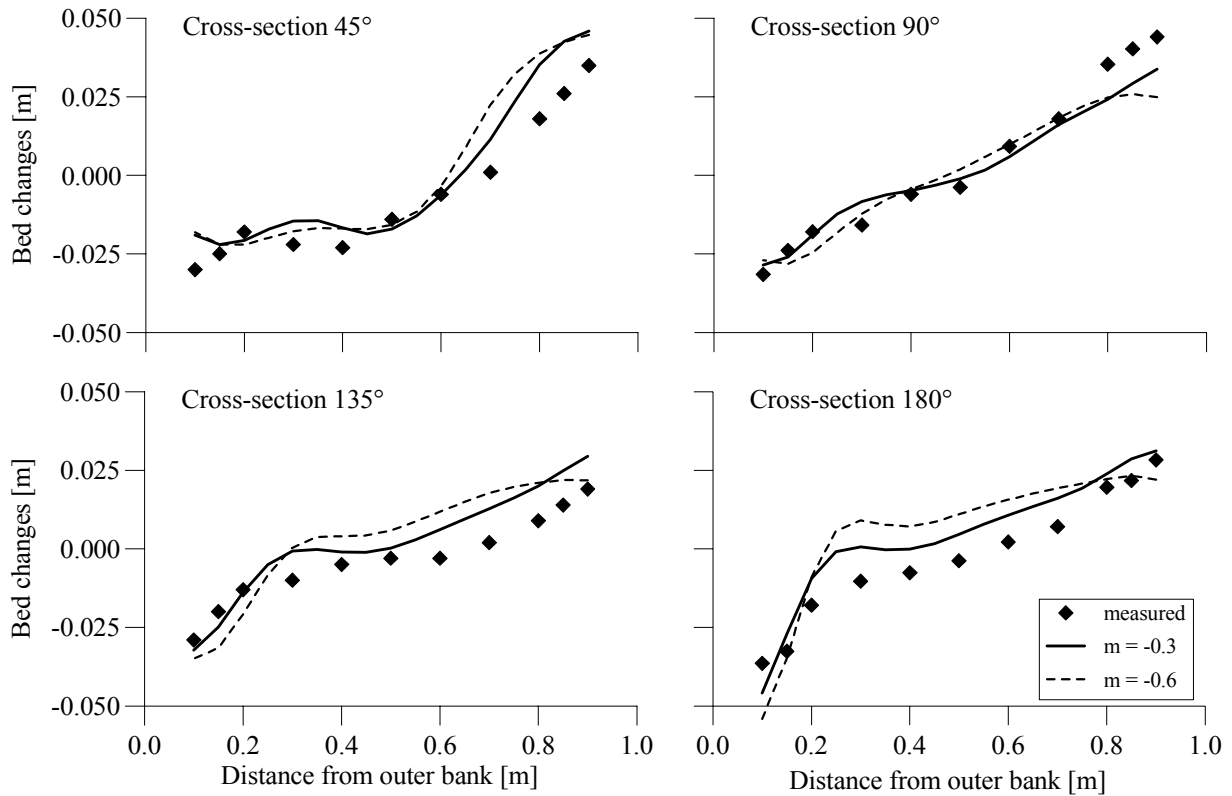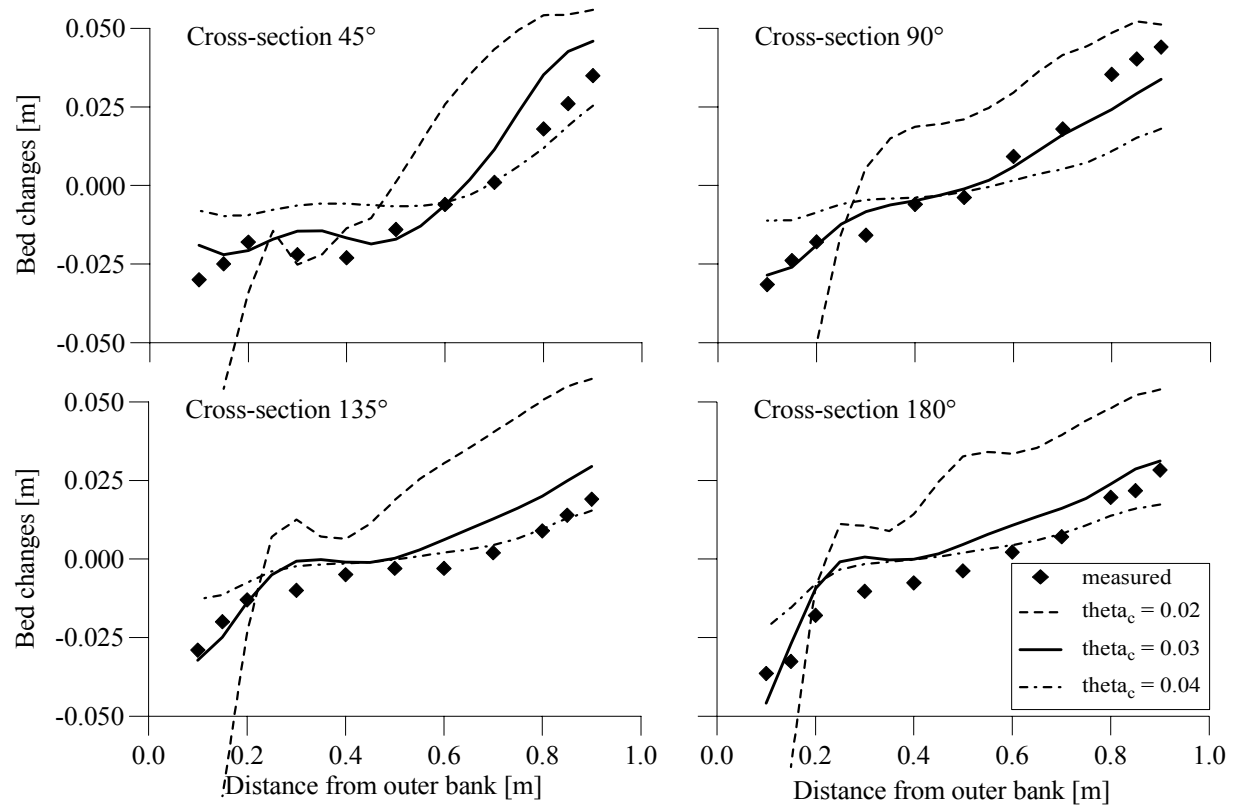

Figure 3.24: Bed changes at four cross-sections, variations of θ_c

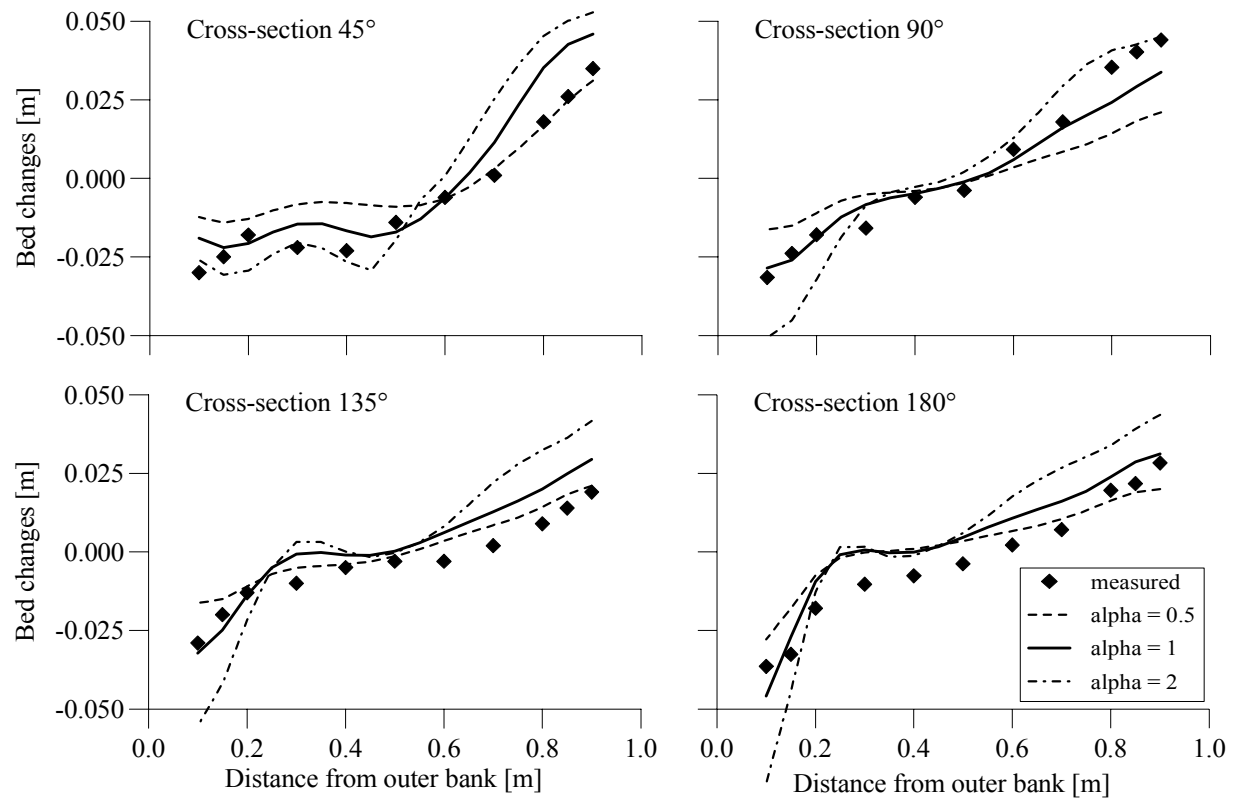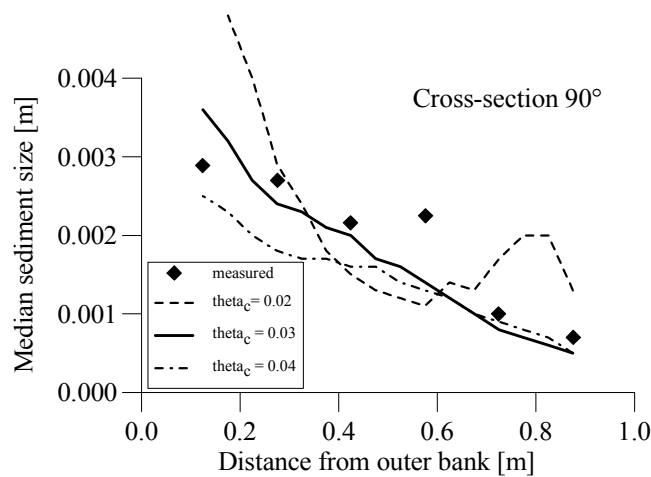Figure 3.25: Median sediment sizes at the bend apex, variations of θ_c

3.5   Summary and conclusions

A three-dimensional numerical model is applied to compute morphological and sorting processes in a laboratory channel bend. Originally the sediment transport formulas of *van Rijn* are applied by the model to compute sediment transport, bed changes, and sorting processes. The sediment transport formulas were developed for uniform sediment with a maximum grain diameter of 2 mm. Possible hiding-exposure effects cannot be modelled by the original *van Rijn* formulas. For mountainous gravel bed rivers, these sediment transport formulas are not appropriate for predicting the correct transport and morphodynamics. The numerical model is modified in a way to compute fractional sediment transport considering hiding-exposure effects that appear when non-uniform sediments are moved by the water flow.

The numerical model is enhanced by incorporating the non-uniform sediment transport formulas presented by *Wu et al. (2000b)*. These formulas are chosen because they

 ➢ were established on a large number of laboratory and field data and have a large range of applicability,

 ➢ have been tested in a comparative study of *Scheer et al. (2002)* and proved to give the best results among the selected formulas, and

 ➢ account for hiding and exposure mechanisms of non-uniform sediment by introducing a hiding-exposure correction factor that is based on a probability approach.

The modified numerical model is validated on complex laboratory experiments in a U-bend introduced by *Yen & Lee (1995)*. The model is validated mainly on measurements of bed deformation and sorting processes in the U-bend. The experiments are challenging for a numerical model because

 ➢ they were conducted in a bend where secondary flow effects prevail,

 ➢ they were performed under unsteady flow conditions using a triangle hydrograph,

 ➢ a vertically mobile bed was applied, and

 ➢ graded sediment on the channel bed was used.

Results of the hydraulic computations of the experiments by *Yen & Lee (1995)*, using the modified numerical model, show that the model is capable of computing the hydraulic features of the unsteady flow in a bend. Both water surface configuration and secondary flow patterns are computed plausibly. The computed lateral gradient of the water surface is compared to an analytical 1D formula and good agreement is achieved. A reason for the good agreement is the computation of a non-hydrostatic pressure field that is of great advantage compared to the assumption of hydrostatic pressure.

The performance of two sediment transport formulas is investigated, the default transport formula in the numerical model introduced by *v.Rijn (1984a)*, and the incorporated transport formulas for nonuniform sediments introduced by *Wu et al. (2000b)*, accounting for the interactions between individual grain sizes by a hiding and exposure approach.

Results show that the three-dimensional model is able to predict both the magnitude and the general tendencies of the measured bed deformations and sediment size distributions of the

laboratory experiments when using the default *van Rijn* configuration. More detailed analysis, however, reveal deviations from measurements with respect to bed level and sediment size changes indicating a remarkable overestimation of bar evolution near the inner bank. Computed results improve significantly when the nonuniform sediment transport approach is applied. The results of the nonuniform approach show less sorting intensity and smaller bar heights, both giving a better fit to the measured data. The computed results of the nonuniform approach in relation with the default approach represent the physical mechanisms of the hiding-exposure effect well. When applying the hiding-exposure approach the inhibited transport of fine materials results in a reduced bar development at the inner bank and reduced sorting processes that both give an improved representation of the measured data. The nonuniform approach by *Wu* predicts the total sediment transport considerably better than the default *van Rijn* approach.

Often the computation of sediment transport and morphodynamics needs adjustments of essential sediment parameters of the applied sediment transport formulas. Following the reasoning of *Kroekenstoel & van Welzen (2003)*, there is little knowledge available in the scientific community on the choice of appropriate sediment transport formulas. The sediment parameters chosen for modification in this study are (1) the exponent m of the hiding-exposure function of *Wu et al. (2000b)*, (2) the factor α for modifying the sediment transport rate, and (3) the non-dimensional critical shear stress θ_c. The best results are achieved for m = -0.3 (default = -0.6), α = 1.0 (= default), and θ_c = 0.03 (=default). A reduction of the absolute value of the exponent m (from –0.6 to –0.3) is physically related to a weaker consideration of the hiding-exposure effect. The reduction of m means that small particles are less protected by hiding behind the coarser particles and coarse particles are less exposed to the flow. As a consequence, segregation or sorting processes are less inhibited by the hiding-exposure effect when using a reduced absolute value for the exponent m.

Sensitivity tests are performed to assess the effect of the sediment parameters on the computed bed changes and sorting processes. While the parameters m and α show medium sensitivity on the results, θ_c reacts sensitive on modifications.

Generally the introduced modified model proves to be able to calculate bed deformation and sorting processes of a complex laboratory experiment with good agreement. The superior results of the nonuniform approach with respect to bed deformation, sorting processes, and total sediment transport compared to the default approach show that hiding-exposure mechanisms play an important role in nature and that they should be considered when modelling morphological changes with nonuniform sediments. However, since sediment transport formulas cover wide ranges of applicability, appropriate sediment parameters have to be determined for each flow situation by comparing computed with measured results.

4 Numerical computation of morphological changes in the Danube river

4.1   Introduction

Sediment transport and morphological changes are important issues in the field of river hydraulics. Variations in water discharge and water levels cause fluctuations of sediment transport rates leading to morphological changes of a river. Even for steady flow, sediment transport is organised in batch-wise movements, bed forms are built that propagate with different velocities. As a consequence of morphological changes, a river can significantly change its curvature over time. Anthropogenic measures such as the installations of hydropower plants, can intensify the variations and consequently cause a sustainable change in river bed morphology. Typical river bed configurations, found in nature are: (1) alternate bars in straight river reaches, (2) meandering rivers, and (3) point bars in river bends. The bed sediment grain size distributions develop as a consequence of bed elevation changes. Longitudinal, lateral and vertical sorting processes in river beds can be observed for nonuniform sediment size distributions. It is often observed in natural rivers that the upper layers of a river bed are composed of coarser sediments that protect the finer sediment layers below, a process denoted as armouring. Morphological changes in rivers, particularly when they are caused by river training measures, have a great impact on ecological functions such as habitat conditions.

It is possible to use numerical methods to gain insight into the morphological processes of a river. In this study, the existing three-dimensional numerical model *SSIIM* was modified in a way to compute nonuniform sediment transport and river bed changes considering the interacting processes of different grain sizes such as hiding and exposure processes. Therefore the sediment transport formulas of *Wu et al. (2000b)* were incorporated into the numerical model. In Chapter 3, the model is validated on complex hydraulic and morphodynamic processes in a 180° bend in a laboratory channel using a mobile bed with a graded sediment size distribution. The model proved successfully to represent the measured features of morphological changes and sorting processes.

In the present Chapter, the numerical model is tested on morphological changes of a reach of the Danube river. The period of the 100 year flood in 2002 is chosen for testing the numerical model. Pre and post flood surveys of the river bed are performed, that document the bed changes as a consequence of the flood event. The model is validated by comparing measured and computed bed changes. A literature review on multidimensional modelling of river dynamics is given in Chapter 4.1.1. The morphological changes of the study reach are summarised in Chapter 4.1.2. The theoretical background for three-dimensional computations of flow and nonuniform sediment transport is summarised in Chapter 3.3. The validity and plausibility of the computed flow features are checked and the results are shown in Chapter 4.3.1. One major objective of this study is to compare measured and calculated erosion-deposition patterns using the modified numerical model. The results are presented in Chapters 4.3.2. The sensitivity of several sediment transport parameters is analysed in Chapter 4.3.3. An error analysis is presented to assess the quality of the computed bed changes when

using different parameter sets. The results are shown in Chapter 4.3.4. Finally, the temporal evolutions of characteristic parameters is analysed in Chapter 4.3.5.

4.1.1 Literature review on multidimensional modelling of river morphodynamics

A number of research studies have been presented over the last decade dealing with numerical computations of sediment transport and morphological changes. Several numerical models were developed and presented in literature. Relevant multidimensional model developments and morphodynamic computations of real river geometries are presented in this Chapter.

In the study of *Marburger (1998)*, computations of real river morphodynamics are performed. The author developed a morphodynamic hydraulic model, that was based on the hydraulic model FAST2D developed at the University of Karlsruhe by *Zhu (1991)* and *Wenka (1992)*. The morphodynamic model uses the finite volume method. The influence of turbulence is considered by a depth-averaged standard k-ε model, which allows to model the shear stress in an improved manner. The shear stress is the significant parameter for morphological computations when using shear stress based empirical bed load transport formulas. According to *Marburger (1998)*, these should be preferred compared to deterministic approaches. The introduced model accounts for fractional bed load and suspended load transport. Suspended load is computed by solving the convection-diffusion equation. Consistency with the bed evolution equation is realised by a source term in the concentration equation. The sediment balance of bed load is based on a first order upwind approach. A single layer concept proves to be sufficient to model stabilising processes in rivers. The morphodynamics of a river reach of 6 km length (stream km 2402 to 2396) of the German Danube river near Bad Abbach was modelled over a period of almost 14 years. On its upstream end a dam was built in the 1970's leading to progressive bed erosion processes that lowered the water levels 2 to 3 cm per year. This situation is comparable to the Danube east of Vienna investigated in the study where the power station Freudenau induces similar bed level reductions. The sediment transport was modelled as fractional bed load transport. Four size fractions with a characteristic sediment diameter of d_{ch} = 0.018 m were used, applying a single-layer approach. The bed load transport formula applied was called 'BAW/Donau-Formel' and was developed at the BAW (Bundesanstalt für Wasserbau, Federal Waterways Engineering and Research Institute, Germany), where the ripple factor was calibrated for this study. The computations showed that the erosion processes were underestimated by the model, which can possibly be explained by dredging measures that were not accounted for in the morphodynamic model. The development of a pool at the outer bend of the Danube reach was modelled with the correct tendency and the general coarsening processes of the bed sediments at the Danube reach caused by the erosion processes was modelled with good agreement.

Bui (1998) developed a two-dimensional depth-averaged model for the prediction of flow and sediment transport in rivers. The hydrodynamic module is based on the FAST2D code developed at the University of Karlsruhe by *Zhu (1991)* and *Wenka (1992)*. Secondary flow effects on sediment transport are taken into account by adjusting the dimensionless diffusivity coefficient in the depth averaged version of the k-ε turbulence model and a quasi-3D flow approach is used to simulate the effects of secondary flows and transverse slope of the bed surface on the direction of bed-load transport. The finite volume method is applied using a curvilinear non-orthogonal and non-staggered

grid. The bed level changes in the sediment transport module are computed using a predictor-corrector scheme. The hydrodynamic and the sediment transport module are linked together on a computational program level, a quasi-steady morphodynamic time-stepping mechanism is applied. During the flow computations the bed levels are assumed to remain constant and during the computations of the bed levels the flow and sediment transport are set invariant to the bed level changes. The model was tested at a river reach of the Elbe river, which covered complex geometric and morphodynamic features. Within the German part of the Elbe river a reach from km 508 to km 521, called Reststrecke, exists where no river training measures were performed. In the vicinity of this reach, *Bui (1998)* simulated the morphodynamics at a sub-reach from km 506 to km 513, that was additionally analysed in the framework of a physical model study at the BAW (Bundesanstalt für Wasserbau) in Berlin. The model was simulating the flood event from December 1993 to January 1994. A mean grain diameter of 1.2 mm was applied. The empirical transport formulas of *v.Rijn (1984a)* and *v.Rijn (1984b)* were used. The computations showed that suspended transport was higher than bed load transport that qualitatively fit the observations. In a bend, the deposition processes were computed at the point bar at the inner bend, and erosion processes were computed at the outer bend. The modelled results were not compared to pre and post flood surveys so that only the plausibility of the computed results was analysed. According to *Bui (1998)*, a straightforward application of the model to real flow situations gives qualitatively correct results, whereas a quantitative prediction requires model calibration. The modelling system served as a useful tool for short-term simulations for practical applications.

Olsen & Kjellesvig (1999) performed computations of sediment flow in a tunnel-type sand trap. The numerical model *SSIIM* was used, solving the transient Navier-Stokes equations by applying the k-ε turbulence model. The sediment flow was calculated by solving the transient convection-diffusion equations for sediment concentrations for five sediment fractions. The suspended sediment formulas of *v.Rijn (1984b)* were used for the sediment concentration as boundary condition for the bed. A vertically adaptive, non-orthogonal grid using the finite-volume method was applied. The processes in the sand trap involved both sedimentation and erosion, as a large volume of sand was formed and moved through the geometry. The modelled results were compared to the results of a physical model test. The temporal evolution of the sand trap was investigated and good agreement was achieved with measured data. A sensitivity analysis of some relevant input parameters showed that variations of the roughness react highly sensitive on the computed bed level changes.

Mewis (2002) developed a three-dimensional morphodynamic model (*SMOR3D*) using finite elements for discretisation. A hydrostatic pressure assumption is made. The bed load formula of *Zanke* was implemented. The model was applied to a river reach of the Elbe river downstream of Magdeburg with a length of 7 km (stream km 506-513) for verification purposes. The reach consists of a strong bend at stream km 509 with a radius of curvature of almost 150°. The bed material was subdivided into four fractions with a mean grain diameter of 1.0 mm. Steady state calculations were performed for a virtual discharge of $Q = 970$ m³/s representing the bankfull discharge at this reach of the Elbe. The Elbe reach was modelled over a period of 19 years under steady state conditions. After 30 % of the computed time, a morphologic equilibrium was achieved. Measurements showed, that bed

forms move in the Elbe with a propagation velocity of 300 to 400 m per year. The propagation velocities of morphologic perturbations were computed significantly larger achieving values in the range of 1500 m per year. At the end of the simulations, the spatial shear stress distribution showed an equalised character. Hydraulics and morphodynamics interacted so that a stable configuration was achieved. The computation of different parameter variations showed that considering side slope effects on the direction of the sediments remarkably improved the plausibility of the computed results. Since a virtual constant discharge was used, it was not possible to compare the computed bed changes to measurements.

Spannring (1999) used a steady two-dimensional depth-averaged hydrodynamic numerical model, developed at the RWTH Aachen University by *Stein (1990)*. The model was extended in a way to compute sediment transport and morphodynamic processes. The original hydrodynamic model was verified on laboratory experiments of a channel equipped with groynes. A focus was drawn on the application of an appropriate turbulence model. The mixing length turbulence model by Prandtl proved to give best results. Parameter studies on straight channels with groynes and a mobile bed were performed to achieve characteristic parameters, such as the maximum erosion depth, to describe the effect of groynes on the development of the bed. According to *Spannring (1999)*, the introduced numerical model is limited to investigations in straight channels, since it does not cover three-dimensional effects such as secondary flow effects that occur in river bends.

Gessler et al. (1999) validated and applied a three-dimensional morphodynamic model (CH3D-SED) to the Deep Draft Navigation Project on the lower Mississippi River. The hydrodynamics were solved with a depth-averaged Reynolds approximation of the momentum equations for the depth averaged velocities. The governing equations in the horizontal plane were solved with a boundary fitted, non-orthogonal, finite difference approximation. The deviation from the depth-averaged velocity was computed for each cell by solving the conservation of mass equation in combination with a *k-ε* closure for vertical momentum diffusion. A hydrostatic pressure assumption was made for simplification. Sediment computations were based on a two-dimensional solution of the conservation of mass equation for the channel bed and the three-dimensional advection-diffusion equation for suspended sediment transport. The model accounts for sorting and armouring and can therefore be used to compute nonuniform sediment transport processes. The algorithms comprise sediment transport of particles with a maximum diameter of 2 mm. The bed load formula of *v.Rijn (1984a)* is used to compute the bed load capacity and the relationship of *v.Rijn (1984b)* is used to compute the reference concentration for suspended sediment transport at the river bed. A reach of 84 km was discretized by a finite difference mesh using a mesh size of 250 to 300 m in longitudinal and 30 to 90 m in lateral direction. The Mississippi reach has a meandering planform, the meanders are divided by eight crossings. Fractional transport was computed using two sediment size fractions. Validation of the model was achieved by comparing observed and calculated sediment deposition processes at a chosen crossing during a period of 9 months. The computed velocities and suspended sediment concentrations at the chosen crossing and a bend downstream the crossing followed typical trends. However, no field data was available to quantify the accuracy of the velocity and suspended sediment predictions of the model.

Fang & Rodi (2003) presented calculations of flow and suspended sediment transport with a three-dimensional morphodynamic model proposed by *Wu et al. (2000a)*. The finite volume method is used for spatial discretisation using a vertically adaptive non orthogonal grid. The model is validated by calculating the development of flow, suspended sediment concentration, and river bed deformation in a 16.7 km reach upstream of a dam in the Yangtze river over a period of 76 years. The Reynolds-averaged Navier-Stokes equations were solved using the k-ε turbulence model. The distribution of suspended sediment concentration was given by the convection-diffusion equation. The reference concentration was determined by the empirical formula given by *v.Rijn (1984b)*. The computed results were compared to laboratory measurements of a physical model experiment. For testing the model, computed velocities at the surface and the computed deformation of the bed resulting from deposition of suspended load were compared to measurements. In the study of *Fang & Rodi (2003)*, lateral flow velocities and cross-sections are shown at the beginning, after 32, and after 54 years. Both the lateral velocity distributions and the bed evolution was modelled with satisfying agreement for all three points of time, even though the morphology changed dramatically over this period with deposition processes of up to 100 m.

4.1.2 The morphology of the Danube river east of Vienna

Morphological structures and river bed changes of the Danube river between Vienna and the Austrian-Slovakian border are analysed in Chapter 2. The results indicate that the morphological structures of the Austrian Danube reach east of Vienna can be divided into three sub-reaches. Within the upper 20 km (from km 1920 to 1900) the reach comprises a pronounced alternate bar configuration. Downstream this reach, from km 1900 to 1890, the morphological structures are less developed due to intensive groyne installations. At the lower reach, from km 1890 to 1880, the curvature of the river leads to typical morphological features such as point bars at the inner bends of the river and scour regions at the opposite sides.

The results of the analysis focussing on the processed erosion and deposition patterns are used to test the modified numerical model. The effect of the 2002 flood on the river bed morphology is analysed by comparing the river bed surveys in spring and autumn 2002. The magnitude of this flood event was on the order of 100 years. Maps showing erosion and deposition patterns were created based on the pre and post flood surveys in 2002. The processed bed level surveys showed that the overall morphological features such as sizes, shapes, and locations of the bars and crossings remained stable over the flood event. Local bed changes in the range of ± 1 m indicated that discontinuities were partially filled up during the flood event. Scour depths increased slightly.

A sub-reach with a length of 8 km (km 1909.5 to 1901.5) was chosen for the numerical computations. It is situated within the upper half of the Danube reach characterised by an alternate bar configuration. The sub-reach was mostly in a stage of deposition. Subtracting 1.5 km upstream, and 0.5 km downstream gives a reduced test reach of 6 km that was chosen for comparing measured and computed results. The test reach comprises alternate bar structures with slight curvature. It is positioned downstream the maintenance reach and is thus free of regular grain feeding measures. Moreover, no dredging measures were performed at the test reach in the chosen period so that the observed morphological changes were based on natural processes.

4.2   Methods

The modified numerical model *SSIIM* is applied on the 8 km long study reach of the Danube river east of Vienna. The nonuniform sediment transport equations of *Wu et al. (2000b)* have been incorporated into the numerical model to account for hiding-exposure effects. A description of the numerical computations of flow, sediment transport, and bed changes is given in Chapter 3.3. Morphological changes that evolved as a consequence of the flood in 2002 are computed and compared to the measured bed changes derived from the pre and post flood surveys.

Figure 4.1 shows a map of the 8 km long Danube reach from stream-km 1909.5 to 1901.5 that is modelled in this study. The reach is situated 11.5 km downstream the hydropower station Freudenau. The flow direction is from left to right, the stream kilometres of the Danube river are counted against the flow direction. The red dots indicate the hectometre points of the stream kilometres.

A numerical grid based on the finite-volume method is generated. The grid consists of quadrilateral cells in the map projection. In Figure 4.1 the intersection points of the grid lines are shown. The width of the grid is limited by the left and right hectometre points. The grid is:

> ➢ non-orthogonal, i.e. it follows the course of the river and it can be described by a curvilinear coordinate system. Thus, the grid is aligned in streamwise direction to decrease false diffusion *Olsen (2002)*.
>
> ➢ vertically adaptive, i.e. the grid can change in vertical direction according to the computed bed level changes,
>
> ➢ structured, i.e. the number of cells in stream-wise, cross-streamwise and vertical direction is invariant.

The grid dimensions are 320 cells in streamwise, 25 cells in cross-streamwise, and 5 cells in vertical direction. In total 40,000 cells are used to resolve the flow field of the study reach. The cell dimensions are 25 m in longitudinal and 12 to 14 m in lateral direction. The vertical size of the cells varies spatially according to the bathymetry of the river and temporally according to the discharge variations (hydrograph). The dimensions of numerical grids based on the finite volume method should fulfil two criteria to adequately represent the hydrodynamics of an open channel flow. The aspect ratio should not exceed a maximum ratio ranging from 2 to 10 *Olsen (2002)*. Here, an aspect ratio of approximately 1.8 is achieved. Furthermore, the difference of one grid cell size compared to the size of its neighbour cell should not exceed 50% (*Olsen (2002)*). This is also fulfilled in the study, since all cells have virtually the same size.

The generation process of the finite volume grid is performed separately for the position and the elevation. The grid generation procedure is developed based on the availability of bathymetric data of the Danube river. Initially, a coarse grid is produced, that is aligned on the hectometre points (100 m distance) using 25 cells in cross-streamwise and 80 cells in streamwise direction. Data of bed levels of the Danube river are available for cross-sections in 100 m distance (see Figure 4.2). The bed cell heights at the intersection points of the grid lines are interpolated from the measured cross-sectional data. Thus, all intersection points lie on the measured profiles, so that only marginal inaccuracies from the interpolation procedure are obtained. The grid is then densified twice in longitudinal direction to obtain the longitudinal grid spacing of 25 m.
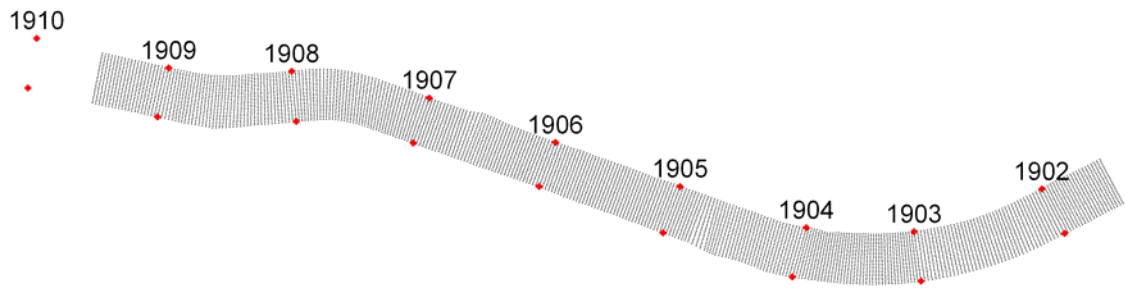
Figure 4.1: Numerical grid in plan view

The vertical elevations of the grid cells are obtained from combined data of different bed level measurements at the Danube river. Both data from echo-sounder measurements in the main channel and data from photogrammetric flights covering the dry and shallow areas are used. For illustration, Figure 4.2 shows a cut-out of the navigation map of the Danube river from km 1904.7 to 1903.4. Superimposed on the navigation map additional information is shown containing:

➢ cross-sectional measurements of bed levels using a single-beam echo-sounder technology (red dots/lines) with a longitudinal distance of 100 m,

➢ hectometre points (yellow dots),

➢ bed data from photogrammetric flight (orange dots),

➢ navigation channel (blue dots),

➢ grid intersection points (black circles).

Figure 4.2 shows, that the single-beam echosounder technology provides dense information of bed levels in lateral direction. However, the measurements are limited to the main channel. A bar that is partly covered by vegetation can be seen from km 1904.6 to 1903.8. Green lines delimit the vegetation areas. For operational reasons, shallow or dry river reaches cannot be surveyed by this technology. These reaches must be surveyed by different measurement techniques. In this study, the bed levels in shallow or dry regions are obtained from a photogrammetric flight technology. Combining both measurement technologies allows to obtain complete river bed level data.
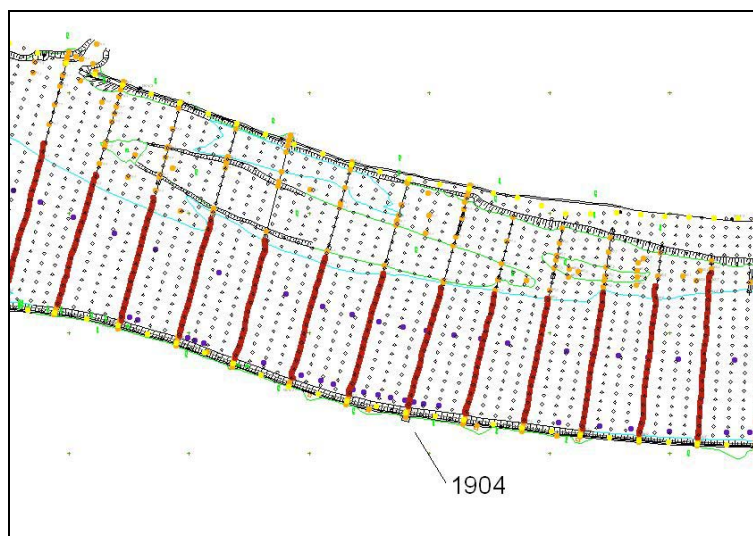

Figure 4.2: Map of river reach around stream-km 1904

An example of the measured data points at a cross-section at km 1904.0 is shown in Figure 4.3. The hectometre points are indicated by the green asterisk. The data densities of the echosounder measurements (red dots) and the photogrammetric survey (black dots) are significantly different. On average, 500 echo-sounder measurements are available per cross-section, while only 10 to 20 photogrammetric points are supplied to cover dry and shallow reaches. Cross-sectional data is obtained by projecting the measured points on pre-defined cross-sectional profile lines. The numerical grid is laterally defined by 25 equidistant cells in cross-streamwise direction. All available bed level data are used and combined to calculate the height elevations of the numerical grid. The combination of data from echosounder measurements and photogrammetric flights allows to represent the geometry of the Danube river with an improved accuracy, especially in the shallow and dry regions of the river bed.
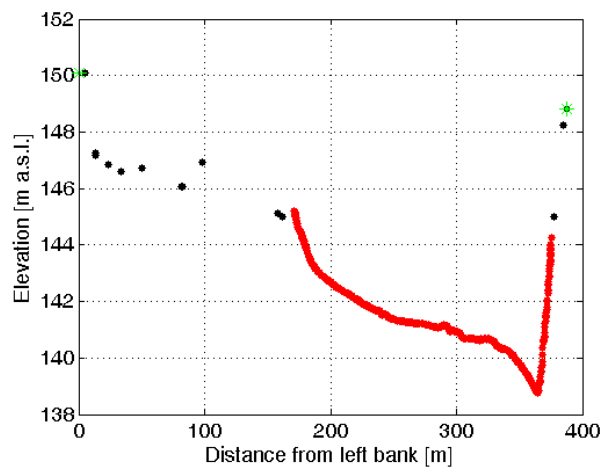

Figure 4.3: Cross-section at km 1904.0

Additionally to the spatial discretisation, the discharge variations of the 2002 flow hydrograph have to be considered for unsteady computations of flow and morphological changes of the Danube river. Figure 4.4 shows the flow hydrograph of the Danube river east of Vienna at the gauge station Wildungsmauer at stream-km 1894.7. This gauge station is used as reference for navigation purposes. The hydrograph is applied in this study, which is justified by the absence of relevant tributaries. Three major flood events are measured in 2002 in this reach of the Danube river, with a maximum discharge exceeding 8,000 m³/s in March and 10,000 m³/s in August 2002. The echo-sounder bed level surveys are performed at the end of February and the beginning of November 2002, so that the effect of the three floods on the morphological changes of the Danube river is completely covered by the bed level surveys. No dredging measures happened during the period between the surveys in the chosen study reach. It is located downstream the maintenance reach. Thus, it is assumed that the study reach is free of anthropogenic influence during the study period. The flood events that are used for the numerical computations in this study are indicated (magenta lines). The chosen peaks are motivated by the assumed initiation of sediment transport at Q = 2000 m³/s (≈MQ) (see Table 2.4). It is thus assumed that all flow periods with respect to relevant morphological processes are covered. This procedure allows to neglect the discharges occurring between, before, and after the floods. In this way, the temporal discretisation is significantly reduced using only the relevant discharges. The first

flood event starts at March, 20 and is finished at April, 4, with a duration of 19 days, and the second event with two peaks starts at August 7 and is finished at August, 31, having a duration of 25 days. In total, 44 flood days are computed.
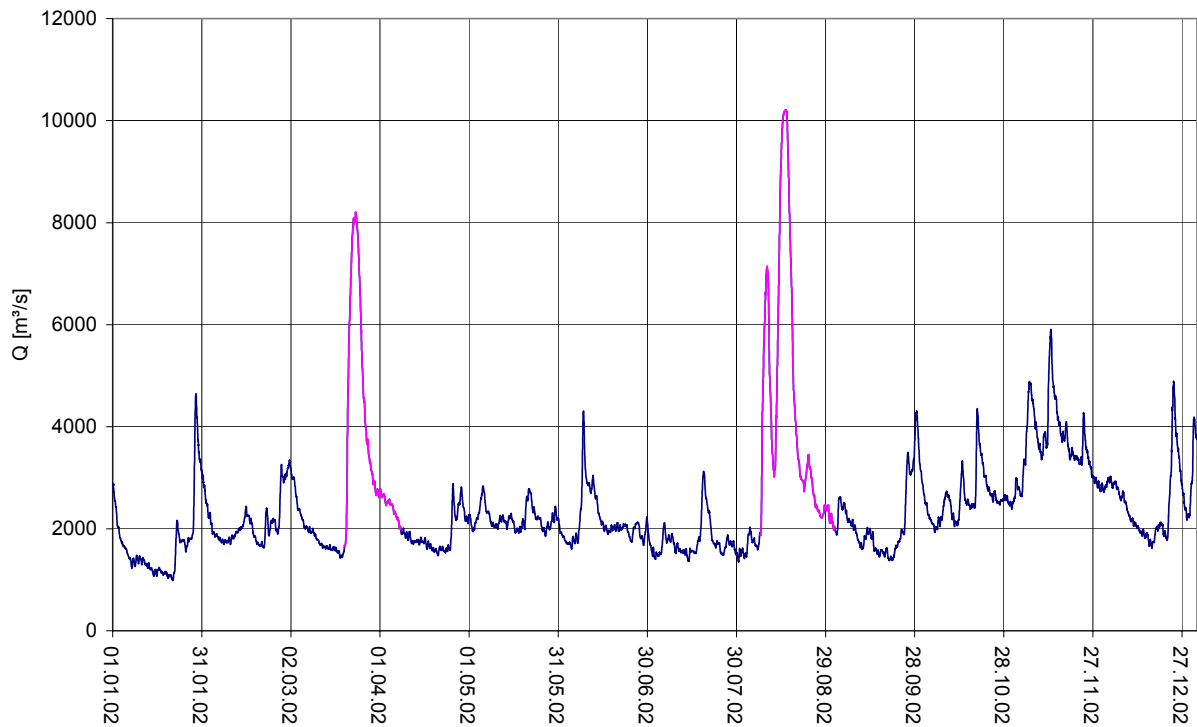
Figure 4.4: Hydrograph 2002 at Wildungsmauer (km 1894.7), magenta: used in *SSIIM*

The flood events used as an input for the morphodynamic model are shown in Figure 4.5. The flood peaks are strung together in a way that immediately after the termination of the first flood, the second and third flood floods start. The hydrograph shows typical flood features with a strongly increasing discharge at the rising limb, a rounded peak discharge followed by a slower decrease of discharge during the falling limb. The third peak measured in August 2002 almost achieves the magnitude of a 100 year flood. Various pre runs are performed to achieve an appropriate time step for the numerical computations. Due to the implicit nature of the morphodynamic model, variations of the time step do not influence the stability of the computations but the accuracy decreases with an increasing time step. A time step of 900 s proves to be sufficiently small to compute the morphological changes. Thus, 4224 outer iterations are performed to compute the flood duration of 44 days. For each time step, inner iterations are employed to achieve convergence for the flow and sediment computations. After each time step, the bed levels are adjusted according to the computed sediment fluxes in each bed cell.
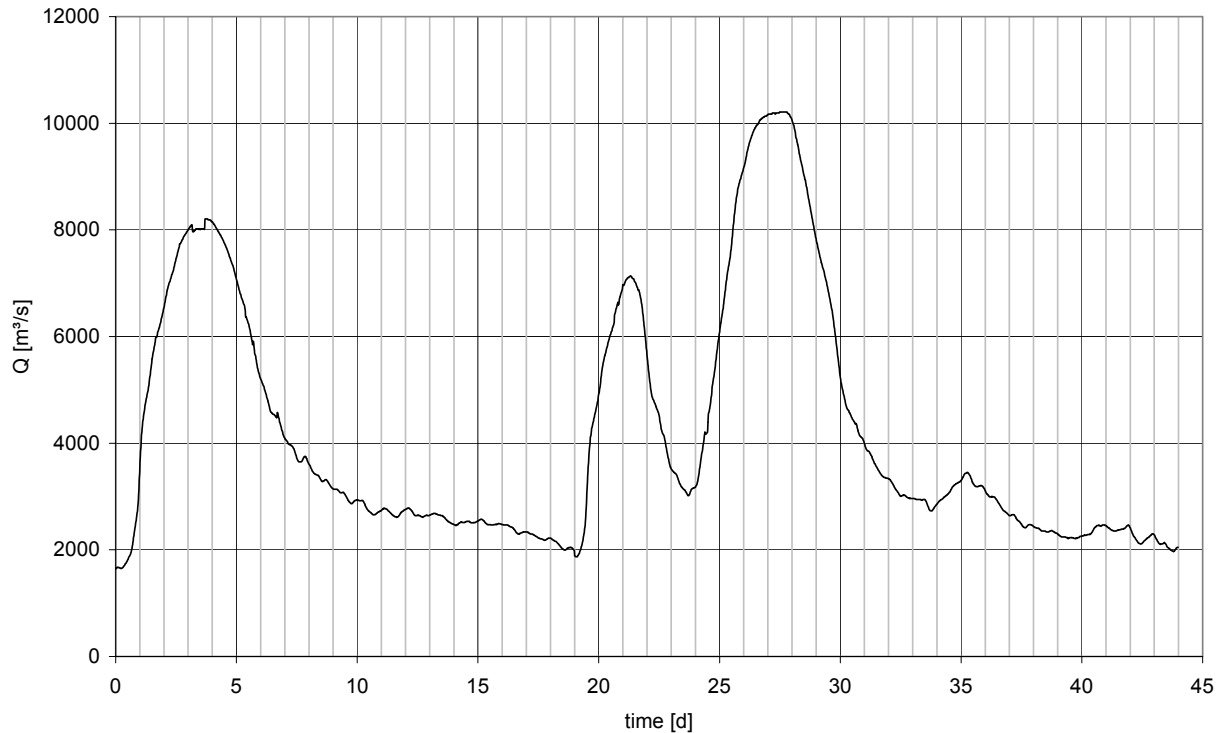
Figure 4.5: Hydrograph used in *SSIIM*

Besides spatial and temporal discretisation, it is necessary to resolve the bed material. Therefore, the sediment size distribution curve is divided into a certain number of sediment fractions represented by a mean fractional sediment diameter. Figure 4.6 shows the measured sediment size distribution of the Danube river bed material and the fractionally decomposed sediment size distribution that is used for the numerical model. Bed material was sampled at 20 locations by *Zottl & Erber (1987)* and averaged to achieve the mean measured sediment size distribution. The sieve curve shows that the Danube bed material consists of a wide range of grain diameters with a d_{50} of 22 mm and a d_{90} of 59 mm.

In this study, the sediment curve is decomposed into seven size fractions for the numerical model. As shown in Figure 4.6, the gradient on the non-logarithmic scale significantly changes with increasing sediment diameters. Therefore a non-uniform distribution of the fractions is chosen. The fractions 20, 20, 20, 20, 10, 5, and 5 % are selected according to the development of the measured sieve curve gradient. A small gradient for the larger sediment sizes requires a finer fractional discretisation while for the steep gradient in the range of small particles a fraction of 20 % is sufficient.
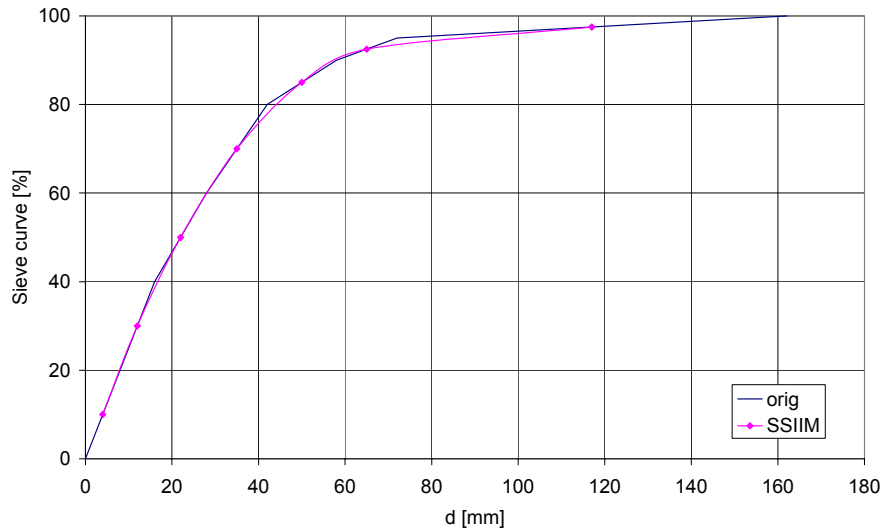
Figure 4.6: Sediment size distribution of river bed material of the Danube river

One boundary condition that needs to be specified for numerical computations is the discharge hydrograph at the upstream end of the river reach. Additionally, the unsteady sediment inflow needs to be specified. In Figure 4.7, the temporal variation of the sediment inflow is shown that is specified at the upstream cross-section. The shape of the sediment inflow follows the flow hydrograph shown in Figure 4.5. The unit of the inflow rate is [m³ sediments per time]. The *Wu et al. (2000b)* formula is used on an idealised inflowing cross-section to estimate the inflowing sediment transport rates for each fraction p_i. The sum of all fractional transport rates q_{bi} gives the total inflowing sediment transport rate. For the peak discharge of Q > 10,000 m³/s, a sediment transport rate of $q_{b,max}$ = 0.14 m³/s is achieved. The upper 1.5 km (km 1909.5 to 1908) are used for numerical development of the flow and sediment transport and are thus not used for the morphological analysis. Thus, possible inaccuracies of the estimated sediment inflow and the flow and sediment computations should not effect the reduced test reach.

The numerical computations are performed by rough adjustment of the threshold for incipient sediment motion. Sensitivity of this parameter and the sensitivities of further parameters to the computed results is discussed thereafter.

Figure 4.7: Sediment inflow

4.3   Results and discussion

4.3.1   Flow

Sediment transport, and, as a consequence the morphodynamic processes in a river are based on the prevailing hydrodynamics. The directions of the flow velocities near the river bed and the bed shear stresses derived from the computed flow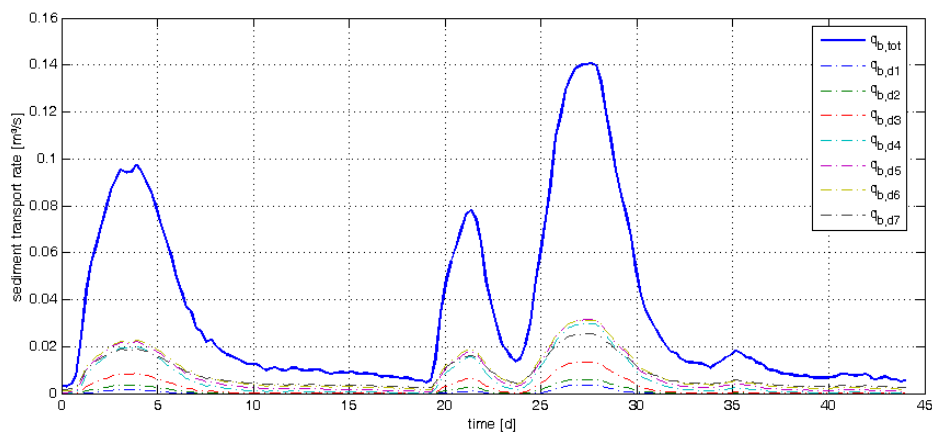 features determine the sediment fluxes in the grid cells of the numerical model. Therefore it is essential for a numerical model to compute the flow features accurately in order to be able to compute sediment transport and morphological changes correctly.

In this study, the plausibility of the computed flow features is investigated for two characteristic discharges. Based on the range of the generated hydrograph (see Figure 4.5), the two characteristic discharges MQ = 1,915 m³/s (mean discharge) and HQ_{100} = 10,400 m³/s (100 year flood) are selected for the plausibility study. The grid of the immobile river bed is generated based on the pre flood survey in March 2002. From a morphological point of view, sediment transport is initiated at a discharge of approximately MQ. For discharges below MQ, it is assumed that only minor bed changes develop.

Figure 4.8 shows contour plots of the flow velocities in streamwise direction for both discharges, MQ = 1,915 m³/s and HQ_{100} = 10,400 m³/s. Both streamwise velocities near the river bed, and near the water surface are shown. Analysis of the computed velocity fields in relation with the river bathymetry as given in Figure 4.18 (top map) shows:

> ➢ lower velocities near the river bed and higher velocities near the water surface follow a logarithmic vertical velocity distribution
> ➢ the velocity distributions of all four maps reflect the bathymetric shape of the river reach. Characteristic lateral and longitudinal velocity variations are computed. Generally low velocities are computed in the bar regions while high velocities appear in the opposite scour regions,
> ➢ a maximum velocity of approx. 4 m/s is achieved for the model run at HQ_{100} in the scour regions and in the narrow crossing upstream km 1907,
> ➢ the wide crossing upstream km 1905 shows reduced velocities,
> ➢ a discontinuity in the morphological structure at km 1902.3 (hole) is reflected by reduced velocities in this region.
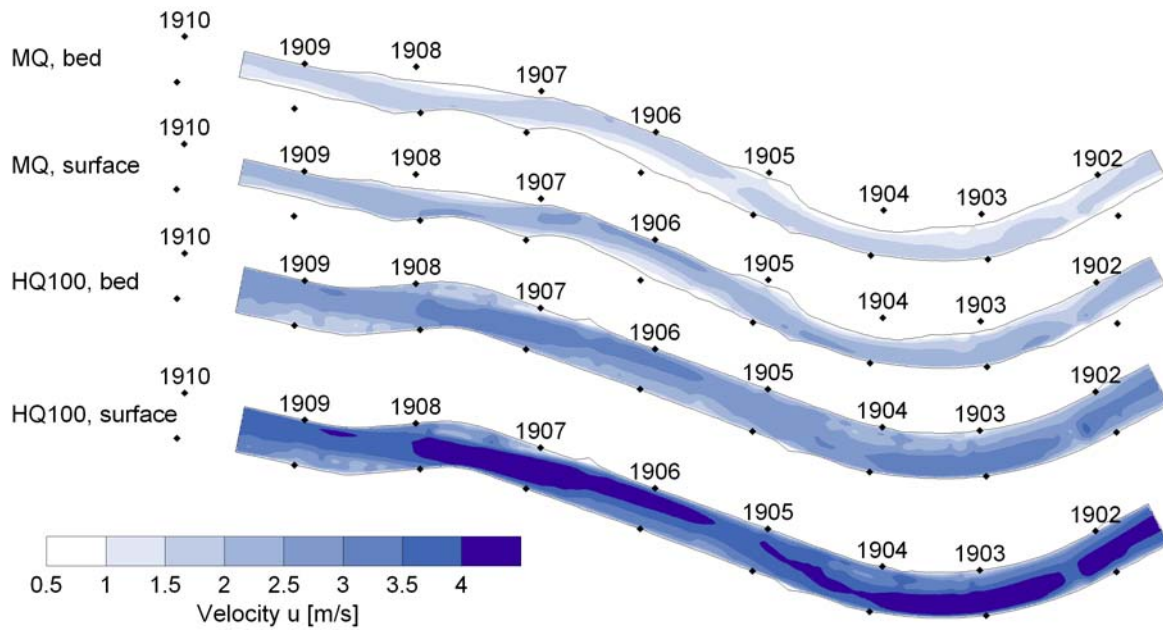
Figure 4.8: Near-bottom and near-surface velocities for *MQ* and *HQ$_{100}$*

Additionally to the contour plots in map view, the velocities in streamwise direction are shown for two cross-sections. Typical cross-sections of a bend (km 1904) and of a crossing (km 1905.2) are given. Figure 4.9 and Figure 4.10 show streamwise velocity contours at km 1904 for mean discharge and for the 100 year flood. Moreover, the inclination of the lateral water level is computed and plotted in the figures. Compared to the cross-sectional variations of the bed levels, the lateral water surface gradients are small. Thus, lateral water level differences are difficult to detect in the plots. The bathymetry of the profile shows an asymmetric shape, that is typically found in river bends. The profile is within a developed bar reach with shallow water levels at the inner bank (bar) with a smooth gradient of the slip-off slope bank and large water depths at the outer bank (scour) with a steep bank gradient at the undercut-slope bank.

To investigate the plausibility of the flow calculations of the model, the computed differences of lateral water levels are compared to an analytical approach of water level differences at river bends as given in Equations (3.30) and (3.31).

Applying the analytical approach for estimating the influence of curvature to the lateral slope of the water surface at the river bend, one obtains good agreement of the values derived by the empirical formula and the numerical model. Analytical and numerical differences of the water surface at the bend apex are given in Table 4.1.

Table 4.1: Analytical and numerical differences of the water surface at the river bend at km 1904

Discharge	Δh, analytical	Δh, numerical model
1,915 m³/s (*MQ*)	4.5 cm	5.5 cm
10,400 m³/s (*HQ$_{100}$*)	20 cm	18 cm

The velocity distribution for *MQ* in Figure 4.9 shows vertically increasing flow velocities from a rough bed to the water surface. The velocity distribution is skewed to the right side towards the scour region where larger water depths are available. A maximum velocity of approximately 2.5 m/s is achieved. The given distribution of the velocities in a river bend gives rise to nonuniform sediment transport processes over the width of a bar. In combination with secondary flow currents (not displayed), the three-dimensional model approach considers these non-uniform sediment transport effects. Thus it outperforms one- or two-dimensional model approaches in curved river flow situations.

A discharge of 10,400 m³/s floods the vegetation regions at this bar profile as shown in Figure 4.2. Therefore, the velocity distribution is more complex than in a compact river channel. This is shown in Figure 4.10. Two velocity maxima are computed, one in the main channel and the other one on the left side of the partly vegetated shallow water region. Considerably higher velocities are computed for HQ_{100} compared to *MQ*. The velocity maximum at the main channel moves slightly inwards for HQ_{100} indicating a more uniformly distributed sediment transport within the main (navigation) reach.

Figure 4.9: Streamwise flow velocities at km 1904 for *MQ*
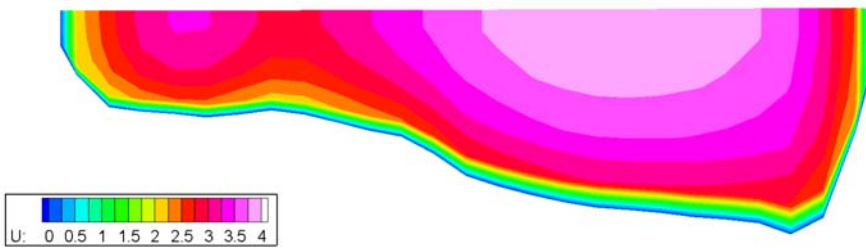
Figure 4.10: Streamwise flow velocities at km 1904 for HQ_{100}

Streamwise velocities are plotted on two levels over the width of the cross-section for both discharges (Figure 4.11). Here, the inwards shift of the velocity maximum for *MQ* is clearly detected which is less pronounced for the HQ_{100} velocities in the main channel. For both discharges, the velocities gradually decrease in the bar region. For HQ_{100} the velocities slightly increase beyond the bar on the left side due to the flow around the vegetated structure as shown in Figure 4.2. The maximum velocities exceed 4 m/s in the scour region, indicating large sediment transport processes there for HQ_{100}.
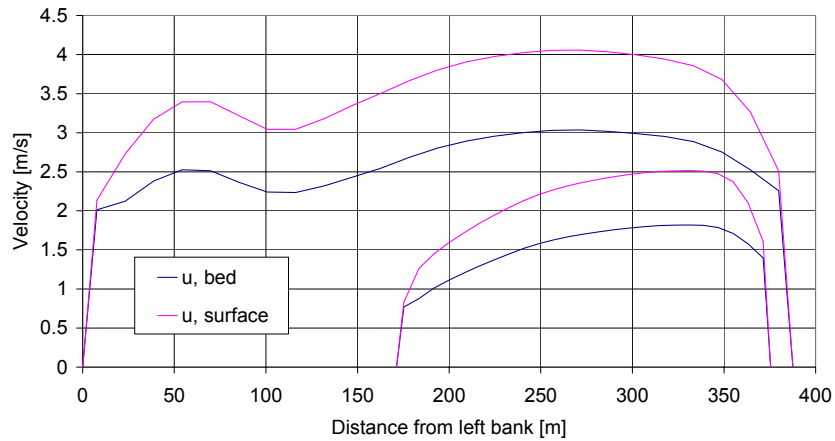
Figure 4.11: Velocities at cross-section km 1904 for *MQ* and *HQ$_{100}$*

For the computation of sediment transport and morphological changes the bed shear stress resulting form the flow computation is used. The lateral distribution of the computed shear stress is shown in Figure 4.12 for both discharges. The shapes of the distributions of bed shear stress and streamwise velocities coincide. In the present model approach the shear stress is computed as a function of the turbulent kinetic energy (see equation (3.9)).
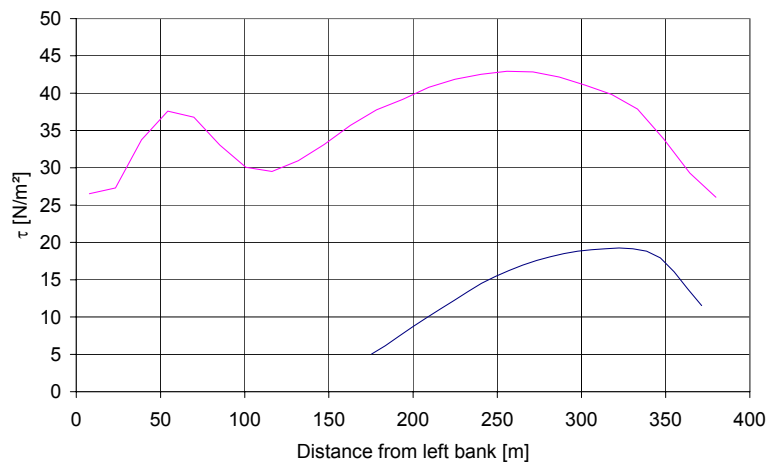
Figure 4.12: Shear stress at cross-section km 1904 for *MQ* and *HQ$_{100}$*

The plausibility of the computed shear stress values is investigated by comparing the model output with averaged one-dimensional approaches. Based on a mean water depth of 5 m and an energy slope of 0.35 m/km for *MQ* and a mean water depth of 8 to 9 m and an energy slope of 0.45 m/km for *HQ$_{100}$* the mean bed shear stresses for the two discharges are given as:

$$\tau_{0,MQ} = \rho \cdot g \cdot h \cdot I = 17 \, N/m^2$$

$$\tau_{0,HQ_{100}} = \rho \cdot g \cdot h \cdot I = 36 \, to \, 41 \, N/m^2$$

The mean bed shear stresses fit well the computed results of the numerical model. Thus, a plausible representation of the numerically computed bed shear stresses can be inferred.

The flow computations are analysed at a second cross-section. The cross-section is situated at km 1905.2 between two alternating bars. Thus, it represents a typical crossing profile. Figure 4.18 (top map) shows that considerably smaller water depths are achieved in this cross-section and the bathymetric profile is considerably more symmetrical and uniform. The velocity maxima in the upstream and downstream vicinity of the crossing profile change from the left side to the right side, respectively (see Figure 4.8).

Figure 4.13 and Figure 4.14 show streamwise velocities in the cross-section. Compared to the bar profile the velocity distribution for *MQ* is considerably more uniform. The flow width is larger compared to the bar cross-section ($B_{1905.2}$ = 320 m, $B_{1904.0}$ = 210 m), thus the flow velocities are smaller here. The computed water levels are virtually constant over the width of the profile. This result is plausible because the profile is positioned in a straight river reach, thus, lateral water level differences induced by the curvature of the river are not developed here. Figure 4.14 shows the velocity distribution for HQ_{100}. Also for this discharge, the river bed geometry is virtually symmetrical. However, the flow here shows a stronger inclination to the left side. Figure 4.8 shows, that this profile is still influenced by the upstream velocity field for HQ_{100} that is inclined to the left side as a consequence of the bar-scour configuration. The velocity maxima here are slightly smaller than at the bar profile.
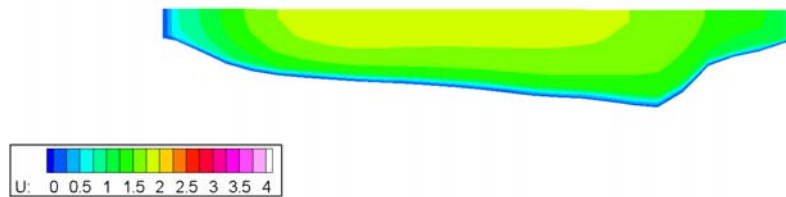
Figure 4.13: Streamwise [e95]flow velocities at km 1905.2 for *MQ*
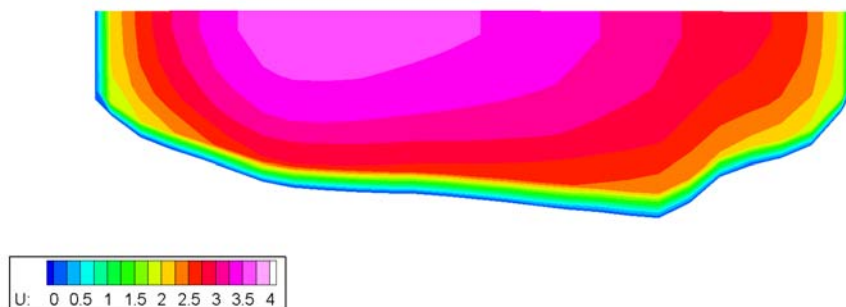
Figure 4.14: Streamwise flow velocities at km 1905.2 for HQ_{100}

In accordance with the bar cross-section, the velocities of the crossing profile are processed for both discharges in two levels, near the water surface and near the river bed. In Figure 4.15, the velocity distributions are shown. Compared to the bar profile, the uniform character of the velocity distribution can be seen that is a consequence of the symmetrical shape of the river bed in this region in a straight river reach. However, for HQ_{100} the velocities are skewed slightly to the left side. The maximum velocity computed for *MQ* slightly exceeds 2 m/s while the maximum velocity at the bar profile is 2.5 m/s.
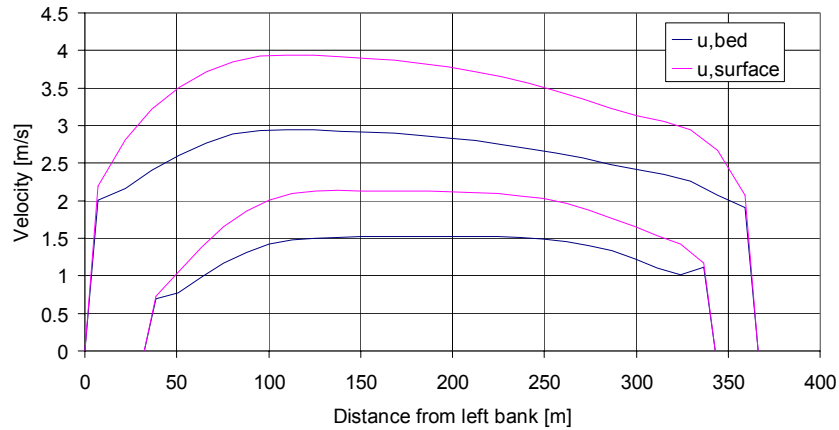
Figure 4.15: Velocities at cross-section km 1905.2 for *MQ* and *HQ$_{100}$*

The shear stress distribution of the crossing profile is shown in Figure 4.16. For *HQ$_{100}$*, the bed shear stresses achieve values that are similar to the values at the bar region. The bed shear stress distribution is considerably skewed to the left side, that is explained by the influence of the neighbouring bar regions. The bed shear stress at *MQ* is rather uniform and approaches smaller values than the shear stress at the cross-section in the bar region. Thus, for the flood discharge, strong sediment transport processes are expected while for mean discharge, a reduced sediment transport capacity is given.
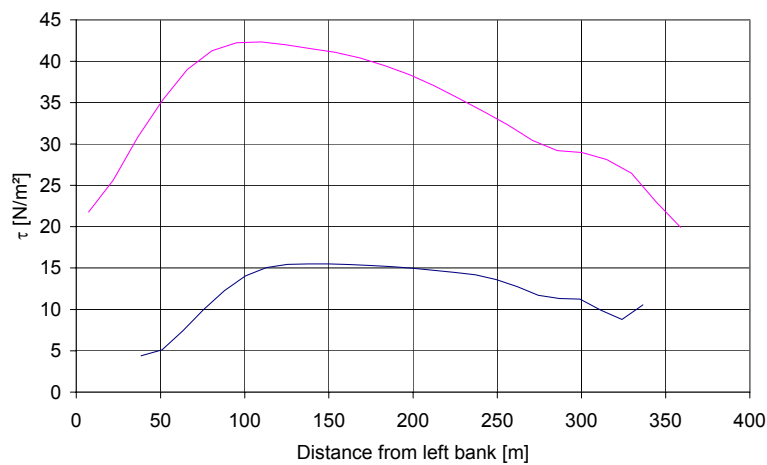
Figure 4.16: Shear stress at cross-section km 1905.2 for *MQ* and *HQ$_{100}$*

The computations of the flow field as shown in Figure 4.8 to Figure 4.16 are used for quantitative analysis of the velocity distribution within the study reach. Plausible computations are obtained showing typical flow patterns in an alternate bar reach. However, velocity measurements are not available, so the validity of the computations has to be controlled implicitly using different data sets. The two chosen discharges are characteristic at the Danube river. Data of measured water levels for both discharges are available.

Figure 4.17 shows measured and calculated water levels for the two characteristic discharges within the study reach. The calculated water levels are extracted from the centre of the grid in

longitudinal direction so that they are virtually free from lateral inclination influences. The results show that the numerical model is able to calculate the water levels with good agreement. Minor deviations are found at HQ_{100} that do not extent 20 to 30 cm. The measured longitudinal water level gradients are different for the two discharges. Gradients of approx.

➢ 0.38 m/km = 3 m / 8 km for *MQ* and

➢ 0.46 m/km = 3.7 m / 8 km for HQ_{100}

are measured. Also the measured gradients are well represented by the model. For both computations, a constant roughness coefficient of k_{st} = 37 m$^{1/3}$/s is chosen. Thus, the chosen roughness coefficient is an appropriate general value to represent the flow. The discontinuity in the bathymetry at km 1902.3 (pool) is reflected by the water levels, which is best seen for the high water levels.

It can be concluded that the flow computations are computed in a plausible way. Comparing the computations with measured water levels shows that good agreement is achieved.
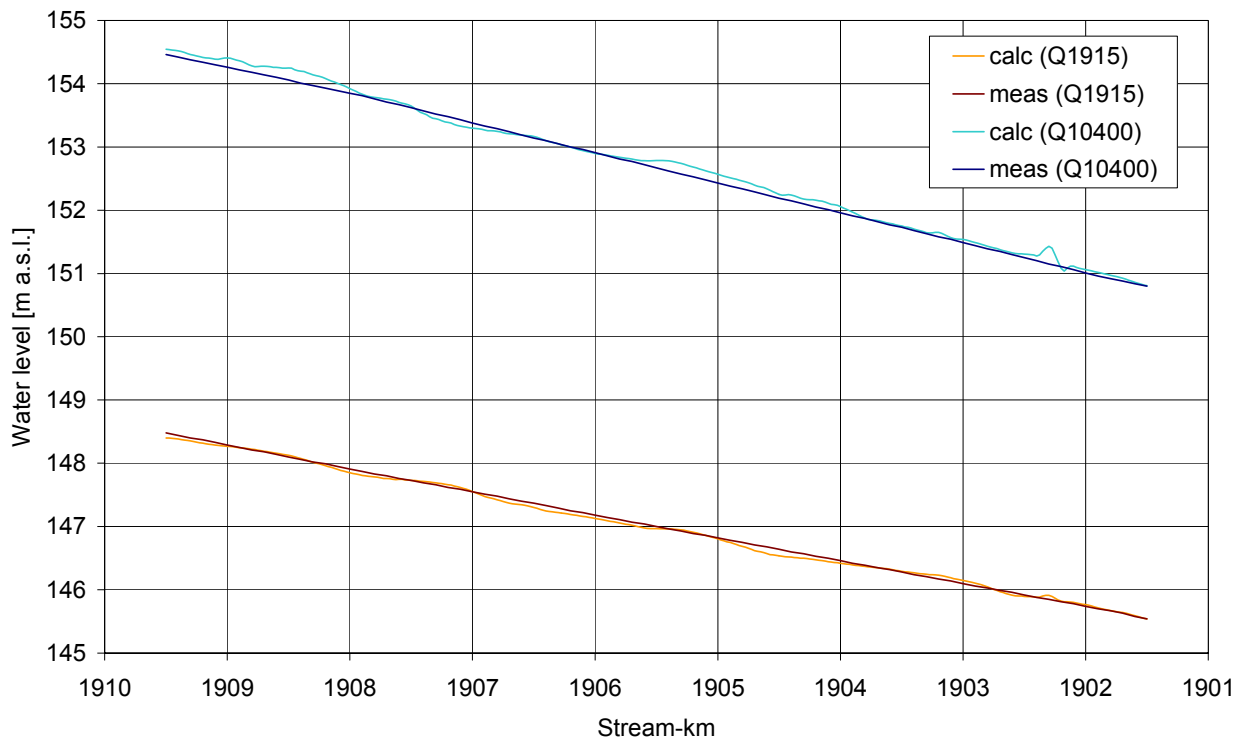
Figure 4.17: Longitudinal water levels for *MQ* and HQ_{100}

4.3.2   Morphological changes

The hydrodynamic computations presented in Chapter 4.3.1 are performed under steady state conditions using an immobile river bed. The computed results are compared to field measurements and to analytical approaches, so that the correct representation of the flow features is assumed. Computing the morphological changes of the Danube river requires two modifications compared to the presented steady flow computations.

(1) The numerical model is applied under unsteady flow conditions using the flow hydrograph shown in Figure 4.5. The flow hydrograph is generated on the basis of the

relevant discharges producing morphological changes for the period between the pre and post flood survey in 2002.

(2) Both flow and sediment computations are performed on a mobile bed according to the flow chart in Figure 3.6.

Thus, the conditions are given to compare the measured morphological changes that developed as a consequence of the 2002 flood to the calculated morphological changes.

The numerical computations are achieved by adjusting the parameter for incipient sediment motion θ_c. In this Chapter, the computed results are obtained by increasing the default value of 0.03 to 0.045. For the other sediment parameters (m, α) default values are chosen. The effect of choosing an increased value for θ_c and the sensitivity of all sediment parameters is discussed in Chapter 4.3.3.

Figure 4.18 shows four contour maps of the study reach of the Danube river ranging from km 1910 to km 1902. Both water depths and bed changes are given. The two maps on top show water depths below the reference low water level. The maps represent the morphology of the Danube river reach at two points of time, before and after the 2002 floods. The pre flood survey was performed in spring 2002 (02-1) and the post flood survey in the late autumn 2002 (02-2). From the two maps it can be seen that the results from the single beam measurements cannot cover the whole width of the Danube reach. Therefore, the bathymetric river bed information is supplemented by photogrammetric flight data to be used for the numerical computations. However, a comparison of two surveys is only possible within the commonly measured river reach.

The morphology of the river shows alternate bar structures. Four bars, two on each side of the banks are present at a length of 8 km giving an average length of 2 km for a bar. The bars are characterised by shallow areas in the bar region and steep scours on the opposite sides. Crossings are situated in the transition reaches between the bars. The crossings exhibit comparably high bed levels lying in between the bed levels of the bars and the scours. Generally the crossings exhibit comparably small water depths and are therefore critical spots for navigation purposes. Comparing the two maps of the surveys 02-1 and 02-2 shows that the general structure and the positions of the bars remain unchanged during the flood event. On a local scale, relevant bed changes can be observed. A noticeable bed development was a hole that was measured at km 1902.3 at the survey in spring 2002 (02-1). It was partially filled up during the flood events, so that it remarkably decayed, what can be observed in the (02-2) map. These strong bed changes impose a relevant test for the numerical model. The observed results are in line with the general conclusions of the whole free flowing Danube river reach from Vienna to the Austrian-Slovakian border that was analysed over a ten year period (see Chapter 2). Also for the long-term development, the bars remained on their positions and changes were observed locally.

For further analysis, the bars and crossings are numbered:

    1   bar from km 1910 to 1908.8 on the right side

    2   bar from km 1908.7 to 1907.5 on the left side

    3   bar from km 1907.2 to 1905.6 on the right side

    4   bar from km 1905.2 to 1902.5 on the left side

    A   crossing between bar 1 and 2

    B   crossing between bar 2 and 3

    C   crossing between bar 3 and 4

The third map (meas) is a difference map and it shows measured bed changes occurring during the two surveys. It was generated by subtracting the two grids of the maps 02-1 and 02-2. In this way, erosion and deposition patterns are obtained, indicated by blue and red colours, respectively. The colour intensity is a measure for the strength of the erosion or deposition.

The measured maps 02-1, 02-2 and the measured bed changes (meas) indicate:

➢ The Danube reach is characterised by strong lateral variations of the water depths (more than 5 meters). The variations are induced by pronounced alternate bar configurations.

➢ Generally the overall morphological features such as size, shape, and location of the bars remain unchanged.

➢ The bed changes are mainly found on a local scale within a range of ± 1 m.

➢ A hole measured near the downstream end of the river reach filled up partially during the flood event. The natural process of smoothing the discontinuity in the river bed geometry produces the largest local bed changes.

➢ Bar 4, the longest bar in the river reach, is influenced by two processes. On one side, it is part of an alternate bar configuration prevailing at this reach that has developed in a general straight river course. On the other side, the bar developed in a slight river bend and therefore shows the characteristics of a point bar. The position of the bar remains unchanged, the gradients of the bar configuration in lateral direction increase as a consequence of the floods. The scour region erodes and at the bar region deposition processes occur.

➢ To a smaller extent, similar processes are also observed for the bars 2 and 3, while bar 1 does not show this tendency.

➢ A small propagation of bar 3 is measured. Material erodes from the centre of the bar and deposits further downstream.

The fourth map is a result of the morphodynamic calculations using the introduced numerical model. The input data comprise (1) the measured bed levels at the pre-flood survey, (2) the photogrammetric data for the shallow water levels, (3) the flow hydrograph shown in Figure 4.5, and (3) the initial grain size distribution of the bed material presented in Figure 4.6. Similar to the processing technique applied to the measured data, the computed bed levels at the end of the run are subtracted from the initial bed levels (02-1) to obtain the bed calculated changes (map 4). For

comparison purposes, the computed results cover the same region as the measured bed changes. The full length of the numerical grid is ranging from km 1909.5 to 1901.5. The results are displayed at a shorter reach (km 1908 to 1902) assuming that a developed flow is reached after the first 1.5 km from the upstream end and that possible inaccuracies initiated by the downstream boundary condition do not propagate more than 0.5 km upstream.

Analysis of measured and calculated bed changes shows:

➢ The magnitude of the bed changes that is mostly in the range of ± 1 m is well reproduced by the model.

➢ The overall erosion and deposition pattern is reproduced with satisfying agreement.

➢ An erosion area at the upstream end of bar 3 and at the crossing B is modelled and measured at approximately the same location. However, the model overestimates the erosion depth.

➢ Downstream the erosion area, at the upper half of bar 3, a deposition area was measured and calculated. While an erosion of the scour is calculated according to the model representation, this only happened partially in nature. The computed erosion of the scour at bar 3 is explained by a significantly increased computed velocity field in this area. The erosion that measured upstream km 1906 at bar 3 is not modelled. Here, the strongest deviation between modelled and measured bed changes occurs. Reasons for the deviation could be an inappropriate consideration of the vegetated parts of the bar region, that might inhibit sediment transport within vegetation and cause erosion downstream the vegetation region, as it was measured. Future research on modelling real rivers morphodynamics should follow this line.

➢ The propagation of bar 3, observed at the downstream end is partially modelled. The succeeding deposition located at the crossing C is modelled with good agreement. Both position and magnitude of the deposition are modelled correctly.

➢ The analysis suggests poor agreement at the upstream end of bar 4. Here, a predominating deposition area is measured, while erosion is modelled. However, analysis of the computed and measured cross-sections shows that in the region only small changes occur that are also modelled (see Appendix A). Thus, the model also performs satisfactory in this area. An integrative measure to quantify the computed results considering the processes of small bed changes is presented later in this study.

➢ The typical morphological processes observed at bar 4, a deposition of the bar and erosion at the scour is well represented by the model. Both the positions and the magnitudes are computed with satisfying agreement.

➢ Another minor movement of bar 4 can be observed upstream km 1903 that is well reproduced by the model.

➢ At the downstream end of bar 4, a discontinuity (hole) is smoothed out during the flood period. This process is characterised by deposition processes at the hole position and erosion processes downstream. These features are well represented by the model.
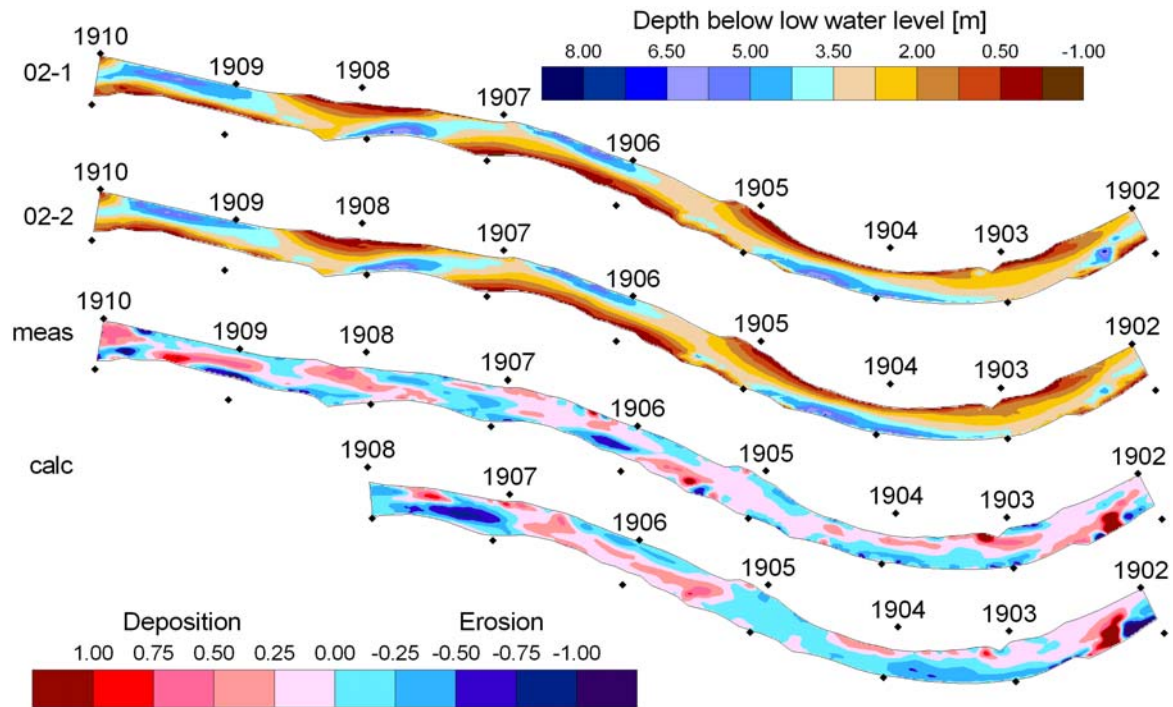
Figure 4.18: Measured bed levels and bed changes versus calculated bed changes

Measured and calculated morphological changes are further analysed on four cross-sectional profiles at characteristic locations. Figure 4.19 shows measured and computed lateral bed levels before and after the flood event allowing to directly compare measured and calculated changes. The chosen profiles represent typical positions at two crossings and two bars. The crossings are plotted on the left side and the bar profiles on the right side. The profile at km 1907.4 represents crossing B which is positioned close to the upstream end of the test reach. The second profile (km 1905.2) represents crossing C. The profile at km 1906.7 characterizes a typical cross-sectional shape of bar 3. The profile at km 1904.0 represents bar 4. This profile was analysed earlier in this study in Chapter 4.3.1. All 400 cross-sectional profiles used for the computation of the Danube river reach are shown in Appendix A.

The profile at km 1905.2 shows that almost no changes happen at this crossing. This process is modelled correctly. While the measurements show minor depositions of a magnitude smaller than 10 cm, the computed results give almost no changes with a slight erosion tendency of a few centimetres. At the crossing at km 1907.4 also minor bed changes are measured. The computed results fit the trend of deposition at the left side and erosion at the right side, but the erosion is considerably overpredicted. The inaccuracy might be explained by an insufficient length of the development reach. The chosen 1.5 km (km 1909.5 to 1908) are possibly too small for a developed numerical flow field.

Comparing the results of bar and crossing profiles show that larger changes are measured and computed at the asymmetric bar profiles than at the symmetric crossing profiles. The profile at km 1906.7 shows deposition processes on the bar that are modelled with perfect agreement. Also, the immobility of the scour is modelled with good agreement. Measured and calculated bed changes are very small here. The profile at km 1904.0 shows deposition processes at the bar that are also

modelled with good agreement. Both the trend and the magnitude is well represented. The bed levels at the scour region are lowered during the flood events. The position of the thalweg remains stable. These processes are represented by the model. The two bar profiles are computed with good agreement compared to the measurements.
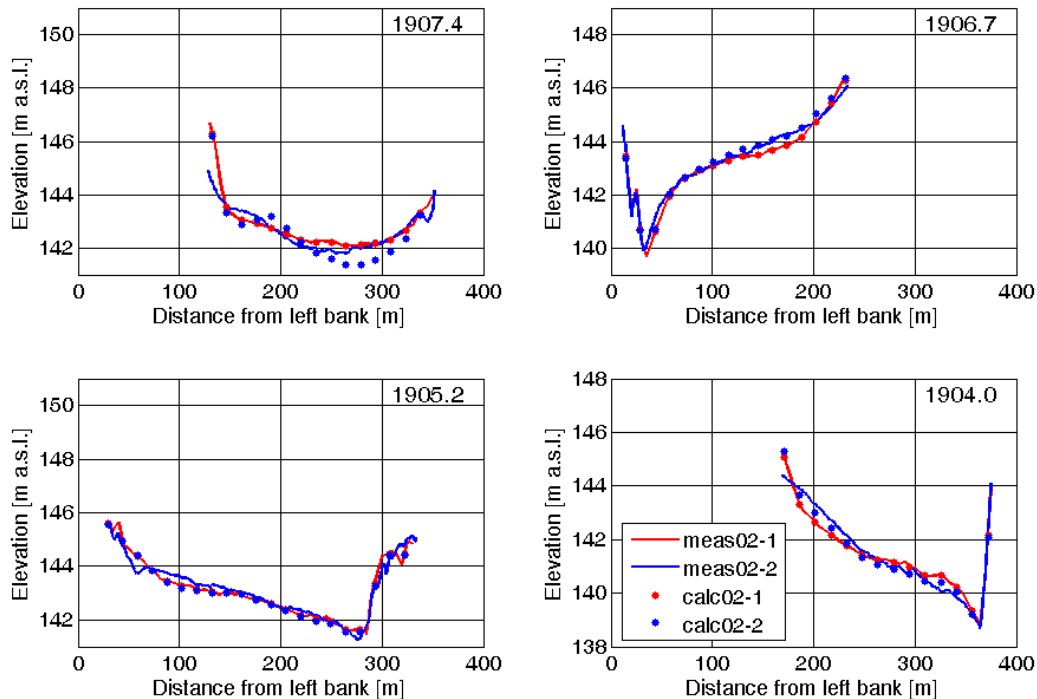

Figure 4.19: Measured and calculated bed levels at two crossings (left) and two bars (right)

The measured and computed longitudinal profiles at the thalweg over the analysed reach from km 1908 to 1902 is shown in Figure 4.20. Bed levels are compared at the thalweg positions derived from the measured profiles of the 02-1 survey. This procedure is chosen to compare bed levels at identical positions.

The figure shows that the thalweg is subject to a certain periodicity. From a virtual mean linear bed level the thalweg deviates approximately 2 m in positive and negative direction. Higher and lower bed levels alternate, the alternate bar and crossing configuration is reflected by the spatial thalweg development. Two outliers are given, one is measured at the 02-1 survey at km 1902.3. This outlier represents the hole measured at the pre flood survey that filled up during the flood event (see Figure 4.18). The second outlier is measured at km 1905.5 where a strong and singular deposition of approx 2 m in the region of the thalweg occurs (see Appendix B at km 1902.3 and 1905.5).

Measured and calculated thalweg development are compared. Good agreement of the thalweg dynamics are computed at the second half of the reach downstream km 1905.5. The thalweg development in the second half is divided into three processes, that are modelled correctly. From km 1905.3 to 1904.4, representing crossing C and the first half of bar 4, the thalweg is invariable over the study period. Downstream this region, the thalweg represents the scour of bar 4. Here, predominating erosion processes are well represented by the model. The third process is the deposition of the

thalweg as a consequence of the deposition process in the vicinity of the hole which is well represented by the model. Upstream km 1905.5, the thalweg is modelled partially correct. In the rising regions from km 1908 to 1907 and km 1906.3 to 1905.8, the measurements show a deposition of the thalweg that is not computed. Here, the model tends to compute degrading bed levels at scour areas within the alternate bar region, while this is only partially measured. The deposition at km 1905.5 is computed with the correct tendency but the model achieves a smaller intensity of the bed changes.
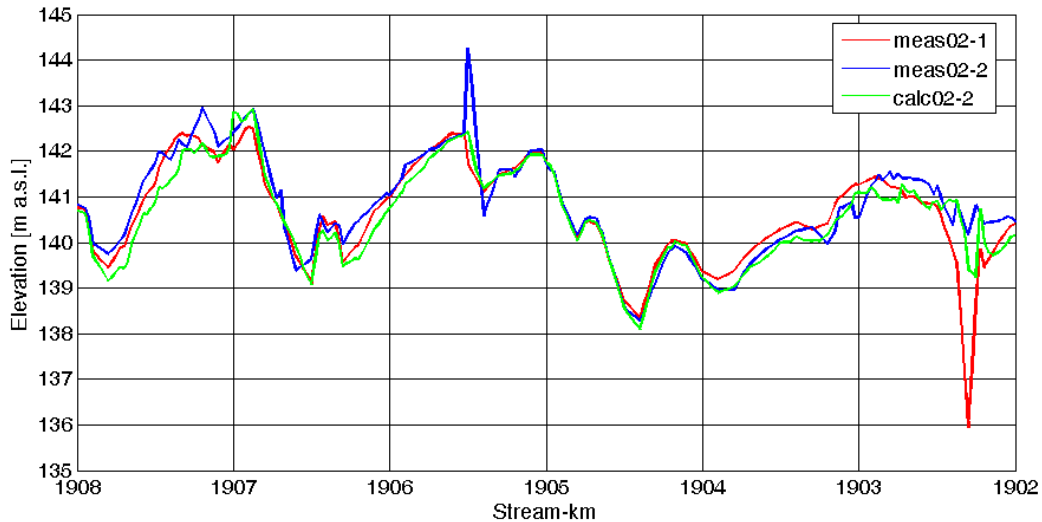

Figure 4.20: Thalweg

The morphodynamic model computes nonuniform sediment transport processes based on the initial sediment size distribution of the Danube bed material (see Figure 4.6). Initially, the bed material is evenly distributed over the entire river reach. In the course of the unsteady flow and sediment computations, sediment sorting processes occur. Figure 4.21 shows the calculated sediment distribution of the d_{50} at the end of the run. Initially, a constant value of d_{50} = 0.022 m is present. The results show a general trend of coarsening in the scour regions and fining on the bars. Field measurements of the lateral distribution of the bed material are not available. Thus, the computed results cannot be compared to measurements. Qualitatively, similar results are obtained at the 180° laboratory bend presented in Chapter 3. Here, the development of a bar and the opposite scour induced fining and coarsening processes, respectively. Therefore, the tendencies of the computed sorting processes in the bar regions of the Danube river can be regarded as plausible. Significant computed coarsening processes can be seen at crossing B, which are possibly related to the over predicted erosion processes in this region. Thus, the accuracy of the sorting processes in this region are debatable. For a detailed analysis on the computed sorting processes at the Danube river, measurements would be obligatory. A detailed analysis of sorting processes at the Danube river is not performed in this study and should be parts of potential future research.
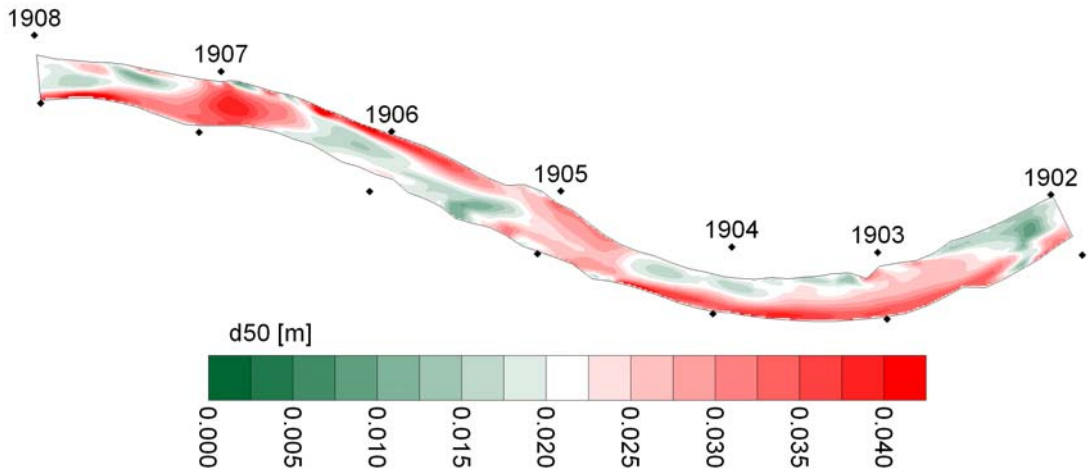
Figure 4.21: Calculated distribution of d_{50}

   The computed sediment inflow and sediment outflow is shown in Figure 4.22. In the numerical model the sediment inflow is user specified at the upstream boundary of the river reach. The upper 1.5 km are used for the development of flow and sediment transport. Therefore the sediment inflow of the reduced 6 km test reach at km 1908 is shown here. The sediment inflow represents the characteristics of the hydrograph. The times of the outflow also coincide with the hydrograph. However, the extent of the outflow deviates from the inflow. The maximum flood (third peak) does not induce the largest sediment outflow. This is due to the general trend of coarsening during the passage of the floods. Thus, the river bed successively stabilises. This phenomenon is further discussed in Chapter 4.3.5.
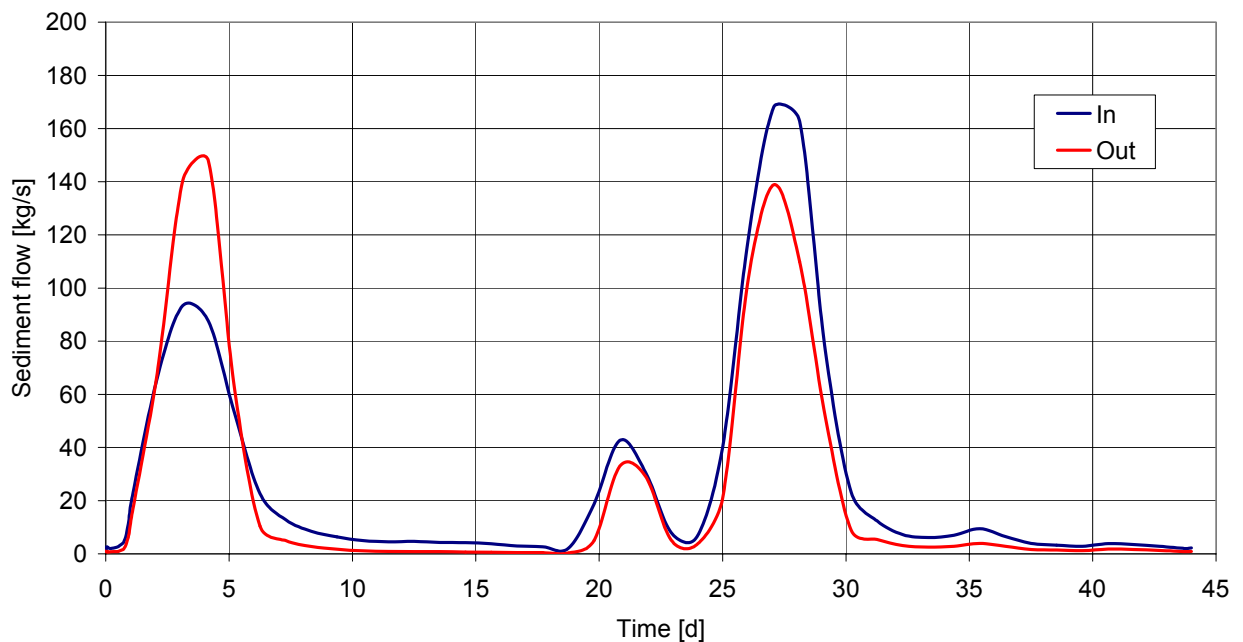
Figure 4.22: Sediment in- and outflow

4.3.3   Sensitivity analysis

In literature, a large choice of formulations for sediment transport can be found. All sediment transport formulas are developed for a specific problem and are limited to a given range of applicability. Some formulas are developed for the transport of coarse material and others are restricted to fine material. Transport formulas can be classified for the type of sieve curve they are applied to. The majority of the transport formulas is developed for uniform sediment material and some formulas consider fractional sediment transport by introducing relationships that describe interaction of the different fractions. In this chapter the sensitivity of several empirically determined parameters is tested that are used to establish a sediment transport formula.

In this study, the results of the morphodynamic computations are performed with a constant Strickler value of k_{st} = 37 m$^{1/3}$/s, a threshold value of incipient sediment motion of θ_c = 0.045, a hiding-exposure coefficient of m = -0.6, a transport rate factor of α = 1.0, and the sediment inflow is estimated on the basis of the *Wu* formula. The results of this parameter set is referred to as 'reference' in the preceding figures. The default parameters at the *Wu* formula are given as θ_c = 0.03, m = -0.6, and α = 1.0. Several sensitivity tests are performed to analyse the sensitivity of the morphodynamic model on different parameter sets. The results are discussed in seven groups: (1) variation of roughness, (2) variation of hiding-exposure coefficient m, (3) variation of bed load rate factor α, (4) variation of the roughness of vegetation regions and consideration of groynes, (5) variation of sediment inflow, (6) variation of threshold for incipient sediment motion θ_c, and (7) variation of the consideration of side slope effects.

The first group summarises parameter studies of the roughness coefficients. In the numerical model, the roughness can be given and varied in two ways. One option is to set a constant overall roughness coefficient, such as the Strickler coefficient k_{st}. Then, the roughness is applied to the whole river reach and remains constant over the entire simulation period, i.e. the roughness is invariable in time and space. A reduced (k_{st} = 34 m$^{1/3}$/s) and an increased (k_{st} = 40 m$^{1/3}$/s) Strickler value is used for the sensitivity tests. The second choice is to define the equivalent roughness k_s as a function of the bed material instead of a constant roughness coefficient k_{st} . Here, k_s = 2*d_{50} and k_s = 4*d_{50} are chosen. When choosing this option, the roughness is initially uniform according to the uniformly distributed bed material at the beginning of the model run. In the course of the simulation the roughness changes according to the re-distribution of bed material, the roughness is then variable in time and space.

Figure 4.23 represents the computed bed changes of the roughness variations. The legend of the contour maps remained unchanged and is given in Figure 4.18. The first map is the result of the reference computations using the parameters as given above. The next two maps show the results of a decreased and increased roughness coefficient k_{st}, respectively. The last two maps show bed changes using temporally varying roughness for the computations. The results show, that the choice of different the roughness options only effects the computed bed change to a minor degree. Both methods of roughness variation lead to minor variations for the bed changes. In most regions, the computed erosion and deposition patterns react insensitive to different k_{st} values. In regions with strong bed changes, the heights of the bed changes are intensified when using a decreased k_{st} value

(i.e. an increased roughness), while the opposite effect is observed for an increased k_{st} value (i.e. a decreased roughness). This is best seen at the scour region of bar 4 and in the pool region at km 1902.3. Variations of the equivalent roughness as a function of the bed material show smaller bed changes in the case of $k_s = 2*d_{50}$. The roughness option $k_s=4*d_{50}$ shows similar bed changes to the reference. Only in the region upstream km 1907, a slightly stronger erosion is observed. This is due to the computed d_{50} distribution, that shows higher values in this region (see Figure 4.21). The chosen roughness coefficient of $k_{st} = 37$ m$^{1/3}$/s in the reference computations appears to be an appropriate value, it gives best results compared to the measured bed changes and it fits the measured water levels in longitudinal and lateral direction.
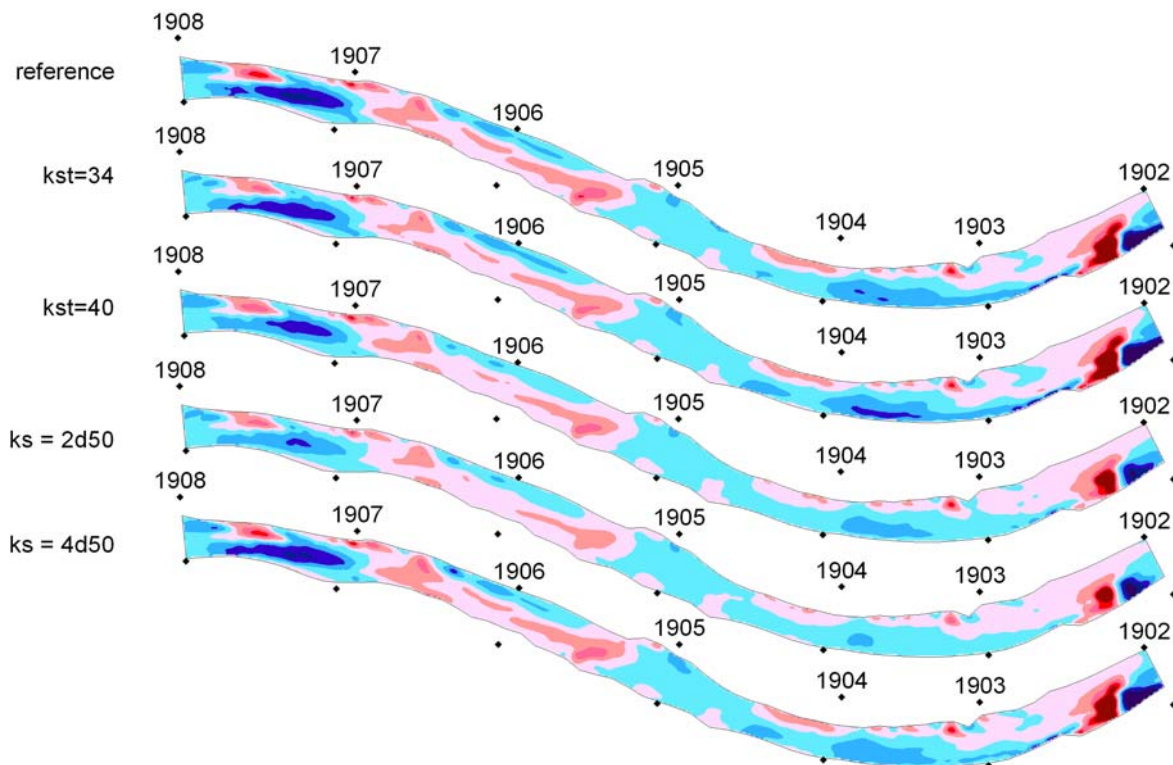
Figure 4.23: Calculated bed changes, variation of roughness

The second group summarises variations of the coefficient in the hiding-exposure function m described in equation (3.14), that is applied in *Wu*'s formula. Applying the model on the 180° laboratory bend (see Chapter 3) showed that the parameter m is sensitive to changes.

Figure 4.24 shows the results of the influence of parameter m on the computed bed changes at the Danube river. The computed results diverge strongly with respect to a variations of m. The first map (reference) was computed with the default value of $m = -0.6$. The effect of the hiding-exposure function is to protect small grain particles from being transported, because of their probability being hidden behind coarse particles. This effect is implemented by increasing the fractional criterion for incipient motion (critical shear stress) for small particles (see equation (3.15)) and vice versa for large particles. Reducing the absolute value of m results in a weaker consideration of the hiding-exposure effect. Then, small grains are less protected by the larger ones. Consequently, a reduced absolute

value of *m* also reduces the computed bed changes, best seen at the erosion area upstream km 1907. Here, a reduction of the absolute value of *m* lead to a better fit to the measured bed changes than the default value. Similar observations were also made at the 180° bend. The variations of *m* had minor influence on the erosion-deposition patterns. However, the bed change heights varied significantly. The strongest effect is computed for an increased absolute value of *m* (from –0.6 to –0.7). Here, patterns remain similar with respect to the reference computations, but the bed change heights increase considerably in both directions, erosion and deposition. Sensitivity tests in this group show that modifications of the hiding-exposure coefficient, especially when increasing the absolute value of *m* significantly influence the computed bed changes.
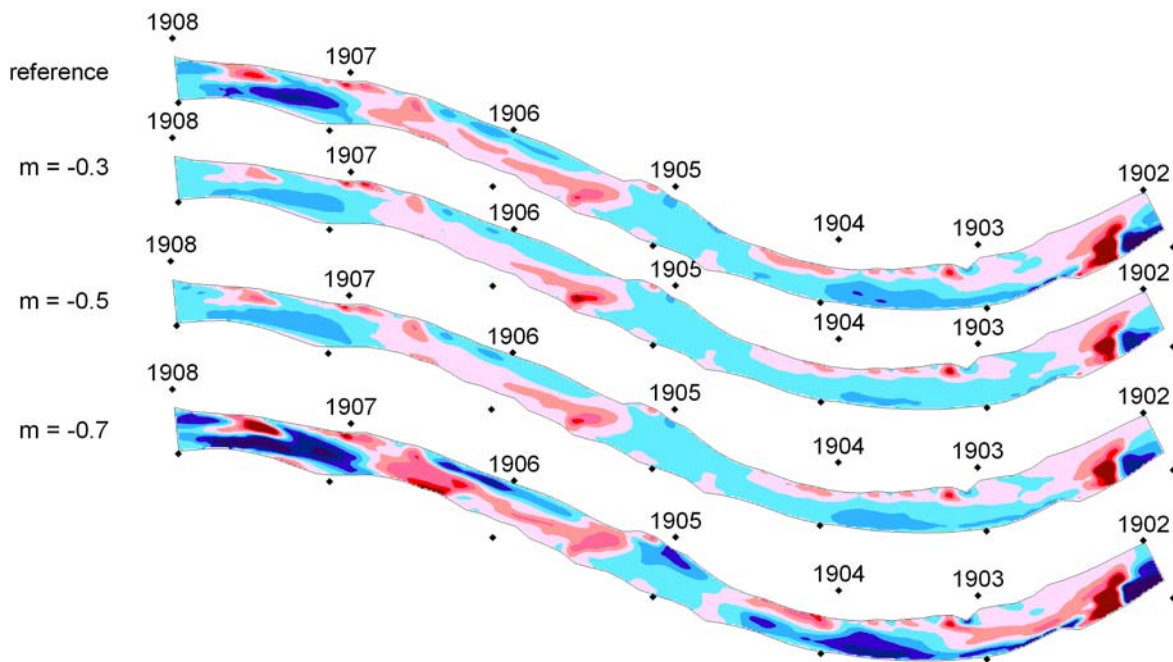
Figure 4.24: Calculated bed changes, variation of hiding-exposure coefficient *m*

According to *Kroekenstoel & van Welzen (2003)*, the parameter α can also be used for parameter studies. In their study, α was significantly varied for calibration purposes in order to achieve agreement of the computed and measured results. The dimensionless fractional transport rate ϕ_{bi}, as defined in the *Wu* formula at equation (3.17), is multiplied by the factor α, so that it linearly modifies the fractional sediment transport rate. A modification of α can be interpreted as a modification of the empirically determined constant of 0.0053 preceding the fractional transport formula. Therefore, the factor is unity by default. Figure 4.25 shows that the factor influences the computed bed changes to a minor degree, even for significant variations of α using half and double the original fractional sediment transport rate. Again, the patterns remain similar, while, as expected, the bed change heights change according to variations of the factor. The effect of a reduction of α is best seen at the erosion region upstream km 1907, where the erosion heights considerably decrease resulting in an improved agreement to the measured bed changes (see Figure 4.18).

Figure 4.25: Calculated bed changes, variation of factor α
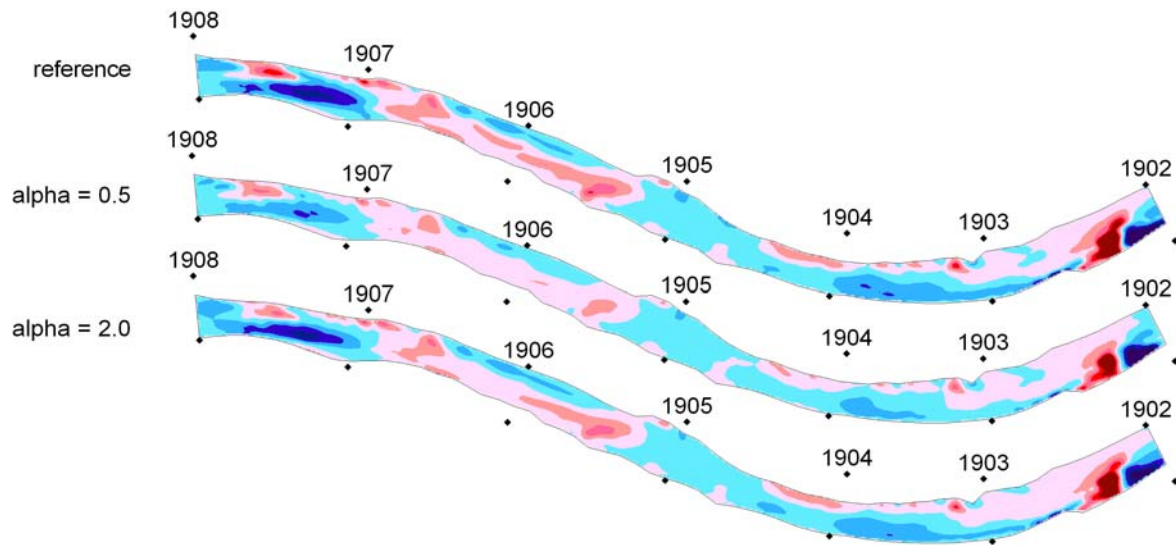
The fourth group of parameter tests deviates from the parameters tested before. Here, the influence of the roughness and the resistance of the flow that is produced by vegetation regions and groynes is tested. As for this study, measured data of the density of the vegetation regions and the heights of the groynes is not available in detail, the implementation is performed using rough assumptions. A total of 19 groynes, three vegetation zones and two guide dykes (triangular elements) are found in the river reach. The vegetation zones are located at km 1908 to 1907 on the left side in stream direction, km 1906.9 to 1906.3 on the right side, and km 1904.7 to 1903.6 on the left side. The guide dykes are located at km 1905.7 to 1905.3 on the left side, and km 1902.9 to 1902.5 on the right side.

In the second map in Figure 4.26 computed results are shown with a doubled roughness of the cells representing the vegetation regions and the guide dykes with respect to the default roughness. The effect of a doubled vegetation roughness on the computed bed changes are of minor relevance, small deviations can be found at the scour of bar 4. Apparently, the long vegetation zone from km 1904.7 to 1903.6 on the left side concentrates the flow to the outer bend resulting in increased shear stresses and increased erosion processes. The doubled roughness for the vegetation zones and the guide dykes is combined by considering the effect of the groynes. Groynes are considered by defining extra walls in the grid. The results are shown in the third map. Here, the patterns of the computed bed changes vary from the reference calculations. The erosion region upstream km 1907 is reduced compared to the reference computations. The erosion region at the scour of bar 4 is less pronounced compared to the results using doubled roughness only (map 2). At the downstream end of the river reach, the erosion after the pool at km 1902.2 is shifted slightly towards the centre of the flow. The fourth map shows results of an alternative consideration of vegetation effects on flow and finally on morphological changes. This approach introduces an additional source term in the Navier-Stokes equations to account for the additional drag induced by vegetation elements on the flow (*Fischer-Antze et al. (2001)*). Vegetation is then modelled by a number of vertical cylinders in each cell. A drag

formula is used to determine the force between the water and the cylinder elements. Results show that the erosion regions on the opposite sides of the vegetation zones increase. The effect is best seen at the scour of bar 4, where considerable erosion processes are computed due to the drag approach. These results represent a tentative attempt to consider the effects of vegetation and groynes for morphodynamic computations. The results show that the morphology reacts plausible on the vegetation and groyne implementations. However, it is not possible to improve the agreement to the measured bed changes when considering vegetation and groyne effects. Flow through vegetation was not a focus of the current study. A detailed analysis of the effects of vegetation and groynes on computed bed changes should be subject to future research activities.
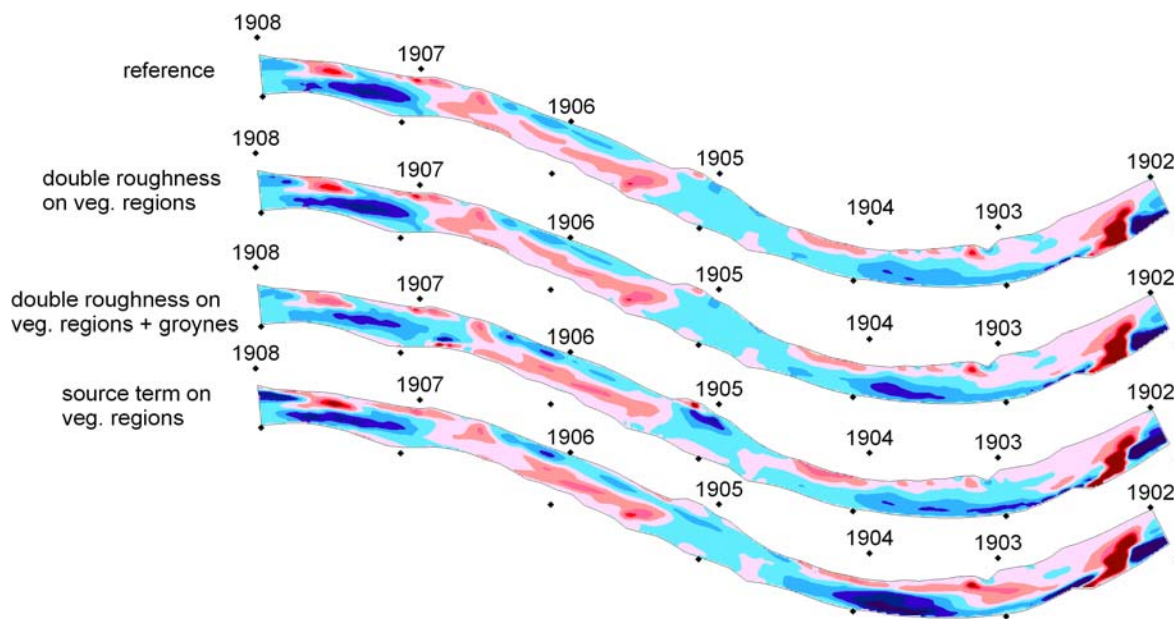

Figure 4.26: Calculated bed changes, variation of flow resistance on vegetation regions and groynes

The sensitivity of another parameter tested is the sediment inflow. The sediment inflow has to be given as a user input. In a pre-processing procedure the inflowing sediments are estimated on the upstream entrance based on the *Wu* formula on an idealised cross-sectional profile. Due to the lack of measured sediment transport rates at the Danube river, the estimated sediment inflow is characterised by a considerable uncertainty. Testing the sensitivity of uncertain input data is therefore an important issue.

For the sensitivity tests, the sediment inflow is neglected, bisected and doubled. The influence of a varied sediment inflow on the computed bed levels in the inflowing region, where its effect is strongest, is not seen here, since the first 1.5 km are cut-off for boundary condition reasons. Within the test reach, the influence of a sediment inflow variation is detectable from the upstream entrance to km 1905.7. Further downstream the inflowing sediment does not influence the computed bed changes. However near the upstream entrance, a variation of the sediment inflow influences the deposition area at km 1907.7. With an increased inflow larger deposition heights are computed while they reduce for smaller sediment inflow rates. The overall erosion-deposition patterns are similar for all chosen

sediment inflow rates. Thus, the sensitivity of the sediment inflow on the computed bed changes is small. Rough assumptions of the sediment inflow are therefore justified.
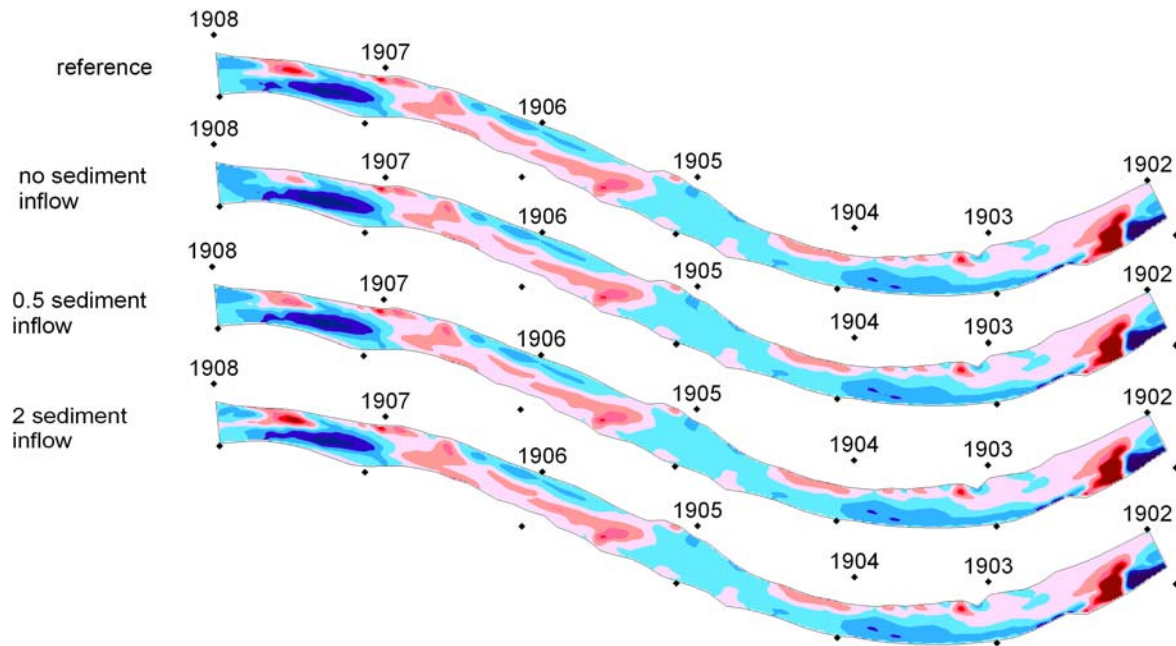

Figure 4.27: Calculated bed changes, variation of sediment inflow

The sixth parameter shows a variation of the threshold value for incipient sediment motion θ_c that is defined with a default value of 0.03 by *Wu et al. (2000b)*. The reference computations are performed with an increased parameter of incipient sediment motion of θ_c = 0.045. At the reference computations, θ_c is the only parameter deviating from the default parameter to achieve the computed results. The results in Figure 4.28 show, that computed bed changes react highly sensitive on changes of this parameter. While good results are obtained using the modified parameter of θ_c = 0.045, the default value gives bed changes, that over predict the measured bed changes considerably. Both the erosion-deposition patterns and the heights of the bed changes are strongly influenced by the choice of the parameter. Therefore, the choice of this parameter is crucial for the accuracy of the computed morphological processes. Obviously, for the Danube river, an increase of the parameter of incipient sediment motion from 0.03 to 0.045 is appropriate to achieve computed bed changes that fit to the observations. A possible reason for an increased value of the parameter θ_c could be related to the fact that *Wu et al. (2000b)* choose this parameter to be constant for all grain Reynolds numbers *Re**. According to the study of *Shields (1936)*, incipient sediment motion is a function of the grain Reynolds number that achieves values of approximately 0.06 for high grain Reynolds number that are usually given for river flow. The experiments of *Meyer-Peter & Müller (1949)* introduce a modified parameter of θ_c = 0.047 in the region of high grain Reynolds numbers, that fits well to the chosen parameter in this study. Further justification of an increase of this parameter can be found in *Kroekenstoel & van Welzen (2003)*. Here, armouring experiments in a laboratory flume are modelled with a one-dimensional morphodynamic model using the nonuniform sediment transport approach of *Wu et al. (2000b)*. The laboratory experiments were performed by *Günter (1971)*. The armouring processes of a

mountainous river are simulated. Best results for the numerical computations of this experiment are obtained using an increased parameter of θ_c = 0.044. Due to the fact that the laboratory experiments deal with mountainous rivers as well as the experiments of *Meyer-Peter & Müller (1949)* and that both experiments use a parameter close to 0.045, the chosen increase of θ_c in this study is justified.
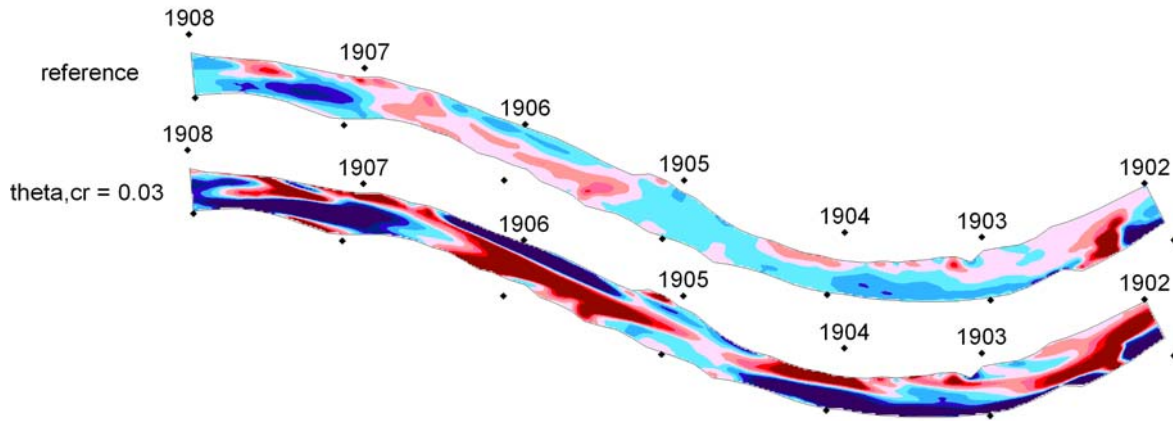
Figure 4.28: Calculated bed changes, variation of threshold value for incipient sediment motion

The last parameter test is performed considering the effects of side slopes on the computed sediment transport and as a consequence on the computed bed changes. The incorporated algorithms accounting for these effect are discussed in Chapter 3.3.2. The results in Figure 4.29 show, that considering side slope algorithms, effects the computed erosion and deposition heights. Also the erosion-deposition patterns are influenced when considering these algorithms. The procedure of reducing the critical shear stress on sloped beds and deviating the angle of sediment transport on lateral slopes in river bends results in reduced bed changes with respect to the reference computations. Thus, the computed tendencies of erosion processes at the scours and deposition processes at the bars induced by secondary flow effects are damped when considering side slope effects. Then material is laterally transported preferentially from high to low bed levels, explaining the smaller gradients of the river bed changes.

Figure 4.29: Calculated bed changes, variation of sediment transport on side slopes

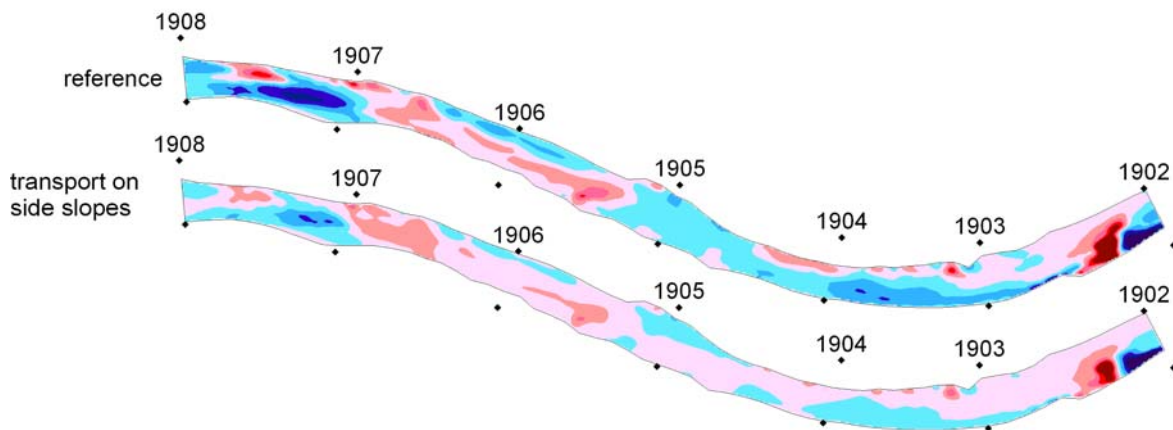### 4.3.4   Error analysis

Numerical computations of flow, sediment transport, and morphological changes are performed at the Danube study reach from km 1909.5 to km 1901.5. The incorporated sediment transport formulas by *Wu et al. (2000b)* are validated on measured bed level changes. The measured data originates from pre and post flood bed level surveys in 2002. The objective of this study is to validate the model on measured bed level changes by comparing measured and computed erosion-deposition patterns visually that are obtained by subtracting the final bed levels (computed or measured) from the initial bed levels. The procedure allows to visually analyse the agreements of computed and measured bed level changes. In this Chapter, the measured and computed erosion-deposition patterns are further processed with respect to agreement and disagreement regions and an approach providing a quantitative assessment of the computed bed changes. The need for providing tools to assess the quality of computed bed changes is based on the complex nature of the morphology and the morphodynamic changes in real rivers. The assessment of the quality of computed bed changes in laboratory experiments is comparably easier. Here, usually an initially flat bed is deformed. The processes can easily be described by analysing a limited number of characteristic cross-sections or longitudinal profiles. This does not apply to real river morphodynamics. Here, computations start from developed morphological structures. Thus, analysis of computed morphological changes needs to employ different methods.

Additionally to visual comparison of computed and measured morphological changes, a quantitative assessment is performed. A binary approach is used to process the computed and measured spatial fields to determine regions of agreement and disagreement. Therefore, both computed and measured bed changes are interpolated onto the same grid having a grid cell size of 10 x 10 meters. For this study, the signs of the interpolated bed levels are investigated. Green pixels are assigned to coinciding signs, i.e. erosion is modelled and measured or deposition is modelled and measured. Red pixels are assigned to disagreement of the signs. The results of the computations are shown in Figure 4.30 (map 3).

When comparing measured and computed bed changes, the accuracy of the measured data introduces uncertainty into the analysis. This especially applies for short term comparisons. The measuring technique as described in Chapter 4.1.2, provides bed levels with a limited accuracy. These limitations have to be considered when comparing computed and measured bed levels. For this study, a total accuracy of the bed level surveys of 10 cm is assumed. Therefore, an additional sign analysis is performed considering the uncertainty by means of a tolerance measure that is included into the post-processing procedure. Here, green pixels are assigned when agreement of erosion or deposition is given within the given tolerance range. The results of the map considering uncertainty are shown in Figure 4.30 (map 5).

The first error analysis map shows that agreement of measured and computed bed changes can be achieved at 65% of the pixels. 35% of the pixels show disagreement. Three large regions of disagreement are computed, the first downstream the upstream entrance of the model in the vicinity of bar 2. The second region is computed at around km 1906. Here, a distinct erosion region is measured at the bar side of bar 3 that is not computed, while the scour on the opposite side slightly deposited, a

bed change process that is not modelled correctly. The third large region of disagreement is detected at around km 1905 covering parts of crossing C and the upstream parts of bar 4. Here, the prevailing deposition processes are not reflected by the model. The erosion and deposition processes at most parts of bar 4 are measured and modelled at similar positions. Introducing the measurement tolerance of 10 cm gives an overall improvement of the computed accuracy of erosion and deposition patterns. In this case, an agreement of 78% is achieved, so the critical regions of the Danube river are reduced to 22%. The error analysis is also performed for a tolerance measure of 20 cm. In this case, 87 % agreement and 13 % disagreement is achieved. The map is not displayed.

Comparing the two binary error maps shows that generally small regions of disagreement reduce. One of the large error regions situated at around km 1905 reduces significantly. Here, minor bed changes are measured. This process is well represented by the morphodynamic model, although the signs of the original map mismatch. These processes of minor changes can also be seen in Appendix B. The two large error regions at around km 1906 remain virtually unchanged. Here, the model results deviate considerably from the measurements. This also applies to the region near the upstream entrance where deviations might be caused by the influence of the upstream boundary conditions.

Figure 4.30: Error maps
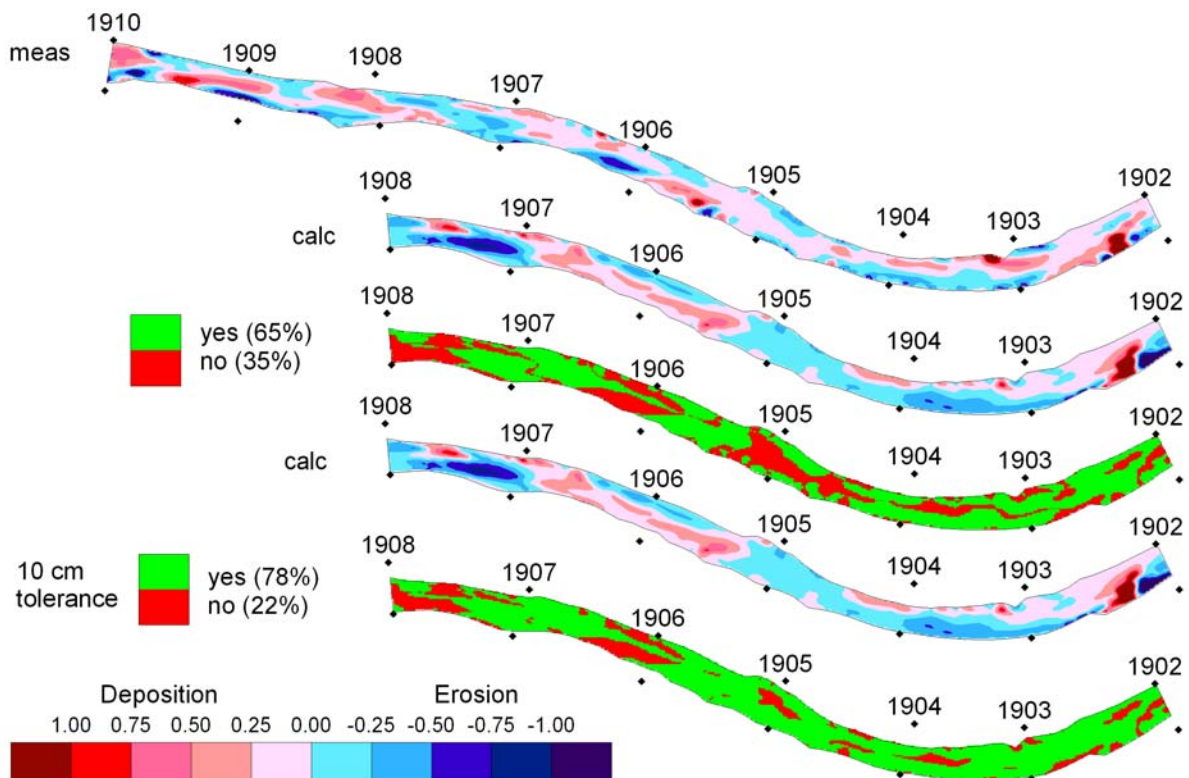
In Chapter 4.3.3, several sensitivity tests using different parameter sets are introduced. Qualitative comparison analysing the computed erosion-deposition patterns is presented. For analysing the benefit of individual parameter variations an assessment factor describing the quality of the computed results is developed in this Chapter. Comparing the assessment factors of different runs

gives information about the efficiency of different model configurations. Different model runs can be rated according to the computed assessment factors. Therefore, two integrative measures of errors are computed for assessing the goodness-of-fit. Basis for the computations are the measured and computed bed changes that are interpolated onto identical grid positions. Then, the errors e_i can be computed for each cell (pixel) i as the difference of observed $\Delta h_{obs,i}$ and calculated $\Delta h_{calc,i}$ bed changes. The two measures of errors shown in Table 4.2 represent mean errors computed from the single errors in each cell e_i. The first measure of error, root mean square error, is often found in literature for estimating the quality of various models. Based on the demands of this study, an additional error is established, referred to as relative error - *RE*. The measure of error *RE* relates the error e_i to the observed bed change $\Delta h_{obs,i}$ at any cell i. In this way, errors are weighed more, when the observed bed changes are small. This results in an improved analysis of the computed bed changes, as larger errors contribute less when the measured bed changes are also large, while they contribute more when small bed changes are measured. The ranges for both measures of errors is [0, ∞) with 0 for the minimum error representing perfect agreement.

Table 4.2: Definition of measures of errors

$e = \Delta h_{obs} - \Delta h_{calc}$	Error
$RMSE = \sqrt{\dfrac{1}{n}\sum e_i^2}$	Root mean square error
$RE = \dfrac{1}{n}\sum \dfrac{e_i^2}{\Delta h_{obs,i}^2 + 0.1}$	Relative error

The measures of errors introduced in Table 4.2 are used to assess the computations of the parameter variations performed for the sensitivity analysis. The results are shown in Table 4.3. A focus is drawn on the values computed for the particularly developed measure of error *RE*. Based on the computed values for *RE*, the results of the numerical computations are classified into three groups. Group 1 represents the best computation that achieve *RE* values smaller 0.5. The second group represents medium quality computations using *RE* values from 0.5 to 0.7, and the third group represents computations with poor agreement achieving *RE* values higher than 0.7. Good results are obtained when the roughness is reduced or computed as a function of the sediment size distribution. Furthermore, a reduction of the absolute value of the hiding-exposure coefficient affects the computed results in a positive way. This is in line with the results obtained from the computations of the morphological changes in the laboratory bend in Chapter 3. Here, both computing the roughness as a function of the sediment size distribution and reducing the absolute value of *m* proved to have positive effects on the computed results. Reducing the sediment transport rate by incorporating the factor α gives slightly better results and also considering sediment transport on side slopes contributes in a positive way to the mean agreement of measured and calculated bed changes. The second group is characterised by a relatively small range of *RE* values (0.5 to 0.7). Nevertheless, most of the runs fall into this group. The reference computations also represent the second group. The third group represents the outliers of the computations. Increasing the absolute value of the hiding-exposure

coefficient that is physically related to a stronger consideration of hiding-exposure effects increases the measure of errors significantly. Moreover, considering both groynes and vegetation regions and running computations by considering the vegetation regions by an additional sink term in the velocity equations does not contribute in a positive way to the agreement of measured and computed bed changes. Since the Danube river reach actually consists of substantial areas of vegetation and groyne elements, apparently further research activities have to be attempted to consider these effects more accurately. Applying the default value of the threshold value of incipient motion of 0.03, results in the highest *RE* values, i.e. the largest deviations of measured and computed bed changes. Reasons for the required modification of the threshold value have been discussed in detail in Chapter 4.3.3.

Table 4.3: Measures of errors

Variation	Parameter	Measure of error		
		RMSE	*RE*	Group
reference	theta,c = 0.045	0.356	0.638	2
roughness	kst = 34	0.360	0.634	2
	kst = 40	0.308	0.430	1
	ks = 2*d50	0.310	0.396	1
	ks = 4*d50	0.359	0.648	2
hiding-exposure coefficient	m = -0.3	0.291	0.369	1
	m = -0.5	0.303	0.427	1
	m = -0.7	0.499	1.530	3
factor transport rate	alpha = 0.5	0.322	0.430	1
	alpha = 2.0	0.330	0.533	2
vegetation/groynes	ks,veg	0.371	0.694	2
	ks,veg + groynes	0.425	0.978	3
	veg sink term	0.446	1.079	3
sediment inflow	sedin = 0	0.352	0.623	2
	0.5 sedin	0.353	0.624	2
	2.0 sedin	0.357	0.648	2
threshold incipient motion	theta,c = 0.03	1.139	9.064	3
transport on side slopes		0.296	0.356	1

4.3.5   Temporal evolution

The computations of morphological changes on a reach of the Danube river are performed under unsteady flow conditions using fractional sediment transport algorithms. The flow hydrograph applied is generated for a period between the pre and post flood surveys in 2002 (see Figure 4.4 and Figure 4.5) in a way that all relevant discharges larger than 2000 m³/s are considered for the morphodynamic computations. This reduction of the flow hydrograph is based on the assumption that discharges smaller 2000 m³/s do not contribute or only to a minor extent to the measured morphological changes. During this period, three flow peaks are measured having a duration of 44 days in total.

In this Chapter the temporal development of the computed flow, sediment transport, and morphological changes is analysed at five positions of the river bed. Therefore, a print-out of the computed results is written every 12 hours for the whole spatial field. Then, the flow, sediment, and

morphology variables are extracted from the spatial fields at the given locations. The five locations chosen for analysis of the temporal evolution are (1) the left side of bar 4 (km 1904.0) at the inner bend (bar side), (2) the right side of bar 4 (km 1904.0) at the outer bend (scour side), (3) the centre of km 1905.5 at crossing C, (4) the left side of bar 3 (km 1906.4) at the outer bend (scour side), and (5) the right side of bar 3 (km 1906.4) at the inner bend (bar side). Four variables are plotted: the flow velocities near the river bed in streamwise direction in [m/s], the water depths in [m], the volumetric sediment concentrations in [m³ (sediment) / m³ (water)], and the river bed levels in [m a.s.l.]. The results of the temporal evolutions at the five locations are shown in Figure 4.31 to Figure 4.35.

The temporal evolution at km 1904 on the left side, that represents the bar side of bar 4 at the inner bend is shown in Figure 4.31. Here, the flow velocities near the bed, the water depths and the sediment concentrations reflect the variability of the flow as given in the input flow hydrograph shown in Figure 4.5. When the flow velocities become smaller than 1m/s or the water depths become smaller than 3 m, the sediment concentrations reduce to zero, i.e. sediment transport stops. Here only the three peaks produce significant sediment concentrations that are related to the sediment transport rates. The near bed flow velocities achieve values of almost 3 m/s at their maximum. The maximum flow velocities are characterised by only small variations for the five reported locations (see Figure 4.31 to Figure 4.35). This is different for the minimum flow velocities that fall below 1 m/s at the bar sides of the bar regions with shallow water depths of less than 3 m, while the minimum velocities at the other locations never fall below 1.5 m/s. The bed levels change according to the flow hydrograph. Deposition processes take place at the bar throughout the whole simulation period. The first peak produces a deposition of less than 10 cm, the second peak, that is the smallest only a few centimetres, and the last and highest peak produces approximately 20 cm deposition, so that here a total deposition of 30 cm is computed that fits well to the measurements (see Chapter 4.3.2 and Appendix B). Although the first and last peak have similar magnitudes, the deposition heights produced by these two peaks are substantially different. This is explained by the sorting processes and the deposition of fine material that is predominantly available for the last peak where it settles mostly during the falling limb until t = 30 days. After this time the river bed remains stable.
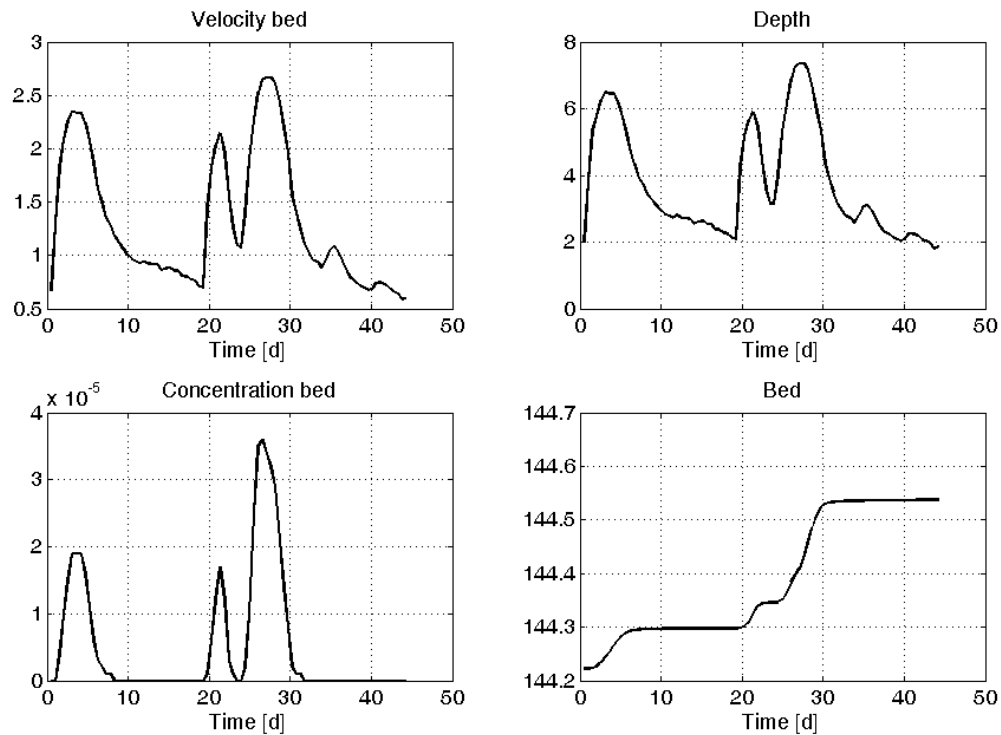
Figure 4.31: Temporal evolution at km 1904.0 left side

The opposite side of km 1904 on the right side represents a typical scour process at the outer bend. Here, the same variables as before are plotted in Figure 4.32. The near bed velocities achieve comparable maximum velocities of approximately 3 m/s. Different from the observations at the bar the minimum velocities reduce only to values slightly below 2 m/s. Therefore, here, sediment transport is available throughout the whole period of the simulations. The scour achieves large water depths ranging from 6 to almost 12 m during the three flood events. The morphological response to the passage of the flood events in this region is characterised by a continuous erosion process at the three peaks and minor bed changes for the small discharges during the falling limbs of the peaks. In total, an erosion of approximately 25 cm is computed that fit well to the measurements. In the course of the flood events, the erosion takes place in three batch-wise movements according to the three flood peaks. The general process of coarsening at the outer bend of bar 4 (see Figure 4.38) explains the uneven erosion depths. While the bed material sediment size distribution at the beginning of the numerical run is evenly distributed over the whole area of the river reach, sorting processes at the course of the run lead to substantial coarsening processes within the scour region. Therefore, the first peak causes en erosion depth of 14 cm, the second and third peak only contribute with erosion depths of 4 and 7 cm, respectively. Therefore, the erosion depth of the largest peak is only half of the erosion depth of the first peak. At the outer bend, where the coarsening processes develop, the river bed is then able to impose an increased resistance to the flow. Here, obviously the fine material is washed out until a comparably stable layer of coarse material remains on the river bed.
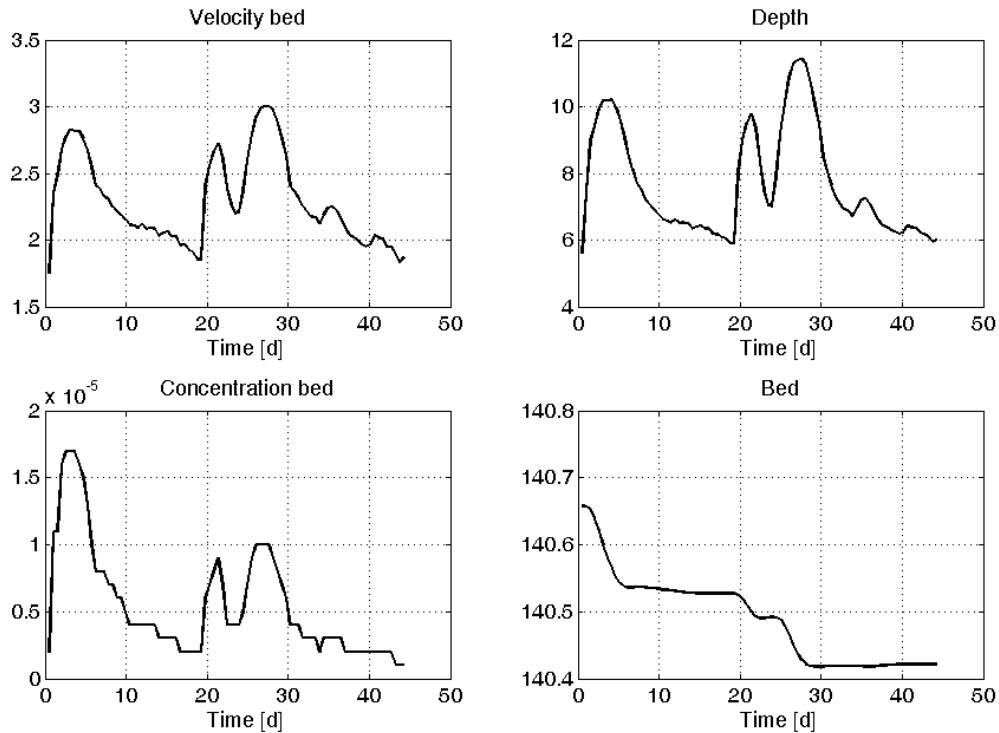
Figure 4.32: Temporal evolution at km 1904.0 right side

The temporal evolution at the centre of km 1905.5 represents flow and morphological processes at a crossing (crossing C). Results are depicted in Figure 4.33. Again, velocity maxima of approximately 3 m/s are achieved while the velocity minima remain above 1.5 m/s. Therefore, sediment transport is available throughout the entire simulation period. Water depths are ranging from 4 to almost 10 metres, they achieve values between the water depths of typical bar and scour locations. The sediment concentrations are also in between typical sediment concentrations of the bar and the scour regions. The location of the crossing is exposed to continuous deposition processes. To a certain degree the deposition processes happen proportionally to the inflowing flow hydrograph. In total a deposition height of 50 cm is measured. Minor deposition processes are computed in the low flow phases where small and almost constant sediment concentrations are computed. The centre location of the crossing is characterised by considerable fining processes representing the settlement of fine particles here. The measurements reflect the computed deposition processes at this location with good agreement.
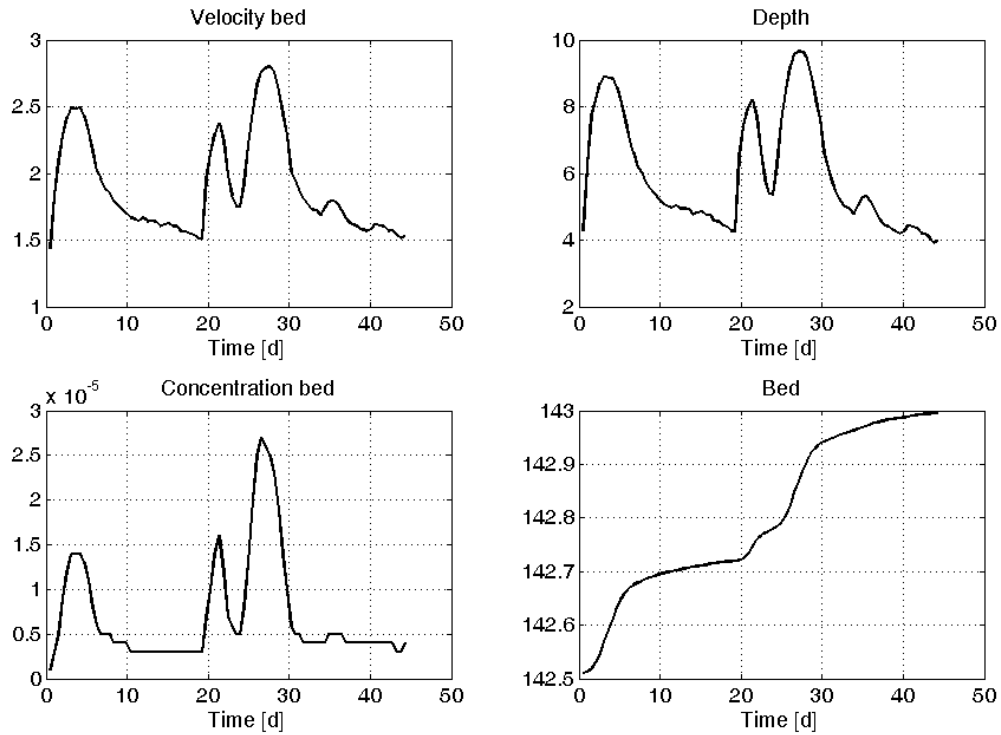
Figure 4.33: Temporal evolution at km 1905.5 centre

In Figure 4.34, the processes at the scour side of bar 3 are represented at km 1906.4 on the left side. Generally similar behaviour to the scour processes of bar 4 (Figure 4.32) are computed here. The aforementioned process of sediment sorting leading to reduced erosion depths at the scour region of a bar reach is also found here. Substantial coarsening processes result in sediment concentrations that are up to 4 times smaller than at the opposite bar side. The lateral differences of sediment concentrations are stronger at this bar than at bar 4. Substantial coarsening processes are reflected by rapid erosion processes. A total of 30 cm is eroded. More than 20 cm are eroded in the course of the first peak. Then, the other two peaks contribute to the erosion processes with significantly reduced erosion depths due to the sorting process.
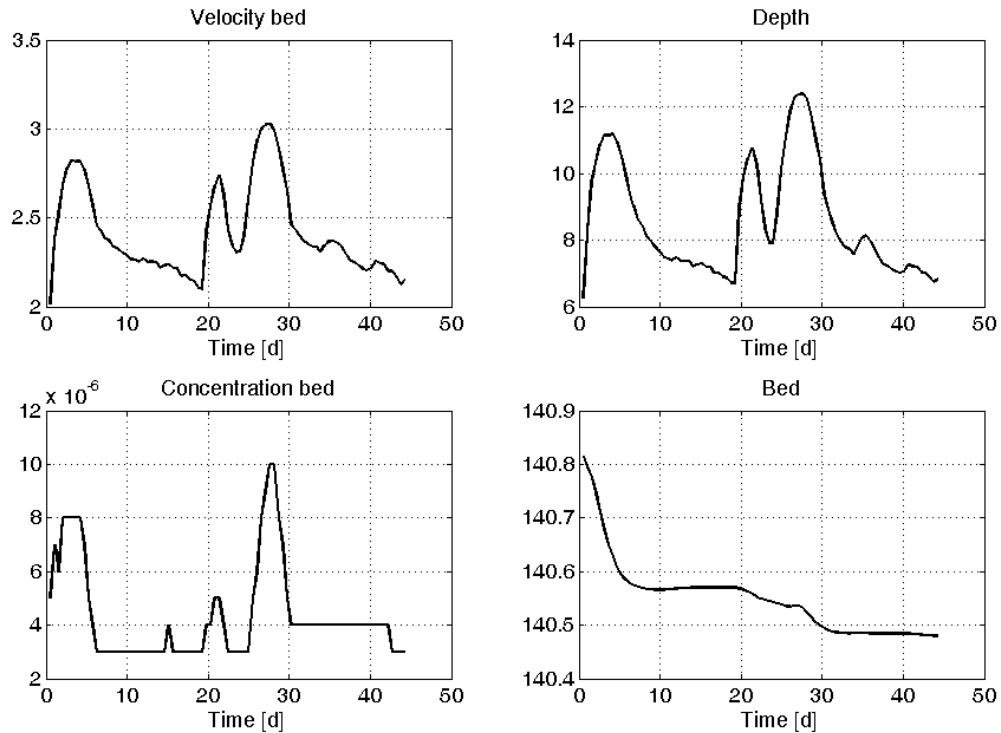
Figure 4.34: Temporal evolution at km 1906.4 left side

The last location is situated at the opposite side, at the bar side of bar 3. The results of the temporal evolution at km 1906.4 on the right side are shown in Figure 4.35. Generally the processes at the bar side of bar 3 are computed similarly to the processes at bar 4. The small water depths here result in flow velocities smaller than 1 m/s for the reduced discharges during parts of the falling limbs of the peaks. Then, the sediment concentrations reduce to zero. For the peak flows and the beginnings of the falling limbs, maximum sediment concentrations of more than $4*10^{-5}$ m³/m³ are achieved. Typical deposition processes are computed at the bar side of bar 3. A total deposition of 50 cm is computed that is settled predominantly within the falling limb of the third peak. Then, the majority of the entrained fine sediment material settles at the low flow location. The deposition process instantaneously reduces to zero when the flow velocities achieve values smaller than 1 m/s.
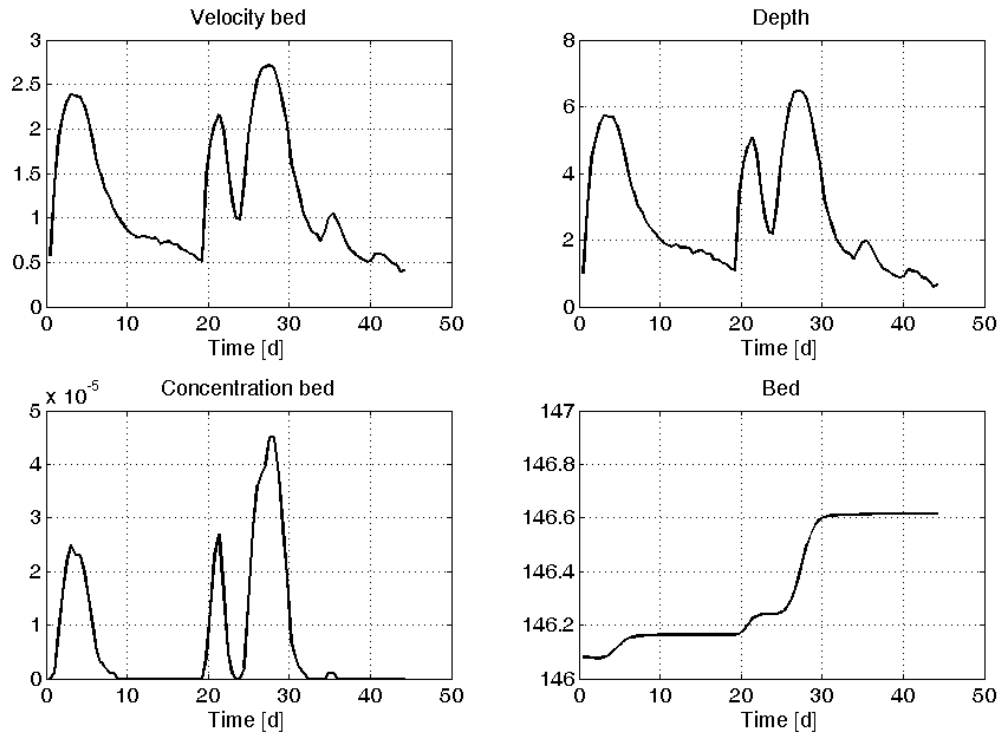
Figure 4.35: Temporal evolution at km 1906.4 right side

The introduced temporal developments of several flow and sedimentologic features at characteristic points in the study reach are supplemented by processing the computed fields of the bed change heights (*bech*) and the sediment size distributions represented by the median grain diameter d_{50} at chosen points of time. The numerical model provides regular print-outs of several computed parameters for the entire numerical grid. The temporal evolution of the spatial fields is investigated at ten characteristic points of time (*t1* to *t10*) of the flow hydrograph. The points of time are shown in Figure 4.36. Morphological changes and sorting processes are analysed at the peaks, the valleys, and the times between the rising and falling limbs of the floods.
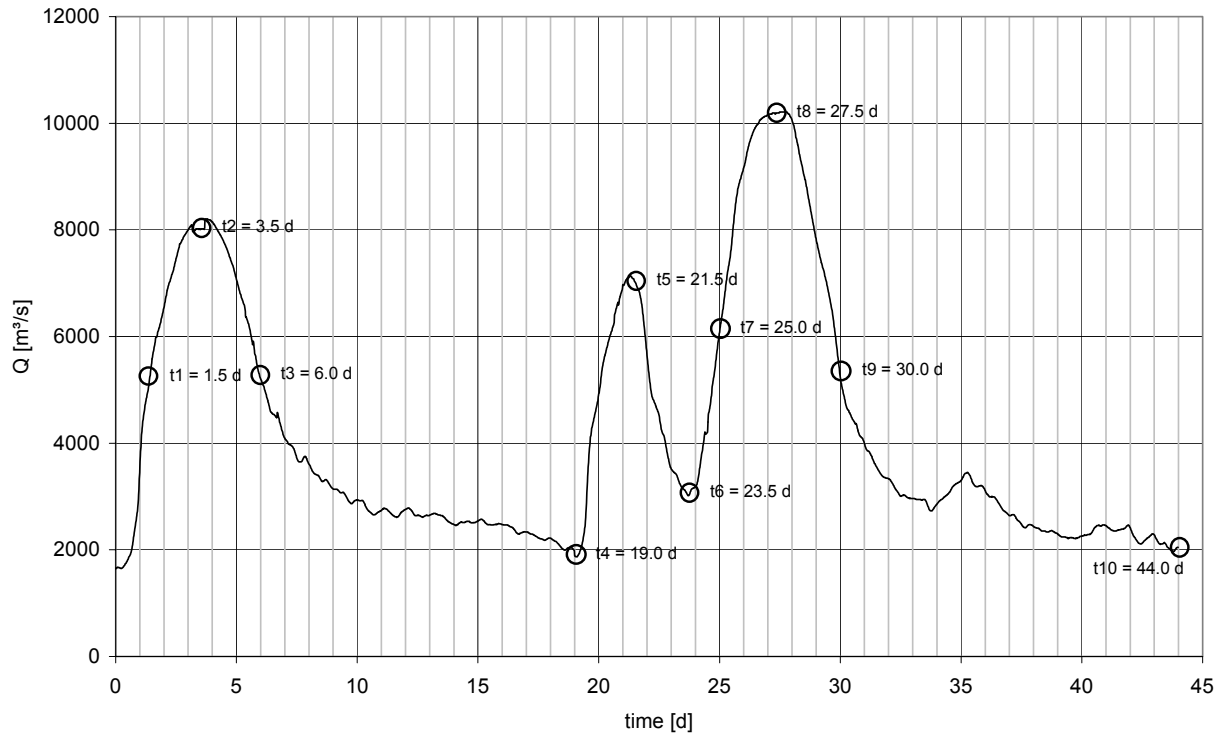
Figure 4.36: Points of time

The development of the river bed of the Danube reach is shown in Figure 4.37. For comparison, the measured bed changes (*meas*) which are generated from the measured data of the pre and post flood surveys are also shown. As can be seen from the maps, the characteristic patterns of erosion and deposition already develop during the passage of the first flood event (*t1* to *t4*). At *t4*, the positions of erosion and deposition regions are determined. Already there, typical morphological changes at the bar and crossing regions can be detected. The bars tend to deposit and the scours show erosion processes. Crossing B and C show erosion and deposition processes, respectively. After that period, the heights of the bed changes develop and finally achieve levels that fit to the measured bed change heights. Also the filling up process of the pool near the downstream end of the channel reach, starts early after initiation of the unsteady run. In this region, the strongest bed changes are observed and measured. As previously discussed, most of the deposition processes occur in the shallow water regions during the falling limb of the third and highest flood. During the second half of the falling limbs, from *t3* to *t4* and from *t9* to *t10*, the dynamics of the morphological changes reduce to a negligible extent. These intervals are characterised by discharges that are predominantly below 4000 m³/s. Figure 4.31 to Figure 4.35 show that these discharges produce minor or zero sediment transport rates.
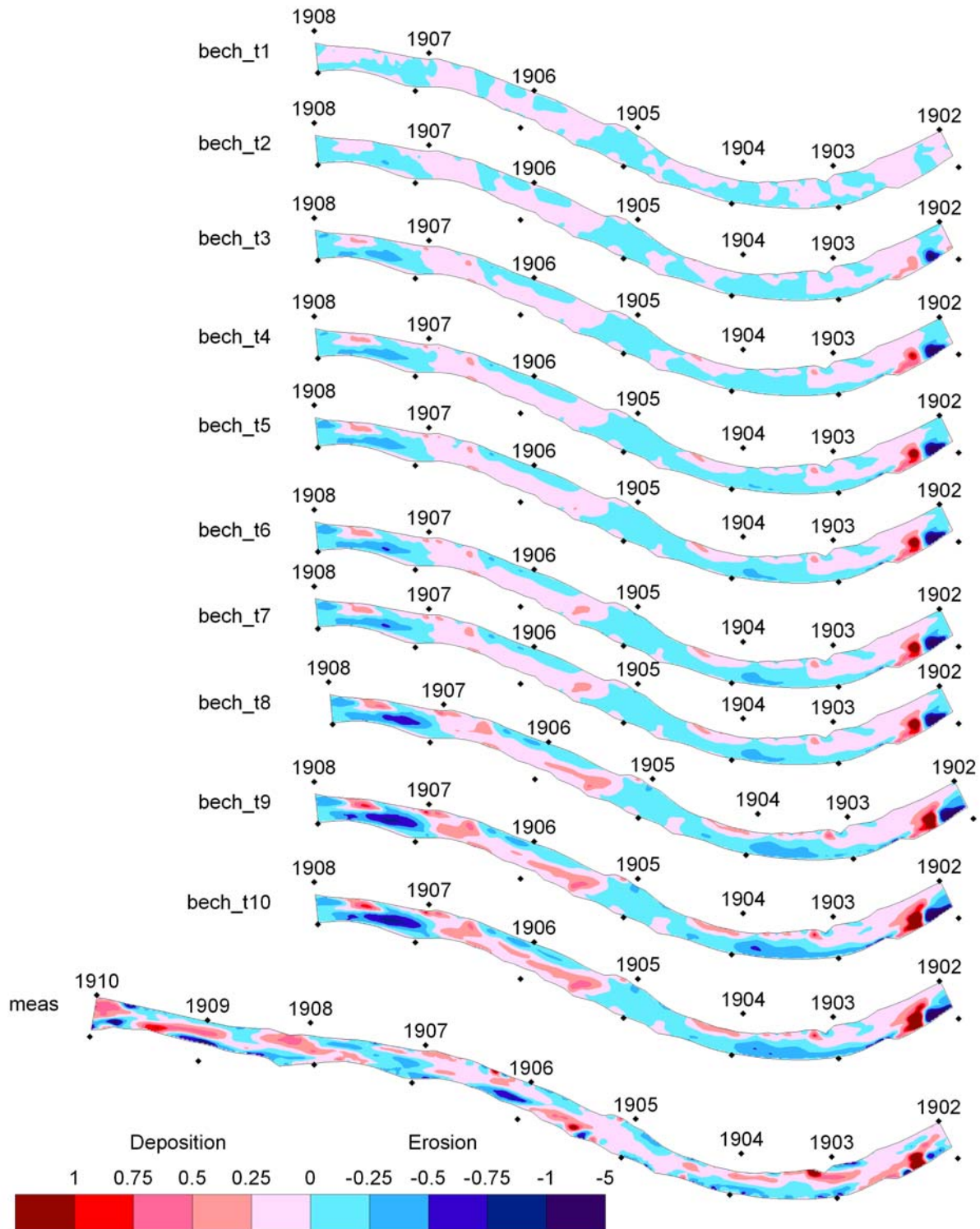
Figure 4.37: Development of bed changes

The distributions of the computed median grain sizes d_{50} at the river bed are plotted at the same points of time in Figure 4.38. Generally the computed grain sorting processes follow the computed trends of morphological changes. Predominating erosion regions (e.g. scours) are characterised by considerable coarsening, while deposition regions (e.g. bars) show fining processes. Similar to the evolution of the bed changes, the sorting pattern is already determined after the passage of the first flood at *t4*. However, the sorting intensities change considerably during rising and falling periods. The

previously discussed deposition process at the bars during the falling limbs is reflected by the fining processes that preferentially occur during these periods. Starting from an initially evenly distributed bed material with a constant d_{50} of 22 mm, the bed material gets considerably redistributed with d_{50} values ranging from very small to almost 40 mm at the end of the run. Considering the results of the sorting processes at the laboratory bend, fining processes are typically found at the shallow regions on bars, while scours are subject to coarsening processes. Thus, the general sorting pattern of the Danube reach is computed plausibly. However, in the scope of this study it is not possible to validate the computed sorting processes since measurements of the bed material size distribution are not available. Furthermore, the variability of the computed sorting dynamics is not validated. Validation would be particularly advisable in regions where the computed d_{50} values change rapidly within one interval, such as the coarsening at km 1907 during the falling limbs of the floods. Detailed validation of sorting processes at the Danube river is a task for future research activities.
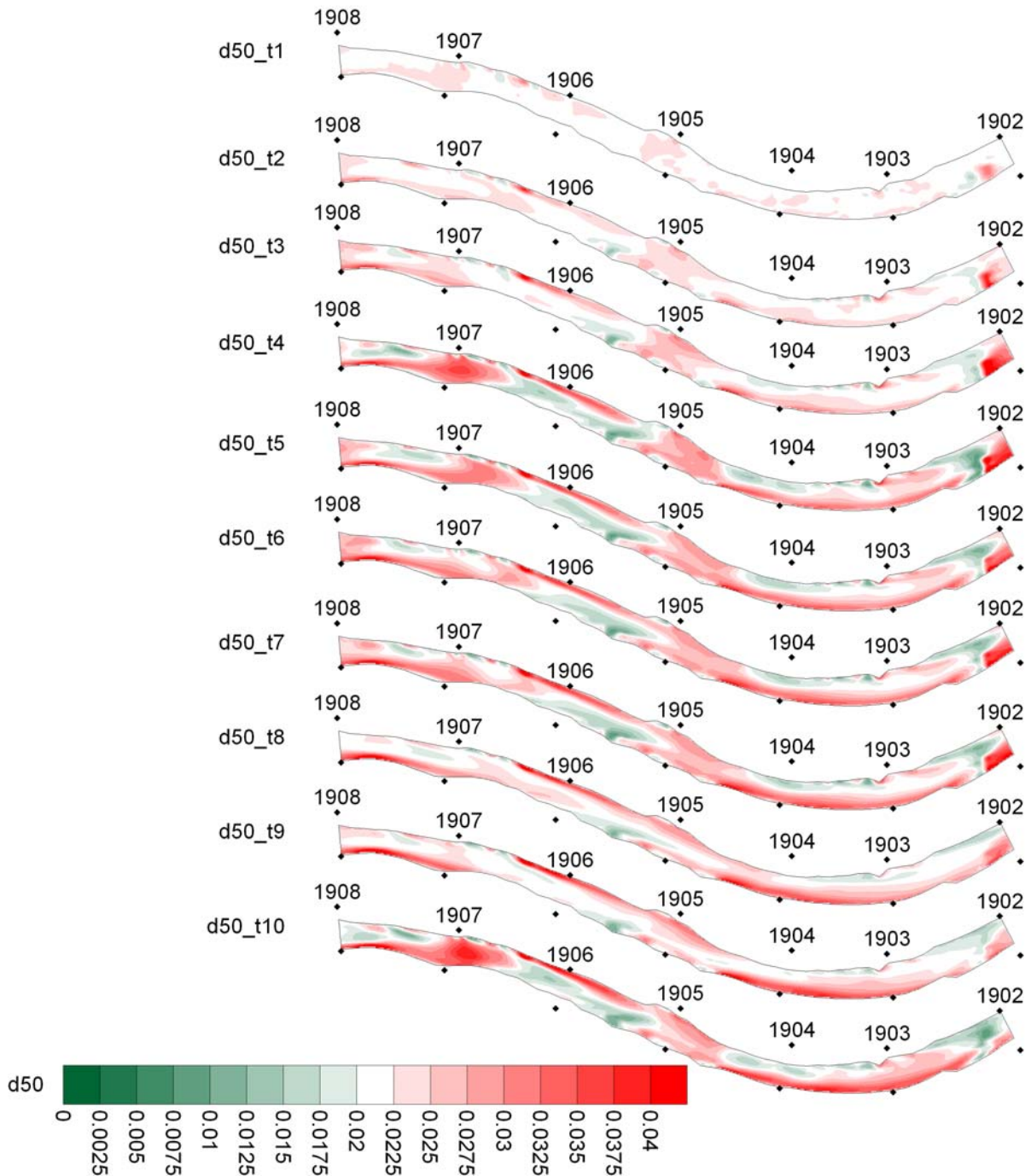
Figure 4.38: Development of d_{50}

4.4   Summary and conclusions

A three-dimensional numerical morphodynamic model is modified to account for the interaction of several grain sizes when computing fractional sediment transport. The sediment transport formulas of *Wu et al. (2000b)* are incorporated to the numerical model *SSIIM*. The performance of the *Wu* formula is tested in the study of *Scheer et al. (2002)*. Here the *Wu* formula performs best among twelve sediment transport formulas including transport formulas of *Meyer-Peter & Müller (1949)*, *Hunziker (1995)*, and *v.Rijn (1984a)*. The *Wu* formula performs best in two tested categories, the prediction of sediment transport rates and the prediction of sediment size distribution.

Within the framework of this study, the newly incorporated model is tested on a real river reach of the free flowing Danube river east of Vienna. A simulation length of 8 km (km 1909.5 to 1901.5) and a processing length of 6 km (km 1908 to 1902) are chosen. The test reach is located 11.5 km downstream the last hydropower station in Austria. The simulation period comprises the 100 year flood event at the Danube river in 2002, where discharges of more than 10,000 m³/s are achieved. Analysing the pre and post flood surveys reveals that the overall morphological features, such as sizes and shapes of the alternating bars have not changed during the flood events. Locally, considerable morphological changes of up to 1 m occur.

The test reach chosen for validating the morphodynamic model is situated in the alternate bar region of the Danube river. This reach was mainly in a stage of deposition during the 2002 flood . The results of the measured bed changes that are achieved from an analysis of the pre and post flood survey in 2002 are used to validate the morphodynamic model. The flow hydrograph measured between the two surveys is simplified to serve as boundary condition for the unsteady model. It is simplified in a way that discharges below a threshold value of 2000 m³/s are neglected as their influence on the morphodynamic changes in a river is assumed to be of minor importance. In this way, the original period of approximately 250 days is reduced to 44 days, giving a reduction of 82 %.

Morphodynamic computations are performed for the 44 day period and the results are compared to the measured bed changes. The threshold for incipient motion θ_c is increased to obtain computed results in the range of the measured bed changes. The adjustment of θ_c is a commonly applied measure and is legitimated by the study of *Kroekenstoel & van Welzen (2003)*. In order to assess the quality of the computed bed changes, difference maps showing the contours of measured and computed bed changes are produced. Thus, a method is given to compare erosion and deposition patterns and the bed change ranges of the measured and the computed results. The agreement of measured and computed erosion-deposition patterns and bed change heights is satisfactory. The model is able to represent the relevant morphodynamic processes, such as deposition processes of a bar and the related erosion processes at the scour on the opposite side.

Moreover, a sensitivity analysis of the morphodynamic model is performed. Parameters of the sediment transport formula are tested with respect to the sensitivity of the computed bed changes. The results show that the parameter for incipient sediment motion, θ_c, gives the largest sensitivity. While an increased value of θ_c gives reasonable results, the default value overestimates the bed change heights. Furthermore, modifications of the hiding-exposure coefficient, especially increasing its absolute value, give highly sensitive results. Other parameters, such as the factor for the sediment transport rate or the sediment inflow show small sensitivity on the computed bed changes.

An error analysis is performed for studying quantitatively the agreement of computed and measured bed changes. Several measures of errors are used as a tool to evaluate the computed results based on using different parameters. Binary maps are developed showing that 78 % of the erosion-deposition patterns are computed at the correct position, when a measurement tolerance of 10 cm is introduced. Two measures of errors are introduced including a measure of error particularly developed to account for the specific situation in this study. The measures of error are computed for all parameter combinations. The results show that some parameter combinations, such as a low absolute

value of the hiding exposure coefficient, using variable roughness computations, and considering side slope effects contribute positively to the agreement of measured and computed bed changes.

Moreover, the temporal evolution of the computed results are assessed. As there is no measured data available for the development of the bed levels between the two surveys, the plausibility of the computed results is tested, and the unsteady processes leading to the morphological changes based on the flood events are analysed. Detailed analysis is performed at two typical cross-sections and on one crossing. The results indicate that the three peaks cause the most significant changes of the river bed. Periods with smaller discharges also result in reduced morphological changes. Within the bar regions, deposition prevails on the bar sides and the scour sides are eroded. Deposition processes are given at the crossing. These processes happen continuously and batch-wise according to the passage of the floods. In areas where the flow velocities fall temporarily below 1 m/s, sediment transport stops resulting in a disruption of the bed change dynamics. These processes are observed during the falling limbs of the hydrograph within the bar regions. The highest peaks do not always produce the most significant bed changes. This is best observed at the erosion regions of the scours. These phenomena are plausibly explained by the coarsening processes that happens at the erosion regions. This results in a stabilisation of the bars during the first two floods, so that the third and highest flood only induces smaller further erosion. This phenomenon is observed analogously on the opposite bar side. While the deposition heights of the first two floods are moderate, the entrainment of fine particles produces the largest deposition processes at the last flood.

The morphodynamic model proves successfully to be able to compute relevant morphodynamic processes in a real river reach. Results and limitations have been discussed in this study. The main recommended fields for further research activities are:

  ➢ Improving the sorting algorithms. At the present stage, a two layer approach is incorporated into the morphodynamic model. For a more detailed analysis of deposition and re-entrainment processes in combination with sorting and armouring processes in the course of flood events, a multi-layer concept should better represent the natural processes.

  ➢ Improving wetting and drying algorithms in the context of unsteady sediment computations. In the present version of the model using structured grid alignment, wetting and drying algorithms are not incorporated. It also exists an unstructured version of the numerical model (denoted as *SSIIM 2*), that should be tested for unsteady morphodynamic computations in the future.

  ➢ Improving the flow computations through vegetation and over groynes. In the present version of the model, vegetation is considered either by defining a separate roughness coefficient in the cells where vegetation is found, or an additional source term is added to the velocity equations in these cells accounting for the additional resistance the vegetation impresses on the flow. Groynes are considered by defining extra walls in the grid. In this study, the vegetation density and the heights of the groynes are unknown, so that rough assumptions have to be drawn.

The introduced analysis allows to enhance the understanding of relevant processes in real rivers. While bed level surveys provide detailed information of the current morphological situation, they

cannot contribute to recognise the underlying processes leading to the momentary bed levels in detail. Thus, the introduced numerical model contributes to the issue of nonuniform sediment transport processes under unsteady flow conditions. The chance of numerical models is to "fill the gap" of the periods between the surveys by reproducing the processes leading from one measured bed level to the next. These computations represent the basis for predicting the river bed development in the future. The computed flow and sediment features indicate that adequate considerations of nonuniform sediment transport processes are essential to compute the morphological changes in a mountainous river like the Danube river correctly.

5 Synopsis

The main aim of the present study is the assessment of river bed changes considering bed deformation and grain sorting processes of graded sediments. Based on regular field measurements, morphological structures and changes are analysed at a 40 km long free flowing reach of the Danube river between Vienna and the Austrian-Slovakian border. Numerical studies are performed to enhance the understanding of the processes leading to measured river bed changes. A three-dimensional numerical model is modified to compute nonuniform sediment transport processes of sand and gravel bed rivers. After validating the model on laboratory experiments, it is tested on a Danube river reach.

In Chapter 2, morphological concepts are introduced to assess the bed changes of the Danube river study reach over a period of ten years. Based on regular bed level surveys, the analysis involves visualisations of bed levels and bed changes by creating bathymetric and difference maps. Erosion-deposition patterns are obtained by comparing different bed level surveys. The patterns are used as a tool to analyse the dynamics of individual morphological structures. Commonly applied parameters such as mean bed levels, thalweg development, cumulative bed volume changes, and width-to-depth ratios, and new parameters such as profile symmetry, lateral slopes, spatial and temporal profile shape similarities are introduced to describe and quantify different aspects of river bed variability and relevant morphological processes. Bed level changes are discussed with reference to river maintenance measures including dredging and grain feeding activities.

The results show that the river reach is in a long-term stage of erosion with an average erosion rate of 2.4 cm per year. River bed morphology is generally characterised by an alternate bar configuration. Clearly developed bar structures are found at the upper half of the study reach while at the lower half which is characterised by intensive groyne installations such clear morphological structures have not developed. The long-term planimetric configuration of the morphological structures, i.e. the positions of bars, scours, and crossings, remain virtually unchanged over the study period. However, detailed analysis of individual structures shows considerable vertical bed changes comprising general erosion of bars, deposition of scours and partly significant erosion of crossings. These local changes are partly ascribed to considerable maintenance measures performed at the study reach. The local changes of the morphological structures have a significant impact on the hydraulics of the flow particularly with regard to the reduced backwater effect of the groynes on the water levels induced by erosion processes. A short-term investigation of the pre and post flood surveys in 2002 shows that the flood has a smoothing effect of local discontinuities of the river bed while the scour depths at some of the bars slightly increase. Shape analysis shows that 80 % of the cross-sectional profiles exhibit distinct asymmetrical features, typically located in the alternate bar regions. Cross-sectional profiles at the bars show mean lateral slopes of approximately 2.5 % which are more than 60 times larger than the mean longitudinal slope at the river reach (0.04 %) giving rise to relevant grain sorting processes at the bars. Analysis of profile shape variations shows a clear relationship of spatial and temporal similarities in the long-term indicating that bed changes at a cross-section are determined by the morphological structures upstream.

To gain more insight in the underlying processes of the morphological changes an analysis on the basis of numerical methods is performed. Starting point is the three-dimensional numerical model *SSIIM* originally developed by *Olsen (1999)* to model sediment movements in water intakes. In this study *SSIIM* is modified to allow to compute nonuniform sediment transport processes in sand and gravel bed rivers. The nonuniform sediment transport approach of *Wu et al. (2000b)* including hiding-exposure effects is incorporated into the model. In Chapter 3, the modified model is validated on laboratory experiments in a 180° channel bend (*Yen & Lee (1995)*) where bed deformation and sorting processes of graded bed material under unsteady flow conditions using a triangle flow hydrograph were investigated. In the default version of the numerical model the sediment transport formulas of *v.Rijn (1984a)* are used. This approach is developed for uniform sediment transport processes of sand with maximum grain diameters of 2 mm. For complex sediment transport processes in gravel bed rivers it is hypothesised that this approach does not give appropriate results. This is verified by comparing the computed results of the newly incorporated and the default approach to the measured bed deformation and sorting processes.

The results show that the general flow features in the 180° bend are well described by the numerical model. Applying the default model (*v.Rijn (1984a)*) it is found that bed deformation and sorting processes in the channel bend are computed qualitatively correct. Bulk morphological features, including bar and scour forming processes at the inner and outer banks, in combination with sediment fining at the bar and coarsening at the scour, are generally represented by the default model. However, the extent of the bed deformation and sorting processes is considerably overestimated. The modified model with the incorporated formulas of *Wu et al. (2000b)* performs substantially better. Here, good agreement of the relevant morphological processes including development of bed changes (bar and scour) and sorting is given. Also, the cumulative transported bed material trapped at the outlet of the laboratory flume is calculated considerably better by the modified model than by the default model. The improved performance is ascribed to the consideration of hiding-exposure algorithms that describe better the physical processes of grain interaction for nonuniform sediment transport. Sensitivity tests of relevant sediment parameters show that best results are obtained when using the default values of the threshold coefficient for incipient motion and the sediment transport rate factor. While changes of the sediment transport rate factor show a small to medium sensitivity to the results, variations of the threshold coefficient for incipient motion are highly sensitive to the computed bed changes. Results can be improved by reducing the absolute value of the exponent in the hiding-exposure function.

The modified numerical model has been successfully validated against measured data from experiments in a laboratory bend providing a number of relevant processes also found in nature such as unsteady flow in river bends and morphological changes of graded bed material. These investigations establish a sound basis for testing the numerical model on a real river application (Chapter 4). Based on the morphological analysis of the Danube river (Chapter 2) an appropriate reach is chosen for the model test. Morphological changes induced by the 100 year flood in 2002 comprising discharges of more than 10,000 m³/s are obtained from pre and post flood surveys of the river bed. Numerical computations of unsteady flow and nonuniform sediment transport of a 6 km long reach of the Danube river are performed including bed change processes of typical morphological

structures (bars and crossings). All discharges exceeding 2,000 m³/s which contribute to sediment transport processes are considered. Detailed tests are performed by analysing measured and computed erosion-deposition patterns. The results show generally satisfactory agreement of measured and computed erosion-deposition patterns when using the modified model. The modified model computes 78 % of the patterns correctly when introducing a measurement uncertainty of 10 cm. Improved agreement is achieved by increasing the threshold for incipient sediment motion. Sediment parameters including the hiding-exposure exponent and the sediment transport rate factor show similar sensitivities to changes as investigated in Chapter 3. The computed sorting processes give plausible results. Analysis of the evolution over time shows that the river bed dynamics are interrelated with the sorting processes of morphological structures. The bed erosion of scour regions is accompanied by progressive coarsening which induces a stabilising effect of the river bed. This is reflected by successively decreasing erosion rates during the 2002 floods at the scour sections.

Morphological processes are analysed in this study by processing bed level surveys and validating and testing a modified numerical model. The combination of both methods allows detailed assessment of morphological structures and bed changes at rivers. The introduced numerical methods can be used to supplement or complement expensive laboratory experiments for predicting bed change developments. Thus, these methods can be used for the decision finding process of river restoration measures such as protecting hot spots from critical erosion processes. The results of this study are particularly relevant for the interdisciplinary field of hydraulics and freshwater ecology. The problem of appropriate habitat conditions (e.g. for fishes) are strongly related to morphological structures and morphological changes.

The analysis in the present study is restricted to the availability of cross-sectional bed level surveys. Here, regularly surveyed data only cover bed levels below a reference low water level. Neither bed levels at shallow water depths nor at the inundation areas are surveyed regularly. Thus, limited cross-sectional bed level data introduce uncertainty to the morphological analysis, particularly with respect to sediment balance computations. Future research should concentrate on the analysis of complete cross-sectional surveys. Furthermore, at chosen pilot reaches bed level measurements should be coupled with measurements of velocities and a survey of the bed material size distribution. Further developments of an underwater camera (*Blaschke et al. (2002)*) can be used in the future for obtaining dense information of the bed material size distribution at the surface. To investigate bed forms such as ripples and dunes, a multibeam technology can be used to measure the river bed with a high longitudinal and lateral resolution.

In the current version of the numerical model the grid has to be adjusted to the groyne geometries by defining extra walls at the appropriate grid lines. Thus, an improved consideration of groynes would simplify the generation process of the finite volume grid. Numerical simulations can be improved by considering further algorithms to better describe the morphological processes, such as loading law approaches (accounting for the non-equilibrium of the sediment transport) or improved algorithms for sediment transport on side slopes. Modelling sorting and armouring processes can be computed more accurately by implementing significantly more bed layers.

6 Notations

B   =   channel width [m]

c   =   volume sediment concentration [m³/m³]

D   =   sediment continuity defect [kg/s]

d_0 =   initial median sediment diameter

d, d_{50} =   grain size of 50 % finer [m] = median sediment diameter

d_{90} =   grain size of 90 % finer [m]

d_m =   mean sediment diameter [m]

f   =   sediment fraction [-]

h_0 =   water depth of base flow [m]

I_0 =   initial energy slope [-]

k   =   turbulent kinetic energy [m²/s²]

m   =   exponent for correction factor [-]

N   =   total number of particle size fractions [-]

n   =   Manning's coefficient for channel bed [s/m$^{1/3}$]

n'   =   Manning's coefficient corresponding to grain roughness [s/m$^{1/3}$]

P   =   pressure [N/m²]

P   =   exponent for hiding-exposure function [-]

p_{bj} =   percentage of the ith fraction of bed material [-]

p_{ei} =   total exposed probabilities of particles d_i [-]

p_{hi} =   total hidden probabilities of particles d_i [-]

P_k =   production of turbulent kinetic energy

Q_0 =   discharge of base flow [m³/s]

q_{bi} =   transport rate of the ith fraction of bed-load per unit width [m³/(s*m)]

r_c	=	radius of curvature [m]
t	=	time [s]
u_{*0}	=	shear velocity of base flow [m/s]
u_i	=	velocity fluctuation [m/s]
U_i	=	average velocity [m/s]
x_i	=	spatial geometrical scale [m]
z_a	=	height of the active layer [m]
z_d	=	height of the deposition [m]
α	=	Factor modifying the fractional sediment transport rate [-]
δ_{ij}	=	Kronecker delta
ε	=	dissipation of turbulent kinetic energy [m²/s²]
ϕ_{bi}	=	non-dimensional fractional bed-load transport rate [-]
η_i	=	correction factor [-]
ν_t	=	eddy viscosity [m²/s]
θ_c	=	non-dimensional critical shear stress [-]
ρ	=	density of water [kg/m³]
ρ_s	=	density of sediments [kg/m³]
σ_0	=	initial standard deviation of sediment size gradation [m]
τ_b	=	bed shear stress
τ_c, τ_{ci}	=	critical shear stress for d_m, d_i
ω	=	dissipation per turbulent kinetic energy [1/s]

7 References

ASCE, 1966, Task Force on Bed Forms, Committee of Sedimentation, Nomenclature for bed forms in alluvial channels, J. Hydraulic Division, 92 (3), pp. 51-64.

Bechteler, W., Hartmann, S., Mergl, C. and Wieprecht, S., 1998, Dynamik von Kiesbänken in der unteren Salzach - ein Vergleich von Naturbeobachtungen mit einem physikalischen Modell, *in* T. Strobl, Hrsg., Planung und Realisierung im Wasserbau, Symposium 15.-17. Oktober 1998, TU München, Wasserbau und Wasserwirtschaft, 82, München.

Blaschke, A. P., Braunshofer, R., Feregyhazy, H. and Gutknecht, D., 2002, Kolmationsprozesse am Beispiel des Stauraums Freudenau, Projektphase II - Vollstau, Verbund und Techn. Univ. Wien, Wien.

Bors, W., 1992, Stromsohlenveränderungen der Donau durch Geschiebe und Schwebstoffe, Landschaftswasserbau, 13 pp. 437-452.

Brasington, J., Rumsby, B. T. and McVey, R. A., 2000, Monitoring and modelling morphological change in a braided gravel-bed river using high resolution GPS-based survey, Earth Surface Processes and Landforms, 25 (9), pp. 973-990.

Brockmann, H., Kraus, K. and Mandlburger, G., 2001, Modellierung digitaler Höhendate zur Bearbeitung hydrologisch/hydraulischer Fragestellungen an Wasserläufen - Am Beispiel des Projektes "HGIS-Saar", Hydrologie & Wasserbewirtschaftung, 45 (3), pp. 112-119.

Brookes, H. N., 1963, Boundary shear stress in curved trapzoidal channels, Journal of Hydraulics Division, ASCE, 89 (3).

Bui, M. D., 1998, Berechnung der Strömung und des Sedimenttransports in Flüssen mit einem tiefengemittelten numerischen Verfahren, Institut für Hydromechanik, Universität Karlsruhe, Karlsruhe.

da Silva, A., 1991, Alternate bars and related alluvial processes, Queen's University, Kingston, Ontario, Canada.

Dittrich, A., 1998, Wechselwirkung Morphologie/Strömung naturnaher Fießgewässer, Institut für Wasserwirtschaft und Kulturtechnik, Universität Karlsruhe, 198, Karlsruhe.

Donauconsult, 1997, Donauausbau östlich von Wien, Verbesserung der Schiffahrtsverhältnisse und granulometrische Sohlverbesserung.

Donaukraft, 1995, Donaukraftwerk Freudenau, Detailprojekt Unterwasserbereich, Geschiebezugabe ohne Kolksicherung, Technischer Bericht, Wien.

Engelund, F., 1974, Flow and bed topography in channel bends, J. Hydraulic Division, 100 (HY11).

Engelund, F., 1981, The motion of sediment particles on an inclined bed, prog. Rep. 53, Inst. Hydrodynamic and Hydraulic Engineering, Tech. Univ. Denmark.

Fang, H. and Rodi, W., 2003, Three-dimensional calculations of flow and suspended sediment transport in the neighborhood of the dam for the Three Gorges Project (TGP) reservoir in the Yangtze River, J. Hydraulic Research, 41 (4), pp. 379-394.

Ferziger, J. and Peric, M., 2002, Computational methods for fluid dynamics, 3rd edition, Springer, Berlin.

Fischer-Antze, T., Gutknecht, D. and Olsen, N. R. B., 2004, 3d numerical modelling of morphological bed changes in the Danube River, Balkema *in* M. Greco, editor, River Flow 2004, Naples, Italy.

Fischer-Antze, T., Stoesser, T. and Bates, P., 2001, 3D numerical modelling of open-channel flow with submerged vegetation, J. Hydraulic Research, 39 (3), pp. 303-310.

Fluent, 2003, FLUENT 6.0, User's guide, Lebanon, New Hampshire, USA.

Fuller, I. C., Large, A. R. G., Charlton, M. E., Heritage, G. L. and Milan, D. J., 2003, Reach-scale sediment transfers: An evaluation of two morphological budgeting approaches, Earth Surface Processes and Landforms, 28 (8), pp. 889-903.

Gessler, D., Hall, B., Spasojevic, M., Holly, F., Pourtaheri, H. and Raphelt, N., 1999, Application of 3d mobile bed, hydrodynamic model, J. Hydraulic Engineering, 125 (7).

Günter, A., 1971, Die kritische mittlere Sohlenschubspannung bei Geschiebemischungen unter Berücksichtigung der Deckschichtbildung und der turbulenzbedingten Sohlenschubspannungsschwankungen, VAW, ETH Zürich, 3, Zürich.

Gutknecht, D. and Fischer-Antze, T., 2005, Durchführung von Wasserspiegellagenberechnungen an der Donau, Institut für Wasserbau, Technische Universität Wien, Vienna.

Habersack, H. and Schneider, J., 2000, Ableitung und Analyse flussmorphologisch relevanter Parameter von historischen Karten, Wasser und Boden, 52 (6), pp. 55-59.

Ham, D. G. and Church, M., 2000, Bed-material transport estimated from channel morphodynamics: Chilliwack River, British Columbia, Earth Surface Processes and Landforms, 25 (10), pp. 1123-1142.

Hervouet, J. M., Hubert, J. M., Janin, J. M., Lepeintre, F. and Peltier, E., 1994, The computation of free surface flows with TELEMAC: An example of evolution towards hydroinformatics, J. Hydraulic Research, 21 (1), pp. 45-65.

Hunziker, R., 1995, Fraktionsweiser Geschiebetransport, ETH Zürich, VAW, 138.

Ikeda, S., 1982, Lateral Bed Load Transport on Side Slopes, Journal of Hydraulics Division, ASCE, 108 (11).

Jäggi, M., 1983, Alternierende Kiesbänke, ETH Zürich, VAW, 62.

Jirka, G. H. and Lang, C., 2005, Gerinnehydraulik, Universität Karlsruhe, Karlsruhe.

Julien, P. Y. and Anthony, D. J., 2002, Bed load motion and grain sorting in a meandering channel, J. Hydraulic Research, 40 (2), pp. 125-132.

Kikkawa, H. S., Ikeda, S. and Kitagawa, A., 1976, Flow and bed topography in curved open channels, J. Hydraulic Division, 102 (9), pp. 1326-1342.

Klasz, G., 2002, Ein Beitrag zur sohlmorphologisch orientierten Untersuchung der Sohlstabilisierung der Donau zwischen Wien und Marchmündung (Vorabzug), Institut für Hydraulik, Gewässerkunde und Wasserwirtschaft, TU Wien, Wien.

Knaapen, M. A. F., 2001, Predicting large waves in erodible sand beds, University of Twente, Netherlands.

Kresser, W., 1988, Die Eintiefung der Donau unterhalb von Wien, Perspektiven, Heft 9/10 pp. 41-43.

Kroekenstoel, D. F. and van Welzen, E. H., 2003, Morphologische Berechnungen mit Sedimentmischungen - Zukunftsmusik oder eine realistische Alternative?, KHR, II-19.

Krouzecky, N., 2004, Buhnen, Wasserspiegelhabeung zufolge nicht überströmter Buhnen bei fester Sohle, Publish Factory Medienproduktion, Wien.

Lanschützer, C., 2005, Personal Communication.

Lanzoni, S., 2000a, Experiments on bar formation in a straght flume, 2. Graded sediment, Water Res. Research, 36 (11), pp. 3351-3363.

Lanzoni, S., 2000b, Experiments on bar formation in a straight flume, 1. Uniform sediment, Water Res. Research, 36 (11), pp. 3337-3349.

Launder, B. E. and Spalding, D. B., 1974, The numerical computation of turbulent flows, Comput. Meths. Appl. Mech. Eng., 3.

Leopold, L. B. and Wolman, M. G., 1957, River channel patterns, braided, meandering and straight, US Geological Survey Prof. Paper, 282-B.

Luijendijk, A. P., 2001, Validation, calibration and evaluation of DELFT3D-FLOW model with ferry measurements, Master's Thesis, University of Utrecht, The Netherlands.

Mangelsdorf, J. and Scheurmann, K., 1980, Flußmorphologie - Ein Leitfaden für Naturwissenschaftler und Ingenieure, Oldenbourg, München.

Marburger, M., 1998, Entwicklung eines tiefengemittelten morphodynamischen Fließgewässermodells, Universität Kassel, Fachgebiet Wasserbau, 8.

Maryono, A., 1999, Inseln und deren Widerstandsverhalten in Fließgewässern, Institut für Wasserwirtschaft und Kulturtechnik, Heft 204, Universität Karlsruhe, Karlsruhe.

Mewis, P., 2002, Morphodynamisch-numerische Modellierung von Flusskurven, Institut für Wasserbau und Wasserwirtschaft, Technische Universität Darmstadt, Darmstadt.

Meyer-Peter, E. and Müller, R., 1949, Eine Formel zur Berechnung des Geschiebetriebs, Schweizerische Bauzeitung, 67 (3).

Minh Duc, B., Wenka, T. and Rodi, W., 2004, Numerical modeling of bed deformation in laboratory channels, J. Hydraulic Engineering, 130 (9), pp. 894-904.

Mohilla, P. and Michlmayr, F., 1996, Donauatlas Wien, Österreichischer Kunst- und Kulturverlag, Wien.

Naudascher, E., 1987, Hydraulik der Gerinne und Gerinnbauwerke, Springer, Wien, New York.

Nestmann, F. and Büchele, B., 2002, Morphodynamik der Elbe, Institut für Wasserwirtschaft und Kulturtechnik, Universität Karlsruhe, Karlsruhe.

Odgaard, A. and Bergs, M., 1988, Flow processes in a curved alluvial channel, Water Res. Research, 24 (1), pp. 45-56.

Olsen, N. R. B., 1991, A three-dimensional numerical model for simulation of sediment movements in water intakes, Division of Hydraulic Engineering, The Norwegian Institute of Technology, Trondheim.

Olsen, N. R. B., 1999, Computational fluid dynamics in hydraulic and sedimentation engineering.

Olsen, N. R. B., 2002, SSIIM - User's Manual, Trondheim.

Olsen, N. R. B., 2003, Three-dimensional CFD modeling of self-forming meandering channel, J. Hydraulic Engineering, 129 (5), pp. 366-372.

Olsen, N. R. B., 2004, Hydroinformatics, fluvial hydraulics and limnology, Department of Hydraulic and Environmental Engineering, The Norwegian University of Science and Technology, www.ntnu.no/~nilsol/cfd, Trondheim.

Olsen, N. R. B. and Kjellesvig, M., 1999, Three-dimensional numerical modelling of bed changes in a sand trap, J. Hydraulic Research, 37 (2), pp. 189-198.

Parker, G. and Andrews, E., 1985a, Sorting of bed load sediment by flow in meander bends, Water Res. Research, 21 (9), pp. 1361-1373.

Parker, G. and Andrews, E. D., 1985b, Sorting of bed load sediment by flow in meander bends, Water Res. Research, 21 (9), pp. 1361-1373.

Patankar, S., 1980, Numerical Heat Transfer and Fluid Flow, T. Francis.

Rhie, C. and Chow, W., 1983, Numerical study of the turbulent flow past an airfoil with trailing edge separation, AIAA Journal, 21 (11).

Ribberink, J. S., 1987, Mathematical modelling of one-dimensional morphological changes in rivers with non-uniform sediment, Delft University of Technology, Delft.

Rinaldi, M., 2003, Recent channel adjustments in alluvial rivers of Tuscany, Central Italy, Earth Surface Processes and Landforms, 28 pp. 587-608.

Rodi, W., 1984, Turbulence models and their application in hydraulics, IAHR state-of-the-art publication.

Rozovskij, I. L., 1957, Flow of water in bends of open channels, Acad. Science Ukranian SSR, Kiev.

Ruether, N. and Olsen, N. R. B., 2004, Three dimensional modeling of sediment transport in a channel bend, Balkema *in* M. Greco, editor, River Flow 2004, Naples, Italy.

Ruether, N. and Olsen, N. R. B., 2005, Three dimensional modeling of sediment transport in a narrow 90° channel bend, J. Hydraulic Engineering. in press.

Savova, S., 2002, Flussmorphologische Charakteristik der österreichischen Donau zwischen Wien und der slowakischen Staatsgrenze, Diplomarbeit, TU Wien, Institut für Hydraulik, Gewässerkunde und Wasserwirtschaft, Wien.

Scheer, P. v. d., Blom, A. and Ribberink, J. S., 2002, Transport Formulas for Graded Sediment - Behaviour ot transport formulas and verification with data, University of Twente, 2002R-002, Enschede.

Scherle, J., 1999, Entwicklung naturnaher Geässerstrukturen, Grundlagen, Leitbilder, Planung, Institut für Wasserwirtschaft und Kulturtechnik, Heft 199, Universität Karlsruhe, Karlsruhe.

Schlichting, H., 1979, Boundary layer theory, McGraw-Hill Book Company, New York.

Schmautz, M., Aufleger, M. and Strobl, T., 2002, Anthropogene Einflussnahme auf die Flussmorphologie der Donau in Österreich, Österr. Ing. und Arch.-Zeitschrift, 147 (5-6).

Schröder, R. and Zanke, U., 2003, Technische Hydraulik - Kompendium für den Wasserbau, Springer.

Seminara, G. and Tubino, M., 1989, Alternate bars and meandering: free, forced and mixed interactions, *in* S. Ikeda and G. Parker, Hrsg., River meandering, AGU, Water Resources Monograph, 12, Washington.

Shields, A., 1936, Anwendung der Ähnlichkeitsmechanik und der Turbulenzforschung auf die Geschiebebewegung, Mitteilungen der Preußischen Versuchsanstalt für Wasserbau und Schiffbau, Heft 26, Berlin.

Spannring, M., 1999, Die Wirkung von Buhnen auf Strömung und Sohle eines Fließgewässers, Lehrstuhl und Versuchsanstalt für Wasserbau und Wasserwirtschaft, Technische Universität München, München.

Stein, C. J., 1990, Mäandrierende Fließgewässer mit überströmten Vorländern - Experimentelle Untersuchung und numerische Simulation, RWTH Aachen, 76, Aachen.

Stiefelmeyer, H., 2001, Dynamische Sohlstabilisierung durch Grobkornanreicherung für einen nationalparkkonformen Donauausbau zwischen Wien und Bratislava, Institut für Konstruktiven Wasserbau, Wien.

Tritthart, M., 2005, Three-dimensional numerical modelling of turbulent river flow using polyhedral finite volumes, Institute for Hydraulic and Water Resources Engineering, Vienna Universoty of Technology, Vienna.

v.Bendegom, 1963, Some considerations on river morphology and river improvement, Technical Translation 1054, Nat. Res. Council Canada.

v.Rijn, L. C., 1984a, Sediment Transport, Part I: Bed Load Transport, J. Hydraulic Engineering, 110 (11), pp. 1431-1457.

v.Rijn, L. C., 1984b, Sediment Transport, Part II: Suspended Load Transport, J. Hydraulic Engineering, 110 (11), pp. 1613-1641.

Verbund, 2005, Die Kraftwerke an der österreichischen Donau.

Wenka, T., 1992, Numerische Berechnung von Strömungsvorgängen in naturnahen Flussläufen mit einem tiefengemittelten Modell, Dissertation, Institut für Hydromechanik, Universität Karlsruhe, Karlsruhe.

WRS, 2000, Wasserwirtschaftliche Rahmenuntersuchung Salzach - Untersuchungen zur Flussmorphologie der Unteren Salzach, Wien, München.

WSD, 1996, Die kennzeichnenden Wasserstände der österreichischen Donau (KWD 1996), Wien.

Wu, W., Rodi, W. and Wenka, T., 2000a, 3d numerical modelling of flow and sediment transport in open channels, J. Hydraulic Engineering, 126 (1), pp. 4-15.

Wu, W. and Wang, S., 2004, Depth-averaged 2-D calculation of flow and sediment transport in curved channels, J. Sediment Research, 19 (4), pp. 241-257.

Wu, W., Wang, S. and Jia, Y., 2000b, Nonuniform sediment transport in alluvial rivers, J. Hydraulic Research, 38 (6), pp. 427-434.

Yalin, M. S., 1992, River Mechanics, Pergamon Press, Oxford.

Yalin, M. S. and da Silva, A., 2001, Fluvial Processes, IAHR, Monograph.

Yen, C. and Lee, K., 1995, Bed topography and sediment sorting in channel bend with unsteady flow, J. Hydraulic Engineering, 121 (8), pp. 591-599.

Zanke, U., 1982, Grundlagen der Sedimentbewegung, Springer, Berlin.

Zarn, B., 1997, Einfluss der Flussbettbreite auf die Wechselwirkung zwischen Abfluss, Morphologie und Geschiebetransportkapazität, ETH Zürich, VAW, 154.

Zarn, B., 2005, Personal Communication.

Zeng, J., Constantinescu, G. and Weber, L., 2005, A fully 3D non-hydrostatic model for prediction of flow, sediment transport and bed morphology in open channels *in* IAHR conference 2005, Seoul, Korea.

Zhu, J., 1991, Fast-2d: A computer program for numerical simulation of two dimensional incompressible flows with comlex boundaries, Institut für Hydromechanik, Universität Karlsruhe, Karlsruhe.
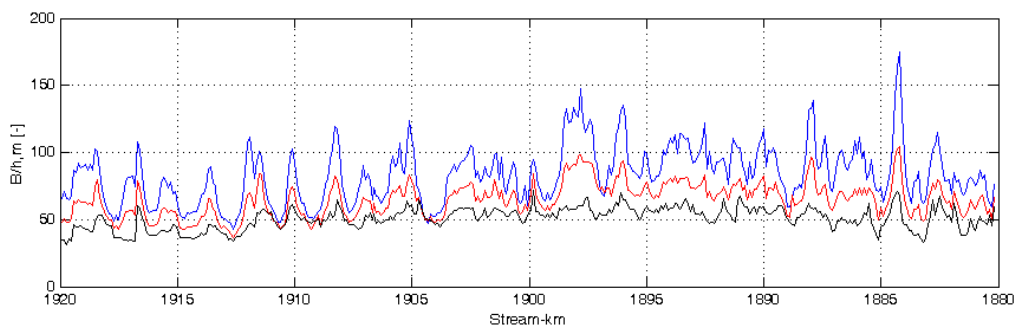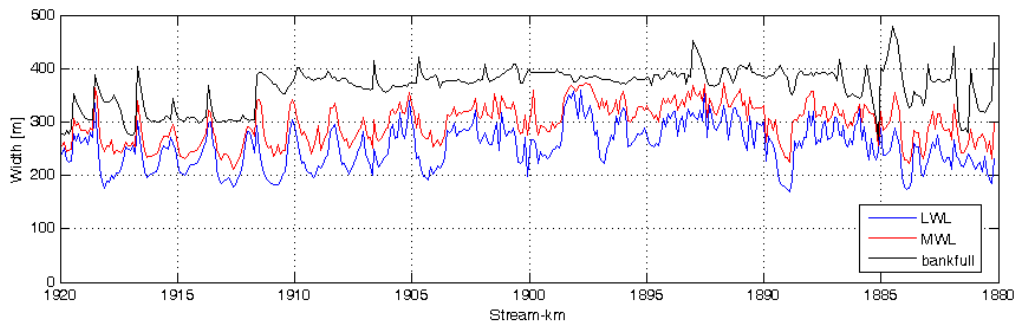
Zimpfer, G., 1975, Development of laboratory river channels, Dept. of Earth Resoruces, Colorado State University, Fort Collins, Colorado.

Zottl, H. and Erber, H., 1987, Untersuchung der Sohlstabilität im Zusammenhang mit der Staustufe Wien, Auftraggeber MA 45, Wien.

Appendix A: Morphological parameters
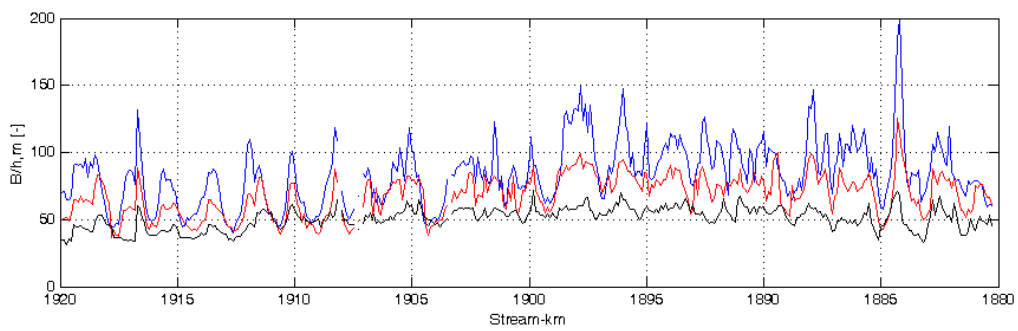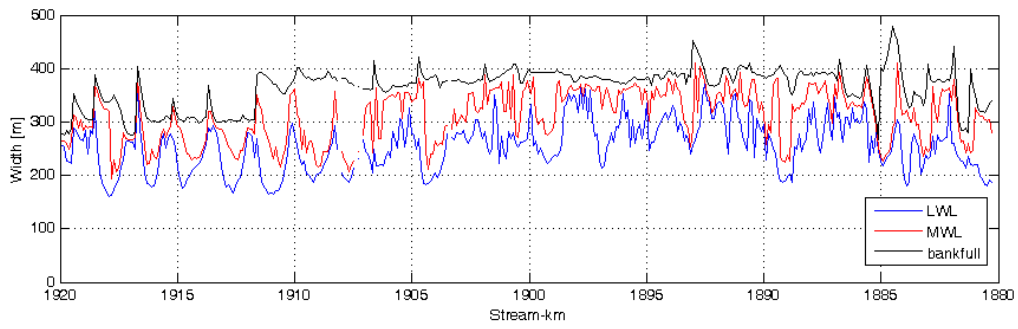
Widths and Width-to-depth ratios 1993

Widths and Width-to-depth ratios 1996
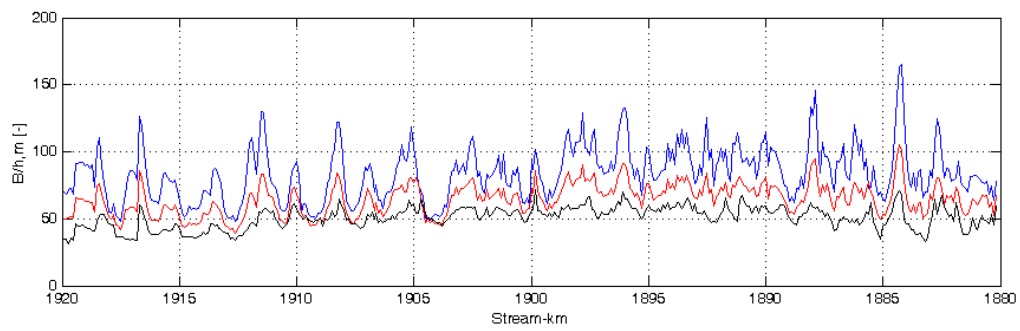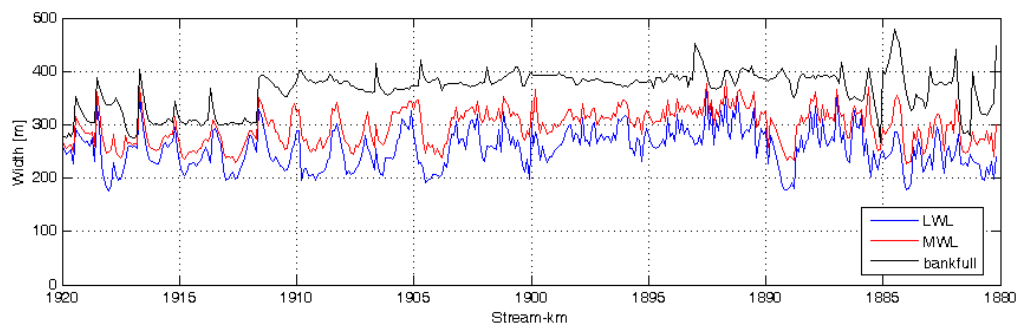
Widths and Width-to-depth ratios 2002(2)
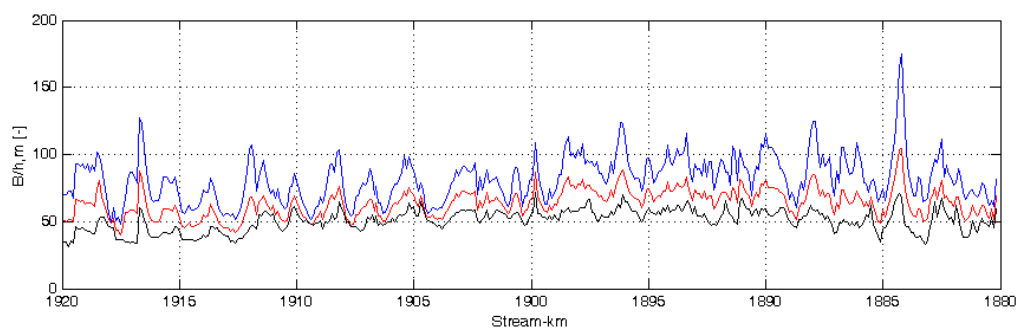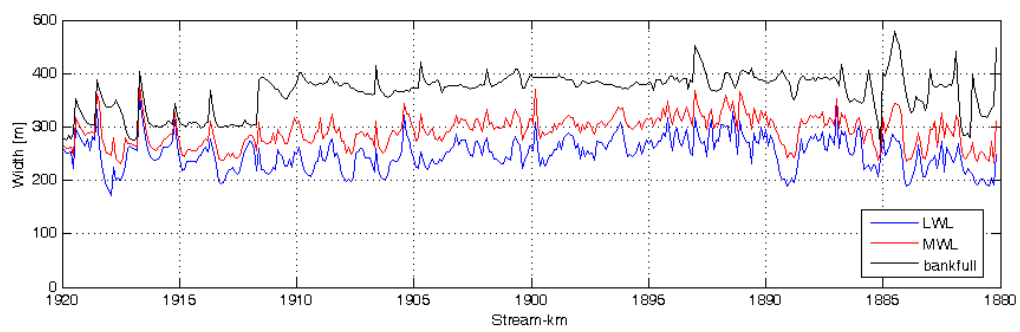
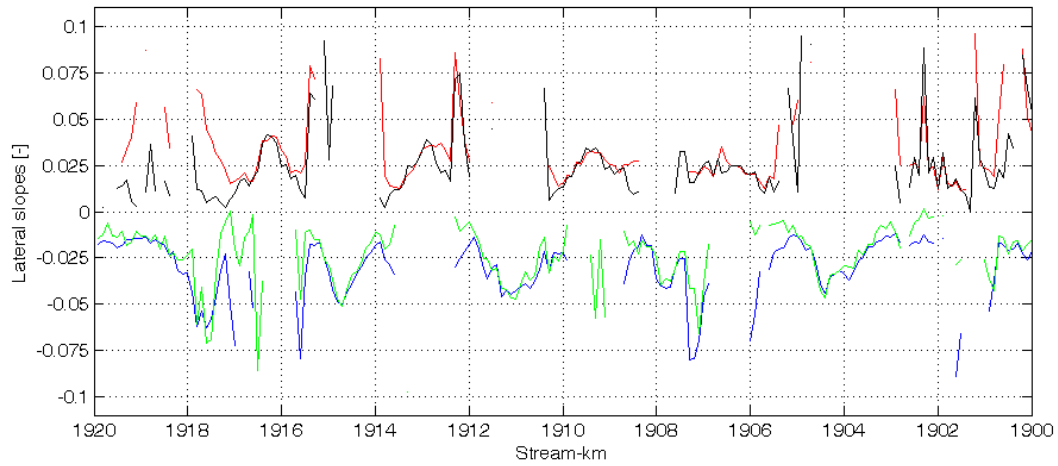Widths and Width-to-depth ratios 2003(2)
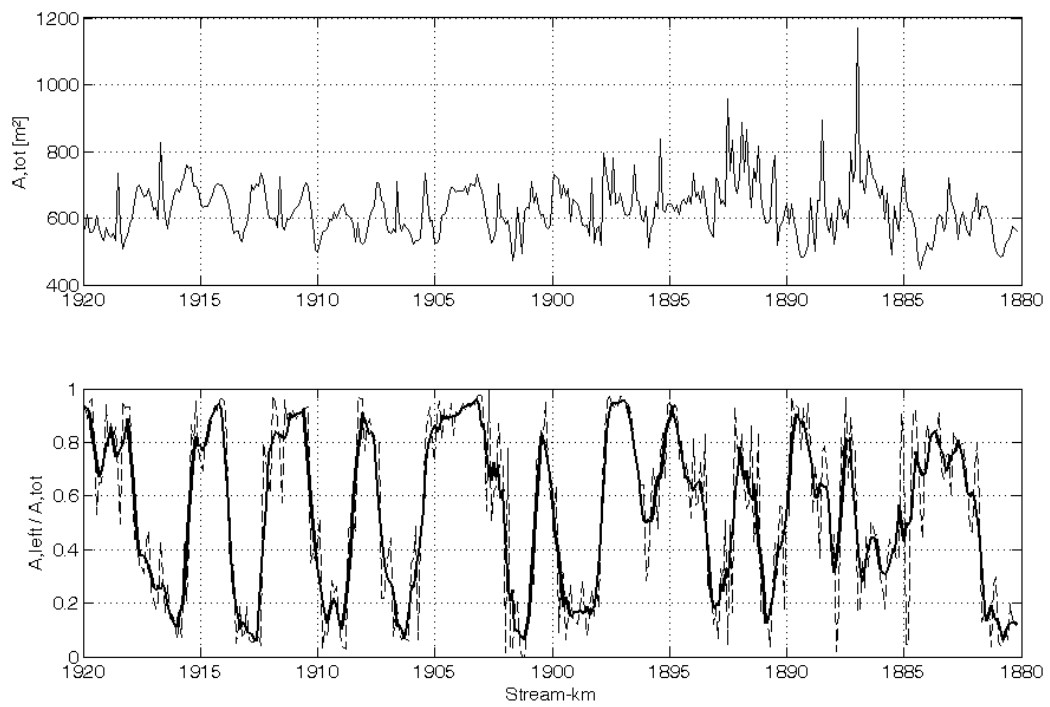
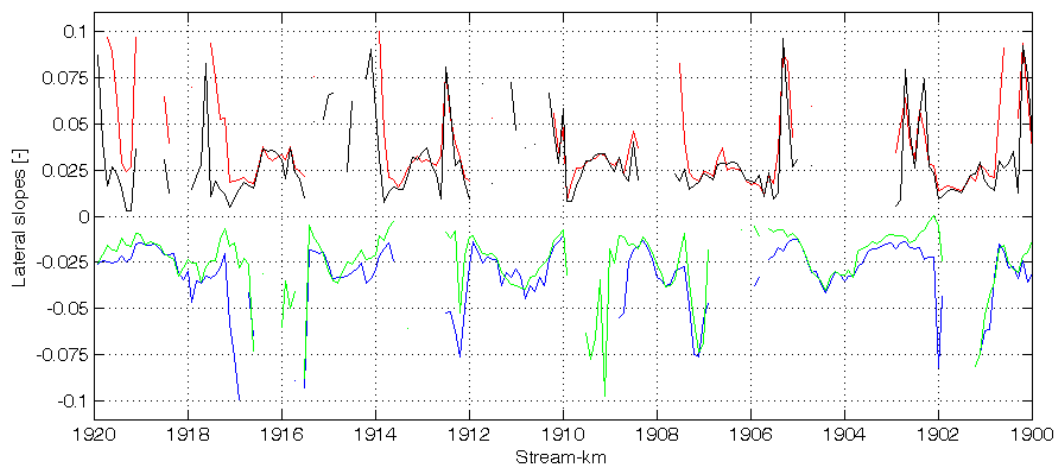Asymmetry in 1993 survey
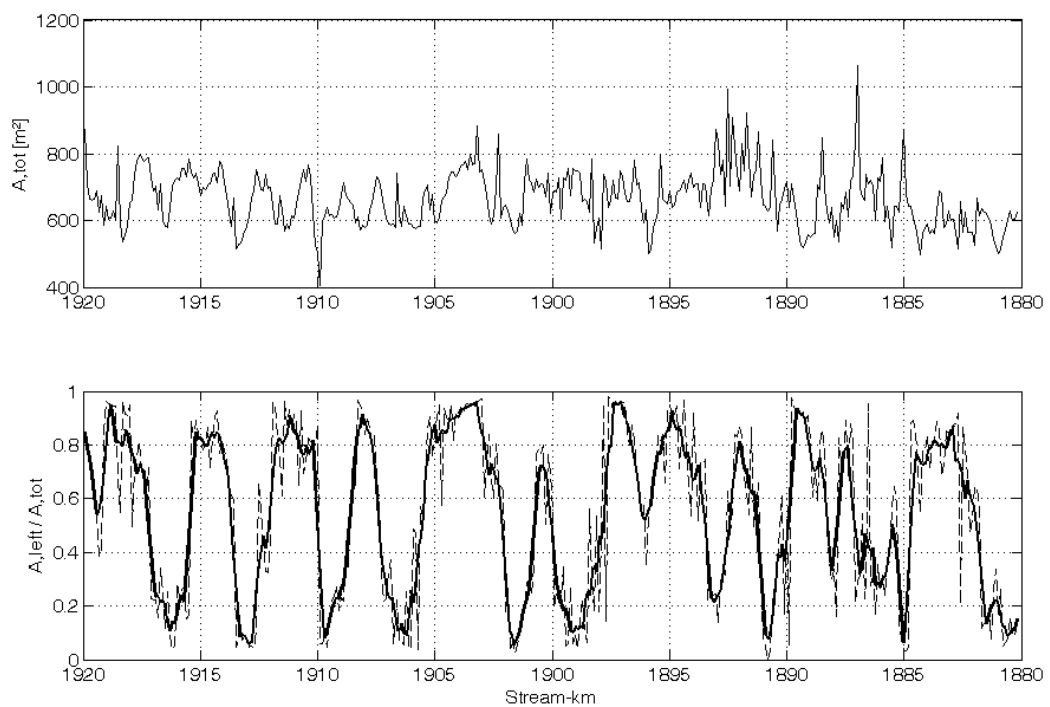
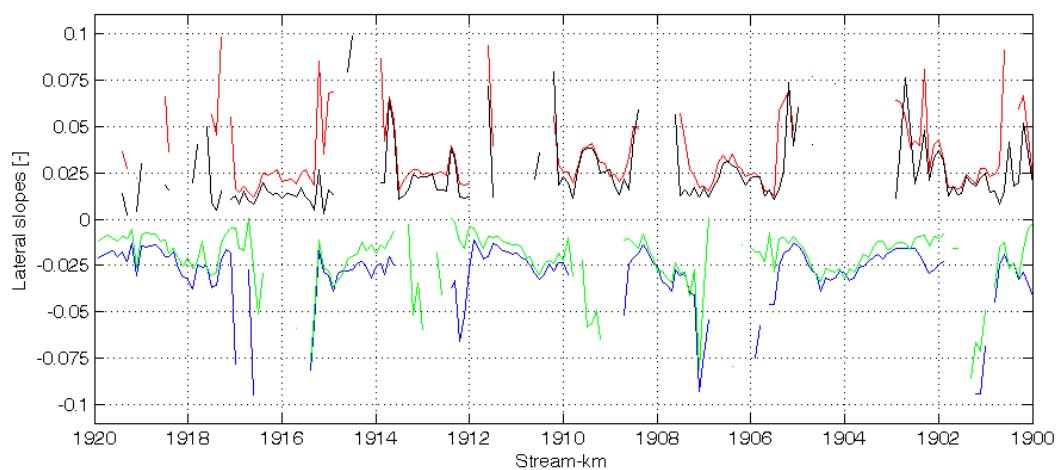Asymmetry in 1996 survey
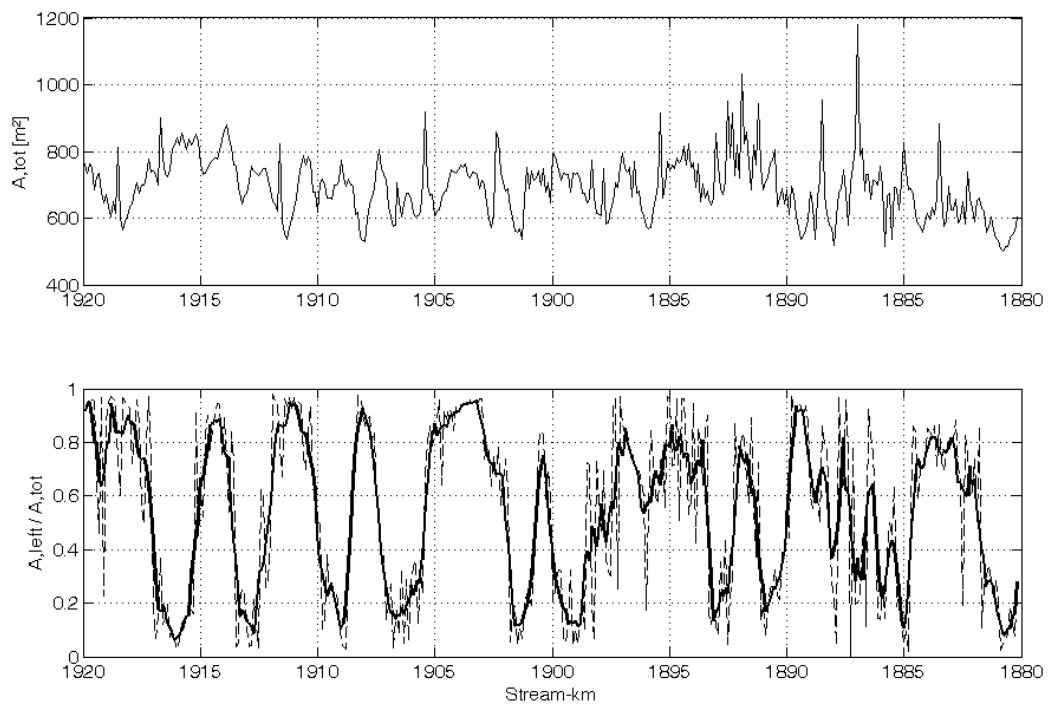
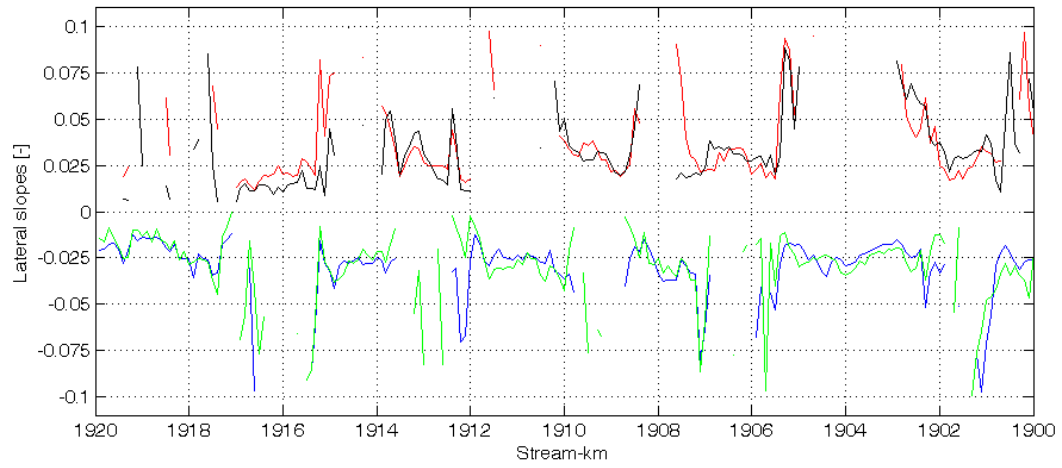Asymmetry in 2002(2) survey
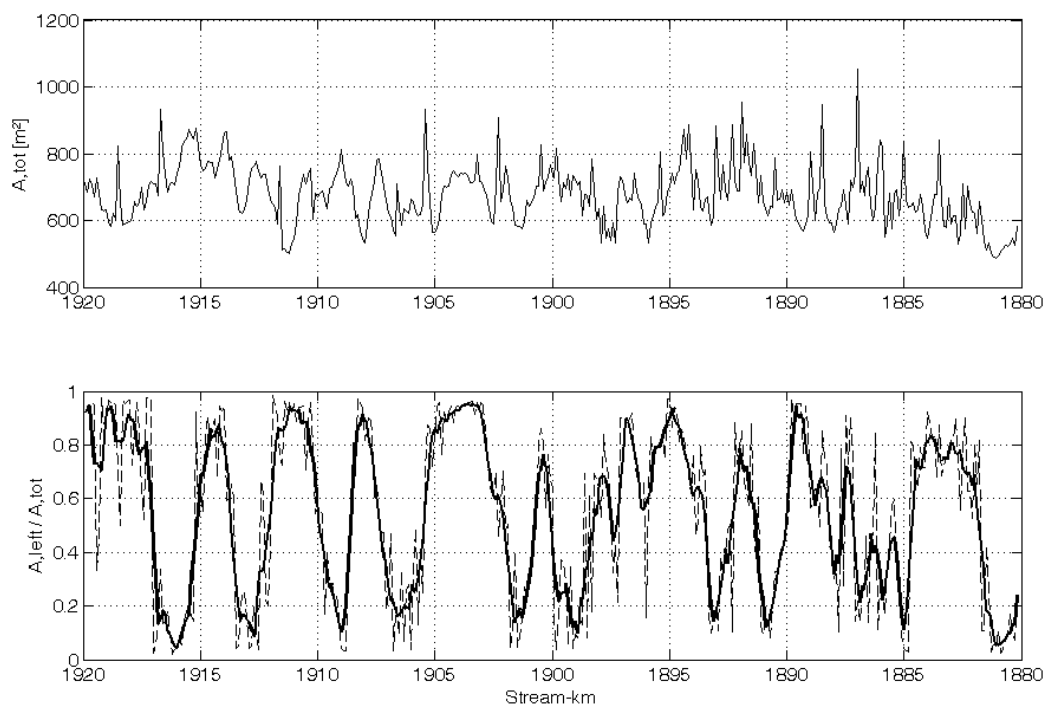
Asymmetry in 2003(2) survey

Lateral slopes on the bars in the survey 1993
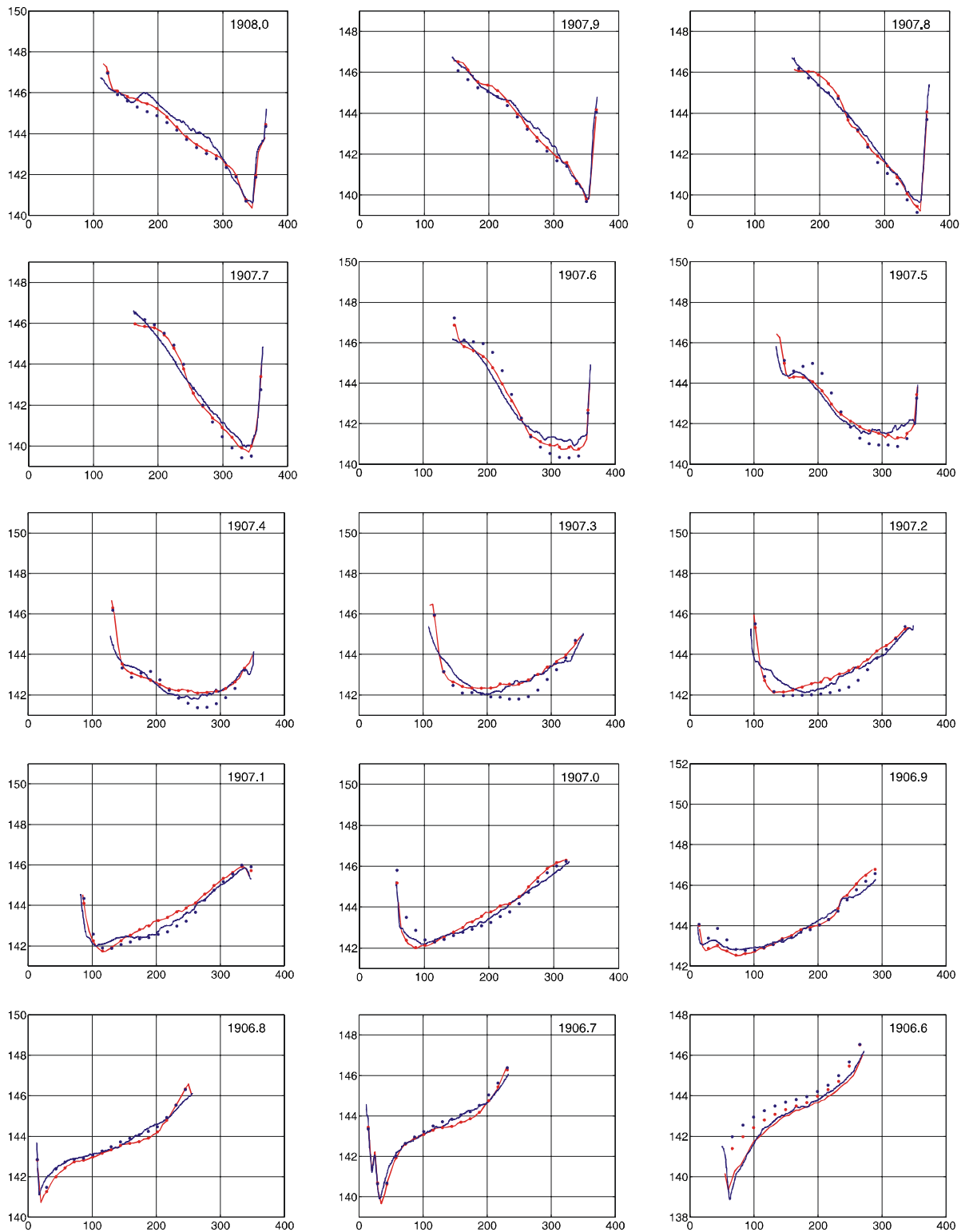

Lateral slopes on the bars in the survey 1996

Lateral [e121]slopes on the bars in the survey 2002(2)

Lateral slopes on the bars in the survey 2003(2)

Appendix B: Measured and computed profiles